UNIVERSIDAD DE GRANADA

FACULTAD DE CIENCIAS

DEPARTAMENTO DE QUÍMICA FÍSICA

KINETIC, STRUCTURAL AND THERMODYNAMIC DETERMINANTS OF AMYLOID FIBRIL FORMATION BY THE ALPHA SPECTRIN SH3 DOMAIN

LORENA VARELA ÁLVAREZ

Tesis Doctoral

GRANADA

2010

UNIVERSIDAD DE GRANADA

FACULTAD DE CIENCIAS

DEPARTAMENTO DE QUÍMICA FÍSICA

KINETIC, STRUCTURAL AND THERMODYNAMIC DETERMINANTS OF AMYLOID FIBRIL FORMATION BY THE ALPHA SPECTRIN SH3 DOMAIN

LORENA VARELA ÁLVAREZ

Tesis Doctoral

GRANADA

2010

Editor: Editorial de la Universidad de Granada
Autor: Lorena Varela Álvarez
D.L.: GR 2875-2010
ISBN: 978-84-693-2516-2

UNIVERSIDAD DE GRANADA

FACULTAD DE CIENCIAS

DEPARTAMENTO DE QUÍMICA FÍSICA

Memoria presentada para aspirar al título de Doctor en Química (con la mención "Doctor europeo")

Fdo. **Lorena Varela Álvarez**

Licenciada en Química por la Universidad de Granada

Granada, a 8 de Marzo de 2010

VºBº

DIRECTORES DE LA TESIS

Fdo. **Francisco Conejero Lara**
Profesor Titular
Departamento de Química Física
Universidad de Granada

Fdo. **Ana I. Azuaga Fortes**
Profesora Ayudante Doctor
Departamento de Química Física
Universidad de Granada

A mis padres
A mi Carlos
A José Luis

AGRADECIMIENTOS

No puedo creer que sea cierto, que ya esté todo listo, que la Tesis esté terminada. Ha sido un periodo duro, muchas horas de trabajo, mucho esfuerzo y dedicación, pero al final lo hemos conseguido, y solo puedo decir que ha merecido la pena. Llegados a este punto por fin tengo la oportunidad de agradecer a tanta gente que ha estado a mi lado, que me ha ayudado en lo profesional y en lo personal a seguir adelante, que ha hecho que todo esto sea posible.

En primer lugar agradezco a Pedro el haberme dado la oportunidad de trabajar en este Departamento, ha sido un honor realizar la Tesis Doctoral en su Grupo de Investigación.

A Quico y Ana, mis directores de tesis, les doy mi más sincero agradecimiento por la magnífica labor realizada durante los 4 años de desarrollo de este trabajo de investigación, por la confianza depositada en mí y por la dedicación absoluta que han mostrado para formarme científicamente. Quico, gracias por transmitirme tus conocimientos y tu pasión por la Ciencia, por guiarme todo este tiempo de forma ejemplar, por enseñarme a investigar de manera rigurosa y por el gran esfuerzo y empeño que has mostrado siempre para sacar la tesis adelante…ha sido una suerte haber podido trabajar bajo tu supervisión. Ana, gracias por transmitirme tu amplia experiencia en el mundo de la Ciencia, por enseñarme a trabajar en un laboratorio, por haber estado siempre dispuesta a ponerte la bata si hacía falta para estar a mi lado guiándome y ayudándome. Mil gracias por haber compartido conmigo tu despacho durante estos últimos meses, por tus sabios consejos, por nuestras conversaciones y confidencias y por tu apoyo incondicional, pero sobre todo, gracias por tu gran amistad. ¡Gracias a los dos por hacer todo esto posible, sin vosotros no lo habría conseguido!.

A Bertrand, mi compañero de proyecto del que tanto he aprendido, gracias por haber estado a mi lado desde el principio enseñándome a trabajar en el mundo de los amiloides y por tu más que importante colaboración en esta Tesis. Siempre has estado dispuesto a ayudarme en el día a día del laboratorio y a resolver las dudas y problemas que se me han ido planteando y eso nunca lo olvidaré.

A Nico le agradezco el haber colaborado tan activamente en el desarrollo de los estudios estructurales llevados a cabo en esta Tesis regalándome siempre su simpatía, cariño, amabilidad y buen humor. Gracias por transmitirme tu pasión por el mundo “erremenero” y por tu alta predisposición a ayudarme en todo momento. Te considero un gran científico y un mejor amigo.

A Salva, mi gran amigo, gracias por estar siempre dispuesto a ayudarme, por tu apoyo incondicional, por interesarte por mí y por mi trabajo a diario. Desde que te conocí has sabido siempre sacarme una sonrisa, hacer amenos los momentos más duros, me has abierto las puertas de tu casa, me has mimado con esas “inigualables tartas de queso”. Gracias por todo Salvi, gracias de corazón.

Gracias a todos los profesores del Departamento porque siempre me he sentido apoyada y respaldada por todos. En especial agradezco a Irene el haberme enseñado a dar los primeros pasos por este laboratorio dirigiéndome las becas de iniciación y de colaboración, y también le agradezco el interés mostrado por mi trabajo a lo largo de estos 4 años; A Jose, el haberme invitado a conocer la investigación que se llevaba a cabo en este Departamento cuando aún era una estudiante de Química y también sus acertados consejos y sabias conversaciones; A Javi, el estar siempre dispuesto a echar una mano para resolver las “dificultades técnicas” del día a día del laboratorio; A Eva, el gran apoyo mostrado, la ayuda prestada y sus acertados consejos; A Obdulio por compartir su gran experiencia y sabiduría; A Enrique agradezco la gran predisposición para arreglar todos los trámites burocráticos y por supuesto su alegría y su buen carácter que me han sacado siempre una sonrisa. A Mª del Mar, por interesarse por mí a diario y por su ánimo en los momentos de desesperación. Gracias por brindarme tu cariño cada día. También agradezco a Mª Paz, del Departamento de Bioquímica, por su gran predisposición en la colaboración de los ensayos “in vivo”, su derroche de amabilidad y sus palabras de ánimo.

A Jose Miguel, el “secre”, porque siempre he contado con él para arreglar todos los papeleos y me ha ayudado sin dudarlo ni un segundo. A Araceli, porque siempre ha estado dispuesta a echar una mano y me ha mostrado un profundo cariño.

I would like to specially thank Fabrizio Chiti for sharing with me his ample scientific experience and his deep knowledge about the amyloid field; I would like to thank André Matagne for his more than valuable collaboration in the kinetic study performed in this thesis project. I would also like to thank all the people that I met in Florence and in Liege during the two short

term stays because they made me feel at home, especially I would like to thank Francesco, Silvia and Roya for all the help given and their sincere friendship.

Agradezco al LPMB, al servicio de TEM y al servicio de espectrometría de masas del CIC de la UGR, todos los servicios prestados, en especial les agradezco a Mª José y a Juande el buen trato recibido.

Agradezco especialmente a la Junta de Andalucía y a los fondos FEDER, el haber financiado la beca de investigación que me ha permitido realizar esta Tesis Doctoral. Agradezco también la financiación recibida por la Junta de Andalucía y las Organizaciones EMBO y FEBS para la realización de las estancias en el extranjero.

A mis hermanos mayores del laboratorio, Adela y Andrés, gracias por haberme enseñado a desenvolverme en el laboratorio cuando aún era una estudiante de carrera, por vuestra ayuda incondicional y por vuestros consejos tan valiosos. Ade, tu cariño y amistad son una de las cosas más importantes que me llevo de este laboratorio. ¡No sabes lo que te he echado de menos desde que te fuiste! Nuestras risas, nuestras confidencias, nuestras excursiones a las tiendas, nuestras cenitas… ¡Gracias de corazón por haberme dado tanto!. Andrés, con tu gran sentido del humor me has hecho pasar muy buenos momentos en el "labo", me pareces una gran persona, muchas gracias por estar ahí. A José Manuel, mi "Crunchi", gracias por estar siempre a mi lado y por compartir tantísimos buenos momentos. Eres una de las mejores personas que he conocido en mi vida, de ti me llevo un amigo para siempre ¡Gracias por todo!; Y a Paqui, su novia, por brindarme su amistad desde el primer momento. También agradezco a Mariano el haber compartido conmigo tantas risas y buenos ratos en los desayunos.

A mis compis del "labo", Manu, Javi, Carles, Mª Ángeles, Sara, María, Ana Mari, Fran y David, gracias por hacer tan ameno el trabajo del día a día, y por los muchos y buenos momentos que hemos compartido. Manu, gracias por tu interés en mi trabajo; Javi, gracias por tus conversaciones tan agradables; Carles, gracias por tu apoyo; María, gracias por preocuparte por mí; Fran, gracias por hacerme reír y por animarme siempre; A David, mi sucesor "amiloidero", también le doy las gracias porque aunque lo conozco de poco tiempo siempre me ha dedicado sus más sinceras palabras de ánimo; Especialmente agradezco a Mª Ángeles, Sara y Ana Mari, "mis niñas", porque conoceros a vosotras ha hecho que todo esto merezca mucho más la pena. Mª Ángeles, "nunca podría dejar de agradecerte" el haberte conocido, el que seas tan divertida y auténtica, el hacerme pasar tan buenos momentos. ¡Gracias de corazón por todo!. Sara, sabes que eres especial para mí. Desde aquel día que te encontré saliendo del despacho de Pedro conectamos de una forma especial y sin tu cariño y amistad nada habría sido lo mismo. Conocerte es una de las mejores cosas que me ha pasado en estos años. ¡Gracias por todo preciosa!. Ana Mari, mi Ana Mari, gracias por regalarme cada día tus risas y tu alegría, ¡me hacen sentir tan bien!, gracias por poder contar contigo siempre. Eres bonita por dentro y por fuera. No sabes lo orgullosa que estoy de tenerte como amiga.

A mis "compis" del Grupo vecino, Inma, Álvaro, Roci, David, Angel, Asun, Mª Carmen, Sisi y Héctor, gracias por todos los buenos momentos compartidos, por vuestro apoyo y vuestras palabras de ánimo en los momentos más duros. Agradezco a Mª Carmen sus conversaciones y su energía y vitalidad que tanto me han animado, a Asun por mostrar siempre tanto interés por mí y por transmitirme tanta serenidad, a Roci por ser ella, por regalarme cada día su "eco-pija" visión de la realidad; A Ángel por sacarme siempre una sonrisa; A Álvaro por todas las conversaciones y risas compartidas; Finalmente a mi Inma, no sabes lo importante que eres para mí dentro y fuera del "Depar". Gracias por tener ese corazón tan grande, por estar siempre ahí, por tus ánimos, por compartir conmigo tantas cosas, por mostrar esa ilusión por todo lo que hago, pero sobre todo, gracias por tu amistad ¡Es una suerte haberte conocido mi "Rubipelirroji"!

Agradezco también a mis amigos de la carrera Macarena, Sisi, José Ignacio y Luis, con los que empecé mis andaduras por esta Facultad, por haberme hecho pasar tantísimos buenos ratos. Especialmente a Macarena, porque aunque estemos lejos sé que siempre está ahí, y a Manolo, su novio, porque hemos compartido grandes momentos.

A mis amigos de siempre, Jessi R., Jessi L., Resu, Leti, Carlos, Salva y Pepe, gracias por ser los mejores amigos que se puede tener, porque me habéis hecho pasar los mejores momentos de mi vida y nunca me habéis fallado cuando os he necesitado, porque durante mis años en este laboratorio siempre os habéis interesado por mí y habéis valorado enormemente mi trabajo apoyándome y animándome insaciablemente. También quiero dar las gracias a Jose

porque aunque hace poco que nos conocemos no ha parado de darme ánimos y apoyo en todo momento. ¡Os quiero muchísimo a todos! ¡Gracias por todo!.

A mis padres, Antonio y Teresa, a los que les debo todo lo que he conseguido en mi vida, todo lo que soy. Si yo he llegado hasta aquí ha sido por vosotros, porque siempre me lo habéis dado todo sin condiciones y porque jamás habéis dejado de confiar en mí. Papá, tú me has transmitido el interés por la Ciencia que me ha permitido llegar aquí y me has enseñado a valorarme y a confiar en mí misma, Mamá, tú me has enseñado a ser responsable y constante para poder alcanzar mis metas y me has guiado y aconsejado siempre para tomar decisiones correctas. No os podéis ni imaginar lo orgullosa que estoy de vosotros, de ser vuestra hija, de ver lo que habéis luchado siempre para conseguir lo mejor para mí y para mi hermano. Sois un ejemplo a seguir. Sois los mejores padres que existen, los mejores padres que se pueden tener. Nunca podré llegar a expresar lo agradecida y feliz que me siento por teneros a mi lado y por apoyarme siempre. Sé lo orgullosos que estáis de que haya hecho el Doctorado y por eso esta Tesis es por y para vosotros. ¡GRACIAS!.

Doy las gracias a mi hermano porque siempre ha confiado en mí y eso me ha dado las fuerzas necesarias para seguir adelante. Carlos, gracias por estar siempre tan orgulloso de mí, por valorar tanto todo lo que he hecho en mi vida, porque sé lo muchísimo que me quieres y ni te imaginas lo que eso me anima y ayuda en todos los ámbitos de mi vida, esta Tesis también es para tí. ¡ Aún no se han inventado las palabras que describan lo que significa mi Carlos para mí!.

A mi “Abueli” Carmela, porque siempre hemos tenido una conexión especial, por estar tan orgullosa de mí y porque siempre me has demostrado tener un corazón gigante. A mi “MamaPaquita”, por confiar en mí como nadie, por darme tanto durante toda mi vida, porque siempre me ha hecho sentir la número 9. A mis abuelos Juan y Carlos, porque sé que desde alguna parte vosotros también estáis orgullosos de que haya llegado hasta aquí. A mi mama, mi Manuelilla, porque me gustaría poder contarte esto y que me dieras un beso y aunque sé que siempre estás conmigo desde algún lugar, llenando mi corazón, no puedo evitar echarte infinitamente de menos.

A mis tíos Mari, Yoli y Felix y mis primos Rober, Adri, Jose, Sergio, Montse, Tolo y Vane por vuestros ánimos y por alegraros siempre tanto por mí. A mi tío “Juanmi”, porque aunque no me lo puedas decir, yo sé lo orgulloso que estás de que tu “mona” haya llegado hasta aquí. A mis tíos Jose, Manoli, Rosa, Nene, Vane, Jessi y David, sabéis que sois mis hermanos, mi ejemplo a seguir. ¡Gracias por aconsejarme tanto y tan bien en toda mi vida!. A mis tíos Antonio S., Mari, Antonio L., José Miguel y Juanjo porque sé lo orgullosos y felices que estáis de que lo haya conseguido. Gracias a mi Jose Carlos, Raúl, Duna, Carla, Claudia, Paula y Hugo, porque sois la alegría de mi vida y llenáis mi corazón cada día con vuestras sonrisas. También agradezco a toda la familia de José Luis su apoyo y sus ánimos, en especial a Carmen, Manolo, Alberto, Mª José y Luna por hacerme sentir una más de la familia.

Y finalmente, a mi José Luis, porque soy la persona más afortunada del mundo por tenerlo a mi lado, porque lleva ya más de 10 años dándolo todo para hacerme feliz y por aportarme tanto, personal y profesionalmente. Jose, si yo he llegado hasta aquí ha sido por tí, porque dentro del laboratorio lo has dejado siempre todo para ayudarme, porque me has enseñado muchísimo, porque me has dedicado tiempo y esfuerzo sin límite para que mis cosas salieran adelante, porque has colaborado conmigo en la parte de RMN con una predisposición y unas ganas desbordantes. Gracias por confiar siempre en mí y por saber animarme y aconsejarme como nadie. Gracias por escucharme en todo momento, por entenderme siempre y por regalarme tu cariño que es tan imprescindible para mí. Ha sido una suerte vivir todo esto a tu lado, sin tí no lo habría logrado. Gracias por no haberte separado de mí ni un segundo durante estos cuatro años, desde lo más profundo de mi corazón te dedico mi Tesis Doctoral.

CONTENTS

CONTENTS

ABBREVIATIONS

ABBREVIATIONS

2D	Two-dimensional
3D	Three-dimensional
Abs	Absorbance
ANS	8-Anilino-naphthalene-1-sulfonic acid
B	Magnetic field
CD	Circular Dichroism
Cp	Heat capacity
D	Translational diffusion coefficient
DLS	Dynamic Light Scattering
DMSO	Dimethylsulphoxide
DNA	Desoxyribonucleic acid
DSC	Differential Scanning Calorimetry
$\Delta\delta$	Chemical shift
Δ**Cp**	Heat capacity change of unfolding
ΔG_u	Gibbs energy change of unfolding
ΔG_{ex}	Gibbs energy change of H/D exchange
ΔH_u	Enthalpy change of unfolding
ΔS_u	Entropy change of unfolding
$\Delta\Delta$**G**	Differences in the Gibbs energies

ABBREVIATIONS

EX1	Type 1 exchange mechanism
EX2	Type 2 exchange mechanism
ε	Molar Extinction coefficient
G^x	Correlation function
HMQC	Heteronuclear Multiple-Quantum Correlation
HSQC	Heteronuclear Single-Quantum Correlation
i	Photon flow
IPTG	Isopropyl-β-D-Thiogalactopyranoside
k	Kinetic rate constant
K	Equilibrium constant
m	slope
n	Refraction index
η	viscosity
NMR	Nuclear Magnetic Resonance
PCR	Polymerase Chain Reaction
PF	Protection Factor
R	Ideal gases constant
R_h	Hydrodynamic radius
SH3	Src-Homology domain 3
SOFAST	Band-Selected Optimized Flip-Angle Short Transient

Spc	Alpha Spectrin
t	Time
T	temperature
TEM	Transmission Electron Microscopy
ThT	Thioflavin T
Tm	Transition temperature of the unfolding
T_{ml}	Primer melting temperature
TOCSY	Total correlation spectroscopy
τ	Lag time
$[\theta]$	Molar ellipticity
UV	Ultraviolet
WT	Wild Type

1.
INTRODUCTION AND OBJECTIVES

1. INTRODUCTION AND OBJECTIVES

1.1. THE IMPACT OF AMYLOID FIBRIL AGGREGATION IN HUMAN HEALTH

The correct folding in proteins is a crucial step in the conversion of genetic information in biologic activity in the living beings. After the synthesis of proteins in the cell, most of them are able to natively fold in their biologically active conformation, either in a spontaneous way or assisted by chaperons and other factors. A small part of the proteins are however incorrectly folded. Figure 1.1 illustrates the different possible fates of a polypeptide chain after its synthesis at the ribosome.

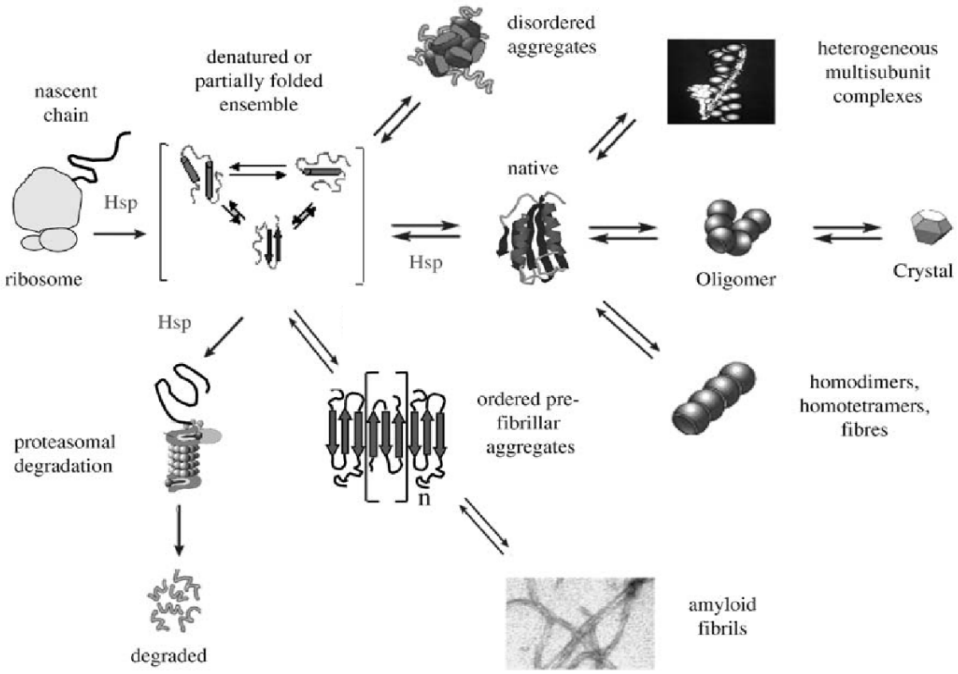

Figure 1.1. *General view of the possible fates of a polypeptide chain after its synthesis in the ribosome.*

Despite the existence of exigent mechanisms of control of protein aggregation in the cell, under certain metabolic circumstances (stress,

cell aging or the presence of exogenous or infectious agents) some misfolded proteins or peptides form highly-organized aggregates, which deposit extracellularly as fibrils or plaques commonly known as amyloids. Fibrillar aggregates structurally and morphologically similar to the amyloid fibrils also form inside the cells in some diseases. In 1907 Alois Alzheimer described for the first time senile plaques and neurofibrillar tangles in a middle-aged woman affected by memory deficits. Since then, the number of diseases related with amyloid aggregates has increased continuously. To date, more than 30 diseases, some sporadic and/or hereditary and some transmissible, have been described as associated with amyloid deposits (Table 1.1), [1]. This type of diseases is known under the generic name of protein deposition diseases. Among these, there are some of the most devastating neurodegenerative diseases, such as Alzheimer, Parkinson and Huntington diseases. In other diseases unrelated to the central nervous system the protein aggregates are deposited in tissues or organs impairing severely their function.

Table 1.1. *Some examples of diseases associated with amyloid deposits.*

Disease	Aggregating protein or peptide
Alzheimer	Amyloid β peptide (Abeta)
Parkinson	α-Synuclein
Huntington	Huntingtin with poly-Q expansion
Spongiform encephalopathies	Prions or fragments of them
Amyotrophic lateral sclerosis	Superoxide dismutase I
Primary Systemic AL Amyloidosis	Immunoglobulin light-chain or fragments
Haemodialysis-related amyloidosis	β2-microglobulin
Type II diabetes	Amylin or islet amyloid polypeptide
Cataracts	γ-crystalline

This group of diseases infringes an enormous social and personal damage and it is crucial therefore to understand in detail the mechanisms of their genesis and to learn how to treat and prevent them.

1.2. MORPHOLOGY AND STRUCTURE OF AMYLOID AGGREGATES AND FIBRILS

Despite the lack of sequence homology between the peptides and proteins associated with each type of disease, the amyloid fibrils exhibit similar external morphology and internal structure. They interact with specific dyes such as Congo red or thioflavin T (ThT) and have characteristic circular dichroism (CD) and infrared spectra, typical of a high content in β-sheet secondary structure [2]. When observed by transmission electron microscopy (TEM) or atomic force microscopy (AFM) *in vitro*, the fibrils consist of a number of filaments (typically between 2 and 6) each 2 to 6 nm thick that twist forming rope-like fibrils (Figure 1.2), [3] or associate laterally to form ribbons [4]. X-ray fiber diffraction analysis indicates that in each filament the protein molecules are arranged in a highly-ordered cross-β structure forming β-sheets that extend throughout the entire length of the fibril [5]. The most recent advances in solid-state NMR spectroscopy applied to amyloid fibrils [6], together with the recent success in growing nano- and micro-crystals of short peptides with amyloid characteristics [7], [8], have allowed to obtain a great level of detail in the internal molecular structure of the fibrils (Figure 1.2). For instance, in the fibrils of amyloid β-peptide (Abeta) each peptide molecule contributes to two β-strands, each one being part of a different parallel and in-register β-sheet [9]. Detailed information about the structure of amyloid fibrils has also come from amide hydrogen-deuterium studies combined with high-resolution NMR and mass spectrometry [10], [11]. This type of

analysis has helped to map at residue level those regions of the polypeptide chain that form the core of the fibrils. Interestingly enough, these methodologies have also established that amyloid fibrils are dynamic structures that can undergo a recycling of molecules in equilibrium between the bulk solution and the fibril ends [11]. This observation has important implications in the design of therapeutic strategies to treat amyloid-related disorders, especially because there is increasing evidence indicating that the dynamic soluble oligomeric species are the true toxic species to cells.

Despite the overall similarity in amyloid fibril structures, there is a significant morphological variability even between the amyloid fibrils formed from the same protein or peptide in vitro [12, 13]. This is related to a heterogeneity in the nano-scale structure of the fibrils, which is influenced by a variety of factors related to the environmental conditions of their formation, such as temperature, pH, ionic strength, or mechanical factors such as the presence or absence of agitation [14]. These results suggest that, in contrast to the unique native conformation of natural proteins, amyloid fibrils can acquire a variety of structures corresponding to several energy minima in their conformational landscape, being the final conformation simply selected by the thermodynamic or, in many cases, kinetic factors that govern under each circumstance.

Although the amino acid sequence can also impact on the particular details of each fibril structure by specific interactions between side chains within the fibril and change strongly the propensity to fibrillate, the common structural properties of amyloid fibrils reflect the fact that amyloid fibril formation is a generic property of polypeptidic chains. In fact, a number of peptides and proteins unrelated to any disease can form amyloid fibrils with similar morphology and structure to those related to disease and it has also

been suggested that almost any protein could be converted to amyloid when submitted to the appropriate conditions [15], [16]. These findings have opened huge possibilities to study *in vitro* amyloid fibrils using a wide range of well-characterized proteins as model systems.

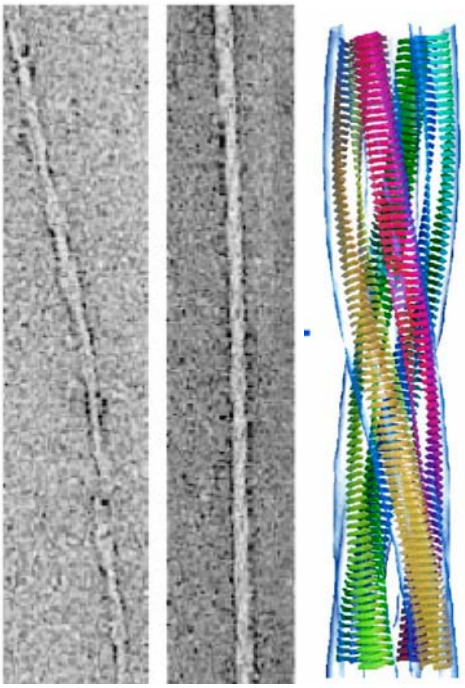

Figure 1.2. *Transmission electron microscopy images of amyloid fibrils of insulin and model of structure of an amyloid fibril formed by filaments of β-sheets [17].*

1.3. THE MECHANISM OF AMYLOID FIBRIL FORMATION

It is nowadays well established that the conversion of a peptide or protein into amyloid fibrils has a kinetic mechanism of nucleation and growth, typical of crystallization. The time course of fibril formation generally shows a typical lag phase of variable length followed by an exponential growth [18]. The lag phase or “nucleation” phase is the time required for the formation of the nuclei of aggregation, being the

rate limiting step of the aggregation process. Once a nucleus is formed, it progresses toward the fibrillation by a series of elongation steps with addition of protein molecules to the ends of the fibrils [19].

As in all nucleation-dependent processes, the lag phase can be shortened or even removed by "seeding" the protein sample with preformed nuclei or fibrillar species prior to the start of the aggregation [20, 21]. The length of the lag phase can also be affected by changes in the experimental conditions or by mutations in the protein sequence that may accelerate the nucleation process, being sometimes no longer the rate limiting step [22]. In some cases, already formed nuclei or fibrils can catalyze the formation of additional nuclei by a secondary nucleation pathway, as observed for insulin [23]. Very recently, an analytical approach to the kinetics of fibril assembly has shown that, in contrast with classical homogeneous nucleation theories, secondary nucleation processes such as filament fragmentation can dominate the process for a majority of examples and conditions [24].

Although it is assumed that fibrils do not appear in a significant amount during the nucleation phase, this is a crucial stage in the overall aggregation process, in which a variety of oligomeric species are formed, many of them rich in β-sheet structure, providing nuclei for the assembly of larger species and finally the fibrils.

1.4. CONFORMATIONAL EVENTS TRIGGERING THE AGGREGATION CASCADE

It is generally believed that an amyloidogenic protein or peptide needs to unfold at least partially (or refold if previously unfolded) to attain a partially structured conformation that can establish, at least transiently, the necessary intermolecular interactions to nucleate aggregation, whereas these interactions are disfavoured in fully unfolded states [25, 26, 27]. Partially-folded species are favoured in

globular proteins by particular conditions such as acidic pH, high pressure, high temperature or moderate concentrations of organic solvents [15, 28, 29, 30]. Remarkably, aggregation of human lysozyme and HypF-N can be initiated by a population of less than 1% of a partially folded states that is in equilibrium with the native conformation [31, 32]. Proteins can achieve a partially-folded conformation prone to aggregation by a variety of structural fluctuations occurring even under native conditions [33, 34, 35]. In fact, recent studies have proposed that destabilization of the native fold results in the modulation of the protein conformational ensemble, disfavouring structural cooperativity and increasing the sampling of partially-folded amyloidogenic conformations [36]. In addition, significant inverse correlations have been reported between the propensity of proteins to aggregate into amyloid-like structures and the thermodynamic stability of the native state [37, 38, 39, 40], although in some examples it is the unfolding rate which correlates with fibrillation propensity [22], [41]. Although the amyloid aggregation usually involves a conformational change, there are some cases in which formation of amyloid fibrils is preceded by an assembly of quasi-native or native-like structures into aggregates. Structural conversion takes place subsequently within the aggregates to transform into pre-fibrillar species that may not yet be fibrillar in their morphologies but have some of the characteristics of amyloid-like structures, such as CD or FT-IR spectra typical of β-sheet structure or binding to Congo-red and ThT dyes [42, 43]. These pre-fibrillar aggregates then convert into amyloid fibrils. Natively unfolded peptides and proteins, as well as fragments of proteins generated by proteolysis and unable to fold in the absence of the remainder of the polypeptide chain, can also adopt conformations that are susceptible to form intermolecular interactions triggering aggregation under some circumstances, for example, if their concentrations become elevated. It

is more and more evident that natural sequences in proteins have evolved to avoid this type of conformations [44].

1.5. CHARACTERISTICS OF THE PRE-FIBRILLAR OLIGOMERIC PRECURSORS

During the last decade a great effort has been made to identify, isolate and characterize the oligomeric and prefibrillar species present in solution before the appearance of the fibrils. The main reason of this active research is based on the increasing evidence supporting that these oligomeric species are involved in the neurotoxic mechanisms of amyloid-related neurodegenerative diseases [45]. The most active research has been centred on the β-amyloid peptide (Abeta) because of its relationship with Alzheimer's disease. The aggregation of Abeta is preceded by the formation of non-fibrillar, metastable species, known as protofibrils, visible by TEM or AFM as globular beads of 2-5 nm of diameter, chains of beads or annular structures [20]. Similar species have been observed for many other proteins such as α-synuclein [46], immunoglobulin light chain [47], transthyretin [48], β2-microglobulin [28], horse lysozyme [49], Sso-acylphosphatase [43] or the PI3-SH3 domain [50]. All these prefibrillar species also possess a high content of β-sheet structure and interact with Congo red and ThT, which suggests a certain degree of structural regularity. Some of these protofibrillar states appear to be on-pathway intermediates in the fibrillation process [51], whereas others can be off-pathway [28], [52].

Preceding the formation of protofibrils, smaller oligomeric states appear, generally soluble and with a low degree of structural order. The assembly and structural reorganization of these species leads to the formation of protofibrils. For example, the 40- or 42-residue forms of Abeta give rise to different oligomeric species in rapid equilibrium with the monomeric forms, with a relatively disordered structure

according to their circular dichroism spectra [53]. Likewise, similar oligomers featuring dynamic structures have been identified during amyloid fibril formation of the yeast prion Sup35p, phosphoglycerate kinase or the PI3K-SH3 domain [50, 51, 54]. These oligomers are capable of nucleating the formation of amyloid fibrils efficiently, reducing the lag phase of aggregation. These results indicate that disordered oligomers appear to be the key precursors of protofibrils and fibrils and therefore the elucidation of their physicochemical and conformational properties is of crucial importance in understanding the determinants of amyloid aggregation in order to design therapeutic strategies to inhibit their formation.

Irrespective of the role of the oligomeric species and prefibrillar aggregates in the overall fibrillation process, the investigation of their mechanism of formation and structural properties is of vital importance because these species appear to constitute the main toxic agents in neurodegenerative diseases [45]. Supporting this hypothesis, some studies established a significant correlation between the levels of soluble Abeta peptide, including its oligomeric forms, and the degree of synaptic alteration, neurodegeneration and cognitive decline in Alzheimer's disease patients, whereas a similar correlation is not observed for the insoluble deposits [55]. Furthermore, the neurotoxicity of Abeta oligomers has been demonstrated in animal brains by injection of purified oligomers into rat hippocampus [56, 57]. Also for α-synuclein increasing evidence suggests that nonfibrillar dimers or oligomers play a major role in the disease progress of Parkinson's disease [58]. Similarly, it has been shown with neuronal cell cultures that there is less cell death in the presence of large aggregates of poly-Q-rich Huntingtin than when only the soluble fraction is present [59]. Certain non-fibrillar aggregates of transthyretin have also been shown

to be toxic to neuronal cells under the conditions where the native tetramers and the mature fibrils have no significant toxicity [60].

The general toxic nature of prefibrillar aggregates has been further underlined by the finding that certain oligomeric species of proteins unrelated to disease, such as HypF-N of E. coli, the SH3 domain of bovine phosphatidyl-inositol kinase and equine lysozyme, are highly toxic in fibroblast and neuron cultures, whereas the amyloid fibrils of the same proteins show little if any toxicity [61, 62].

The reasons of the toxic behaviour of these prefibrillar aggregates to cells are currently at the front of research. This investigation is however hampered by the lack of structural information available for the toxic oligomeric species and also the mechanism of their pathological action remains unclear. For instance, it is possible that A-beta neurotoxic effects are the result of an interaction between oligomers and neurotransmitter receptors, interfering with signalling pathways in the synaptic plasma membranes [45]. Other hypotheses imply the formation of specific ion channels or the non-selective permeabilization of the plasmatic membrane [63]. The main obstacle to this investigation is that these oligomeric states are relatively short-lived and rapidly convert into an amyloid fibril state and, therefore, are difficult to detect or study. Among the few exceptions to this is a recently reported study, in which two types of stable oligomers of HypF-N with similar morphological, structural and tinctorial properties have been shown to have very disparate cellular toxicity. This difference appears to be related to their different structural flexibility and hydrophobic exposure that are related to their capability to permeabilize the cell membrane and trigger citotoxic processes [64]. Understanding the stability and life-time of toxic oligomers under physiological conditions could turn out to be a key factor in the progress against amyloid-related diseases.

Given the complexity and limited information about amyloid structures and the mechanisms and factors controlling their formation, the high stability of the fibril inclusions and the incomplete knowledge about the identity of the toxic species and their mechanisms of toxicity, designing effective strategies of therapy and prevention for these diseases is a very complex task.

Current lines of action involve several different approaches [65], such as interfering with posttranslational modifications of proteins that promote protein aggregation, up-regulating molecular chaperones or stimulating aggregate clearance, targeting cellular pathways affected by protein aggregation (e.g. apoptosis, transcription) or directly targeting proteins that undergo misfolding and aggregation.

1.6. AMYLOID AGGREGATION PROPENSITY IS STRONGLY DEPENDENT ON SEQUENCE

A large body of work has established that polypeptide chains with different sequences have markedly different aggregation rates, even when the aggregation occurs from unfolded states or disordered short peptides. In particular, hydrophobic side chains at key positions in the sequence (for example, if they are important in nucleation) can influence strongly the rate of aggregation [66, 67]. Net charge and β-sheet propensity of the sequence can also impact considerably on the aggregation rate [68, 69, 70]. Remarkably, the changes in the rate of aggregation of unstructured peptides and proteins following a series of mutations could be rationalized using a phenomenological equation, based on simple physicochemical principles [71]. This provides strong support to the idea that aggregation of polypeptide chains reflects the typical behaviour of a simple polymer, in contrast to the process of folding of globular proteins, where the folding rates are strongly coupled to the specific structures of the native states determined by

highly evolved sequences. The increasing knowledge about the sequence effects on aggregation has led to the development of algorithms to identify the regions of the sequence that promote aggregation within an unstructured polypeptide chain [72, 73, 74]. The success of this type of approach is particularly well illustrated by the very good agreement between the regions of the sequence predicted to promote the aggregation of the Abeta peptide and α-synuclein and those found experimentally to form and stabilize the fibril core and/or to play a primary role in fibril formation [73].

1.7. SPC-SH3 DOMAIN, A MODEL TO STUDY THE AMYLOID FIBRIL FORMATION MECHANISM

The work body of this thesis has been focused in the α-spectrin SH3 domain (Spc-SH3) (Figure 1.3). This small domain of 62 residues has become the subject of intense investigation by many groups including ours and there is now a wealth of both thermodynamic and kinetic information available about its folding mechanism and conformational stability from both experimental [34, 75, 76, 77, 78, 79, 80] and computational approaches [81, 82].

More than a decade ago, a highly homologous SH3 domain (PI3-SH3) was shown to form amyloid fibrils under acidic conditions [29], being one of the first amyloidogenic proteins unrelated to disease. Since then, a vast amount of data about the biophysics and structure of amyloid fibrils has been generated with this model system [13, 83, 84, 50, 85]. Intriguingly, the Spc-SH3 domain did not form amyloid fibrils under similar conditions and the molecular reasons behind of this different behaviour were a subject of particular interest [86]. It was later described than transplanting a small sequence stretch of 6 amino acids from PI3-SH3 to Spc-SH3, comprising residues of the diverging turn and adjacent RT loop, creates an amyloidogenic protein closely

similar in its behaviour to the original PI3-SH3 [87]. This indicated the importance of specific residues or "hotspots" in controlling the aggregation propensity of the protein.

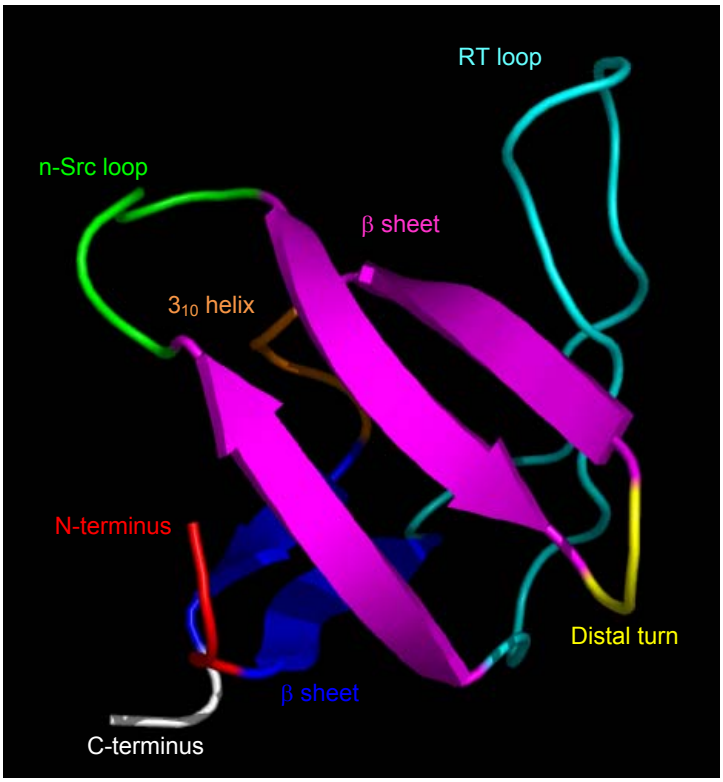

Figure 1.3. *Schematic ribbon representation of the 3D structure of the Spc-SH3 domain.*

During the course of previous research in our group, it was found that the single mutation N47A, placed at the distal turn within the folding nucleus of the Spc-SH3, favours the rapid formation of amyloid fibrils at mildly acidic conditions, under which the majority of the protein is natively folded [88]. The reasons of the amyloidogeneicity of the N47A mutation were unclear since algorithms of prediction of

aggregation [72, 73] did not anticipate any increased aggregation propensity for this mutant compared to the WT domain.

The effect of the N47A mutation on the folding, stability and structural cooperativity of the Spc-SH3 domain had been studied previously [89, 90, 91]. This mutation produces a destabilization of the native state of about 2 kJ mol^{-1}, mainly due to a decrease in the folding rate, without an important influence in the unfolding rate, which is indicative of the involvement of the distal turn in the folding transition state of the domain [78]. The increase in the energy barrier of folding produced by this mutation is, however, rather small and it could not be ruled out that the mutation exerts additional changes in the folding landscape by stabilization of alternative aggregation-prone conformations, thus affecting the kinetic partitioning between folding and aggregation.

This previous study of amyloid formation, together with the wealth of kinetic and thermodynamic data available for the folding mechanism and the conformational stability of the Spc-SH3 domain, make it an ideal model protein to study the determinants of amyloid formation.

Given the lack of a profound understanding of the molecular and physicochemical determinants of formation of amyloid structures and, particularly, of the soluble precursor species that precede the fibrillation process, it is required further investigation of the details of the mechanism of fibrillation and the factors that control it. For instance, it is necessary to establish unequivocal links between the energy landscapes controlling the folding and the conformational stability of proteins and those governing their aggregation. It is also crucial to understand how amyloidogenic early precursors and aggregation nuclei arise from normally folded proteins and how environmental variables affect their formation. And finally it is important

to elucidate how these early stages affect to final structure and morphology of the amyloid aggregates.

The work presented in the Thesis is aimed at tackling these aspects of amyloid aggregation by making use of a very suitable model protein to analyze a variety of stages of the mechanism of amyloid fibrillation, ranging from the early conformational effects occurring prior to the nucleation to the final structure and morphology of the amyloid fibrils.

All this information is essential to devise future strategies of therapy or prevention of these devastating pathologies related to amyloids. For instance, since key precursors of fibrillation appear to share common structural features in many proteins, including those unrelated to disease, their detailed structural characterization may serve to enlighten the design of compounds inhibiting their formation or even to design mimetic molecules that may act as vaccines preventing these disorders. Moreover, a better understanding of the influence of environmental conditions in vitro upon fibrillation and, especially, upon formation of oligomeric species, toxic to cells, may shed light on the way to avoid *in vivo* metabolic states that promote protein deposition.

1.8. OBJECTIVES

Our main hypothesis, supported by previous research in our group, was that, with the use of an appropriate, well-characterized model system such as the Spc-SH3 domain, it is possible to characterize in detail the kinetics amyloid fibril formation and their precursors and to find significant relationships between their properties, their structure, the environmental conditions and the mechanism of their formation.

The main objective of this Thesis project was to identify and characterize the most relevant states of the protein during the amyloid

cascade in order to elucidate the mechanism of the process in detail. To achieve this goal, we used a wide variety of biophysical methods and techniques to explore structurally and kinetically all the stages of amyloid fibrillation, ranging from the initial conformational events that the protein chain undergoes under amyloidogenic conditions, to the final structure and morphology of the amyloid fibrils at the end of the process.

The specific aims of the Thesis include:

1. To elucidate the relationship between thermodynamic stability of the native Spc-SH3 domain and its amyloid aggregation propensity.

2. To understand the effect of environmental variables (temperature, salt concentration and pH) on the fibrillation kinetics, the pathway of assembly and the final fibril morphology.

3. To identify early intermediates and oligomeric precursors in the fibrillation pathway and how environmental conditions influence their accumulation in equilibrium and kinetics experiments.

4. To characterize structurally at the level residue the native conformational ensemble of Spc-SH3 under conditions near those of fibrillation using amide hydrogen-deuterium exchange methods combined with high-resolution NMR. The structural information will be essential in the molecular interpretation of the early events of fibril formation.

5. To analyse structurally the mechanism of the conformational changes triggering fibril formation using a site-directed mutagenesis approach probing all secondary structure elements in the Spc-SH3 backbone.

6. To obtain structural information about the amyloid fibril core of the N47A Spc-SH3 domain.

1.9. BIBLIOGRAPHY

[1] Chiti, F. and Dobson, C.M. (2006). Protein misfolding, functional amyloid, and human disease. Annu Rev Biochem 75, 333-66.

[2] Nilsson, M.R. (2004). Techniques to study amyloid fibril formation in vitro. Methods 34, 151-160.

[3] Serpell, L.C. (2000). Alzheimer's amyloid fibrils: structure and assembly. Biochim Biophys Acta 1502, 16-30.

[4] Saiki, M., Honda, S., Kawasaki, K., Zhou, D., Kaito, A., Konakahara, T. and Morii, H. (2005). Higher-order molecular packing in amyloid-like fibrils constructed with linear arrangements of hydrophobic and hydrogen-bonding side-chains. J Mol Biol 348, 983-98.

[5] Makin, O.S., Atkins, E., Sikorski, P., Johansson, J. and Serpell, L.C. (2005). Molecular basis for amyloid fibril formation and stability. Proc Natl Acad Sci U S A 102, 315-20.

[6] Heise, H. (2008). Solid-state NMR spectroscopy of amyloid proteins. Chembiochem 9, 179-89.

[7] Nelson, R., Sawaya, M.R., Balbirnie, M., Madsen, A.O., Riekel, C., Grothe, R. and Eisenberg, D. (2005). Structure of the cross-beta spine of amyloid-like fibrils. Nature 435, 773-8.

[8] Sawaya, M.R. et al. (2007). Atomic structures of amyloid cross-beta spines reveal varied steric zippers. Nature 447, 453-7.

[9] Tycko, R. (2006). Solid-state NMR as a probe of amyloid structure. Protein Pept Lett 13, 229-34.

[10] Hoshino, M., Katou, H., Hagihara, Y., Hasegawa, K., Naiki, H. and Goto, Y. (2002). Mapping the core of the beta(2)-microglobulin amyloid fibril by H/D exchange. Nat Struct Biol 9, 332-6.

[11] Carulla, N. et al. (2005). Molecular recycling within amyloid fibrils. Nature 436, 554-8.

[12] Bauer, H.H., Aebi, U., Haner, M., Hermann, R., Muller, M. and Merkle, H.P. (1995). Architecture and polymorphism of fibrillar supramolecular assemblies produced by in vitro aggregation of human calcitonin. J Struct Biol 115, 1-15.

[13] Jimenez, J.L., Guijarro, J.I., Orlova, E., Zurdo, J., Dobson, C.M., Sunde, M. and Saibil, H.R. (1999). Cryo-electron microscopy structure of an SH3 amyloid fibril and model of the molecular packing. EMBO J 18, 815-21.

[14] Pedersen, J.S. and Otzen, D.E. (2008). Amyloid-a state in many guises: survival of the fittest fibril fold. Protein Sci 17, 2-10.

[15] Chiti, F., Webster, P., Taddei, N., Clark, A., Stefani, M., Ramponi, G. and Dobson, C.M. (1999). Designing conditions for in vitro formation of amyloid protofilaments and fibrils. Proc Natl Acad Sci U S A 96, 3590-4.
[16] Dobson, C.M. (2003). Protein folding and misfolding. Nature 426, 884-90.
[17] Jimenez, J.L., Nettleton, E.J., Bouchard, M., Robinson, C.V., Dobson, C.M. and Saibil, H.R. (2002). The protofilament structure of insulin amyloid fibrils. Proc Natl Acad Sci U S A 99, 9196-201.
[18] Ferrone, F. (1999). Analysis of protein aggregation kinetics. Methods Enzymol 309, 256-74.
[19] Wetzel, R. (2006). Kinetics and thermodynamics of amyloid fibril assembly. Acc Chem Res 39, 671-9.
[20] Harper, J.D. and Lansbury, P.T., Jr. (1997). Models of amyloid seeding in Alzheimer's disease and scrapie: mechanistic truths and physiological consequences of the time-dependent solubility of amyloid proteins. Annu Rev Biochem 66, 385-407.
[21] Uversky, V.N., Li, J., Souillac, P., Millett, I.S., Doniach, S., Jakes, R., Goedert, M. and Fink, A.L. (2002). Biophysical properties of the synucleins and their propensities to fibrillate: inhibition of alpha-synuclein assembly by beta- and gamma-synucleins. J Biol Chem 277, 11970-8.
[22] Pedersen, J.S., Christensen, G. and Otzen, D.E. (2004). Modulation of S6 fibrillation by unfolding rates and gatekeeper residues. J Mol Biol 341, 575-88.
[23] Librizzi, F. and Rischel, C. (2005). The kinetic behavior of insulin fibrillation is determined by heterogeneous nucleation pathways. Protein Sci 14, 3129-34.
[24] Knowles, T.P. et al. (2009). An analytical solution to the kinetics of breakable filament assembly. Science 326, 1533-7.
[25] Uversky, V.N. and Fink, A.L. (2004). Conformational constraints for amyloid fibrillation: the importance of being unfolded. Biochim Biophys Acta 1698, 131-53.
[26] Kelly, J.W. (1998). The alternative conformations of amyloidogenic proteins and their multi-step assembly pathways. Curr Opin Struct Biol 8, 101-6.
[27] Dobson, C.M. (1999). Protein misfolding, evolution and disease. Trends Biochem Sci 24, 329-32.
[28] Gosal, W.S., Morten, I.J., Hewitt, E.W., Smith, D.A., Thomson, N.H. and Radford, S.E. (2005). Competing pathways determine fibril morphology in the self-assembly of beta2-microglobulin into amyloid. J Mol Biol 351, 850-64.

[29] Guijarro, J.I., Sunde, M., Jones, J.A., Campbell, I.D. and Dobson, C.M. (1998). Amyloid fibril formation by an SH3 domain. Proc Natl Acad Sci U S A 95, 4224-8.

[30] Jansen, R., Grudzielanek, S., Dzwolak, W. and Winter, R. (2004). High pressure promotes circularly shaped insulin amyloid. J Mol Biol 338, 203-6.

[31] Canet, D., Sunde, M., Last, A.M., Miranker, A., Spencer, A., Robinson, C.V. and Dobson, C.M. (1999). Mechanistic studies of the folding of human lysozyme and the origin of amyloidogenic behavior in its disease-related variants. Biochemistry 38, 6419-27.

[32] Marcon, G., Plakoutsi, G., Canale, C., Relini, A., Taddei, N., Dobson, C.M., Ramponi, G. and Chiti, F. (2005). Amyloid formation from HypF-N under conditions in which the protein is initially in its native state. J Mol Biol 347, 323-35.

[33] Lindorff-Larsen, K., Best, R.B., Depristo, M.A., Dobson, C.M. and Vendruscolo, M. (2005). Simultaneous determination of protein structure and dynamics. Nature 433, 128-32.

[34] Sadqi, M., Casares, S., Abril, M.A., Lopez-Mayorga, O., Conejero-Lara, F. and Freire, E. (1999). The native state conformational ensemble of the SH3 domain from alpha-spectrin. Biochemistry 38, 8899-906.

[35] Hilser, V.J., Dowdy, D., Oas, T.G. and Freire, E. (1998). The structural distribution of cooperative interactions in proteins: analysis of the native state ensemble. Proc Natl Acad Sci U S A 95, 9903-8.

[36] Dumoulin, M. et al. (2005). Reduced global cooperativity is a common feature underlying the amyloidogenicity of pathogenic lysozyme mutations. J Mol Biol 346, 773-88.

[37] Ramirez-Alvarado, M., Merkel, J.S. and Regan, L. (2000). A systematic exploration of the influence of the protein stability on amyloid fibril formation in vitro. Proc Natl Acad Sci U S A 97, 8979-84.

[38] Kim, Y.S., Wall, J.S., Meyer, J., Murphy, C., Randolph, T.W., Manning, M.C., Solomon, A. and Carpenter, J.F. (2000). Thermodynamic modulation of light chain amyloid fibril formation. Journal of Biological Chemistry 275, 1570-1574.

[39] Chiti, F., Taddei, N., Bucciantini, M., White, P., Ramponi, G. and Dobson, C.M. (2000). Mutational analysis of the propensity for amyloid formation by a globular protein. EMBO J 19, 1441-9.

[40] Espargaro, A., Castillo, V., de Groot, N.S. and Ventura, S. (2008). The in vivo and in vitro aggregation properties of globular proteins correlate with their conformational stability: the SH3 case. J Mol Biol 378, 1116-31.

[41] Hurshman Babbes, A.R., Powers, E.T. and Kelly, J.W. (2008). Quantification of the thermodynamically linked quaternary and tertiary structural stabilities of transthyretin and its disease-associated variants: the relationship between stability and amyloidosis. Biochemistry 47, 6969-84.

[42] Bouchard, M., Zurdo, J., Nettleton, E.J., Dobson, C.M. and Robinson, C.V. (2000). Formation of insulin amyloid fibrils followed by FTIR simultaneously with CD and electron microscopy. Protein Sci 9, 1960-7.

[43] Plakoutsi, G., Taddei, N., Stefani, M. and Chiti, F. (2004). Aggregation of the Acylphosphatase from Sulfolobus solfataricus: the folded and partially unfolded states can both be precursors for amyloid formation. J Biol Chem 279, 14111-9.

[44] Dobson, C.M. (2001). The structural basis of protein folding and its links with human disease. Philos Trans R Soc Lond B Biol Sci 356, 133-45.

[45] Haass, C. and Selkoe, D.J. (2007). Soluble protein oligomers in neurodegeneration: lessons from the Alzheimer's amyloid beta-peptide. Nat Rev Mol Cell Biol 8, 101-12.

[46] Conway, K.A., Harper, J.D. and Lansbury, P.T., Jr. (2000). Fibrils formed in vitro from alpha-synuclein and two mutant forms linked to Parkinson's disease are typical amyloid. Biochemistry 39, 2552-63.

[47] Ionescu-Zanetti, C., Khurana, R., Gillespie, J.R., Petrick, J.S., Trabachino, L.C., Minert, L.J., Carter, S.A. and Fink, A.L. (1999). Monitoring the assembly of Ig light-chain amyloid fibrils by atomic force microscopy. Proc Natl Acad Sci U S A 96, 13175-9.

[48] Quintas, A., Vaz, D.C., Cardoso, I., Saraiva, M.J. and Brito, R.M. (2001). Tetramer dissociation and monomer partial unfolding precedes protofibril formation in amyloidogenic transthyretin variants. J Biol Chem 276, 27207-13.

[49] Malisauskas, M., Zamotin, V., Jass, J., Noppe, W., Dobson, C.M. and Morozova-Roche, L.A. (2003). Amyloid protofilaments from the calcium-binding protein equine lysozyme: formation of ring and linear structures depends on pH and metal ion concentration. J Mol Biol 330, 879-90.

[50] Bader, R., Bamford, R., Zurdo, J., Luisi, B.F. and Dobson, C.M. (2006). Probing the mechanism of amyloidogenesis through a tandem repeat of the PI3-SH3 domain suggests a generic model for protein aggregation and fibril formation. J Mol Biol 356, 189-208.

[51] Serio, T.R., Cashikar, A.G., Kowal, A.S., Sawicki, G.J., Moslehi, J.J., Serpell, L., Arnsdorf, M.F. and Lindquist, S.L. (2000). Nucleated conformational conversion and the replication of conformational information by a prion determinant. Science 289, 1317-21.

[52] Morozova-Roche, L.A. et al. (2004). Fibrillation of carrier protein albebetin and its biologically active constructs. Multiple oligomeric intermediates and pathways. Biochemistry 43, 9610-9.

[53] Bitan, G., Kirkitadze, M.D., Lomakin, A., Vollers, S.S., Benedek, G.B. and Teplow, D.B. (2003). Amyloid beta -protein (Abeta) assembly: Abeta 40 and Abeta 42 oligomerize through distinct pathways. Proc Natl Acad Sci U S A 100, 330-5.

[54] Modler, A.J., Gast, K., Lutsch, G. and Damaschun, G. (2003). Assembly of amyloid protofibrils via critical oligomers--a novel pathway of amyloid formation. J Mol Biol 325, 135-48.

[55] McLean, C.A., Cherny, R.A., Fraser, F.W., Fuller, S.J., Smith, M.J., Beyreuther, K., Bush, A.I. and Masters, C.L. (1999). Soluble pool of Abeta amyloid as a determinant of severity of neurodegeneration in Alzheimer's disease. Ann Neurol 46, 860-6.

[56] Shankar, G.M. et al. (2008). Amyloid-beta protein dimers isolated directly from Alzheimer's brains impair synaptic plasticity and memory. Nat Med 14, 837-42.

[57] Martins, I.C. et al. (2008). Lipids revert inert Abeta amyloid fibrils to neurotoxic protofibrils that affect learning in mice. EMBO J 27, 224-33.

[58] El-Agnaf, O.M. et al. (2003). Alpha-synuclein implicated in Parkinson's disease is present in extracellular biological fluids, including human plasma. FASEB J 17, 1945-7.

[59] Schaffar, G. et al. (2004). Cellular toxicity of polyglutamine expansion proteins: mechanism of transcription factor deactivation. Mol Cell 15, 95-105.

[60] Sousa, M.M., Cardoso, I., Fernandes, R., Guimaraes, A. and Saraiva, M.J. (2001). Deposition of transthyretin in early stages of familial amyloidotic polyneuropathy: evidence for toxicity of nonfibrillar aggregates. Am J Pathol 159, 1993-2000.

[61] Malisauskas, M., Ostman, J., Darinskas, A., Zamotin, V., Liutkevicius, E., Lundgren, E. and Morozova-Roche, L.A. (2005). Does the cytotoxic effect of transient amyloid oligomers from common equine lysozyme in vitro imply innate amyloid toxicity? J Biol Chem 280, 6269-75.

[62] Bucciantini, M., Calloni, G., Chiti, F., Formigli, L., Nosi, D., Dobson, C.M. and Stefani, M. (2004). Prefibrillar amyloid protein aggregates share common features of cytotoxicity. J Biol Chem 279, 31374-82.

[63] Jang, H., Zheng, J., Lal, R. and Nussinov, R. (2008). New structures help the modeling of toxic amyloidbeta ion channels. Trends Biochem Sci 33, 91-100.

[64] Campioni, S. et al. A causative link between the structure of aberrant protein oligomers and their toxicity. Nat Chem Biol 6, 140-7.

[65] Rochet, J.C. (2007). Novel therapeutic strategies for the treatment of protein-misfolding diseases. Expert Rev Mol Med 9, 1-34.

[66] Otzen, D.E., Kristensen, O. and Oliveberg, M. (2000). Designed protein tetramer zipped together with a hydrophobic Alzheimer homology: a structural clue to amyloid assembly. Proc Natl Acad Sci U S A 97, 9907-12.

[67] Chiti, F., Taddei, N., Baroni, F., Capanni, C., Stefani, M., Ramponi, G. and Dobson, C.M. (2002). Kinetic partitioning of protein folding and aggregation. Nat Struct Biol 9, 137-43.

[68] Chiti, F., Calamai, M., Taddei, N., Stefani, M., Ramponi, G. and Dobson, C.M. (2002). Studies of the aggregation of mutant proteins in vitro provide insights into the genetics of amyloid diseases. Proc Natl Acad Sci U S A 99 Suppl 4, 16419-26.

[69] Lopez De La Paz, M., Goldie, K., Zurdo, J., Lacroix, E., Dobson, C.M., Hoenger, A. and Serrano, L. (2002). De novo designed peptide-based amyloid fibrils. Proc Natl Acad Sci U S A 99, 16052-7.

[70] Kim, W. and Hecht, M.H. (2005). Sequence determinants of enhanced amyloidogenicity of Alzheimer A{beta}42 peptide relative to A{beta}40. J Biol Chem 280, 35069-76.

[71] Chiti, F., Stefani, M., Taddei, N., Ramponi, G. and Dobson, C.M. (2003). Rationalization of the effects of mutations on peptide and protein aggregation rates. Nature 424, 805-8.

[72] Fernandez-Escamilla, A.M., Rousseau, F., Schymkowitz, J. and Serrano, L. (2004). Prediction of sequence-dependent and mutational effects on the aggregation of peptides and proteins. Nat Biotechnol 22, 1302-6.

[73] Pawar, A.P., Dubay, K.F., Zurdo, J., Chiti, F., Vendruscolo, M. and Dobson, C.M. (2005). Prediction of "aggregation-prone" and "aggregation-susceptible" regions in proteins associated with neurodegenerative diseases. J Mol Biol 350, 379-92.

[74] Conchillo-Sole, O., de Groot, N.S., Aviles, F.X., Vendrell, J., Daura, X. and Ventura, S. (2007). AGGRESCAN: a server for the prediction and evaluation of "hot spots" of aggregation in polypeptides. BMC Bioinformatics 8, 65.

[75] Sadqi, M., Casares, S., Lopez-Mayorga, O. and Conejero-Lara, F. (2002). The temperature dependence of the hydrogen exchange in the SH3 domain of alpha-spectrin. FEBS Lett 527, 86-90.

[76] Casares, S., Sadqi, M., Lopez-Mayorga, O., Conejero-Lara, F. and van Nuland, N.A. (2004). Detection and characterization of partially unfolded oligomers of the SH3 domain of alpha-spectrin. Biophys J 86, 2403-13.

[77] Viguera, A.R., Martinez, J.C., Filimonov, V.V., Mateo, P.L. and Serrano, L. (1994). Thermodynamic and kinetic analysis of the SH3 domain of spectrin shows a two-state folding transition. Biochemistry 33, 2142-50.

[78] Martinez, J.C., Pisabarro, M.T. and Serrano, L. (1998). Obligatory steps in protein folding and the conformational diversity of the transition state. Nat Struct Biol 5, 721-9.

[79] Kortemme, T., Kelly, M.J., Kay, L.E., Forman-Kay, J. and Serrano, L. (2000). Similarities between the spectrin SH3 domain denatured state and its folding transition state. J Mol Biol 297, 1217-29.

[80] Cobos, E.S., Filimonov, V.V., Vega, M.C., Mateo, P.L., Serrano, L. and Martinez, J.C. (2003). A thermodynamic and kinetic analysis of the folding pathway of an SH3 domain entropically stabilised by a redesigned hydrophobic core. J Mol Biol 328, 221-33.

[81] Periole, X., Vendruscolo, M. and Mark, A.E. (2007). Molecular dynamics simulations from putative transition states of alpha-spectrin SH3 domain. Proteins 69, 536-50.

[82] Lee, S.Y., Fujitsuka, Y., Kim, D.H. and Takada, S. (2004). Roles of physical interactions in determining protein-folding mechanisms: molecular simulation of protein G and alpha spectrin SH3. Proteins 55, 128-38.

[83] Zurdo, J., Guijarro, J.I., Jimenez, J.L., Saibil, H.R. and Dobson, C.M. (2001). Dependence on solution conditions of aggregation and amyloid formation by an SH3 domain. J Mol Biol 311, 325-40.

[84] Polverino de Laureto, P. et al. (2003). Protein aggregation and amyloid fibril formation by an SH3 domain probed by limited proteolysis. J Mol Biol 334, 129-41.

[85] Orte, A., Birkett, N.R., Clarke, R.W., Devlin, G.L., Dobson, C.M. and Klenerman, D. (2008). Direct characterization of amyloidogenic oligomers by single-molecule fluorescence. Proc Natl Acad Sci U S A 105, 14424-9.

[86] Ventura, S., Lacroix, E. and Serrano, L. (2002). Insights into the origin of the tendency of the PI3-SH3 domain to form amyloid fibrils. J Mol Biol 322, 1147-58.

[87] Ventura, S. et al. (2004). Short amino acid stretches can mediate amyloid formation in globular proteins: the Src homology 3 (SH3) case. Proc Natl Acad Sci U S A 101, 7258-63.

[88] Morel, B., Casares, S. and Conejero-Lara, F. (2006). A single mutation induces amyloid aggregation in the alpha-spectrin SH3 domain: analysis of the early stages of fibril formation. J Mol Biol 356, 453-68.

[89] Vega, M.C., Martinez, J.C. and Serrano, L. (2000). Thermodynamic and structural characterization of Asn and Ala residues in the disallowed II' region of the Ramachandran plot. Protein Sci 9, 2322-8.

[90] Casares, S., Sadqi, M., Lopez-Mayorga, O., Martinez, J.C. and Conejero-Lara, F. (2003). Structural cooperativity in the SH3 domain studied by site-directed mutagenesis and amide hydrogen exchange. FEBS Lett 539, 125-30.

[91] Casares, S., Lopez-Mayorga, O., Vega, M.C., Camara-Artigas, A. and Conejero-Lara, F. (2007). Cooperative propagation of local stability changes from low-stability and high-stability regions in a SH3 domain. Proteins 67, 531-47.

2.
ANALYSIS OF THE RELATIONSHIPS BETWEEN NATIVE STATE STABILITY AND AMYLOID FIBRILLATION PROPENSITY

2. ANALYSIS OF THE RELATIONSHIPS BETWEEN NATIVE-STATE STABILITY AND AMYLOID FIBRILLATION PROPENSITY

A number of studies have reported an inverse correlation between the propensity of proteins to aggregate into amyloid-like structures and the thermodynamic stability of the native state [1-3]. Furthermore, recent studies have proposed that stabilization of the native fold results in the modulation of the conformational ensemble favouring structural cooperativity and reducing sampling of partially-folded amyloidogenic conformations [4,5]. This has led in some cases to devise promising therapeutic strategies for amyloid-related diseases based on stabilization of the native-state by specific drugs [6]. There are however examples in which kinetic stability, rather than thermodynamic stability, controls fibrillation [7] and in some cases the formation of amyloid fibrils is preceded by an assembly of quasi-native or native-like structures into aggregates [8,9]. Thus, a detailed understanding of the thermodynamic and kinetic factors determining accumulation of amyloidogenic species in proteins still remains far from complete.

In the case of the Spc-SH3 domain the amyloidogenic mutation N47A strongly accelerates the formation of amyloid fibrils in the presence of moderate salt concentration [10], whereas the fibrillation of the WT domain is much slower under similar conditions. The N47A mutation, located at the tip of the distal loop (a type II' β-turn) within the folding nucleus of the domain [11], has a significant destabilizing effect of the native state [12,13]. We wondered whether the increased tendency of the N47A mutant to form amyloids relative to the WT domain is exclusively due to a thermodynamic destabilization on the native structure or it is related to other specific effects exerted by the mutation.

To answer this question we compared the thermodynamic stability of the native state and the amyloid aggregation propensity between the WT Spc-SH3 domain and several single mutants located in the 3_{10} helix at the A56 position (A56E and A56G, destabilizing; and A56K stabilizing). In addition, we compared the kinetics of fibril formation of the WT protein and the N47A mutant under conditions where the thermodynamic stability of both variants is identical.

2.1. THERMODYNAMIC STABILITY OF SINGLE MUTANTS AND ITS CORRELATION WITH THE PROPENSITY TO FORM AMYLOID AGGREGATES

The propensity to form amyloid fibrils of the WT Spc-SH3 and several single-point mutants was analyzed by monitoring ThT fluorescence under the conditions described previously for the N47A mutant [10], i.e., at 37 ºC in 100 mM glycine buffer pH 3.2, in the presence of 100 mM NaCl and a protein concentration of 8.2 mg/mL (Figure 2.1). The mutations in the variants analyzed are located at two different regions within the putative folding nucleus of the Spc-SH3 domain [14]. Most of the variants except the A56K mutant formed amyloid fibrils when incubated at 37 ºC for long periods, with morphologies similar to those of the N47A mutant, as observed by TEM (not shown). The aggregation rates of the WT domain and the A56G and A56E mutants were quite similar but they all aggregated considerably slower than the N47A mutant and their kinetics presented longer lag phases, suggesting a slower formation of aggregation nuclei.

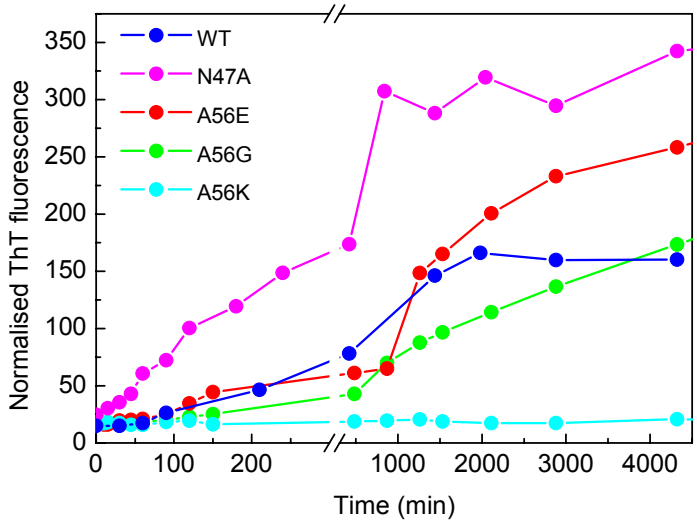

Figure 2.1. *Kinetics of amyloid fibril growth of variants of Spc-SH3 domain measured by ThT fluorescence. Aggregation was followed at 37 ºC in 100 mM glycine buffer pH 3.2, with 100 mM NaCl, at an equal protein concentration of 8.2 mg mL^{-1}.*

The thermodynamic stability of all the variants was analyzed by DSC at pH 3.2 and at protein concentrations sufficiently low (0.8 mg mL^{-1}) to avoid aggregation during the thermal unfolding. The WT and the N47A mutant were also studied by DSC at different pH values between 2.0 and 3.5. Under these conditions, the thermal unfolding of all variants was highly reversible and followed the two-state unfolding model. Identical DSC thermograms were obtained for some of the variants using different scan rates, between 1 and 2 ºC min^{-1} (not shown), indicating that the thermal unfolding occurs under equilibrium during the entire DSC scan.

The thermodynamic parameters (Table 2.1) do not correlate whatsoever with the aggregation propensities of the mutants. For instance, the A56E and A56G mutants, with stabilities similar to the N47A mutant, form amyloid fibrils at slower rate than the latter but at similar rate as the more stable WT domain. In contrast, the A56K

mutant has practically identical stability as the WT domain but it does not form amyloid aggregates within the time period analyzed.

Table 2.1. *Thermodynamic parameters of the equilibrium thermal unfolding of Spc-SH3 variants determined by DSC.*

Variants	pH	Tm (ºC)	ΔH_u (Tm) (kJ mol^{-1})	ΔG_u (37 ºC) (kJ mol^{-1})
WT	3.2	53.9	165	7.28
N47A		50.9	149	5.59
A56E		50.1	146	5.15
A56G		49.3	148	4.94
A56K		53.3	160	6.91
WT	2.0	43.1	125	2.19
	2.5	49.5	144	4.83
	3.0	52.4	159	6.14
	3.2	54.8	168	7.28
	3.5	58.9	182	9.31
N47A	2.0	36.8	106	-0.08
	2.5	40.0	114	1.03
	3.0	49.5	148	4.83
	3.2	51.2	152	5.59
	3.5	55.4	170	7.56

2.2. WT AND N47A Spc-SH3 DOMAINS: PROPENSITY TO FORM AMYLOIDS UNDER CONDITIONS OF IDENTICAL STABILITY

A plot of the unfolding enthalpies, ΔH_u (Tm), versus the unfolding temperatures, Tm, measured for the different variants at pH 3.2 and for the WT and N47A variants at several pH values, shows a single linear dependence (Figure 2.2a). This indicates that the changes in enthalpy of unfolding are only due, within the experimental error, to its dependence with temperature due to the heat capacity change of unfolding, $\Delta C_p = d\Delta H/dT$, common to all domain variants [15]. This is consistent with insignificant changes in the native structure produced by the pH or the mutations.

Using the heat capacity change of unfolding derived from the slope of the plot (3.6 ± 0.1 kJ K^{-1} mol^{-1}) and the thermodynamic data of Table 2.1, we calculated the Gibbs energy change of unfolding at 37 ºC as described elsewhere [16] as a function of pH and determined that the WT Spc-SH3 domain at pH 2.78 and the N47A mutant at pH 3.20 have the same Gibbs energy change of unfolding, i.e., identical thermodynamic stability (Figure 2.2b).

Thus, to exclude the influence of the native-state stability, we compared the kinetics of amyloid formation of the WT Spc-SH3 domain at pH 2.78 and the N47A mutant at pH 3.20 (Figure 2.3).

The N47A mutant still aggregates much faster than the WT domain, which indicates that the amyloidogenic effect of this mutation is not related to a global destabilization of the native state. This difference is neither due to the pH difference affecting the net charge of the protein because the rate of fibrillation of the N47A mutant increases with the reduction of pH (see Chapter 3).

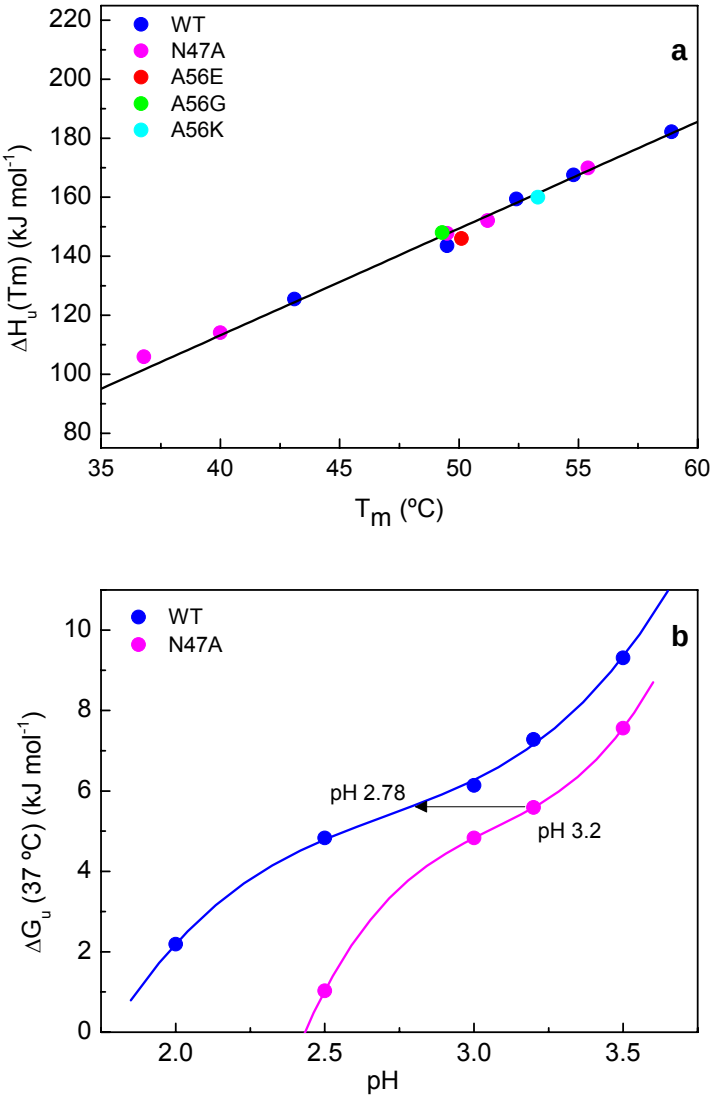

***Figure 2.2**. The effect of the single-point mutations upon the thermodynamic stability of the Spc-SH3 domain. **a)** Plot of the enthalpy change of unfolding, ΔH_u (Tm) , versus the unfolding temperature, Tm, obtained from the two-state analysis of the DSC thermograms measured for all variants at pH 3.2 and low protein concentration where thermal unfolding occurs under equilibrium. Values were also measured for WT and N47A mutant at different pH values (pH 2.0, 2.5, 3.0, 3.2 and 3.5). In all cases the buffer was 100 mM glycine, 100 mM NaCl, and the sample concentration was 0.8 mg mL^{-1}. The solid line represents the linear regression of the experimental data corresponding to a heat capacity change of unfolding of 3.6 ± 0.1 kJ K^{-1} mol^{-1}. **b)** pH dependence of the folding stability of WT and N47A Spc-SH3 at 37 ºC. The solid line was calculated by polynomial regression to facilitate interpolation.*

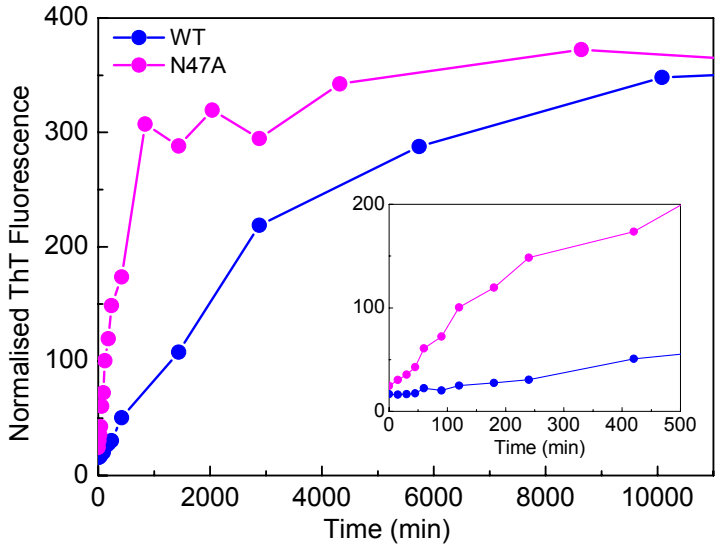

Figure 2.3. *Kinetics of amyloid fibril growth of the WT and N47A variants of Spc-SH3 measured by ThT fluorescence. Aggregation was followed as in Figure 2.1 but at pH 2.78 for WT and pH 3.20 for N47A. The inset shows an expansion of the first 500 min of incubation.*

2.3. AMYLOID FIBRIL MORPHOLOGY OF WT AND N47A SPC-SH3

We compared by TEM the morphology of the aggregates appearing during the aggregation process of WT and N47A Spc-SH3 under conditions of equal thermodynamic stability (Figure 2.4). At early times of incubation (30 min) the N47A forms protofibrillar and amorphous aggregates of protein (Figure 2.4a), which quickly reorganize after only 60 min of incubation into small curly fibrils with diameter of 6-7 Å and lengths between few tenths and several hundreds of nanometres (Figure 2.4b). These fibrils elongate further for longer incubation times. In the case the WT domain, at 30 min of incubation only few small globular and amorphous aggregates were sparsely visible (not shown) but a variety of irregular aggregate clusters form at 60 min of incubation (Figure 2.4d), which become reorganized later to form fibrillar structures as observed at 180 min of incubation (Figure 2.4e). After long incubation times both variants

presented a tangle of amyloid fibrils with similar apparent curly morphology and diameter (Figures 2.4c and 2.4f) and few mature amyloid fibrils already appeared in the N47A samples.

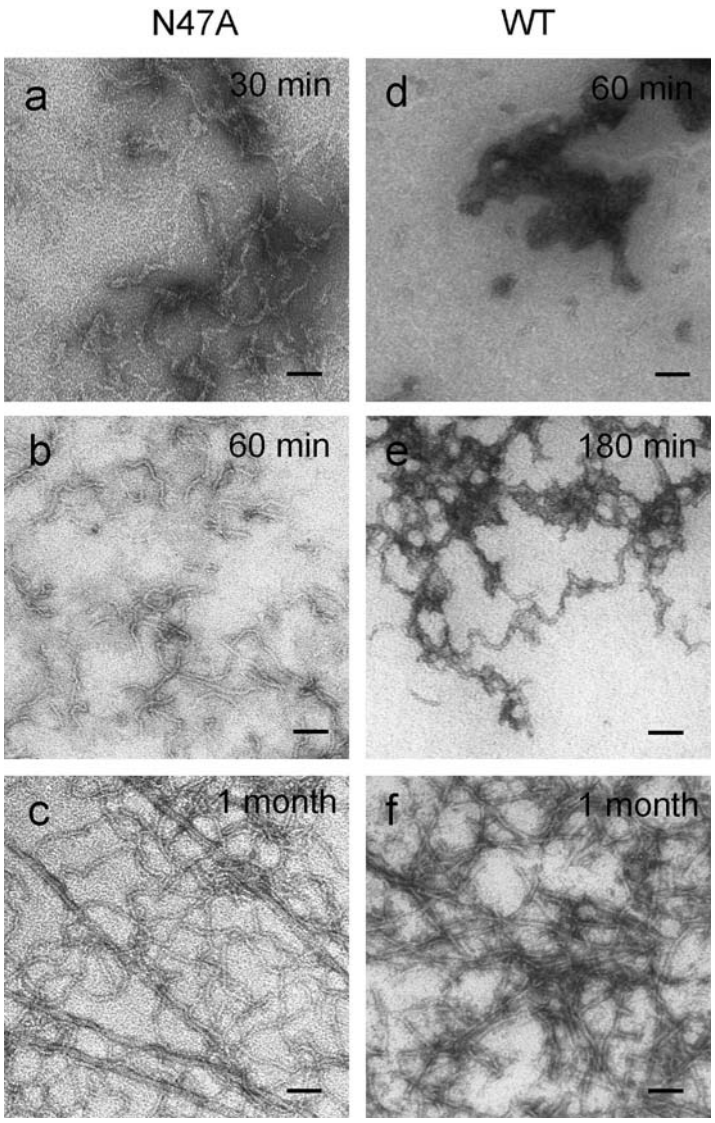

Figure 2.4. *Electron microscopy images of aggregated N47A (panels a, b and c) and WT (panels d, e and f) Spc-SH3 variants after different times of incubation at 37 ºC: (a) 30 min; (b and d) 60 min; (e) 180 min; (c and f) 1 month. Incubation conditions are identical to those of Figure 1b for each variant. The length of the black segments corresponds to 100 nm in all images.*

It appears that for both protein variants amyloid fibril formation involves similar early events, i.e., an initial formation of amorphous prefibrillar aggregates and a subsequent reorganization of these aggregates into fibrils. Both events occur more rapidly in the N47A mutant than in the WT form.

2.4. STUDY OF THE EARLY PARTICLES FORMED DURING AGGREGATION

We followed by DLS the early stages of aggregation of the WT and N47A variants at 37 ºC under conditions of identical thermodynamic stability (Figure 2.5 and 2.6). The growth of the scattering signal for the N47A mutant had a much shorter lag time than for the WT form (Figure 2.6a), indicating a faster formation of aggregation nuclei. From the DLS data we calculated the size distribution of particles in the mixture as a function of the incubation time. The time evolution of the apparent hydrodynamic radius, R_h, for the two smallest peaks in the distributions are shown in Figure 2.6b. At the start of the incubation, the size distributions show for both protein variants only particles with an apparent R_h of ≈ 1.7 nm, consistently with the value reported for native Spc-SH3 [17]. This R_h increases from ≈1.7 nm to ≈3.2 nm in N47A at around 100 minutes of incubation. In our previous work we interpreted this observation as indicative of oligomerisation following a conformational change in the protein [10]. In the case of the WT domain this event is delayed more than 300 minutes of incubation, corresponding approximately to the duration of the lag phase observed by ThT fluorescence.

Simultaneously, within few minutes from the start of the incubation additional species appeared with an apparent R_h starting at ≈ 7-9 nm and increasing progressively with the incubation time. These particles were identified previously as small protofilaments of 6-7 nm in

diameter elongating as the aggregation progresses [10]. The fibril elongation is slightly slower for the WT, as indicated by the slower increase in their average R_h, which reaches ≈40 nm at ≈300 min (≈ 150 min for the N47A mutant). The apparent R_h of the fibrils stops increasing because of the lack of linear persistence of the fibrils. This apparent R_h would correspond to fibril lengths of about 250-500 nm [18]. Finally, at long incubation times larger particles with apparent R_h reaching up to several micrometers became developed for both proteins corresponding to long amyloid fibrils (Figure 2.5).

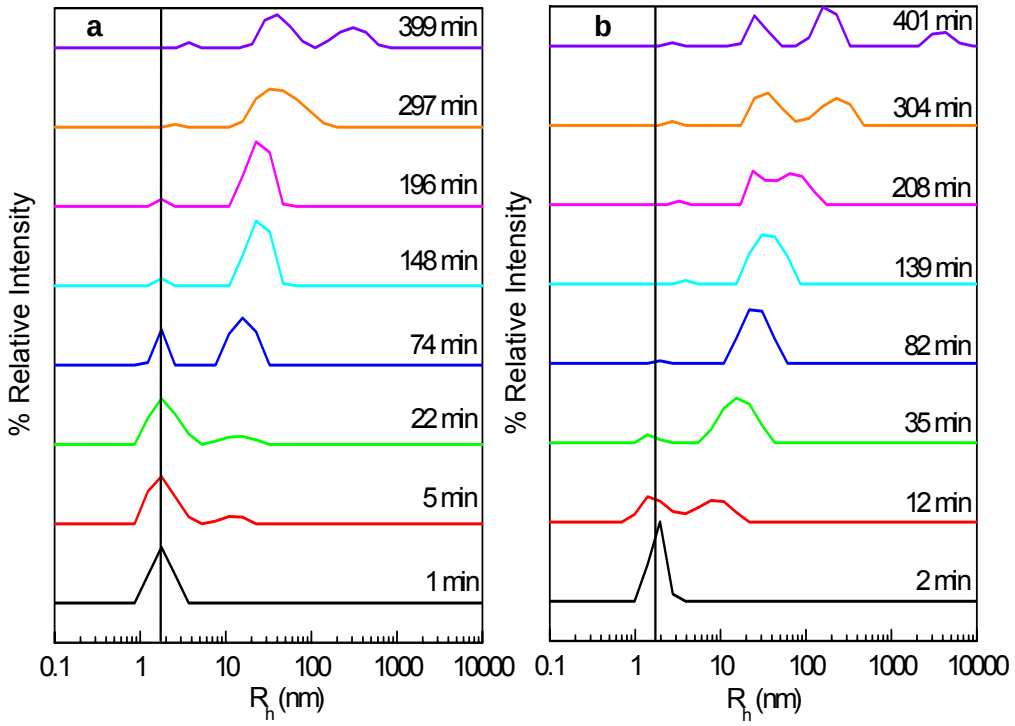

***Figure 2.5**. DLS analysis of the hydrodynamic radius (R_h) of the species present during the time evolution of the amyloid aggregation of WT (a) and N47A (b). Times of incubation indicated alongside each curve. Sample concentration is 8 mg mL^{-1} and the aggregation conditions are 37 ºC, 100 mM Gly, 100 mM NaCl, pH 2.78 for WT and pH 3.2 for N47A.*

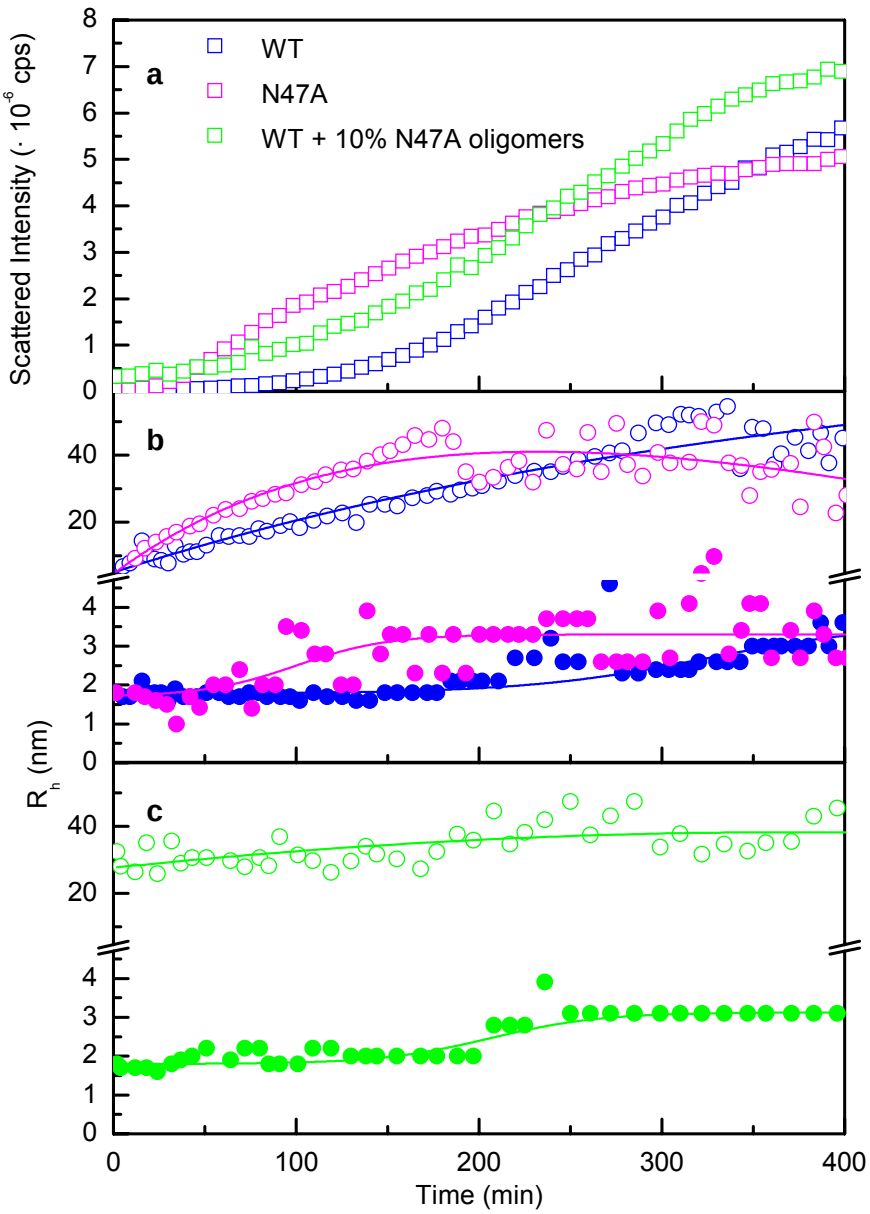

***Figure 2.6**. Aggregation kinetics at 37 ºC of WT and N47A Spc-SH3 followed by DLS. Experimental conditions are identical to those of Figure 1b. **a)** Time dependence of the scattering intensity for WT (blue open squares), N47A (magenta open squares) and WT in the presence of 10 % N47A preincubated for 100 min (green open squares). **b)** Apparent hydrodynamic radius, R_h, determined by DLS for the two smallest species during the course of aggregation at 37 ºC observed in the size distributions for WT (blue), N47A (pink). **c**) Same as in (b) for WT in the presence of 10 % N47A preincubated for 100 min (green). Symbols in b) and c) correspond to the maximum of each peak in the size distributions. The lines are drawn only for the sake of clarity.*

To test the effect of the presence of preformed nuclei of N47A mutant upon the fibril nucleation of the WT protein, we preincubated an 8.2 mg mL^{-1} sample of N47A mutant at 37 ºC for 100 min allowing formation of oligomeric species. Then, we immediately added a 10 % of this sample to an identical fresh sample of WT protein and incubated the mixture at 37 ºC while measuring the DLS signal (Figures 2.6a and 2.6c).

The presence of N47A nuclei reduced significantly the lag phase of aggregation of WT but did not affect importantly the growth rate of fibrils as observed by the similar slope of the increase in the DLS signal. Interestingly, the formation of oligomeric species of WT Spc-SH3 with apparent R_h of $\approx$ 3.2 nm was accelerated significantly, indicating that pre-existing N47A oligomers could catalyze formation of WT oligomers and facilitate nucleation.

2.5. DISCUSSION

Here we have demonstrated that the effect of mutations in Spc-SH3 upon the thermodynamic stability of the native state does not correlate with the changes in the rates of amyloid aggregation. Whilst the destabilizing mutation N47A at the tip of the distal loop of the domain greatly enhances amyloid aggregation, other similarly destabilizing mutations at the 3_{10} helix do not change importantly the aggregation propensity. We have also shown that even under conditions where the WT and the N47A mutant have identical stability their kinetics of aggregation are markedly different. These results demonstrate unequivocally that thermodynamic destabilization of the native state produced by the mutation is not the main factor favoring fibril formation by this small domain.

The fibrillation presents a much shorter lag phase for the N47A mutant than for the WT domain, suggesting a faster formation of

aggregation nuclei. In addition, the rate of fibril elongation observed by DLS is roughly 2-fold higher for the N47A mutant than for the WT, in great contrast with a roughly 10-fold difference in the growth of fibril mass observed by ThT fluorescence. This indicates that the amyloidogenic effect of the N47A mutation occurs mainly at the stage of the conformational events previous to nucleation or at the nucleation step itself. In fact, the analysis by DLS shows that formation of early oligomers occurs earlier for the N47A mutant than for the WT and this event appears to be crucial in the development of fibrillar aggregates, thus conditioning all the subsequent fibrillation process. Indeed, for both variants the duration of the lag phase in fibril formation is very similar to that of formation of oligomers (see Figures 2.1b and 2.3). This suggests that these oligomers may be the competent species of fibril nucleation or may even constitute themselves the aggregation nuclei. The presence of oligomeric species in rapid equilibrium with the monomeric form has also been reported as critical for fibril nucleation as for example in Abeta [19] or yeast prion Sup35p [20] and the importance of their characterization is emphasized by their implication in a number of neurotoxic processes [21].

Of particular interest is the observation that preformed aggregation nuclei of the N47A mutant could accelerate significantly nucleation of the WT protein, whereas the rate of fibril elongation was not affected. This suggests that nuclei pre-existing in the mixture can catalyze formation of additional aggregation nuclei, likely through transient intermolecular interactions.

Our results may appear in conflict with previous studies, which have found a significant inverse correlation between native stability and the propensity to form amyloids. For instance, several mutants of the B1 domain IgG-binding protein G induced amyloid aggregation in inverse correlation with their native stability [3,22]. Similarly, a

significant inverse correlation has been found between native stability of a series of acylphosphatase mutants and their susceptibility to amyloid fibrillation induced by TFE [1]. These studies concluded that key requirement for fibril formation was an increase in the population of intermediate folding conformations that become favoured by destabilizing the native state. On the other hand, a mutational analysis of the fibrillation of the thermophilic protein S6 has revealed no correlation whatsoever between native stability and fibril formation [8]. Instead, the unfolding rates correlated directly with the lag phases of amyloid aggregation suggesting that the nucleation occurs from a quasi-native state. In this case, certain amino acid residues locally grouped in the structure were found to act as “gate keepers” inhibiting the access to specific states that trigger the aggregation cascade. Additional evidence supporting the importance of local effects has been provided by the study of two amyloidogenic variants of human lysozyme [4,23], in which transient unfolding of a specific region of the protein including the beta domain and the C-helix is enhanced by the mutations.

Our previous studies by native-state hydrogen-deuterium exchange have revealed that under native conditions at acid pH the Spc-SH3 domain undergoes a variety of conformational fluctuations ranging from local distortions of flexible regions to extensive unfoldings [24, 25]. Moreover, we reported that single mutations changing the native stability produced redistributions of the conformational ensemble that differed depending of the mutational position [12, 26]. Although both the 47 and 56 positions are located within the putative folding nucleus of the Spc-SH3 domain [14], they differ in conformational flexibility in the native state. A local destabilization at position A56 affects the whole domain’s core lowering the energy of highly unfolded states but leaving unchanged the distribution of the

most accessible states. By contrast, the N47A mutation destabilizing the flexible distal loop produces a redistribution of highly populated states, which may favour particular states prone to aggregation. This view is consistent with our finding that similarly destabilizing mutations such as N47A and A56G produce disparate amyloidogenic effects.

It appears, therefore, that although transient exposure of certain regions of the polypeptide chain is a common and obligatory step in amyloid fibril formation by globular proteins, the precise details of the mechanism by which this event conducts to nucleation and the subsequent aggregation cascade may strongly differ between proteins and determine whether or not a correlation between stability of the native state and amyloid aggregation propensity is found in mutational analyses. In the case of the small Spc-SH3 domain, not every mutation destabilizing the native state are intrinsically amyloidogenic and it seems that the N47A mutation may produce a particular redistribution of the conformational ensemble of the protein leading specifically to a significant reduction in the energy barrier of nucleation of the fibrillation process.

2.6. BIBLIOGRAPHY

[1] Chiti, F., Taddei, N., Bucciantini, M., White, P., Ramponi, G. and Dobson, C.M. (2000). Mutational analysis of the propensity for amyloid formation by a globular protein. EMBO J 19, 1441-9.

[2] Kim, Y.S., Wall, J.S., Meyer, J., Murphy, C., Randolph, T.W., Manning, M.C., Solomon, A. and Carpenter, J.F. (2000). Thermodynamic modulation of light chain amyloid fibril formation. Journal of Biological Chemistry 275, 1570-1574.

[3] Ramirez-Alvarado, M., Merkel, J.S. and Regan, L. (2000). A systematic exploration of the influence of the protein stability on amyloid fibril formation in vitro. Proc Natl Acad Sci U S A 97, 8979-84.

[4] Dumoulin, M. et al. (2005). Reduced global cooperativity is a common feature underlying the amyloidogenicity of pathogenic lysozyme mutations. J Mol Biol 346, 773-88.

[5] Espargaro, A., Castillo, V., de Groot, N.S. and Ventura, S. (2008). The in vivo and in vitro aggregation properties of globular proteins correlate with their conformational stability: the SH3 case. J Mol Biol 378, 1116-31.

[6] Rochet, J.C. (2007). Novel therapeutic strategies for the treatment of protein-misfolding diseases. Expert Rev Mol Med 9, 1-34.

[7] Hurshman Babbes, A.R., Powers, E.T. and Kelly, J.W. (2008). Quantification of the thermodynamically linked quaternary and tertiary structural stabilities of transthyretin and its disease-associated variants: the relationship between stability and amyloidosis. Biochemistry 47, 6969-84.

[8] Pedersen, J.S., Christensen, G. and Otzen, D.E. (2004). Modulation of S6 fibrillation by unfolding rates and gatekeeper residues. J Mol Biol 341, 575-88.

[9] Plakoutsi, G., Taddei, N., Stefani, M. and Chiti, F. (2004). Aggregation of the Acylphosphatase from Sulfolobus solfataricus: the folded and partially unfolded states can both be precursors for amyloid formation. J Biol Chem 279, 14111-9.

[10] Morel, B., Casares, S. and Conejero-Lara, F. (2006). A single mutation induces amyloid aggregation in the alpha-spectrin SH3 domain: analysis of the early stages of fibril formation. J Mol Biol 356, 453-68.

[11] Martinez, J.C. and Serrano, L. (1999). The folding transition state between SH3 domains is conformationally restricted and evolutionarily conserved. Nat Struct Biol 6, 1010-6.

[12] Casares, S., Sadqi, M., Lopez-Mayorga, O., Martinez, J.C. and Conejero-Lara, F. (2003). Structural cooperativity in the SH3 domain studied by site-directed mutagenesis and amide hydrogen exchange. FEBS Lett 539, 125-30.

[13] Vega, M.C., Martinez, J.C. and Serrano, L. (2000). Thermodynamic and structural characterization of Asn and Ala residues in the disallowed II' region of the Ramachandran plot. Protein Sci 9, 2322-8.

[14] Martinez, J.C., Pisabarro, M.T. and Serrano, L. (1998). Obligatory steps in protein folding and the conformational diversity of the transition state. Nat Struct Biol 5, 721-9.

[15] Privalov, P.L. (1979). Stability of proteins: small globular proteins. Adv Protein Chem 33, 167-241.

[16] Viguera, A.R., Martinez, J.C., Filimonov, V.V., Mateo, P.L. and Serrano, L. (1994). Thermodynamic and kinetic analysis of the SH3 domain of spectrin shows a two-state folding transition. Biochemistry 33, 2142-50.

[17] Casares, S., Sadqi, M., Lopez-Mayorga, O., Conejero-Lara, F. and van Nuland, N.A. (2004). Detection and characterization of partially unfolded oligomers of the SH3 domain of alpha-spectrin. Biophys J 86, 2403-13.

[18] Lomakin, A., Teplow, D.B., Kirschner, D.A. and Benedek, G.B. (1997). Kinetic theory of fibrillogenesis of amyloid beta-protein. Proc Natl Acad Sci U S A 94, 7942-7.

[19] Bitan, G., Kirkitadze, M.D., Lomakin, A., Vollers, S.S., Benedek, G.B. and Teplow, D.B. (2003). Amyloid beta -protein (Abeta) assembly: Abeta 40 and Abeta 42 oligomerize through distinct pathways. Proc Natl Acad Sci U S A 100, 330-5.

[20] Serio, T.R., Cashikar, A.G., Kowal, A.S., Sawicki, G.J., Moslehi, J.J., Serpell, L., Arnsdorf, M.F. and Lindquist, S.L. (2000). Nucleated conformational conversion and the replication of conformational information by a prion determinant. Science 289, 1317-21.

[21] Haass, C. and Selkoe, D.J. (2007). Soluble protein oligomers in neurodegeneration: lessons from the Alzheimer's amyloid beta-peptide. Nat Rev Mol Cell Biol 8, 101-12.

[22] Ramirez-Alvarado, M. and Regan, L. (2002). Does the location of a mutation determine the ability to form amyloid fibrils? J Mol Biol 323, 17-22.

[23] Booth, D.R. et al. (1997). Instability, unfolding and aggregation of human lysozyme variants underlying amyloid fibrillogenesis. Nature 385, 787-93.

[24] Sadqi, M., Casares, S., Abril, M.A., Lopez-Mayorga, O., Conejero-Lara, F. and Freire, E. (1999). The native state conformational ensemble of the SH3 domain from alpha-spectrin. Biochemistry 38, 8899-906.

[25] Sadqi, M., Casares, S., Lopez-Mayorga, O. and Conejero-Lara, F. (2002). The temperature dependence of the hydrogen exchange in the SH3 domain of alpha-spectrin. FEBS Lett 527, 86-90.

[26] Casares, S., Lopez-Mayorga, O., Vega, M.C., Camara-Artigas, A. and Conejero-Lara, F. (2007). Cooperative propagation of local stability changes from low-stability and high-stability regions in a SH3 domain. Proteins 67, 531-47.

3.

EFFECT OF ENVIRONMENTAL FACTORS UPON THE FIBRILLATION KINETICS AND FIBRIL MORPHOLOGY

3. EFFECT OF ENVIRONMENTAL FACTORS UPON THE FIBRILLATION KINETICS AND FIBRIL MORPHOLOGY

As summarized in the Introduction, the kinetics of amyloid fibril formation generally follows a nucleation-growth mechanism, in which non-native forms of partially folded protein molecules slowly associate to form aggregation nuclei. These species grow subsequently through the sequential incorporation of other precursor molecules [1,2]. The distinctive feature of the nucleation-growth mechanism is a lag period followed by a rapid extension reaction. The length of the lag phase can be affected by changes in the experimental conditions (pH, salt ions, temperature, etc.) that may accelerate the nucleation process, being no longer the rate limiting step [3]. In addition, certain proteins appear to fibrillate through entirely non-nucleated processes [4,5] or by secondary nucleation mechanisms [6,7].

Despite a considerable similarity in their overall structural and morphological properties, amyloid fibrils can be remarkably diverse. This heterogeneity appears to be related to significant variation in the nano-scale structure of the fibrils, which is influenced by a variety of factors related to the environmental conditions controlling their formation, such as temperature, pH, ionic strength, or mechanical factors such as the presence or absence of agitation [8-14].

In the previous chapter we have demonstrated that the amyloidogenic effect of the N47A mutation is not due to a destabilization of the native state of the protein but to an acceleration of the series of conformational events taking place during the nucleation stage of the fibrillation process. To achieve a better understanding of the nature of these early kinetic events and how these variables influence the morphology of the fibrils, we have extended the study of the fibril formation by the N47A mutant of Spc-SH3 under a broad range of experimental conditions. We have systematically explored the effect of salt concentration, temperature

and pH using a variety of biophysical techniques that report about different stages and aspects of the aggregation process.

Most of the experiments related to salt and temperature studies were performed by Dr. Bertrand Morel, who has collaborated intensely in the development of this work.

3.1. EFFECT OF SALT CONCENTRATION ON THE MORPHOLOGY OF THE AMYLOID FIBRILS OF N47A Spc-SH3

Our research group has previously shown that the N47A mutant of the Spc-SH3 domain forms readily amyloid fibrils at mild acid pH (100 mM glycine buffer, pH 3.2) and that an increase in NaCl concentration enhances the fibrillation considerably [15]. Here we examined in detail the morphologies of the fibrillar aggregates produced under different NaCl concentrations by transmission electron microscopy (TEM) (Figure 3.1).

Incubating during three days a high protein concentration sample (20 mg mL^{-1}) at 37 ºC and at pH 3.2 in the absence of NaCl produced fibrils with a curly morphology (see figure 1c in reference [15]). The fibrils had an approximate diameter of 6-7 nm as estimated from the TEM pictures and have a curly and tangled appearance similar to those described as protofilaments or protofibrils [16]. A complete study of TEM images (not shown) with the time dependence of fibril assembly was performed. Strikingly, after 2 months of incubation at 37 ºC the curly fibrils had disappeared and only straight and twisted amyloid fibrils were visible in the samples (Figure 3.1a). These fibrils are formed by twisted protofilaments with an approximate diameter of 6.9 ± 0.8 nm, similar to that of the protofibrils assembled at long incubation times.

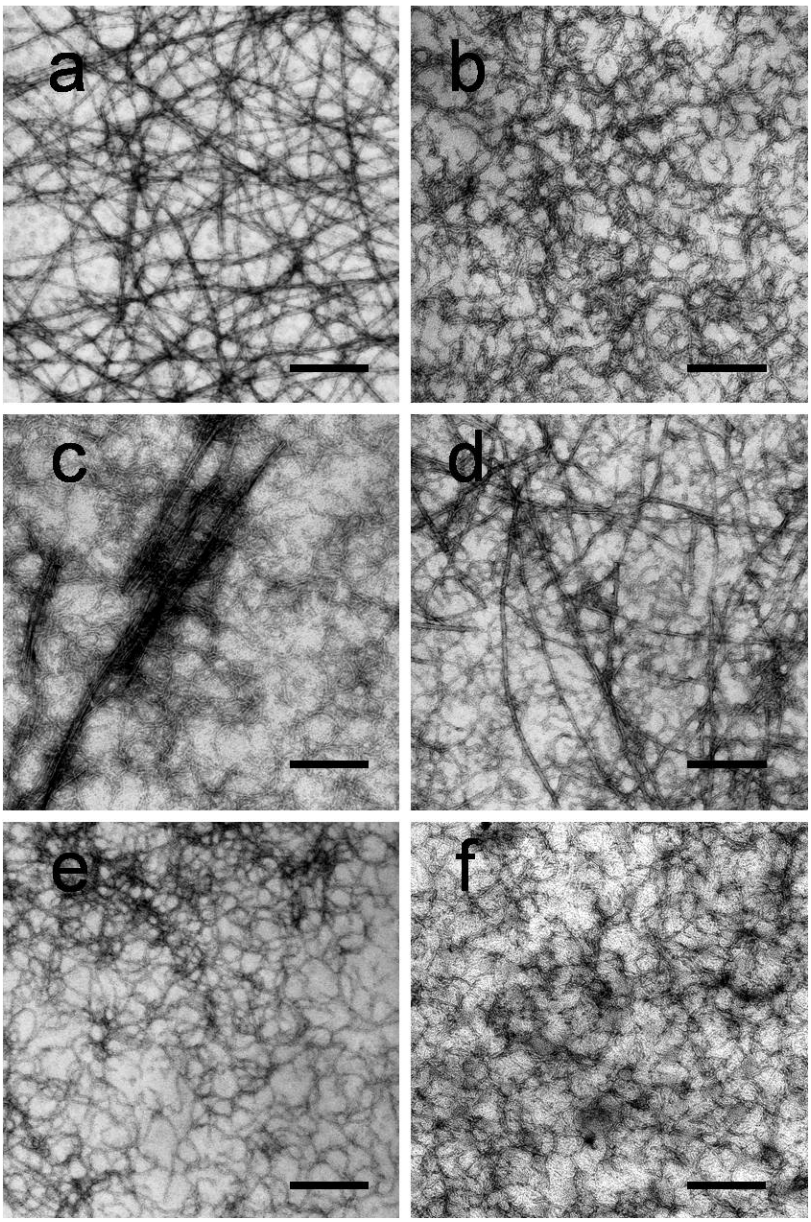

Figure 3.1. *Effect of environmental conditions upon the morphology of amyloid fibrils of N47A Spc-SH3. Transmission electron microscopy images were taken with samples incubated in 100 mM glycine buffer pH 3.2 at different NaCl concentration, temperature, sample concentration and incubation time: (a) 0 M NaCl, 37 ºC, 20 mg mL^{-1}, 2 months; (b) 0.05 M NaCl, 37 ºC, 8 mg mL^{-1}, 10 days; (c) (b) 0.1 M NaCl, 37 ºC, 8 mg mL^{-1}, 10 days; (d) 0.1 M NaCl, 37 ºC, 8 mg mL^{-1}, 1 month; (e) 0.2 M NaCl, 37 ºC, 8 mg mL^{-1}, 10 days; (f) 0.1 M NaCl, 70 ºC, 8 mg mL^{-1}, 6 hours. The length of the black segment corresponds to 100 nm for each panel.*

The amyloid fibrils have considerable linear persistence and several morphological subtypes characterized by different twists of a number of coiled protofilaments, as usually observed for many other amyloids [17].

At intermediate salt concentrations (0.05 M and 0.1 M NaCl) the aggregates formed at early times of incubation at 37 ºC consisted of only curved protofibrils reaching lengths of up to several μm [15]. The diameter of the filaments is about 6-7 nm (Table 3.1). Interestingly, after about 10 days of incubation thin curved filaments and straight twisted amyloid fibrils coexisted in the samples (Figures 3.1b and 3.1c), with the latter appearing earlier in the mixture at the lower NaCl concentration. At long incubation times of more than 1 month the twisted fibrils prevailed in the samples, indicating that the curly filaments convert into straight and twisted fibrils (figure 3.1d). We cannot fully discern from these results whether the curved filaments can assemble directly to form the twisted amyloid fibrils or they are off-pathway to their formation, as it has been described elsewhere [14].

Incubation of an 8 mg mL^{-1} protein sample at pH 3.2 and high salt concentration (0.2 M NaCl) resulted in the rapid formation (within few minutes) of a tangle of curved protofibrils (Figure 3.1e). The average diameter of these curly filaments estimated from the TEM pictures was 4.5 ± 0.6 nm, significantly lower than that of the protofibrils formed at lower salt concentrations, which suggest a different internal structure. Importantly, these protofibrils persisted for more than one month of incubation under these conditions without any apparent change in morphology or diameter. A similar fibrillar material could also be obtained by incubating at 70 ºC during 6h an 8 mg mL^{-1} protein solution at pH 3.2 in the presence of 0.1 M NaCl (Figure 3.1f).

Table 3.1. *Apparent diameter of protofibrils and protofilaments determined using TEM images. Data correspond to mean values of 15 measurements.*

Incubation time at 37ºC	[NaCl] (M)	Apparent diameter (nm)
10 days	0.05	6.9 ± 0.3
	0.1	6.2 ± 0.8
	0.2	4.5 ± 0.6
1 month	0.05	6.4 ± 0.8
	0.1	6.4 ± 0.8
	0.2	4.9 ± 0.8

These results indicate that the N47A Spc-SH3 domain can form amyloid fibrils of different morphologies depending on the environmental conditions and the time of incubation. Low to moderate salt concentrations favour the initial formation of protofibrils with a diameter of about 6-7 nm that convert into long and twisted mature fibrils after prolonged incubation. High salt concentration promotes the rapid assembly of protofibrils with significantly lower diameters, which remain stable despite incubation for several months at 37 ºC.

To elucidate if the different ability between each type of protofibril to convert into the mature amyloid fibrils may be caused by the conditions of incubation or by some difference in their intrinsic structural properties, samples of each type of curly protofibrils were prepared by three-day incubation at 37 ºC of 8.5 mg mL^{-1} protein samples at pH 3.2 in buffers containing either 0.05 M NaCl or 0.2 M NaCl. The fibrillar materials were centrifuged and the fibrils were resuspended in the opposite buffer, adjusting the final volume to keep the original protein concentration. The samples were then incubated during 2 months and analyzed by TEM at several time intervals (not shown). Interestingly, only curly fibrils were visible in both samples during 1 month of incubation and only after 2 months a few twisted amyloid fibrils appeared very sparsely in both samples. This indicates that the morphological conversion is much slower than that observed

for the protofibrils formed and incubated under moderate NaCl concentration, suggesting that neither type of protofibrils can in isolation evolve efficiently into amyloid fibrils irrespective of the buffer condition. It is possible that soluble species present in the supernatant at low NaCl concentration and removed by centrifugation are essential in the morphological conversion.

These results suggest that the fibril structure appears to be determined and directed by the environmental conditions occurring during the early events of fibrillation.

3.2. EFFECT OF SALT CONCENTRATION IN THE KINETICS OF AMYLOID FORMATION

In order to relate the morphological effects observed with possible changes in the early fibrillation kinetics, we carried out an extensive kinetic analysis of the fibril formation by the Spc-SH3 N47A mutant as a function of NaCl concentration. Typically, protein samples at a concentration of 8.3 mg mL^{-1} were incubated at 37 ºC and the aggregation process was followed by several biophysical techniques. NaCl concentration was explored from 0 to 0.3 M. Figure 3.2a shows the CD spectra of the protein after 180 min of incubation at 37 ºC at several salt concentrations. At this high protein concentration the CD signal could be measured only from 210 nm, due to saturation of the instrument signal at shorter wavelengths. At time zero the spectrum of N47A was identical to that of the native wild-type (WT) Spc-SH3 domain independently of the NaCl concentration (not shown). In Figure 3.2b it is shown how as aggregation progressed during incubation at 37 ºC under various NaCl concentrations, the far-UV CD spectrum changed considerably and developed a negative band at ≈ 215 nm, typical of β-sheets in amyloid fibrils. This band became gradually more intense upon prolonged incubation of the protein.

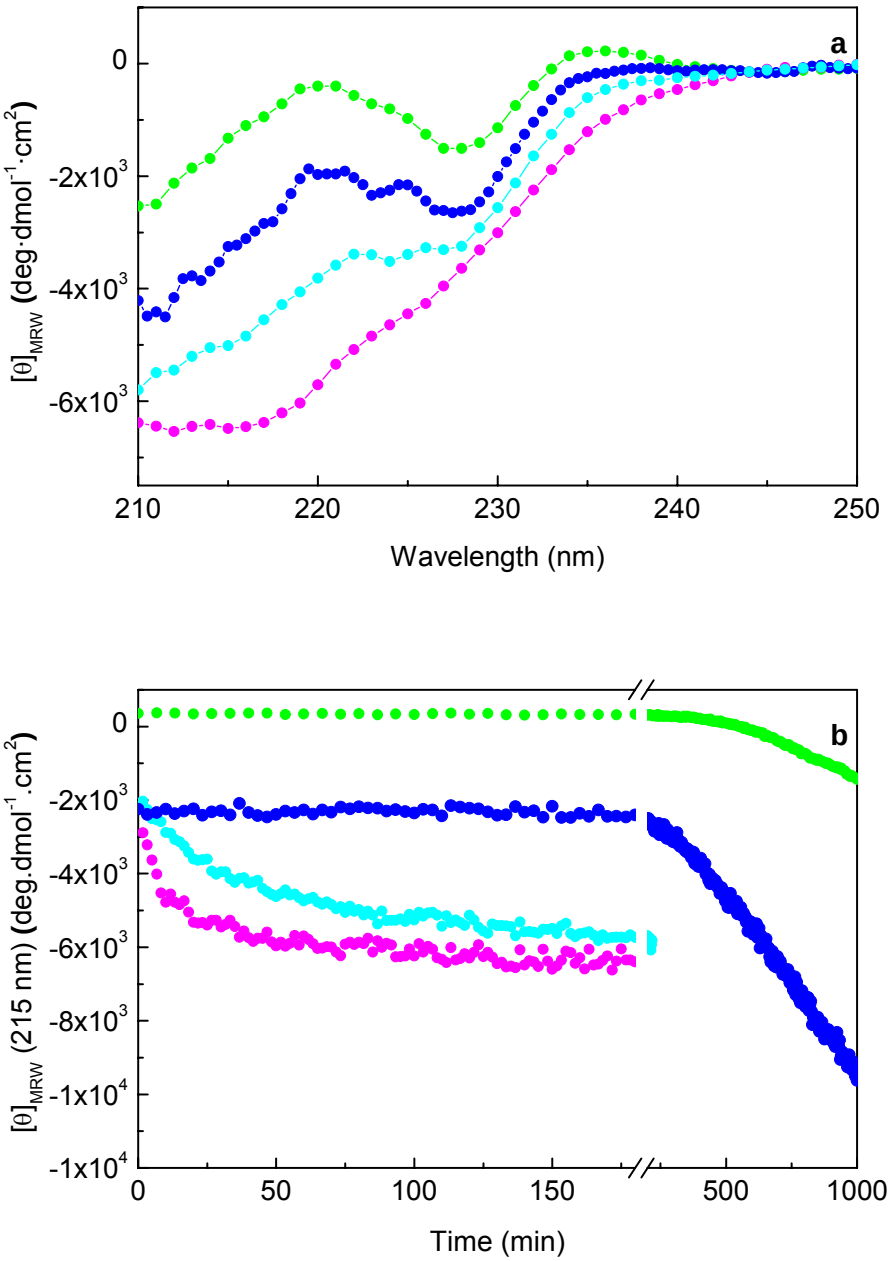

Figure 3.2. *Time dependence of aggregation of N47A Spc-SH3 at 37 ºC in 100 mM Glycine pH 3.2 at different concentrations of NaCl. (a) Far-UV CD spectra after incubation for 180 minutes in a 0.1 mm pathlength CD cuvette. (b) Time dependence of the far-UV CD signal. Colours correspond to 0 mM NaCl, green, 0.05 M NaCl, blue, 0.1 M NaCl, cyan, and 0.2 M NaCl, magenta. The green trace was obtained at 235 nm and 20 mg mL^{-1}, whereas the other experiments were recorded 215 nm and 8.3 mg mL^{-1}.*

The rise in NaCl concentration increased dramatically the speed of the process. At 0 M NaCl and 8 mg mL^{-1} fibrillation did not take place after months of incubation but it occurred within 3 days if protein concentration was elevated up to about 20 mg mL^{-1} (not shown). At a concentration of 0.05 M NaCl, there was a considerable lag phase and the far-UV CD spectrum changed very slowly during the first 200 min of incubation and then a negative ellipticity started to evolve (Figure 3.2b). After 24 hours of incubation, a pronounced negative band centred at 215 nm became developed (not shown). The presence of a lag phase is consistent with a nucleation-growth mechanism for the fibrillation process [18].

At salt concentrations of 0.1 M and 0.2 M, the lag phase in the CD kinetics disappeared and the curves displayed two distinct, well-defined phases. The kinetics could be fitted to a single exponential decay superimposed to a slow and approximately linear decay.

The fast phase involves considerable changes in secondary structure and takes place in about 100 min at 0.1 M NaCl and about 20 min at 0.2 M NaCl. The time constant (38 ± 9 min at 0.1 M NaCl) and the amplitude of the fast phase is practically independent of the protein concentration (figure 3.3), which suggests a first-order rate-limiting step for this conformational conversion. On the other hand, the rate of formation of additional β-sheet structures during the subsequent slower decay is strongly dependent on the concentration of protein, consistent with a polymerization process. At 0.3 M NaCl the protein underwent very fast amorphous aggregation as evidenced by electron microscopy (not shown).

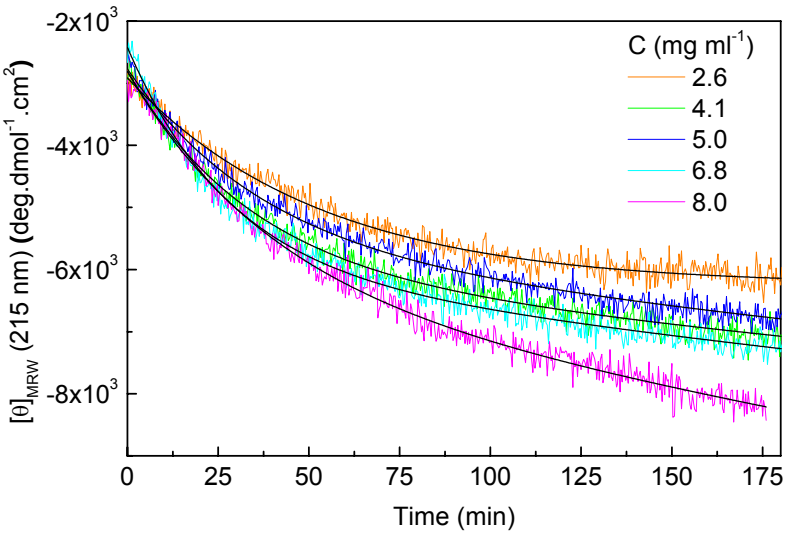

Figure 3.3. *Time dependence of aggregation of the far-UV CD signal at 215 nm of N47A Spc-SH3 at different concentrations at 37 ºC in 100 mM Glycine pH 3.2 at 100 mM NaCl.*

The kinetics of aggregation was also followed by thioflavine T (ThT) fluorescence and dynamic light scattering (DLS) (see figures 3.4a and 3.4b). In the presence of 0.05 M NaCl the development of ThT fluorescence and scattering intensity showed lag phases of about 100-200 min consistent with the changes observed by CD. The scattering intensity is proportional to the second power of the particle mass and, therefore, the contribution from the larger particles dominates the scattering signal [19]. This indicates that during the lag phase the protein does not form large aggregate particles such as oligomers or aggregation nuclei.

At 0.1 mM and 0.2 mM NaCl concentrations the lag times in the DLS and ThT fluorescence kinetics practically disappeared, indicating a much higher rate of nucleation of fibrils and, as a consequence, the mass of fibrils grew much faster. Under these conditions the kinetics followed by CD, ThT and DLS are highly similar indicating that the

process of conformational conversion is almost concomitant with the fibril nucleation and growth.

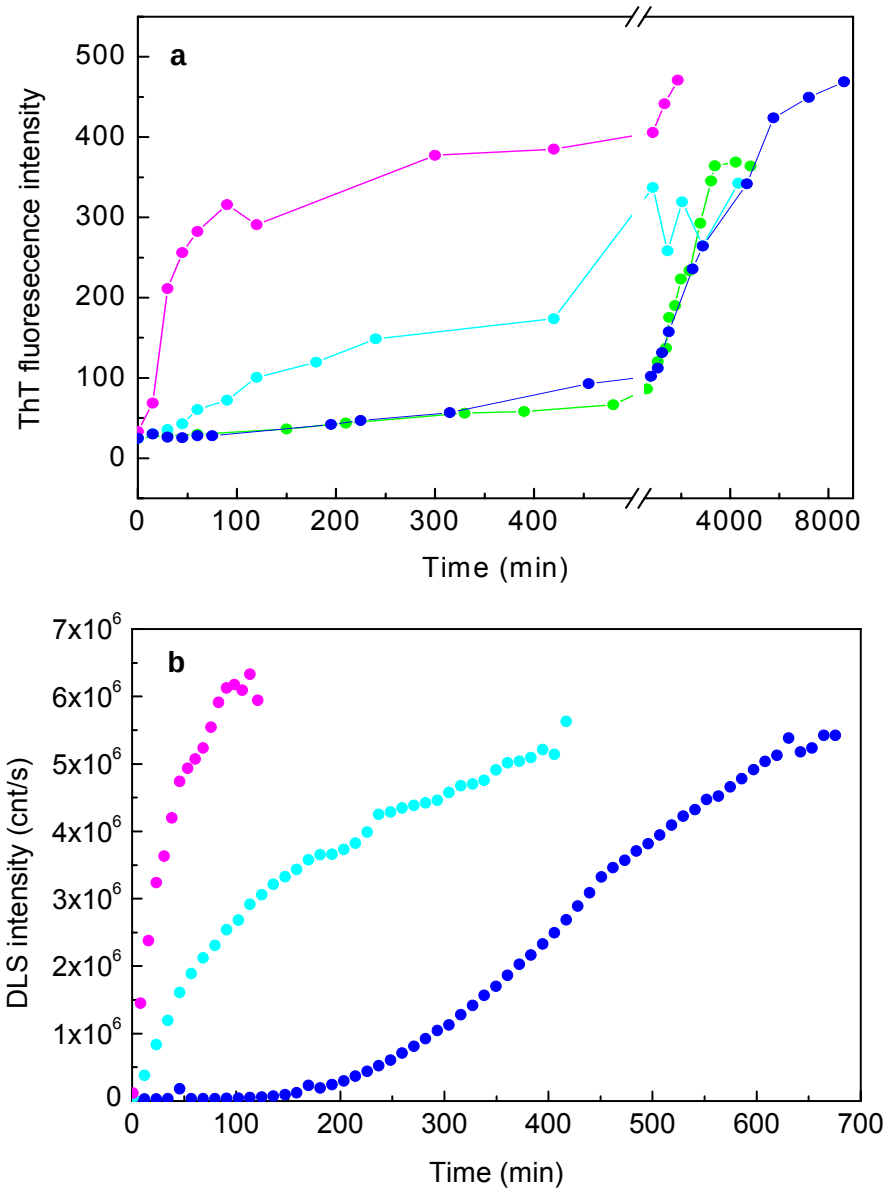

Figure 3.4. *Time dependence of aggregation of N47A Spc-SH3 (8.3 mg mL^{-1}) at 37 ºC in 100 mM Glycine pH 3.2 at different concentrations of NaCl. (a) Time dependence of thioflavine T fluorescence. (b) Time dependence of the scattering intensity. Colours correspond to 0 mM NaCl, green, 0.05 M NaCl, blue, 0.1 M NaCl, cyan, and 0.2 M NaCl, magenta.*

Consistent with these conclusions are the results of an experiment in which we followed the fibrillation process at 37 ºC by recording a series of two-dimensional ^{15}N-^{1}H-HSQC NMR spectra with an 8 mg mL^{-1} ^{15}N-labelled sample at pH 3.2 in the presence of 0.1 M NaCl. All the spectra showed only native signals that decreased in intensity with the time of incubation as aggregation progressed (Figure 3.5).

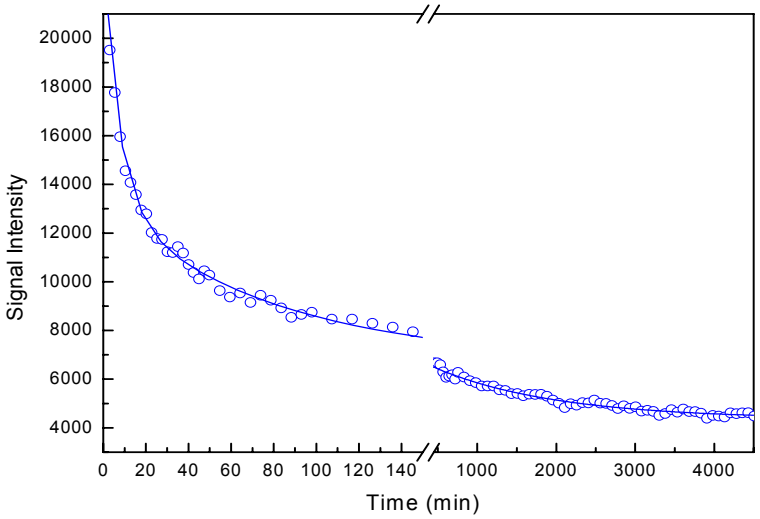

Figure 3.5. *Time dependence of aggregation of the native NMR signal intensity for residue Leucine 10 in a sample at 8 mg mL^{-1}of N47A Spc-SH3 at 37 ºC in 100 mM Glycine pH 3.2 at 100 mM NaCl.*

The kinetic traces obtained by plotting the intensity of each signal against the incubation time are all identical, which indicates that the native protein is converted cooperatively into species with large molecular size, not detectable by NMR. These kinetic curves show two phases, a fast intensity decrease taking place within about 100-150 min and followed by a slower intensity decrease, in good consistency with the CD kinetics. The fast phase could not be fitted, however, to a single exponential decay, suggesting complex mechanism for this

process, although this might be due to the effect of some delay in the temperature equilibration of the sample after its introduction in the NMR probe. The amplitude of the fast phase accounts for more than 50 % of the initial intensity indicating that the conformational conversion and oligomerisation affects to a large fraction of the protein. The presence of the slow phase is consistent with the dissapearance of additional native molecules during fibril elongation.

A detailed analysis of the DLS data allowed us to follow the distribution of particle size during the early times of the aggregation process at 37 ºC (Figure 3.6). Before incubation, only particles with the native hydrodynamic radius (R_h) of ≈1.6 nm were detected, independently of the salt concentration used. As aggregation progressed, larger particle radii appeared in the distributions. The series of events observed is however markedly different depending of the NaCl concentration. Figure 3.6a shows the evolution with the time of incubation of the average R_h for the two smallest peaks in the distributions. At 0.05 M NaCl, the majority of the protein remained in particles with native R_h for about 300 min and then there was a slight expansion of the apparent R_h up to about 2.5 nm, which took place between 200 and 400 min. Well before this event, after just about 100 min a peak with average R_h of about 10 nm appeared in the distributions and grows progressively reaching up to 40 to 50 nm. These particle sizes had been assigned previously to small elongating protofibrils as shown by electron microscopy [15]. This is supported by the observation by TEM of few small fibrillar structures appearing at early incubation times (not shown). Further incubation produced particles of up to several μm in the size distributions and simultaneously the apparent R_h of the protofibrils decayed.

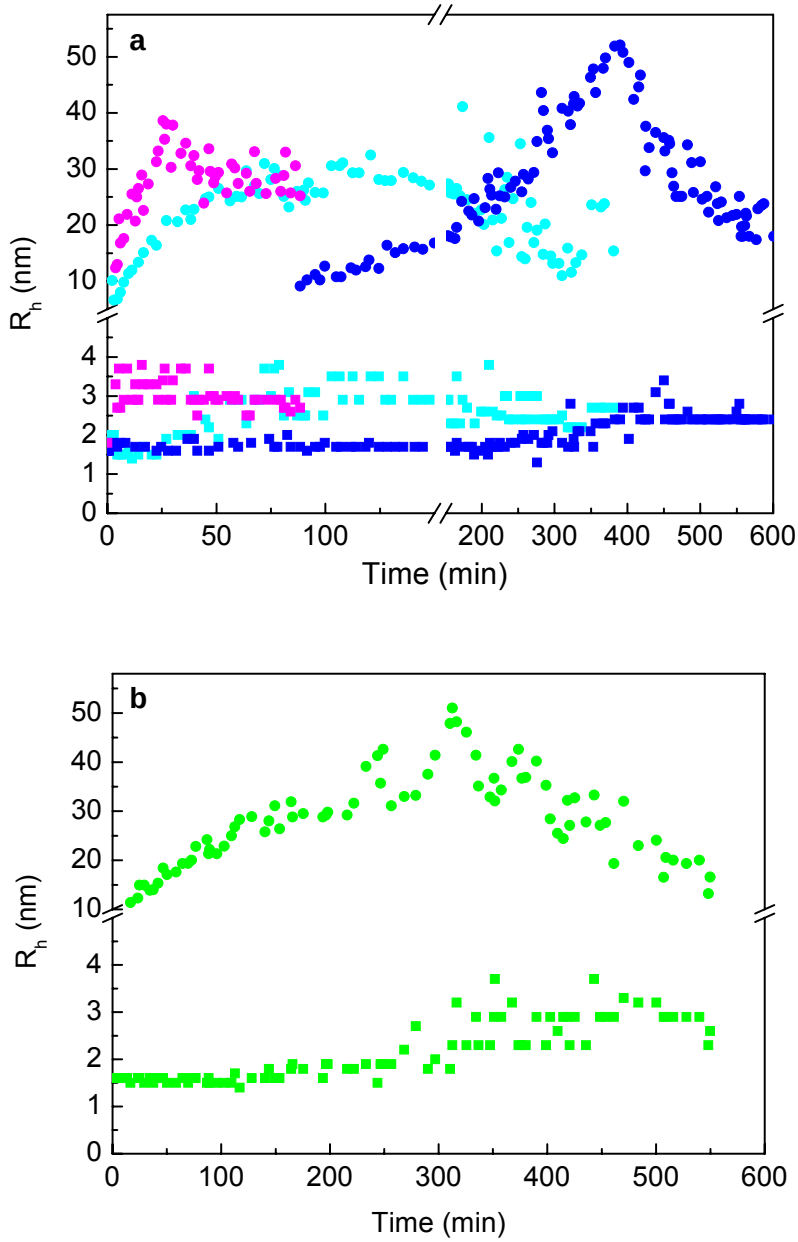

Figure 3.6. *Time evolution of particle sizes determined by dynamic light scattering during fibrillation of N47A Spc-SH3. The average hydrodynamic radii of the two smallest peaks in the distributions have been plotted as a function of the time of incubation. (a) Effect of NaCl concentration at 37 ºC: 0.05 M (blue), 0.1 M (cyan) and 0.2 M (magenta). (b) A 20 mg mL^{-1} sample incubated at 37 ºC without NaCl (green).*

At 0 M NaCl and a 20 mg mL^{-1} protein concentration, the expansion of the monomeric particles to an R_h of about 2.9 nm was also delayed more than 250 min. The apparent R_h reached in this event is significantly higher than that expected for a fully unfolded monomer (2.3 nm) and suggests the formation of small oligomers under these conditions. The appearance in the size distributions of protofibrils with R_h starting in about 10 nm occurred just after 15 min of incubation (Fig 3.6b).

The time evolution of the size distributions at 0.2 M NaCl is markedly different: the expansion in R_h of the native particles occurred within the dead time of the experiment, reaching an R_h of ≈3 nm. Larger particles corresponding to protofibrils also appeared immediately at the very beginning of the incubation and grew much faster than at low salt concentration. The situation observed at 0.1 M NaCl is intermediate between those of 0.05 M and 0.2 M, with an initial expansion in the R_h of the monomeric protein ending at about 100 min, in good agreetment with the end of the fast phase observed by CD [15] and an intermediate rate of growth of the protofibrils.

These results show that the fibrillation of the N47A Spc-SH3 domain takes place in two stages. In an early stage, a fraction of the native protein undergoes extensive conformational changes involving β-sheet formation accompanied by the formation of small oligomers. In a second stage, nucleated protofibrils elongate to incorporate additional native monomers. The increase in NaCl concentration strongly accelerates the first stage, which results in a dramatic enhancement of the overall fibrillation process.

3.3 THE EFFECT OF TEMPERATURE UPON THE RATE OF OLIGOMER FORMATION

The kinetic of aggregation was also analyzed at different temperatures of incubation by following the CD signal at 215 nm.

Samples of 8 mg ml^{-1} of protein concentration were incubated in the presence of 0.05 M, 0.1 M and 0.2 M NaCl. The interval of temperatures of incubation was chosen according to the velocity of the process under each salt concentration. The kinetic curves could be well fitted using a single exponential decay for the first phase plus a linear decay for the slow phase.

The apparent first-order rate constant of the fast phase increased strongly with temperature indicating a high activation energy for the process. In contrast, the rate of the second phase did not change importantly with temperature, suggesting a down-hill polymerization for the slow phase.

The Arrhenius plots obtained for the first phase at different salt concentrations are shown in Figure 3.7.

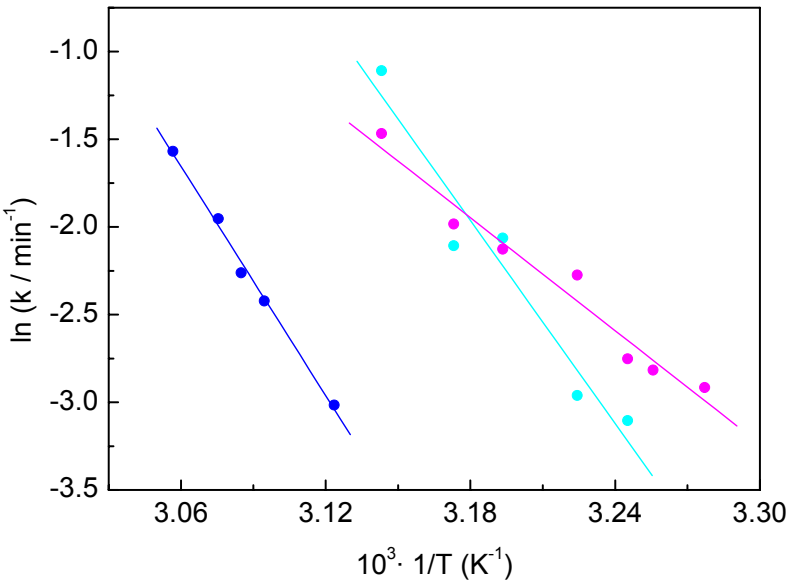

Figure 3.7. *Arrhenius plot for the first phase of the conformational change of N47A Spc-SH3 at different NaCl concentration: 0.05 M, blue, 0.1 M, cyan and 0.2 M, magenta.*

The activation enthalpies are 178 ± 8 kJ mol^{-1} at 0.05 mM NaCl and 157 ± 23 kJ mol^{-1} at 0.1 mM NaCl, which are significantly higher than the total enthalpy change of unfolding of the native protein at similar temperatures (see Table 3.2, below). At 0.2 mM NaCl the activation enthalpy diminishes to 86 ± 8 kJ mol^{-1}, being in this case lower than the unfolding enthalpy. These results indicate that an increase in NaCl concentration decreases considerably the balance of interactions involved in the energy barrier.

The distributions of particle sizes followed by DLS during aggregation were also strongly affected by the temperature increase, as shown in Figure 3.8.

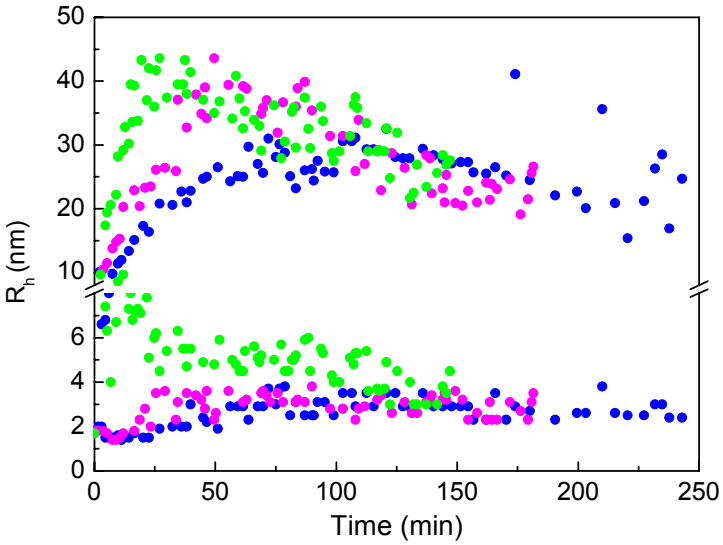

Figure 3.8. *Effect of temperature in the time evolution of particle sizes determined by dynamic light scattering during fibrillation of N47A Spc-SH3 at 0.1 M NaCl. The average hydrodynamic radii of the two smallest peaks in the distributions have been plotted as a function of the time of incubation. 37 ºC (blue), 42 ºC (magenta); 55 ºC (green).*

It is evident that a temperature rise accelerates the shift in the apparent R_h of the early oligomers, in good consistency with the increase in the rate of the conformational change observed by CD. Importantly, the maximum R_h value attained after this phase augmented significantly with temperature. For instance, in the presence of 0.1 M NaCl the apparent R_h grew up to 2.5 nm at 37 ºC, 3.0 nm at 42 ºC, and up to 7-8 nm at the very beginning of the incubation at 55 ºC. These observations suggest that a temperature increase favours the accumulation of larger oligomeric species. Interestingly, the R_h value decreased slightly as aggregation progressed, suggesting that depletion of soluble protein to form fibrillar aggregates may shift back the oligomerization equilibrium toward smaller species.

3.4 THERMALLY-INDUCED FIBRILLATION AND FIBRIL MELTING

In previous work [15] it was reported the potential of differential scanning calorimetry (DSC) to analyze thermally-induced amyloid formation. Here we analyzed the thermally-induced aggregation of N47A Spc-SH3 within the DSC instrument at pH 3.2 in 0.1 M glycine buffer at several NaCl concentrations. The effects of protein concentration were also investigated (Figures 3.9a-c). Under the conditions favouring fibrillation, the DSC thermograms presented a complicated shape containing essentially three peaks. The first peak may be associated with a competition between the equilibrium thermal unfolding and the time-dependent fibrillation. It is evident from the figures that the latter process is strongly favoured by the increase in protein or NaCl concentration, which is reflected in significant shift of the maximum of the peak, Tm, to lower temperature and in considerable decrease of its area. Assuming that at high protein concentration the dominant process is the fibrillation, the area under

the first peak is a rough estimate of the overall enthalpy change of this process. These amounts are in the range of 50-60 kJ mol^{-1} at 0.05 M and 0.1 M NaCl and about 45 kJ mol^{-1} at 0.2 M NaCl.

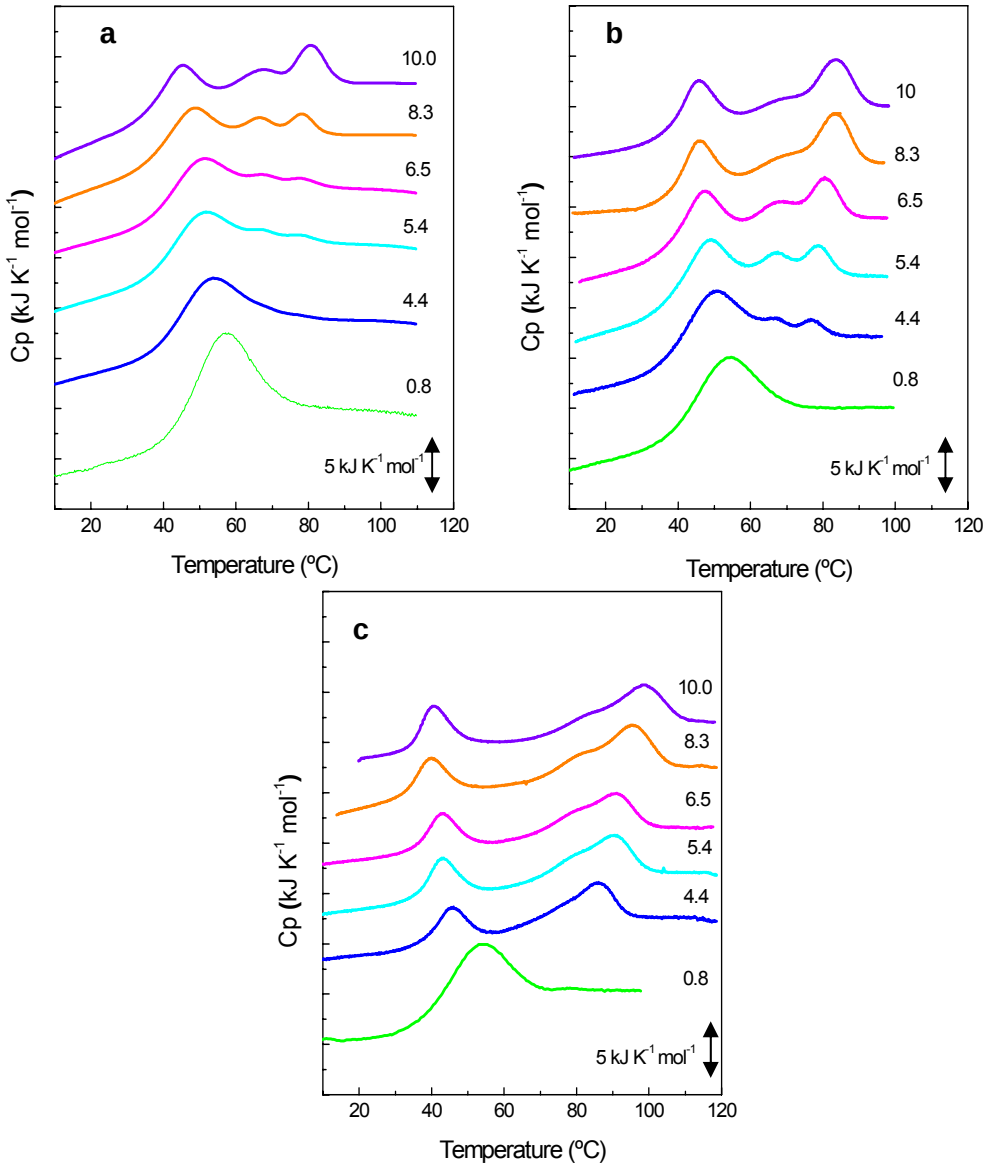

Figure 3.9. *DSC analysis of the N47A Spc-SH3 samples under fibrillation conditions. Effect of sample concentration on the DSC thermograms measured with native protein in the presence of 0.05 M NaCl (a), 0.1 M NaCl (b) and 0.2 M NaCl (c). Numbers alongside each curve indicate sample concentration in mg mL^{-1}. Scan rate was 2 ºC min^{-1} in all experiments. The curves have been displaced artificially along the ordinate axis for clarity.*

This indicates that net balance of interactions accompanying these transitions is much lower than that corresponding to the global unfolding of the protein [15] and indicates that the thermally-induced fibrils are formed by partially-unfolded protein molecules, consistent with the CD data shown above. It would also appear that an increase in salt concentration from 0.05 M to 0.2 M lowers slightly the net balance of interactions accompanying fibrillation.

A second smaller transition appeared in the DSC thermograms around 65-70ºC at 0.05 M and 0.1 M NaCl and as a shoulder near 80 ºC at 0.2 M NaCl. This transition was attributed in previous work to intermediate oligomers that did not have time to evolve into amyloid fibrils during the DSC scan [15]. It is clear that the stability of these species is higher at 0.2 M NaCl, in good consistency with the effect of NaCl enhancing oligomerisation as observed by DLS.

Finally, the third high-temperature peak corresponds to the thermal melting of the amyloid fibrils to yield the fully unfolded state [15]. At 0.05 M and 0.1 M NaCl the normalized area under this peak and its Tm increased with the total protein concentration in the sample, reflecting the formation of higher amounts of aggregates during the DSC scan. At 0.2 M NaCl the area of this peak did not show any significant increase with the protein concentration within the interval investigated, which indicated that the amount of aggregates had reached a plateau under these conditions. The melting temperature of the fibrils (Tm) increased with the NaCl concentration by more than 10 ºC indicating a considerable stabilization of the fibrils by salt.

We also analyzed by DSC protein samples of 8 mg mL^{-1} preincubated at 37 ºC for different time periods in the presence of 0.05 M NaCl, 0.1 M NaCl and 0.2 M NaCl (Figures 3.10a-c).

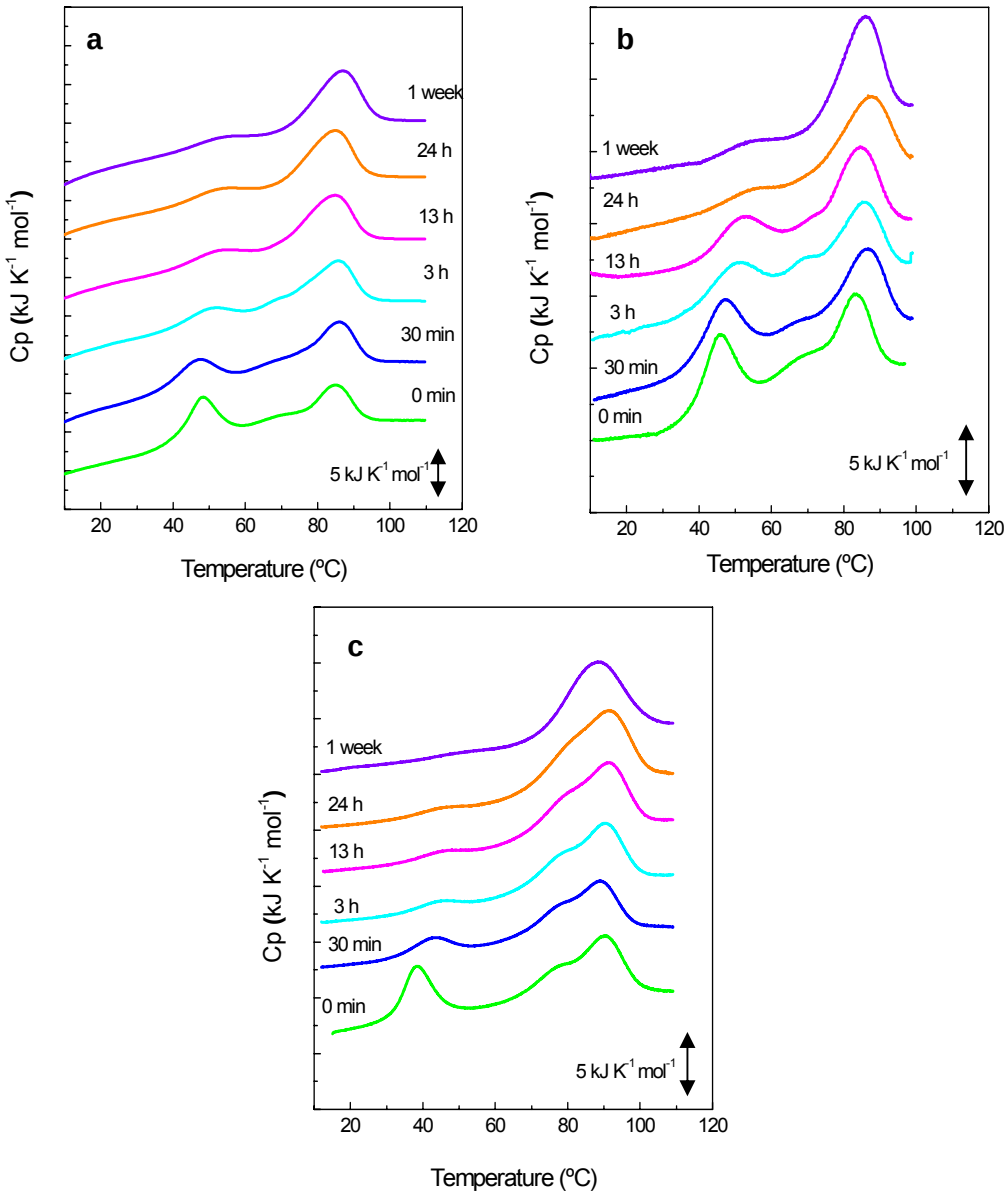

Figure 3.10. *DSC analysis of 8.3 mg mL^{-1} samples preincubated at 37 ºC during different times in 0.05 M NaCl (a), 0.1 M NaCl (b) and 0.2 M NaCl (c). Incubation times are indicated alongside each curve. Scan rate was 2 ºC min^{-1} in all experiments. The curves have been displaced artificially along the ordinate axis for clarity.*

In the presence of 0.05 M and 0.1 M NaCl, within 3 h of incubation the first transition at ≈ 46 ºC reduces its area by more than 50 % and shifts considerably toward higher temperature reaching the approximate Tm of the transition of unfolding at equilibrium (see Table 3.2, bellow). The duration of this event is largely coincident with the initial conformational phase observed in the aggregation kinetics and reflects the conversion of a large fraction of the native protein into oligomers or fibrils. The remaining area of this peak disappears by subsequent incubation at 37 ºC due to the incorporation of the native protein into aggregates. A similar event takes place during incubation in the presence of 0.2 M NaCl but at a faster rate and with a higher efficiency. The first transition at 40 ºC shifts to 48 ºC and is reduced by more than 90 % in area indicating a high degree of conversion of the native protein into oligomers and aggregates. At longer incubation times, the transition taking place at ≈ 48 ºC disappears, indicating full incorporation of native protein into the fibrils. The small DSC transition at intermediate temperature is clearly visible for samples incubated during short periods but disappears for long times of incubation, suggesting a progressive conversion of oligomers into fibrils.

The high-temperature transition is prominent for all samples but its area increases significantly with the time of pre-incubation, which correlates with a more complete formation of amyloid fibrils. For samples preincubated for long time periods, in which fibril formation is essentially complete, the enthalpy of fibril melting is about 100 kJ mol^{-1} and relatively independent of the experimental conditions. It is noticeable the higher Tm observed for the melting of the fibrils at 0.2 M NaCl concentration assembled either by preincubation at 37 ºC or by direct heating of the native state. This highlights the importance of salt in both the assembly pathway and the stability of the amyloid fibrils.

3.5 DEPENDENCY OF THE NATIVE STATE THERMODYNAMIC STABILITY WITH THE SALT CONCENTRATION AND pH

It has been proposed elsewhere that the stability of the native state has a decisive influence on the formation of amyloid fibrils [13,22,23]. Our previous studies have shown that the thermodynamic stability of the Spc-SH3 domain depends strongly on the pH [24] (see also the Chapter 2) but the effect of salt had not been analyzed so far. To characterize this effect, the thermal unfolding of the N47A mutant of Spc-SH3 domain was followed by DSC under the conditions of the fibrillation experiments, but at protein concentrations sufficiently low to avoid significant aggregation (0.8 mg mL^{-1}). Under these conditions, all unfolding curves were highly reversible and followed the two-state unfolding model.

Table 3.2 highlights the thermodynamic parameters for the thermal unfolding of the protein under the different conditions. We also analyzed the effect of pH at 0.1 M NaCl concentration.

Table 3.2. *Thermodynamic parameters of the equilibrium thermal unfolding of N47A Spc-SH3 measured by DSC at different pH values and NaCl concentrations. Values have been obtained by two-state analysis of the unfolding transitions at 0.8 mg* mL^{-1}.

pH	[NaCl] (M)	Tm (ºC)	ΔH_u (Tm) ($kJ.mol^{-1}$)	$\Delta C_{p,u}$ (Tm)[a] ($kJ.K^{-1}.mol^{-1}$)
3.2	0	54.5	168	3.67 ± 0.15
	0.05	54.8	164	
	0.1	51.2	152	
	0.2	49.3	144	
2.0	0.1	36.8	105.9	
2.5		39.9	114.1	
3.0		49.5	147.7	
3.5		55.4	169.9	

[a]The heat capacity change of unfolding was determined by linear regression to all the ΔH_u vs T_m data.

Whilst the decrease in pH produced a strong destabilizing effect as previously reported for the WT Spc-SH3, there was only a moderate destabilisation produced by the increase in NaCl concentration. Nevertheless, the unfolding enthalpy does not appear to change with either the ionic strength or the pH, except for the expected temperature dependence due to the heat capacity change of unfolding, as shown by the single linear correlation between ΔH_u (Tm) and Tm (Figure 3.11). This indicates that the net balance of interactions separating the native structure and the globally unfolded state is practically unaffected by these variables. We conclude therefore that the influence of salt concentration upon the fibrillation rate of the Spc-SH3 domain is not related to a significant structural destabilization of the native state relative to the unfolded state, which is fully consistent with the results described in the Chapter 2.

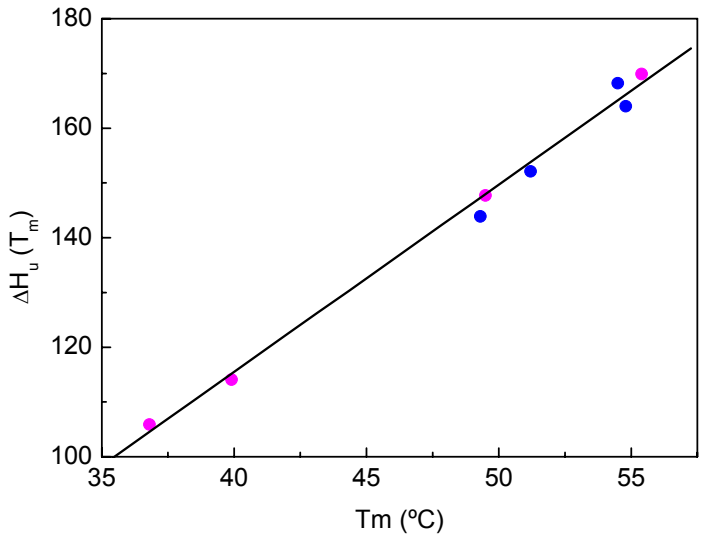

Figure 3.11. *Enthalpy change (ΔH_u) versus temperature (Tm) for the thermal unfolding of N47A Spc-SH3 under equilibrium conditions. Data correspond to the results of the analysis of the DSC unfolding curves using a two-state unfolding model summarized in Table 3.2. Experiments made at different pH values in the presence of 0.1 M NaCl, magenta. Experiments made at pH 3.2 and different NaCl concentrations, blue.*

3.6 DEPENDENCY OF THE FIBRILLATION RATE WITH THE pH

Several studies have proposed that a critical balance between electrostatic repulsion and hydrophobic interactions is required to trigger amyloid formation [25-27]. Moreover, net charge of the polypeptide chain has been shown to impact considerably the fibrillation rates of polypeptides [28,29]. We hypothesized that salt may be acting by weakening repulsive electrostatic interactions via a Debye-Huckel screening effect or by direct ion binding [27], favouring oligomerization of partially unfolded species and accelerating the aggregation cascade. To test further this hypothesis, we have analyzed the effect of pH on the kinetics of formation of amyloid fibrils by N47A Spc-SH3. By modifying the pH in the range where the carboxylic groups become protonated and the net positive charge of the protein is changed.

The fibrillation of the N47A Spc-SH3 mutant at 37 ºC was followed by ThT fluorescence at several pH values between 2.0 and 3.5, in the presence of 0.1 M NaCl (Figure 3.12). The rate of aggregation increased moderately as pH is reduced. This is in striking contrast with the large effects exerted by salt on the kinetics of aggregation. In addition, the observed effects were opposite to those expected according to our initial hypothesis, since an increase in positive charge should have resulted in higher intermolecular repulsion and less aggregation. At 3.5 there is some lag phase period lasting about 50 minutes, whereas at lower pH the lag time is almost insignificant suggesting a higher rate of nucleation. The total mass of fibrils reached a plateau after about 3 days of incubation at all pH values but the mass of fibrils was significantly higher at lower pH according to the intensity in ThT fluorescence achieved. The far-UV CD spectra at different pH values after one day of incubation at 37 ºC also developed an intense negative band at around 215 nm indicating formation

extensive β-sheet structure (Figure 3.13). The changes in secondary structure also occurred in two phases as described above.

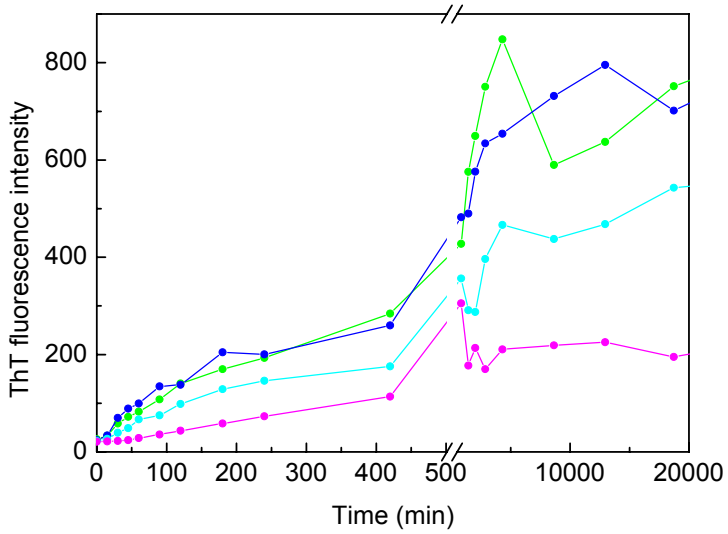

Figure 3.12. *Time course of fibrillation of N47A Spc-SH3 at 37 ºC in 100 mM glycine buffer at different pH in the presence of 0.1 M NaCl monitored by thioflavine T fluorescence. Sample concentration was 8 mg mL^{-1} in all samples. pH 2.0, green, pH 2.5, blue, pH 3.0, cyan, pH 3.5, magenta.*

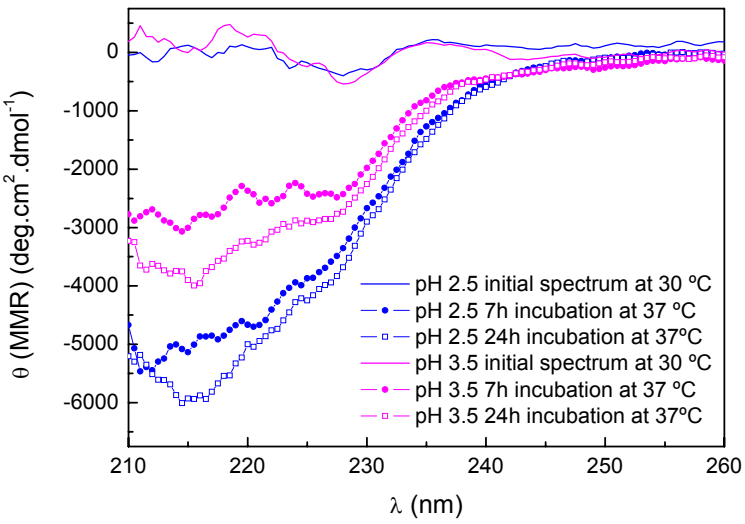

Figure 3.13. *Far-UV CD spectra of a 8 mg mL^{-1} N47A Spc-SH3 sample at 100 mM NaCl after different incubation times in a 0.1 mm pathlength CD cuvette at different pH values.*

The species present in solution during the aggregation process at different pH values were also analyzed by DLS (Figure 3.14).

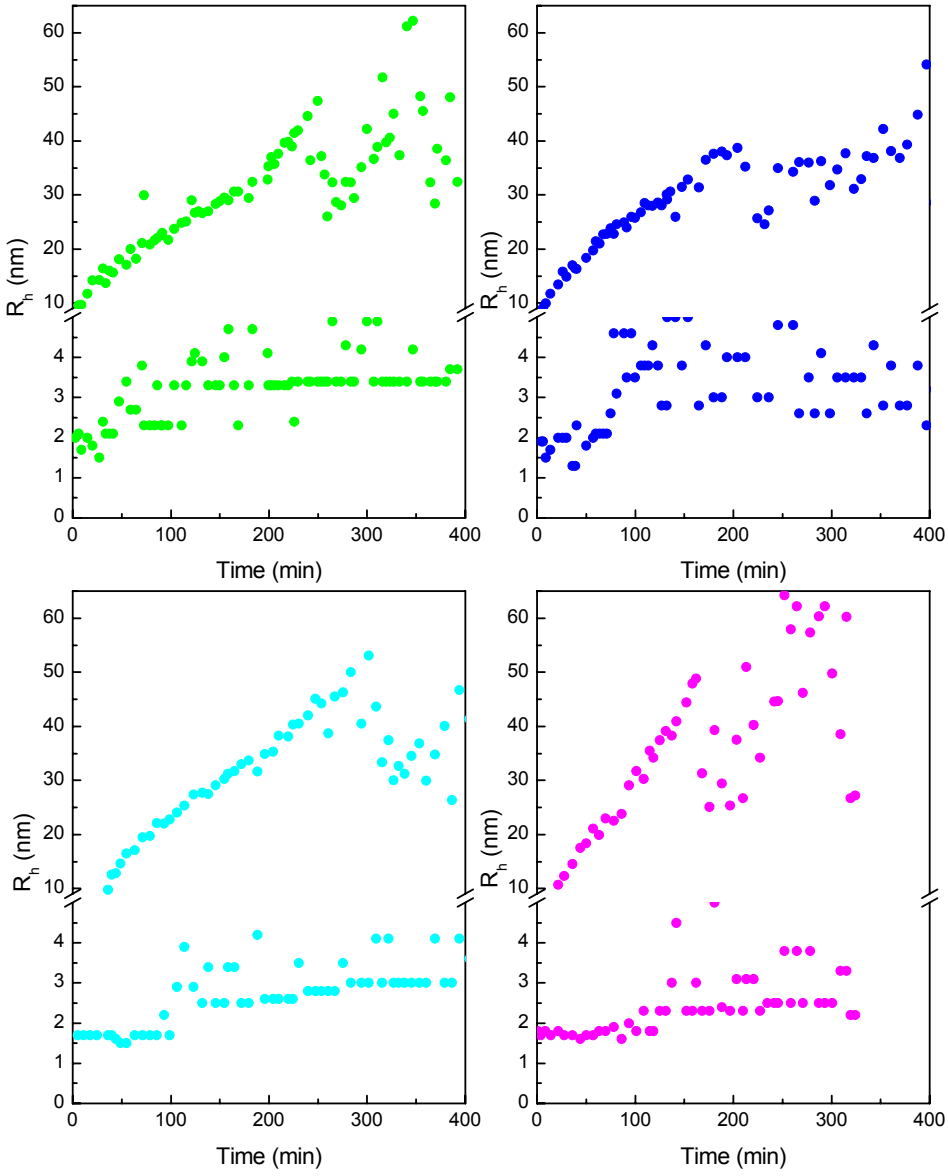

Figure 3.14. *Time evolution of particle sizes determined by dynamic light scattering during fibrillation of N47A Spc-SH3 at different pH values. The average hydrodynamic radii of the two smallest peaks in the distributions have been plotted as a function of the time of incubation. Sample concentration was 8 mg mL^{-1} in all samples. pH 2.0, green, pH 2.5, blue, pH 3.0, cyan, pH 3.5, magenta.*

The series of events were similar to those observed at pH 3.2 in the presence of 0.1 M. The initial expansion of the apparent R_h of the smallest particles reflecting the formation of small oligomers was accelerated by the reduction of pH but this effect was much less dramatic than that produced by the increase in salt concentration or temperature.

As shown above, the onset of the fibrillation process was approximately coincident with the R_h expansion at all pH values. We conclude from these results that lowering the pH increases the rate of fibril nucleation enhancing fibrillation but to a lesser extent than the other environmental variables.

We have also explored the time course of the fibrillation process at various pH values by TEM. Figure 3.15 shows the images obtained for solutions incubated at different times of incubation at 37 ºC and at different pH values.

At pH 3.0 and 3.5, where the lag phase lasts longer, some globular an amorphous aggregates were still visible at 30 min of incubation (figure 3.15c). These species converted into short protofibrils after 60 min incubation, and then grew progressively. At lower pH, only protofibrillar filaments were detected at 30 min incubation (figure 3.15a).

The decrease in pH resulted in a faster appearance of fibrillar aggregates likely due to a higher rate of formation of oligomeric precursors. At longer incubation times the fibrils looked very similar at all pH values (figure 3.15b and 3.15d).

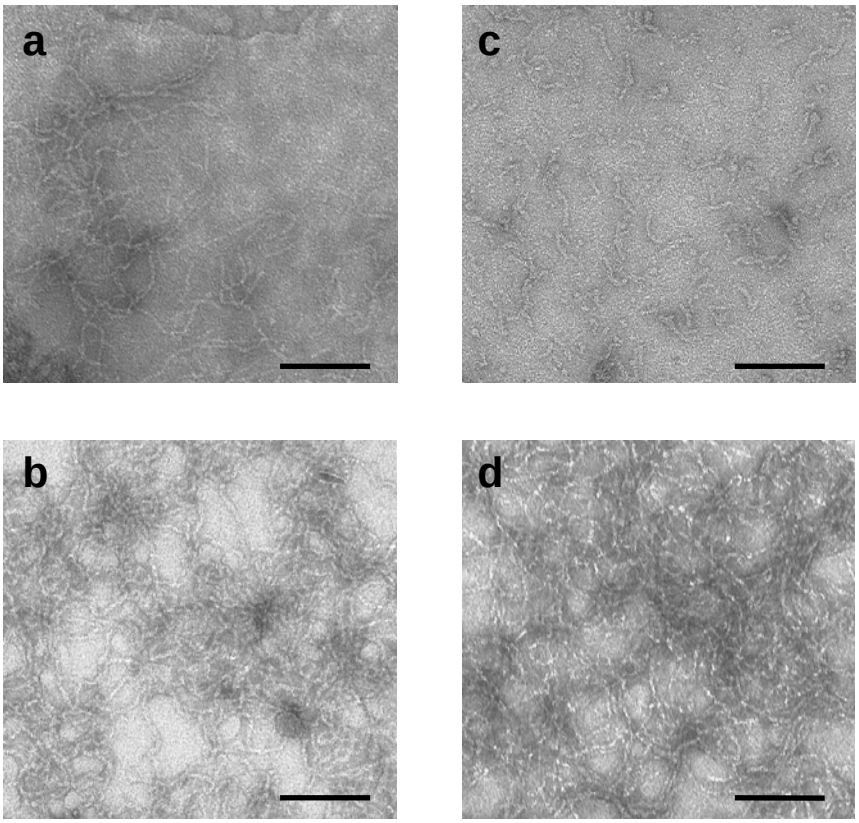

***Figure 3.15**. Effect of pH upon the morphology of amyloid fibrils of N47A Spc-SH3. Transmission electron microscopy images were taken with samples of 8 mg mL^{-1} incubated at 37 ºC in 100 mM glycine buffer and 100 mM NaCl at different pH values and incubation time: (a) pH 2, 30 minutes; (b) pH 2, 30 days (c) pH 3.5, 30 minutes; (d) pH 3.5, 30 days. The length of the black segment corresponds to 100 nm.*

3.7 DISCUSSION

Here we have shown that the kinetics amyloid fibril formation of the N47A Spc-SH3 domain at low salt concentration shows the existence of a prolonged lag phase, indicating that the process takes place by a nucleation and growth mechanism under these conditions [1,2]. The lag phase is progressively reduced by increasing either the NaCl concentration or the temperature and to a lower extent by lowering the pH. This suggests that the processes leading to fibril nucleation are considerably accelerated by changes in these

environmental variables, so that the lag phase can be the completely abrogated if these processes are not longer rate-limiting. This has also been observed for Abeta fibrillation in the presence of moderate concentrations of trifluoroethanol, which facilitates partially folded helix-containing conformers that appear to be intermediates in fibril assembly [30].

During the series of conformational events leading to fibril nucleation the native protein undergoes a remarkable conformational change involving substantial structural changes according to the CD spectra and a net balance in interactions considerably lower than that of the global unfolding, as evidenced by DSC. This indicates that the amyloidogenic species are partially unfolded states of the protein. When these species have accumulated sufficiently, they show a strong tendency to oligomerize and trigger the fibrillation process. In fact, under all conditions studied here the end of the lag period is approximately coincident with the formation of small oligomeric species with average hydrodynamic radii ranging between 2.5 and 8 nm depending of the conditions as detected by DLS. The rate of fibril growth increases strongly after this event indicating that oligomer formation is crucial in the mechanism of fibrillation.

Fibrillation via soluble oligomeric species is a common theme in the mechanism of amyloid formation and oligomerization appears to play a crucial role in amyloid nucleation. More than one decade ago, small metastable protofibrillar aggregates were already described as transient intermediates of the Abeta-40 and Abeta-42 fibrillation pathway [31]. Further work [32] has shown that Abeta-40 and Abeta-42 form earlier and smaller oligomeric assemblies with a distribution of molecular sizes including monomer, dimer, trimer, tetramer and higher-order oligomers, with the latter strongly favoured for Abeta-42 relative to Abeta-40. The relative tendency to oligomerize of the two Abeta variants appears to be crucial in their different fibrillation propensity.

Transient oligomeric intermediates have also been detected for example during the lag phases of fibrillation of alpha-synuclein [33,34], mouse prion protein [35] and human insulin [36]. Formation of distinct morphological types of fibrils of β2-microglobulin by either nucleated or non-nucleated mechanism also occurs via the transient formation of a range of oligomeric species [37]. When fibrillation takes place from stable and well-populated soluble oligomers, as it occurs in barstar fibrillation, there kinetics do not show any lag phase indicating that nucleation is no longer a rate limiting step [38]. The importance of oligomeric species is further supported by the observation that amyloid formation by a tandem repeat of the PI3-SH3 domain, highly homologous to the Spc-SH3 domain, is strongly accelerated by the presence of preformed amorphous oligomers with a critical size of roughly 20 molecules [39]. This so-called “molten oligomer” state has been proposed to facilitate the structural conversion of the protein into small amyloid-like structures that then act as templates for fibril growth. Similarly, the prion protein Sup35 has been shown to form structurally fluid oligomeric species that are crucial intermediates in nucleating amyloid fibrils [40]. Interestingly, these authors also report a remarkable independence of the rate of fibril nucleation with protein concentration, as we also show here for the Spc-SH3. Although in principle this concentration independence may suggest that the rate limiting step of the nucleation process is a monomolecular partial unfolding previous to a rapid oligomerization, other explanations may also be possible, such as a conformational conversion taking within preformed oligomers or nuclei [40,41]. Our results do not allow discerning between these alternative interpretations, given that under our conditions the conformational change and the formation of oligomeric species are practically simultaneous processes.

An increase in NaCl concentration or in temperature of incubation accelerates dramatically the fibrillation process by increasing the rate

of the structural change of the protein and favouring the subsequent formation of oligomeric species. This results in a drastic reduction of the lag phase (nucleation step). Likewise, the amyloidogenic effect of the N47A mutation is also mainly due to an increase in the rate of formation of aggregation nuclei relative to the WT domain, as we have shown in the previous Chapter [42]. Lowering the pH from 3.5 to 2.0 while keeping constant all other factors also leads to some increase in the aggregation rate and a decrease of the lag phase but the effect of pH is much less intense than that of the salt or temperature. These results are in marked contrast with the strong reduction in stability observed for this domain as pH decreases, as compared with the moderate destabilizing effect exerted by the increase in salt concentration.

Whilst destabilising the native conformation has been shown to increase the propensity of several proteins to aggregate into amyloid fibrils [22,23,43,44], no correlation between native stability and fibrillation propensity has been found in a mutational analysis of the fibrillation of the thermophilic protein S6 [3] and even a direct correlation between protein stability and amyloid formation enhancement by salts has been recently reported for an immunoglobulin light chain [45]. These results together with those of Chapter 2 indicate that amyloid formation in the Spc-SH3 domain is not directly correlated with the native-state thermodynamic stability. Accordingly, the enhancement of amyloid formation by environmental factors must have physicochemical reasons different from the destabilization of the native state.

It has been shown in recent studies that a critical balance between electrostatic repulsion and hydrophobic interactions is required to trigger amyloid formation at acidic pH [25-27]. This balance could be altered by the presence of ions, pH, temperature, co-solvents, pressure, etc. The effect of salt ions is the most extensively studied. In

general, an increase in salt concentration accelerates fibrillation, although the extent of this effect is strongly dependent on the aggregating protein and the type of salt. Several possible mechanisms by which salts exert aggregation triggering effects have been proposed. Salts may favour intermolecular interactions by weakening repulsive electrostatic interactions via a Debye-Huckel screening effect or by direct ion binding [27]. They could also perturb the hydration shell of the protein molecule [45,46]. A combination of both direct protein-salt interactions and changes in water structure has also been proposed [47] and saline ions may even interact directly as structural ligands with fibrils where they coordinate charges and assist in formation of new fibrils [12]. In general all these studies have related the amyloid-enhancing effect of salt ions with their influence upon the establishment of protein-protein interactions.

On the other hand, the results of our work indicate that salt appears to affect mainly the stage of an initial conformational change that the protein must undergo to favour the nucleation of fibrils. Salt also influences the fibril elongation step to some extent, although this effect could be just the result of a higher availability of amyloidogenic precursors. If the the rate-limiting step of nucleation were a first-order conformational change as observed by CD, an enhancement of intermolecular association by screening of charge-charge repulsion would not be crucial in triggering fibrillation, in agreement with the observation that increasing the net positive charge of the protein by lowering pH does not result in less aggregation but just in the opposite effect. It is thus possible that the role of salt in enhancing fibrillation is related to its influence upon the hydration shell of the protein or to a direct interaction of salt ions with the protein groups. Nevertheless, our data did not allow us to establish a complete kinetic mechanism for the conformational change-nucleation process.

An important result of this work is that an increase in the NaCl concentration lowers considerably the activation enthalpy of the conformational change that leads to the accumulation of amyloidogenic oligomers. Interestingly, the events occurring during early fibrillation processes of a number of proteins usually have relatively high activation energies, as it happens with our system. An activation energy of 95 kJ mol^{-1} was determined for the fibril elongation rate of Abeta-40 at acid pH, where fibrils appear to grow from a micellar precursor [48]. Higher values have been measured for non-nucleation-dependent fibrillation of mouse prion protein (130 kJ mol^{-1}) [35] and barstar (100 to 120 kJ mol^{-1}) [38]. Activation energies for nucleation and elongation of alpha-synuclein amyloid fibrils were determined to be 75 and 84 kJ mol^{-1} respectively [49]. Insulin fibrillation also shows an activation energy of about 105 kJ mol^{-1} [50]. These values are of a similar magnitude as those measured in this work, although there may be additional variability related to the different protein systems, as well as the different experimental conditions and methods of analysis used in each study. In general, these high activation energies have been attributed to the complex molecular changes accompanying the early events of fibrillation.

The existence of robust enthalpic activation barriers in protein folding has been recently attributed to desolvation of protein surfaces [51]. These barriers have been associated with the cooperative desolvation of relatively large protein surface areas that is needed to establish intramolecular interactions during protein folding. From the point of view of protein unfolding, the barrier could be viewed as arising from an asynchrony between water penetration and the disruption of internal interactions and in this case it would be described as a solvation barrier [52]. The typical experimental activation enthalpies of folding-unfolding of small globular proteins fall in the

range of 70 to 160 kJ mol^{-1}, comparable to those measured for amyloid formation and also to the values reported here. Since amyloid formation of natively folded proteins is usually accompanied by partial unfolding, as in the case of the Spc-SH3 domain, it is likely that activation enthalpies of both types of processes share a common physicochemical origin. Likewise, formation of intermolecular contacts in nucleation and fibril formation also require the desolvation of extensive protein surface areas, which would also result in considerable enthalpy barriers as it is observed experimentally.

We speculate here that the reduction of activation enthalpy produced by the increase in salt concentration might then be related to its influence upon the protein hydration shell. Salt ions may act by altering the structure and the cooperativity of the solvation layer of the protein, either by a direct ion binding to the protein surface that would change the effective protein surface or by interacting with the water of the first hydration layer [53]. In support of each of these two mechanisms are the observations that the effects of different salt ions upon amyloid formation rates of some proteins correlate well with the electroselectivity series [47], whereas in other cases they correlate with the Hofmeister series [45] [46]. In any case, the alteration of the cooperativity of protein hydration by salt may have dramatic consequences in the energy landscape of the protein, promoting alternative folding or unfolding pathways accessible to the polypeptide chain and then leading to amyloidogenic species as we observed in this work.

It should be also underlined that salt concentration and temperature of incubation affect significantly the morphology of the finally formed fibrils by the N47A Spc-SH3 domain. Under conditions where the rate of the conformational change that leads to nucleation is low, curly fibrils are initially favoured but well-ordered, straight and twisted fibrils dominate the mixture at long incubation times. This is

observed at low and intermediate NaCl concentration. At high salt concentration or high temperature only curly filaments are obtained and these remain for long incubation times. These filaments appear thinner and shorter than those formed at intermediate salt concentration suggesting a different internal structure between them. Despite their different morphologies, all these types of fibrils have been shown to be amyloid-like. The pH does not appear to affect however the apparent final morphology of the mature fibrils within the interval analyzed.

High resolution electron microscopy images have revealed in the past that the fibrils of many different proteins show a high degree of polymorphism, in many cases modulated by environmental conditions [9,11-14,25,54]. These observations has been often used to support a linear hierarchical mechanism of fibril assembly, in which less-ordered fibrillar aggregates, such as the curly protofibrils described here, would be on-pathway kinetic intermediates of the long and twisted amyloid fibrils that constitute the most thermodynamically stable ones [55]. Although this hypothesis would be apparently supported in this work by the early appearance of protofibrils that gradually convert into the twisted amyloid fibrils at intermediate salt concentrations, the protofibrils do not convert efficiently into amyloid fibrils under any of the conditions studied if they are separated from the soluble species. This suggests that the soluble oligomeric species play a crucial role in the morphological conversion.

On the other hand, the coexistence of different fibril morphologies has also led to the alternative hypothesis that there are alternative competing pathways of assembly, which would be selected by the influence of environmental conditions upon the energy landscape. This has been established for instance for β2-microglobulin [14], in which assembly of different kinds of fibrils can occur by two diverging routes depending on the conditions of their formation: a first route occurs with

characteristics non-nucleation dependent growth kinetics and results in the formation of the short, seemingly flexible fibrils with low linear persistence. This route is favoured at pH 3.5 in the presence of 0.2 M NaCl or using a high temperature of incubation, where the native protein is predominantly unfolded. By contrast, in the absence of salt at similar or lower pH the formation of long and straight fibrils that are comprised of several twisted filaments occurs via a nucleation-dependent kinetics involving a considerable lag phase [2]. These results are highly similar to those obtained by us suggesting that this type of mechanism may also hold for the Spc-SH3 domain. It is thus likely that high salt concentration promotes an alternative fibrillation pathway by altering the conformational landscape accessible to the polypeptide chain at the early conformational events prior to nucleation.

3.8 BIBLIOGRAPHY

[1] Harper, J.D., Lieber, C.M. and Lansbury, P.T., Jr. (1997). Atomic force microscopic imaging of seeded fibril formation and fibril branching by the Alzheimer's disease amyloid-beta protein. Chem Biol 4, 951-9.

[2] Naiki, H., Gejyo, F. and Nakakuki, K. (1997). Concentration-dependent inhibitory effects of apolipoprotein E on Alzheimer's beta-amyloid fibril formation in vitro. Biochemistry 36, 6243-50.

[3] Pedersen, J.S., Christensen, G. and Otzen, D.E. (2004). Modulation of S6 fibrillation by unfolding rates and gatekeeper residues. J Mol Biol 341, 575-88.

[4] Hurshman Babbes, A.R., Powers, E.T. and Kelly, J.W. (2008). Quantification of the thermodynamically linked quaternary and tertiary structural stabilities of transthyretin and its disease-associated variants: the relationship between stability and amyloidosis. Biochemistry 47, 6969-84.

[5] Modler, A.J., Gast, K., Lutsch, G. and Damaschun, G. (2003). Assembly of amyloid protofibrils via critical oligomers--a novel pathway of amyloid formation. J Mol Biol 325, 135-48.

[6] Knowles, T.P.J. et al. (2009). An Analytical Solution to the Kinetics of Breakable Filament Assembly. Science 326, 1533-1537.

[7] Librizzi, F. and Rischel, C. (2005). The kinetic behavior of insulin fibrillation is determined by heterogeneous nucleation pathways. Protein Sci 14, 3129-34.

[8] Pedersen, J.S. and Otzen, D.E. (2008). Amyloid-a state in many guises: survival of the fittest fibril fold. Protein Sci 17, 2-10.

[9] Bauer, H.H., Aebi, U., Haner, M., Hermann, R., Muller, M. and Merkle, H.P. (1995). Architecture and polymorphism of fibrillar supramolecular assemblies produced by in vitro aggregation of human calcitonin. J Struct Biol 115, 1-15.

[10] Zurdo, J., Guijarro, J.I., Jimenez, J.L., Saibil, H.R. and Dobson, C.M. (2001). Dependence on solution conditions of aggregation and amyloid formation by an SH3 domain. Journal of Molecular Biology 311, 325-340.

[11] Jimenez, J.L., Nettleton, E.J., Bouchard, M., Robinson, C.V., Dobson, C.M. and Saibil, H.R. (2002). The protofilament structure of insulin amyloid fibrils. Proc Natl Acad Sci U S A 99, 9196-201.

[12] Pedersen, J.S., Flink, J.M., Dikov, D. and Otzen, D.E. (2006). Sulfates Dramatically Stabilize a Salt-Dependent Type of Glucagon Fibrils. Biophysical Journal 90, 4181-4194.

[13] Kad, N.M., Myers, S.L., Smith, D.P., Alastair Smith, D., Radford, S.E. and Thomson, N.H. (2003). Hierarchical Assembly of [beta]2-Microglobulin Amyloid In Vitro Revealed by Atomic Force Microscopy. J. Mol. Biol. 330, 785-797.

[14] Gosal, W.S., Morten, I.J., Hewitt, E.W., Smith, D.A., Thomson, N.H. and Radford, S.E. (2005). Competing pathways determine fibril morphology in the self-assembly of beta2-microglobulin into amyloid. J Mol Biol 351, 850-64.

[15] Morel, B., Casares, S. and Conejero-Lara, F. (2006). A single mutation induces amyloid aggregation in the alpha-spectrin SH3 domain: analysis of the early stages of fibril formation. J Mol Biol 356, 453-68.

[16] Kodali, R. and Wetzel, R. (2007). Polymorphism in the intermediates and products of amyloid assembly. Current Opinion in Structural Biology Folding and binding / Protein-nucleic interactions 17, 48-57.

[17] Serpell, L.C. (2000). Alzheimer's amyloid fibrils: structure and assembly. Biochim Biophys Acta 1502, 16-30.

[18] Harper, J.D. and Lansbury, P.T., Jr. (1997). Models of amyloid seeding in Alzheimer's disease and scrapie: mechanistic truths and physiological consequences of the time-dependent solubility of amyloid proteins. Annu Rev Biochem 66, 385-407.

[19] Lomakin, A., Benedek, G.B. and Teplow, D.B. (1999). Monitoring protein assembly using quasielastic light scattering spectroscopy. Methods Enzymol. 309, 429-459.

[20] Wilkins, D.K., Grimshaw, S.B., Receveur, V., Dobson, C.M., Jones, J.A. and Smith, L.J. (1999). Hydrodynamic radii of native and denatured proteins measured by pulse field gradient NMR techniques. Biochemistry 38, 16424-31.

[21] Casares, S., Sadqi, M., Lopez-Mayorga, O., Conejero-Lara, F. and van Nuland, N.A. (2004). Detection and characterization of partially unfolded oligomers of the SH3 domain of alpha-spectrin. Biophys J 86, 2403-13.

[22] Booth, D.R. et al. (1997). Instability, unfolding and aggregation of human lysozyme variants underlying amyloid fibrillogenesis. Nature 385, 787-93.

[23] Ramirez-Alvarado, M., Merkel, J.S. and Regan, L. (2000). A systematic exploration of the influence of the protein stability on amyloid fibril formation in vitro. Proc Natl Acad Sci U S A 97, 8979-84.

[24] Sadqi, M., Casares, S., Abril, M.A., Lopez-Mayorga, O., Conejero-Lara, F. and Freire, E. (1999). The native state conformational ensemble of the SH3 domain from alpha-spectrin. Biochemistry 38, 8899-906.

[25] Zurdo, J., Guijarro, J.I., Jimenez, J.L., Saibil, H.R. and Dobson, C.M. (2001). Dependence on solution conditions of aggregation and amyloid formation by an SH3 domain. J Mol Biol 311, 325-40.

[26] Smith, D.P., Jones, S., Serpell, L.C., Sunde, M. and Radford, S.E. (2003). A systematic investigation into the effect of protein destabilisation on beta 2-microglobulin amyloid formation. J Mol Biol 330, 943-54.

[27] Raman, B. et al. (2005). Critical balance of electrostatic and hydrophobic interactions is required for beta 2-microglobulin amyloid fibril growth and stability. Biochemistry 44, 1288-99.

[28] Chiti, F., Stefani, M., Taddei, N., Ramponi, G. and Dobson, C.M. (2003). Rationalization of the effects of mutations on peptide and protein aggregation rates. Nature 424, 805-8.

[29] Lopez De La Paz, M., Goldie, K., Zurdo, J., Lacroix, E., Dobson, C.M., Hoenger, A. and Serrano, L. (2002). De novo designed peptide-based amyloid fibrils. Proc Natl Acad Sci U S A 99, 16052-7.

[30] Fezoui, Y. and Teplow, D.B. (2002). Kinetic Studies of Amyloid beta -Protein Fibril Assembly. Differential effects of alpha -helix stabilization 10.1074/jbc.M204168200. J. Biol. Chem. 277, 36948-36954.

[31] Harper, J.D., Wong, S.S., Lieber, C.M. and Lansbury, P.T. (1997). Observation of metastable Abeta amyloid protofibrils by atomic force microscopy. Chem Biol 4, 119-25.

[32] Teplow, D.B. et al. (2006). Elucidating Amyloid Î²-Protein Folding and Assembly: A Multidisciplinary Approach. Accounts of Chemical Research 39, 635-645.

[33] Kaylor, J., Bodner, N., Edridge, S., Yamin, G., Hong, D.-P. and Fink, A.L. (2005). Characterization of Oligomeric Intermediates in [alpha]-Synuclein Fibrillation: FRET Studies of Y125W/Y133F/Y136F [alpha]-Synuclein. Journal of Molecular Biology 353, 357-372.

[34] Dusa, A., Kaylor, J., Edridge, S., Bodner, N., Hong, D.-P. and Fink, A.L. (2006). Characterization of Oligomers during Î±-Synuclein Aggregation Using Intrinsic Tryptophan Fluorescenceâ€ Biochemistry 45, 2752-2760.

[35] Jain, S. and Udgaonkar, J.B. (2008). Evidence for Stepwise Formation of Amyloid Fibrils by the Mouse Prion Protein. Journal of Molecular Biology 382, 1228-1241.

[36] Mirco Sorci, Robert A. Grassucci, Ingrid Hahn, Joachim Frank and Georges Belfort. (2009). Time-dependent insulin oligomer reaction pathway prior to fibril formation: Cooling and seeding. Proteins: Structure, Function, and Bioinformatics 9999, NA.

[37] Smith, A.M., Jahn, T.R., Ashcroft, A.E. and Radford, S.E. (2006). Direct Observation of Oligomeric Species formed in the Early Stages of Amyloid Fibril Formation using Electrospray Ionisation Mass Spectrometry. Journal of Molecular Biology 364, 9-19.

[38] Kumar, S., Mohanty, S.K. and Udgaonkar, J.B. (2007). Mechanism of Formation of Amyloid Protofibrils of Barstar from Soluble Oligomers: Evidence for Multiple Steps and Lateral Association Coupled to Conformational Conversion. Journal of Molecular Biology 367, 1186-1204.

[39] Bader, R., Bamford, R., Zurdo, J., Luisi, B.F. and Dobson, C.M. (2006). Probing the mechanism of amyloidogenesis through a tandem repeat of the PI3-SH3 domain suggests a generic model for protein aggregation and fibril formation. J Mol Biol 356, 189-208.

[40] Serio, T.R., Cashikar, A.G., Kowal, A.S., Sawicki, G.J., Moslehi, J.J., Serpell, L., Arnsdorf, M.F. and Lindquist, S.L. (2000). Nucleated conformational conversion and the replication of conformational information by a prion determinant. Science 289, 1317-21.

[41] Plakoutsi, G., Bemporad, F., Calamai, M., Taddei, N., Dobson, C.M. and Chiti, F. (2005). Evidence for a Mechanism of Amyloid Formation Involving Molecular Reorganisation within Native-like Precursor Aggregates. Journal of Molecular Biology 351, 910-922.

[42] Varela, L., Morel, B., Azuaga, A.I. and Conejero-Lara, F. (2009). A single mutation in an SH3 domain increases amyloid aggregation by accelerating nucleation, but not by destabilizing thermodynamically the native state. FEBS Lett 583, 801-6.

[43] Kad, N.M., Thomson, N.H., Smith, D.P., Smith, D.A. and Radford, S.E. (2001). beta(2)-microglobulin and its deamidated variant, N17D form amyloid fibrils with a range of morphologies in vitro. Journal of Molecular Biology 313, 559-571.

[44] Chiti, F., Taddei, N., Bucciantini, M., White, P., Ramponi, G. and Dobson, C.M. (2000). Mutational analysis of the propensity for amyloid formation by a globular protein. EMBO J 19, 1441-9.

[45] Sikkink, L.A. and Ramirez-Alvarado, M. (2008). Salts enhance both protein stability and amyloid formation of an immunoglobulin light chain. Biophysical Chemistry 135, 25-31.

[46] Munishkina, L.A., Henriques, J., Uversky, V.N. and Fink, A.L. (2004). Role of protein-water interactions and electrostatics in alpha-synuclein fibril formation. Biochemistry 43, 3289-300.

[47] Klement, K., Wieligmann, K., Meinhardt, J., Hortschansky, P., Richter, W. and Fändrich, M. (2007). Effect of Different Salt Ions on the Propensity of Aggregation and on the Structure of Alzheimer's A[beta](1-40) Amyloid Fibrils. Journal of Molecular Biology 373, 1321-1333.

[48] Kusumoto, Y., Lomakin, A., Teplow, D.B. and Benedek, G.B. (1998). Temperature dependence of amyloid Î²-protein fibrillization. Proceedings of the National Academy of Sciences of the United States of America 95, 12277-12282.

[49] Uversky, V.N., Li, J. and Fink, A.L. (2001). Evidence for a Partially Folded Intermediate in alpha -Synuclein Fibril Formation. 10.1074/jbc.M010907200. J. Biol. Chem. 276, 10737-10744.

[50] Mauro, M., Craparo, E.F., Podestà, A., Bulone, D., Carrotta, R., Martorana, V., Tiana, G. and San Biagio, P.L. (2007). Kinetics of Different Processes in Human Insulin Amyloid Formation. Journal of Molecular Biology 366, 258-274.

[51] Liu, Z. and Chan, H.S. (2005). Desolvation is a Likely Origin of Robust Enthalpic Barriers to Protein Folding. Journal of Molecular Biology 349, 872-889.

[52] Rodriguez-Larrea, D., Ibarra-Molero, B. and Sanchez-Ruiz, J.M. (2006). Energetic and Structural Consequences of Desolvation/Solvation Barriers to Protein Folding/Unfolding Assessed from Experimental Unfolding Rates. Biophysical Journal 91, L48-L50.

[53] Zhang, Y. and Cremer, P.S. (2006). Interactions between macromolecules and ions: the Hofmeister series. Current Opinion in Chemical Biology. Model systems / Biopolymers 10, 658-663.

[54] Goldsbury, C.S. et al. (1997). Polymorphic fibrillar assembly of human amylin. J Struct Biol 119, 17-27.

[55] Zerovnik, E. (2002). Amyloid-fibril formation. Proposed mechanisms and relevance to conformational disease. Eur J Biochem 269, 3362-71.

4.

STRUCTURAL CHARACTERIZATION OF THE CONFORMATIONAL ENSEMBLE OF THE SPC-SH3 DOMAIN UNDER AMYLOIDOGENIC CONDITIONS

4. STRUCTURAL CHARACTERIZATION OF THE CONFORMATIONAL ENSEMBLE OF THE SPC-SH3 DOMAIN UNDER AMYLOIDOGENIC CONDITIONS

Structural characterization of intermediate states in conformational processes in proteins is a very complicated task and even more challenging if aggregation is involved. There are however a number of approaches that can be used to circumvent this problem and to obtain structural information at the level of residue about the states key in the fibrillation process. One approach is to analyze the soluble states using methods that are mainly based on the use of hydrogen-deuterium (H/D) exchange detected by NMR (see chapter 8) under amyloidogenic conditions but minimizing aggregation by a choice of the appropriate experimental variables.

The patterns of H/D exchange protection under native conditions indicate that protein structures fluctuate in such a way that many amide groups are exposed to the solvent as a result of local or sub-global unfolding events [1]. Our research group has previously shown using NMR-detected H/D exchange that under mild acid conditions the Spc-SH3 domain undergoes a variety of conformational changes, which range from local fluctuations affecting flexible regions of the domain to extensive unfolding affecting most of the domain structure [2-6]. Although these studies were made under conditions disfavouring amyloid aggregation, it was hypothesized that some of these conformational fluctuations may be involved in triggering the amyloid cascade.

The aim of this research was elucidate if the factors favouring amyloid formation modify the conformational landscape of the Spc-SH3 domain in such a way that a population of partially folded conformational states may result enhanced and trigger the formation of misfolded states or amyloid aggregation precursors.

4.1. NMR CHEMICAL SHIFT ANALYSIS

To explore possible conformational changes in the Spc-SH3 structure induced by the N47A mutation or by the different experimental conditions, the assignments of the NMR chemical shifts of the backbone amide groups were made for the WT and the N47A variants under conditions approaching those of fibrillation but avoiding significant aggregation during the experiments. We achieved this goal by decreasing the protein concentration and temperature to values (1 mg mL^{-1} and 30 ºC), where aggregation is not significant during the course of the experiments. We measured the two-dimensional ^{15}N-^{1}H HSQC NMR spectra for both proteins in 100 mM glycine buffer, in the presence of 100 mM or 200 mM NaCl under conditions of equal stability (pH 3.20 for N47A and pH 2.78 for WT). Figure 4.1 shows the changes in chemical shifts produced by the N47A mutation and by the increase of NaCl concentration. The chemical shift changes were calculated using equation 4.1.

$$\Delta\delta = \sqrt{\left(\Delta H_N\right)^2 + \left(\Delta N / 6.51\right)^2} \qquad (4.1)$$

Where $\Delta\delta$ is the global chemical shift change, ΔH_N and ΔN are the chemical shift changes for the amide proton and nitrogen, respectively, all expressed in ppm.

Under the two conditions analyzed the N47A mutation results in very small chemical shift changes. Significant changes are only observed at the place of mutation and the adjacent residue (positions 47 and 48) at the distal turn, and smaller changes are visible for residue 41 in the β_3 strand and residue 18 in the RT-loop. The increase of NaCl concentration does not have a significant effect on the chemical shifts. These results indicate that the amyloidogenic

factors do not produce significant changes in the native structure of the Spc-SH3 domain.

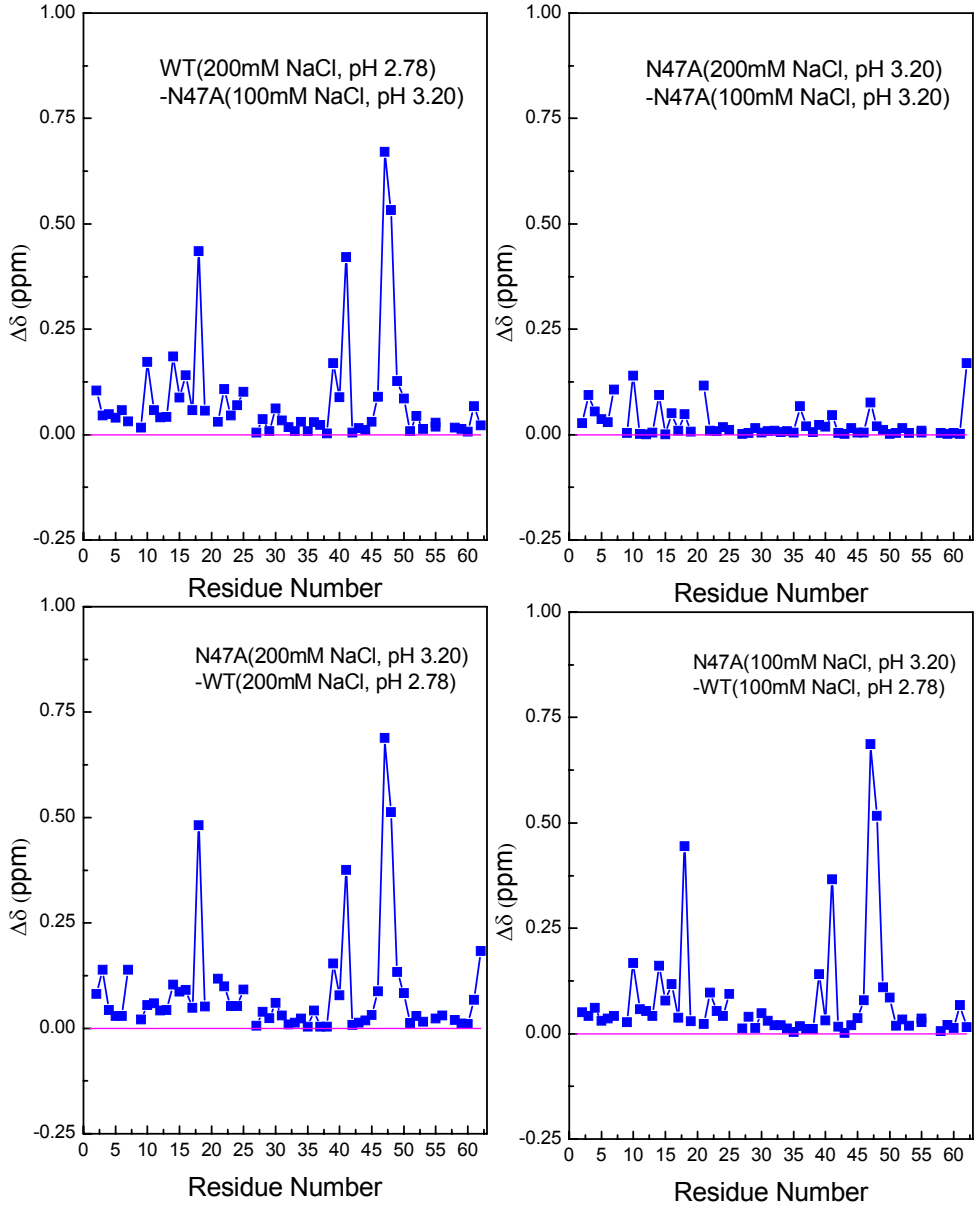

Figure 4.1. *Effect of the N47A mutation and the NaCl concentration on the backbone NMR chemical shifts of the Spc-SH3 domain, as indicated in each panel.*

4.2. CHANGES IN GLOBAL STABILITY.

We investigated the thermodynamic magnitudes of global unfolding of the N47A mutant and the WT Spc-SH3 domain at each different salt concentration under the same conditions described above. In all cases both domains unfolded reversibly according to a two-state model. Table 4.1 contains the relevant thermodynamic parameters of unfolding as determined from the two-state fittings of the DSC thermograms (not shown).

Table 4.1. *Thermodynamic parameters of the equilibrium thermal unfolding of N47A and WT Spc-SH3 measured by DSC at different salt concentrations under the same stability conditions. The values have been obtained by two-state analysis of the unfolding transitions.*

Variant	pH	[NaCl] (M)	Tm (ºC)	ΔH_u (Tm) (kJ.mol^{-1})	$\Delta C_{p,u}$ (Tm)[a] (kJ.K^{-1}.mol^{-1})	ΔG_u (30ºC) (kJ.mol^{-1})
N47A	3.20	0.1	50.9±0.8	149±3	3.67 ± 0.15	7.1±0.4
		0.2	48.7±0.8	144±3		6.4±0.4
WT	2.78	0.1	50.8±0.8	149±3		7.1±0.4
		0.2	48.8±0.8	146±3		6.5±0.4

[a]The heat capacity change of unfolding was determined by linear regression to all the ΔH_u vs T_m data.

As expected, the stability of the two variants is the same at each salt concentration. In both domains we observed a decrease in stability with the increase of the NaCl concentration, as observed before (see Chapter 3).

4.3. AMIDE H/D EXCHANGE IN THE NATIVE STATE UNDER AMYLOIDOGENIC CONDITIONS

To investigate in more detail the changes in conformational stability and cooperativity of the Spc-SH3 variants and their relationship with the amyloid fibril formation, we analyzed the H/D exchange of the N47A mutant and the WT Spc-SH3 under conditions

approaching those of fibrillation but avoiding aggregation during the experiments as described in Section 4.1. The H/D exchange kinetics was measured for each variant by NMR at 30 ºC in the presence of 100 mM NaCl (Figure 4.2a) and 200 mM NaCl (Figure 4.2b). In all cases studied the H/D exchange process occurred in all residues with exponential decays of proton occupancies within less than one day. The data were analyzed assuming an EX2 mechanism of exchange to calculate the apparent Gibbs energies of exchange per residue (ΔG_{ex}), as described elsewhere [4]. The Gibbs energy changes of global unfolding (ΔG_u) (Table 4.1) have been represented in Figures 4.2 for comparison's sake.

We also represented the most protected residues against exchange on a schematic drawing of the native Spc-SH3 structure to obtain a direct observation of the differences between the two variants when the exchange Gibbs energy was compared with the ΔG_u global obtained by DSC under the same conditions (Figure 4.3 and Figure 4.4).

There is significant variability in the values of the apparent Gibbs energies of exchange, ΔG_{ex}, along the polypeptide chain for both protein variants. The exchange profiles are similar for both variants under each concentration of salt, consistent with the similar stability of the two variants.

The most protected regions are mainly coincident with the secondary structures, whereas the N- and C-terminal ends and the different loops show less protection. In particular, residues 1-8 at the N-terminus and residues 47 and 48 the distal turn exchanged completely within the dead time of the experiment for both protein variants.

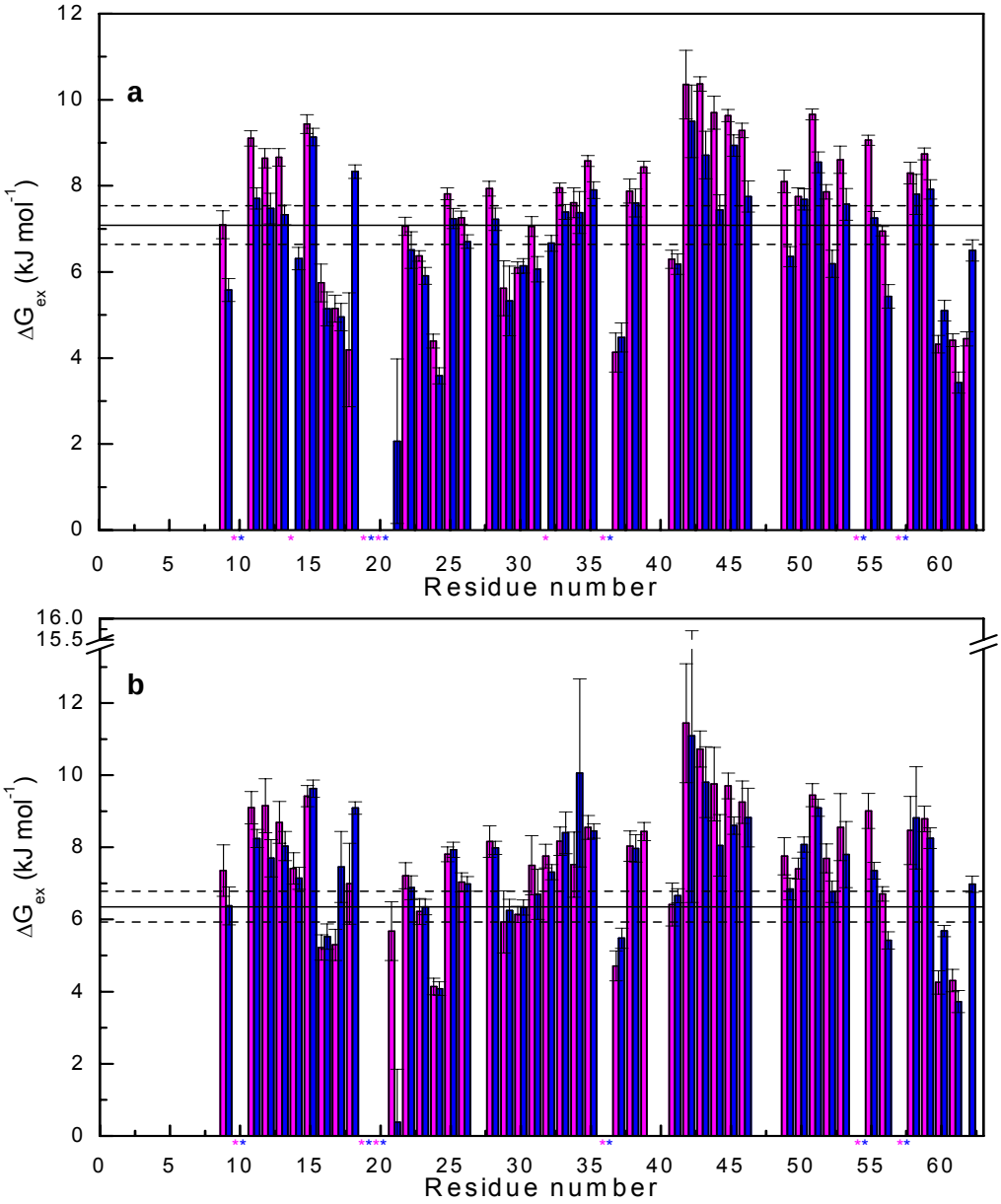

Figure 4.2. *Histogram plot showing the apparent Gibbs energies of exchange per residue of N47A and WT Spc-SH3 at 1 mg/mL, 100 mM Gly and a) 100 mM NaCl and b) 200 mM NaCl at 30 ºC. N47A mutant at pH 3.20, magenta. WT variant at pH 2.78, blue. The estimated errors of these quantities are represented above each bar. The global unfolding Gibbs energy at 30 ºC is indicated by a horizontal continues line and the estimated errors are represented in dashed lines. The missing bars marked with asterisk correspond to residues for which H/D exchange could not be measured, either because they are proline residues or because they are overlapping in the spectrum. The rest of the bars not shown correspond to residues for which the exchange occurred during the dead time of the experiment.*

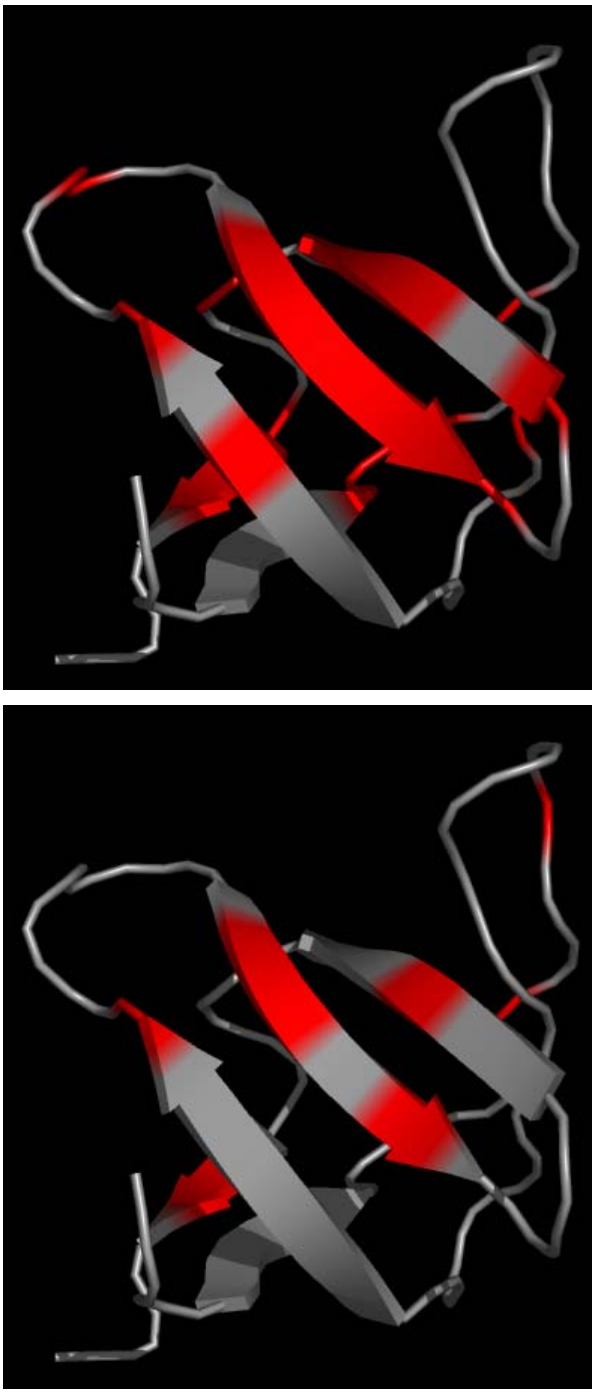

Figure 4.3. *Schematic ribbon representations of the protein native structure showing in red colour residues with Gibbs energies of H/D exchange higher than the global unfolding Gibbs energy obtained by DSC under the same experimental conditions, i.e, 100 mM NaCl, 100 mM Gly and 30 ºC. a, N47A mutant at pH 3.20 and b, WT variant at pH 2,78.*

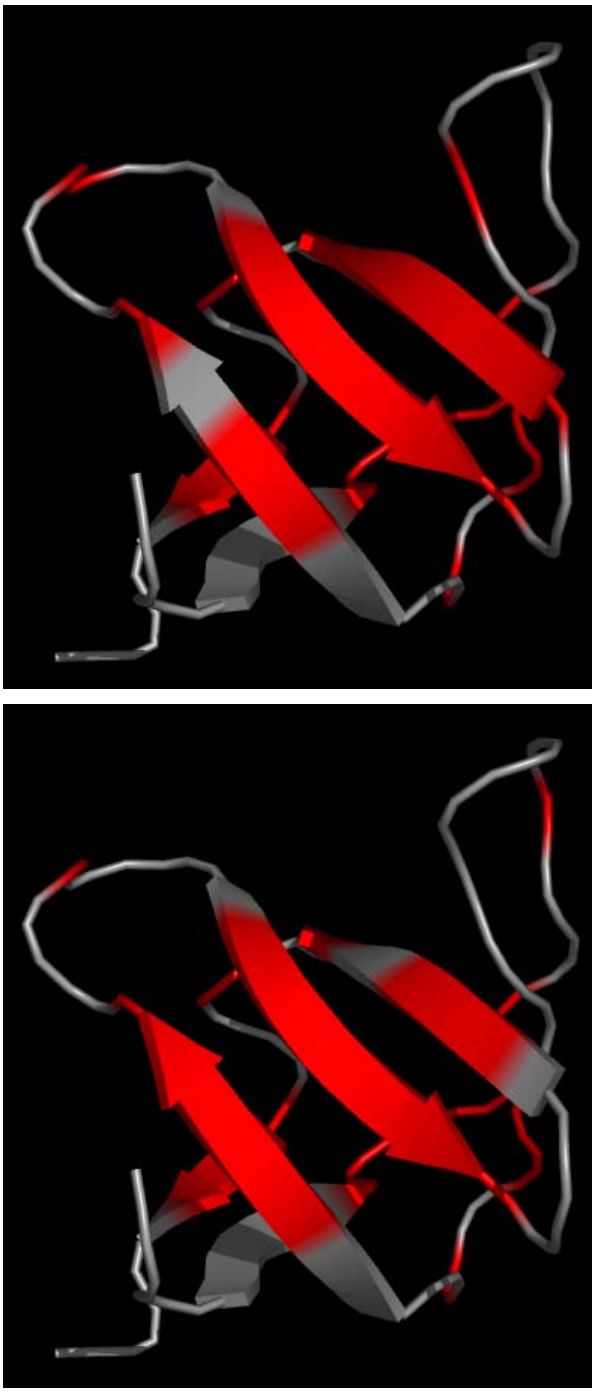

Figure 4.4. *Schematic ribbon representations of the protein native structure showing in red colour residues with Gibbs energies of H/D exchange higher than the global unfolding Gibbs energy obtained by DSC under the same experimental conditions, i.e, 200 mM NaCl, 100 mM Gly and 30 ºC. a, N47A mutant at pH 3.20 and b, WT variant at pH 2,78.*

Remarkably, for a significant number of residues the apparent Gibbs energies of exchange are clearly higher than the global unfolding Gibbs energy, ΔG_u. This effect is more evident for the N47A mutant than for the WT form at 100 mM NaCl and becomes even more pronounced at 200 mM NaCl for both domain variants. Most super protected residues are grouped in the secondary structure elements, except for some of them located at the RT loop and n-src loop (Figure 4.3 and 4.4).

This superprotection against H/D exchange of considerable areas of the polypeptide chain has not been observed in our previous studies of H/D exchange of Spc-SH3 under similar conditions but in the absence of NaCl, where amyloid formation is very slow [2-4].

The differences in the Gibbs energies of exchange ($\Delta\Delta G_{ex}$) per residue between each pair of domains are relatively small under the two conditions studied and many of these differences do not exceed the uncertainty in the measurements (Figure 4.6). Nevertheless, at 100 mM NaCl, groups of residues at the β-strands 1, 3 and 4 and the 3_{10} helix show significant increases in ΔG_{ex} of more than 1 kJ/mol for the N47A mutant relative to the WT form. At 200 mM NaCl the differences are more homogeneous but smaller in magnitude despite few residues, which show higher $\Delta\Delta G_{ex}$ values but they are affected by great errors.

These results suggest that the N47A mutation has a relatively small but significant impact on the distribution of conformational states in the native-state ensemble under conditions of equal overall stability.

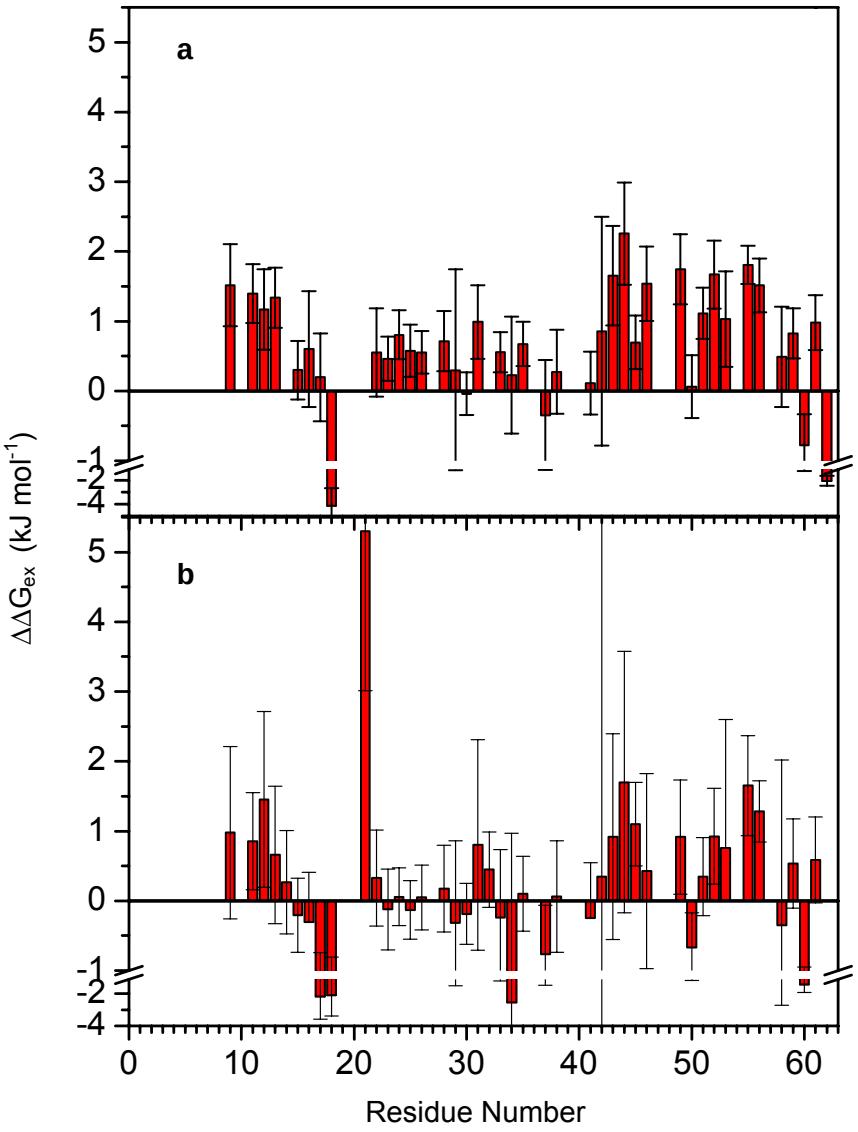

Figure 4.6. *Effect of the mutation N47A on the apparent Gibbs energies of H/D exchange ($\Delta\Delta G_{ex}$) measured by NMR under the same conditions indicated in Figure 4.2. a, differences at 100 mM NaCl and b, differences at 200 mM NaCl. Error bars correspond to the sum of the uncertainties in the ΔG_{ex} values for each mutant.*

4.4. DISCUSSION

In this study we have compared the effect of amyloidogenic factors, i.e. the N47A mutation and the increase in NaCl concentration, upon the native state conformational dynamics and cooperativity of the Spc-SH3 domain

NMR chemical shift analysis clearly indicates that the N47A mutation does not produce significant changes in the solution structure of the SH3 domain, consistently with previous data [5], which confirms further that structural distortion of the native state structure is not the cause of amyloid aggregation.

Under our experimental conditions, the H/D exchange of the N47A and WT variants has allowed us mapping the regions of the domain that are either largely unstructured or involved in local unfolding, as well as those regions protected against exchange by persistent native structure. Overall, the H/D exchange profiles of protection are consistent with previous analyses in the absence of NaCl [2-4] and indicate a remarkable structural cooperativity in the Spc-SH3 domain under the experimental conditions studied [5,6]. Our results here support the proposal that native-state H/D exchange in Spc-SH3 occurs via a wide distribution of conformational fluctuations extending even above the transition state barrier of folding [7].

The similarity in the ΔG_{ex} profiles between the two variants indicates that the amyloidogenic mutation has a relatively low impact on the structural cooperativity of the domain and does not produce any important increase in the population of specific partially unfolded species that may be amyloidogenic. This is in contrast with the results obtained with human lysozyme amyloidogenic pathogenic mutants [8], for which the reduction in global cooperativity produced by the mutations results in an increased population of transiently, partly unfolded intermediates that trigger the aggregation process.

In contrast to our previous studies, the N47A mutation and presence of a moderate NaCl concentration have favoured for many residues to have ΔG_{ex} values higher than the global unfolding Gibbs energy, ΔG_u. This situation, usually called super protection, has often been attributed to the presence of residual structure in the unfolded ensemble [9, 10, 11]. The term residual structure needs not to be related to any specific stable structure but rather to an ensemble of transient and dynamic structures that may impair solvent accessibility to amide protons.

The existence of compact denatured states involving both native-like and non-native dynamic interactions has been described for the drkN-SH3 domain [12]. Also, the amyloid-forming, acid-denatured state of the PI3-SH3 has been found by pulsed-gradient NMR methods to be significantly more compact than the GdnHCl-denatured state and, moreover, the presence of moderate concentrations of salts decreased even further the apparent hydrodynamic radius [13]. A more recent NMR study of the acid-denatured conformational ensemble of the PI3-SH3 domain under amyloidogenic conditions has reported reduced mobility for several regions corresponding to some of the β-strands and the RT loop, which appear to be involved in non-native long-range interactions [14].

It is possible therefore that the amyloidogenic factors analyzed here could be favouring a more compact conformation of the unfolded ensemble of the Spc-SH3 domain that may be more prone to intermolecular association. In fact, Radford and coworkers have recently shown that the amyloid aggregation of β-microglobulin at acid pH is determined by a competition between intra- and intermolecular interactions mediated by residual structure at the acid-denatured state [15]. Reduced hen lysozyme also has a residual structure involving long-range interactions, which affect amyloid formation [16] and, similarly, several recombinant human lambda6 immunoglobulin light

chains have shown a relationship between residual structure in a highly denatured state at pH 2 and amyloid aggregation propensity [17].

The results presented here support our discussion of Chapter 3, in which we hypothesized that salts may favour aggregation by altering the energy landscape of the protein due to its effects upon the hydration of the protein groups.

4.5. BIBLIOGRAPHY

[1] Luque, I., Leavitt, S.A. and Freire, E. (2002). The linkage between protein folding and functional cooperativity: two sides of the same coin? Annu Rev Biophys Biomol Struct 31, 235-56.

[2] Sadqi, M., Casares, S., Abril, M.A., Lopez-Mayorga, O., Conejero-Lara, F. and Freire, E. (1999). The native state conformational ensemble of the SH3 domain from alpha-spectrin. Biochemistry 38, 8899-906.

[3] Sadqi, M., Casares, S., Lopez-Mayorga, O. and Conejero-Lara, F. (2002). The temperature dependence of the hydrogen exchange in the SH3 domain of alpha-spectrin. FEBS Lett 527, 86-90.

[4] Sadqi, M., Casares, S., Lopez-Mayorga, O., Martinez, J.C. and Conejero-Lara, F. (2002). pH dependence of the hydrogen exchange in the SH3 domain of alpha-spectrin. FEBS Lett 514, 295-9.

[5] Casares, S., Sadqi, M., Lopez-Mayorga, O., Martinez, J.C. and Conejero-Lara, F. (2003). Structural cooperativity in the SH3 domain studied by site-directed mutagenesis and amide hydrogen exchange. FEBS Lett 539, 125-30.

[6] Casares, S., Lopez-Mayorga, O., Vega, M.C., Camara-Artigas, A. and Conejero-Lara, F. (2007). Cooperative propagation of local stability changes from low-stability and high-stability regions in a SH3 domain. Proteins 67, 531-47.

[7] Parker, M.J. and Marqusee, S. (2000). A statistical appraisal of native state hydrogen exchange data: evidence for a burst phase continuum? J Mol Biol 300, 1361-75.

[8] Dumoulin, M. et al. (2005). Reduced global cooperativity is a common feature underlying the amyloidogenicity of pathogenic lysozyme mutations. J Mol Biol 346, 773-88.

[9] Grantcharova, V.P. and Baker, D. (1997). Folding dynamics of the src SH3 domain. Biochemistry 36, 15685-92.

[10] Neira, J.L., Sevilla, P., Menendez, M., Bruix, M. and Rico, M. (1999). Hydrogen exchange in ribonuclease A and

ribonuclease S: evidence for residual structure in the unfolded state under native conditions. J Mol Biol 285, 627-43.

[11] Liang, X., Lee, G.I. and Van Doren, S.R. (2006). Partially unfolded forms and non-two-state folding of a beta-sandwich: FHA domain from Arabidopsis receptor kinase-associated protein phosphatase. J Mol Biol 364, 225-40.

[12] Marsh, J.A., Neale, C., Jack, F.E., Choy, W.Y., Lee, A.Y., Crowhurst, K.A. and Forman-Kay, J.D. (2007). Improved structural characterizations of the drkN SH3 domain unfolded state suggest a compact ensemble with native-like and non-native structure. J Mol Biol 367, 1494-510.

[13] Zurdo, J., Guijarro, J.I., Jimenez, J.L., Saibil, H.R. and Dobson, C.M. (2001). Dependence on solution conditions of aggregation and amyloid formation by an SH3 domain. J Mol Biol 311, 325-40.

[14] Ahn, H.C., Le, Y.T., Nagchowdhuri, P.S., Derose, E.F., Putnam-Evans, C., London, R.E., Markley, J.L. and Lim, K.H. (2006). NMR characterizations of an amyloidogenic conformational ensemble of the PI3K SH3 domain. Protein Sci 15, 2552-7.

[15] Routledge, K.E., Tartaglia, G.G., Platt, G.W., Vendruscolo, M. and Radford, S.E. (2009). Competition between intramolecular and intermolecular interactions in an amyloid-forming protein. J Mol Biol 389, 776-86.

[16] Ohkuri, T., Yasumatsu, K., Shigemura, N., Yoshida, R. and Ninomiya, Y. (2006). Amiloride inhibition on NaCl responses of the chorda tympani nerve in two 129 substrains of mice, 129P3/J and 129X1/SvJ. Chem Senses 31, 565-72.

[17] Mishima, T., Ohkuri, T., Monji, A., Kanemaru, T., Abe, Y. and Ueda, T. (2009). Residual structures in the acid-unfolded states of Vlambda6 proteins affect amyloid fibrillation. J Mol Biol 392, 1033-43.

5.

DETECTION OF EARLY FOLDING INTERMEDIATES THAT MAY BE AMYLOIDOGENIC

5. DETECTION OF EARLY FOLDING INTERMEDIATES THAT MAY BE AMYLOIDOGENIC

It is widely accepted that amyloid fibril formation requires the accumulation of a critical concentration of partially folded protein species [1]. These protein states are usually favoured by mutations or environmental conditions that destabilize the native state, such as for instance, extreme pH, high ionic strength, high temperature, moderate concentration of denaturant agents or organic solvents, etc. These factors have been described to act by decreasing the structural cooperativity of the native structure and favouring the critical states in the amyloid fibril formation [2], [3].

In spite of this, we have shown in previous Chapters that the amyloidogenic effect of the N47A is neither related to its destabilizing effect upon the native state or to any significant decrease in the cooperativity of the SH3 structure that may result in an increase of the population of amyloidogenic states under equilibrium conditions. We have shown however that the amyloidogenic mutation and the environmental conditions that favour fibrillation increase the rate of conformational events that lead to oligomerization and fibril nucleation and these events seem to be crucial in determining the amyloid formation cascade.

We questioned ourselves if the precursor states of fibrillation were only transiently populated or if their population was too low so that they were silent under the conditions investigated so far.

The folding and unfolding of the WT Spc-SH3 domain and many mutant variants was extensively studied in the past under low ionic strength conditions [4], [5], [6]. The process was described as a two-state process following first-order kinetics without any significantly populated intermediate states. We decided to investigate if the N47A mutation and/or the presence of moderate concentrations of salt

induced the accumulation of partially folded forms that may be amyloidogenic. With this aim we analyzed the equilibrium and kinetic folding and unfolding processes of both the WT Spc-SH3 domain and the N47A mutant under the conditions that favoured amyloid aggregation. This study was carried out in collaboration with Prof. André Matagne in the Center of Protein Engineering of the University of Liege (Belgium).

5.1. EQUILIBRIUM FLUORESCENCE STUDIES TO DETECT INTERMEDIATE STATES

To elucidate whether partially folded species may become populated under equilibrium by effect of the N47A mutation, we carried out equilibrium urea unfolding experiments of the two Spc-SH3 domain variants in the presence of 25 μM ANS following simultaneously both the intrinsic tryptophan (Figure 5.1a) and the ANS fluorescence signals (Figure 5.1b). To avoid fibrillation during the experiments the protein concentration was kept low (0.2 mg mL^{-1}) in the samples. The experiments were conducted at 37 ºC under conditions were both variants have identical stability (see Chapter 2 and [7]), i.e., 100 mM NaCl, 100 mM Gly, pH 2.78 for WT and 3.20 for N47A.

The unfolding profiles monitored by intrinsic Trp fluorescence did not show any significant difference, with very similar $[urea]_{1/2}$, for the two variants. In the case of the unfolding profiles followed by ANS fluorescence, there was a slight increase in ANS fluorescence at low urea concentrations for the N47A mutant relative to the WT, but the data were not very conclusive because the fluorescence signal was very low in these measurmements. This indicates that under equilibrium at 37 ºC the population of partially folded species is very low for both variants.

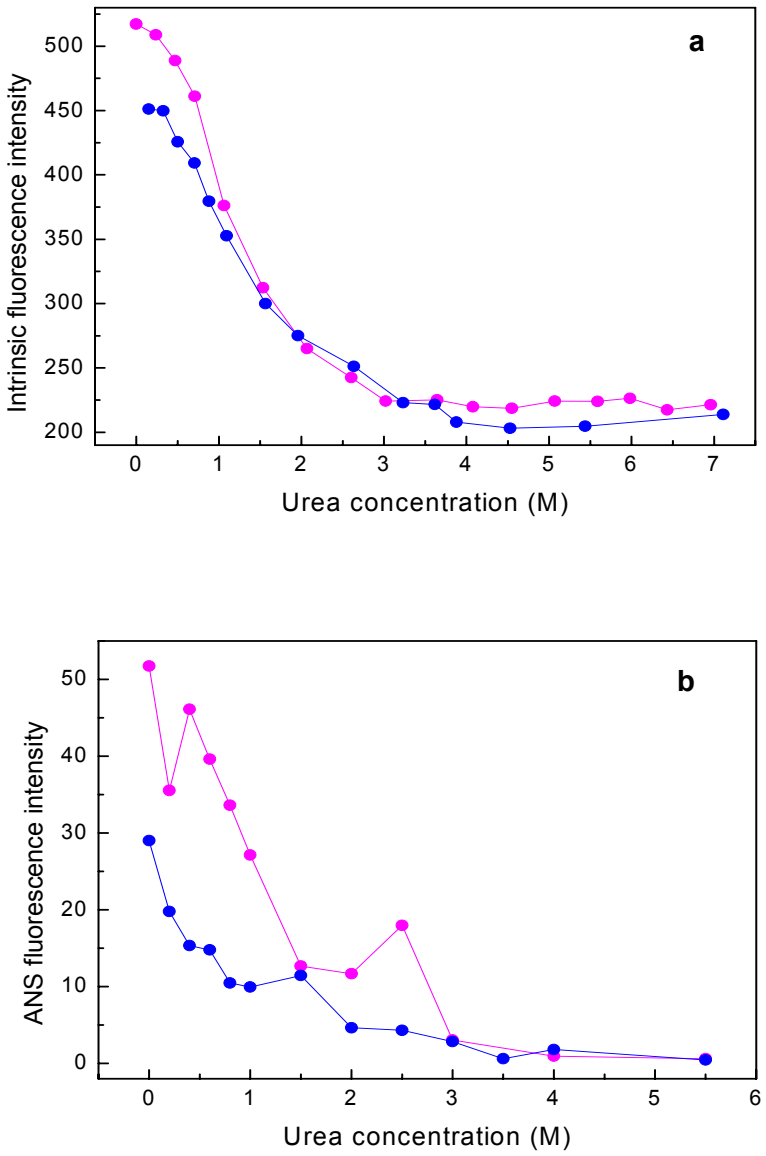

Figure 5.1. *Equilibrium urea unfolding of WT (blue) and N47A (magenta) at 37 ºC in 100 mM glycine buffer, 100 mM NaCl, pH 2.78 and pH 3.20 respectively. The protein concentration was 0.2 mg* mL^{-1} *in both cases. (a) Intrinsic Trp fluorescence; (b) ANS Fluorescence.*

We also made thermal unfolding experiments following intrinsic tryptophan fluorescence and ANS fluorescence at the same time using different protein concentrations and different NaCl concentrations. The buffer conditions were 100 mM glycine, 25 μM ANS at pH 3.20 for N47A and 2.78 for WT, (Figure 5.2).

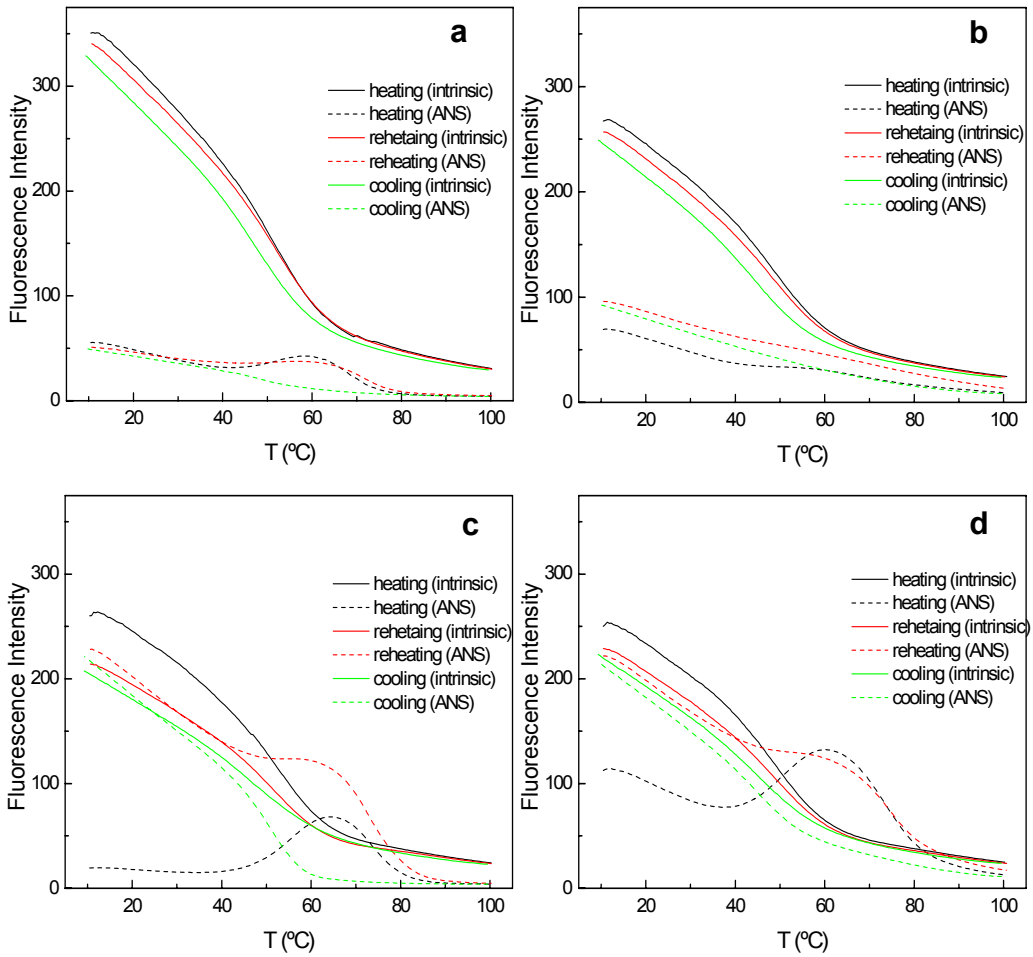

Figure 5.2. *Thermal unfolding profiles monitored by intrinsic Trp fluorescence and ANS fluorescence. a) and b) represent N47A and WT respectively at 100 mM NaCl and at a concentration of protein of 0.8 mg mL^{-1}. c) and d) represent N47A and WT respectively at 200 mM NaCl and at a concentration of protein of 0.6 mg mL^{-1}.*

In the presence of 100 mM NaCl, the unfolding profiles followed by intrinsic Trp fluorescence showed a single reversible transition with a Tm value similar to that measured by DSC, indicating that the majority of the protein unfolds and refolds in a two-state transition. In contrast, the thermal unfolding profiles followed by ANS fluorescence showed a small but significant signal increase at intermediate temperatures, with a maximum around 60 ºC. This effect was considerably more pronounced for the N47A mutant relative to the WT form. These increases in ANS fluorescence indicate the formation a small population of partially-unfolded species at intermediate temperatures during the heating. Interestingly, the enhancement did not occur during the cooling indicating that the partially-unfolded species cannot not be efficiently formed from the unfolded protein.

At higher salt concentration (200 mM) the increase in ANS fluorescence at intermediate temperatures was strongly enhanced for both variants and shifted to higher temperatures but the thermal unfolding and refolding followed by intrinsic fluorescence were not completely reversible, indicating that, even at this low protein concentration (0.6 mg mL^{-1}), the higher salt concentration could have favoured partial aggregation of the protein.

Once again, the partially-unfolded species did not form during the cooling, suggesting that these species are not kinetically accessible from the unfolded state within the time scale of these experiments.

These results indicate that the factors favouring amyloid formation, i.e., the N47A mutation and the increase in salt concentration, also enhance the transient accumulation of partially unfolded species during the thermal unfolding of the native protein. This suggests an implication of these species in the amyloid cascade for the Spc-SH3 domain.

5.2. FOLDING AND UNFOLDING KINETICS OF THE N47A MUTANT

On the basis of our previous observations we hypothesized that the transient formation of partially-folded species favoured by amyloidogenic factors may become reflected in the folding or unfolding kinetics and, if these species were prone to associate intermolecularly as we have observed before, there would be a significant effect of protein concentration on the kinetics.

To investigate this effect we used stopped-flow fluorescence to reinvestigate the folding and unfolding kinetics of WT Spc-SH3 and the N47A mutant under the buffer conditions that induced amyloid formation.

Initially, the folding-unfolding kinetics of the N47A mutant were studied at 4 different protein concentrations under the same experimental conditions (Figure 5.3).

The kinetics fitted quite well to single-exponential functions (Table 5.1), except for small deviations during the first 100 ms. A small increase with the protein concentration was observed in the rate constant of unfolding , whereas the folding rate constant changed only slightly.

Nevertheless, a closer look to the folding and unfolding kinetics indicates significant deviation from two-state behaviour. According to the two-state folding model, the ratio between the folding and the unfolding amplitudes should be close to 1 and the signal level at time zero in each kinetic trace should be approximately coincident with that of the end point of the other. The amplitude ratio was however significantly higher than 1 and increased with the protein concentration. In addition, the fluorescence intensity level at time zero in the unfolding kinetics (Figure 5.3, black) was considerably lower than that of the end point of the folding trace corresponding to the

native protein (Figure 5.3, red). These effects are incompatible with a two-state folding-unfolding process and suggest that there may be an accumulation of partially folded states during the dead time of the unfolding kinetics.

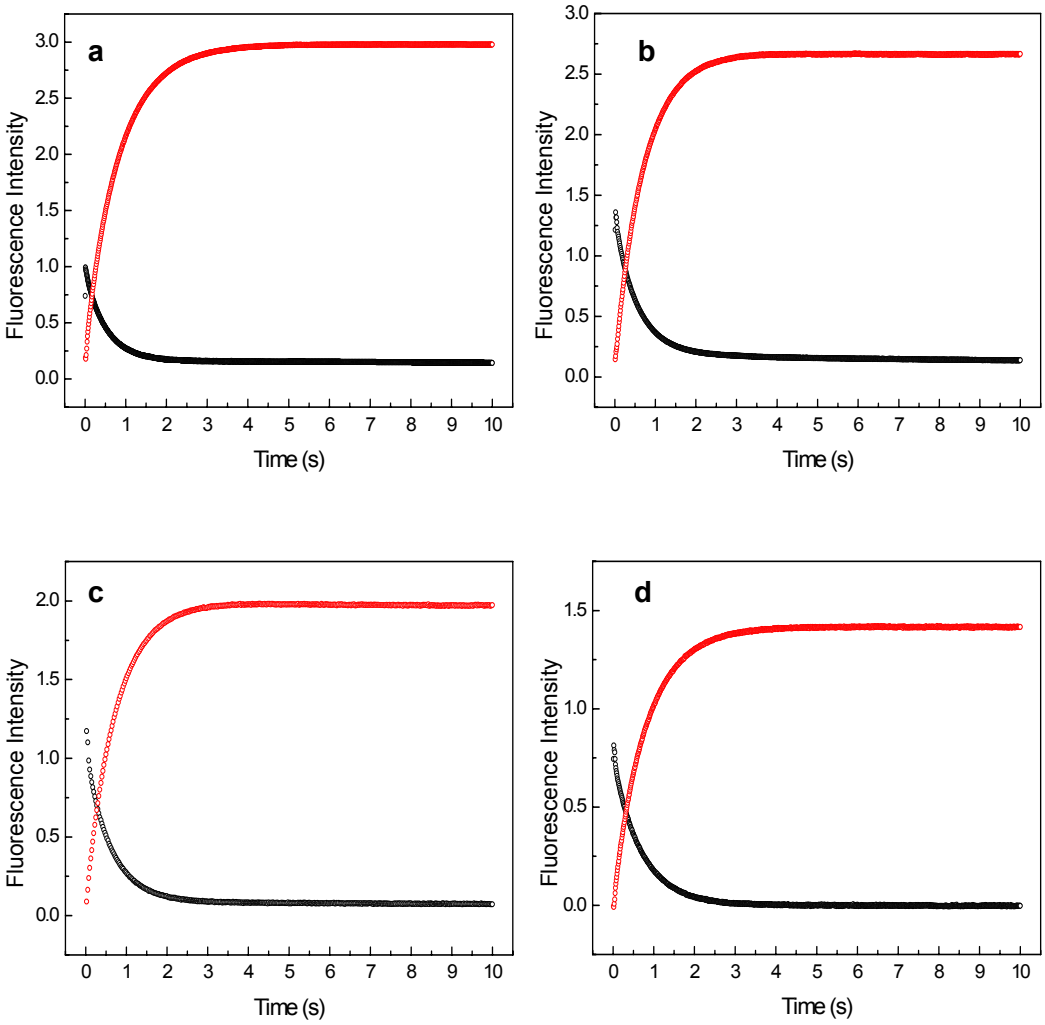

***Figure 5.3**. Folding (from 6 M to 0.55 M urea, red) and unfolding (from 0 M to 5.45 M urea, black) kinetics of N47A Spc-SH3 at 25 ºC at different protein concentrations: a) 1 mg mL^{-1}, b) 0.35 mg mL^{-1}, c) 0.1 mg mL^{-1} and d) 0.02 mg mL^{-1}.*

Table 5.1. *Kinetic parameters derived from fittings to single-exponential functions of the curves represented in Figure 5.3.*

Concentration (mg/mL)	$k_{\ddagger\text{-U,urea}}$ (s^{-1})	Folding amplitude	$k_{\ddagger\text{-N,urea}}$ (s^{-1})	Unfolding amplitude	Amplitude ratio
1.00	1.25±0.01	2.77±0.01	1.85±0.02	0.81±0.01	3.42
0.35	1.43±0.01	2.59±0.01	1.67±0.02	1.15±0.01	2.25
0.10	1.43±0.02	1.94±0.01	1.71±0.02	1.02±0.01	1.90
0.02	1.27±0.02	1.42±0.01	1.57±0.02	0.77±0.01	1.84

We also analyzed the folding and unfolding kinetics for both the WT and N47A Spc-SH3 variants over a wide range of urea concentrations under the same stability conditions using a protein concentration of 0.15 mg mL^{-1} (Figure 5.4). The kinetics fitted well to single-exponential functions for both variants and the chevron plots complied well with the two-state unfolding model (Table 5.2).

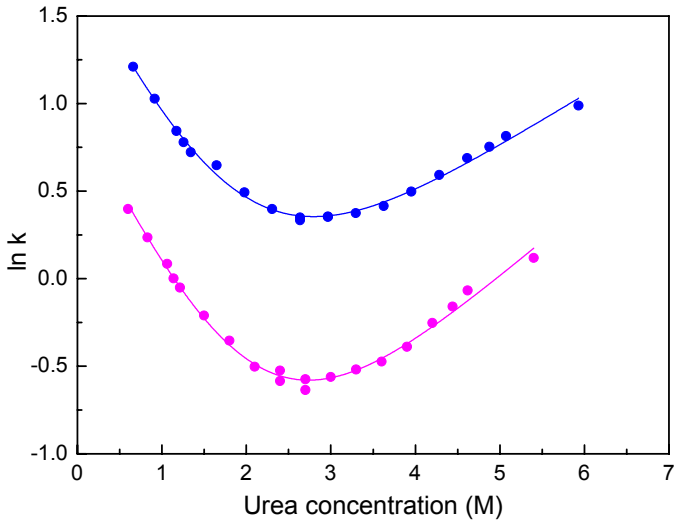

Figure 5.4. *Chevron plots for the folding and unfolding kinetics of the WT (blue) and N47A (magenta) Spc-SH3 variants with 100 mM NaCl at 25 ºC under conditions of identical stability (pH 2.78 and 3.20 respectively). The protein concentration used was 0.15 mg mL^{-1} in all experiments. The lines correspond to the best fit according to the two-state model.*

Table 5.2. *Kinetic and thermodynamic parameters of the folding and unfolding of WT and N47A Spc-SH3 under amyloidogenic conditions.*

Variant	Conditions	$k^{\neq-U}$ (s^{-1})	$k^{\neq-N}$ (s^{-1})	$m^{\neq-U}$ (M^{-1})	$m^{\neq-N}$ (M^{-1})	$[urea]_{1/2}$ (M)
N47A	100 mM NaCl, pH 3.20, 25 ºC	2.47±0.11	0.13±0.02	–0.99±0.06	0.41±0.03	2.1±0.3
WT	100 mM NaCl, 2.78, 25 ºC	5.38±0.24	0.48±0.04	–1.00±0.05	0.30±0.02	1.9±0.2
N47A	200 mM NaCl, pH 3.20, 25 ºC	3.3±0.3	0.12±0.03	-0.92±0.09	0.43±0.05	2.5±0.6
N47A[a]	100 mM NaCl, pH 3.20, 37 ºC	4.3±0.5	1.1±0.12	-1.23±0.23	0.23±0.03	1.0±0.4

[a] These parameters correspond to the analysis of the rate constants of the major kinetic phase.

Figure 5.5 represents the dependence of the amplitudes of the kinetics with the concentration of urea as compared with the predictions of the two-state model. For the N47A mutant the amplitudes of unfolding are markedly decreased (about 30%) compared to those of folding. This confirms a clear deviation from the two-state model since the amount of native protein at the start of the unfolding reaction seemed smaller than the amount of unfolded protein that folds into native. In the case of the WT Spc-SH3 the decrease in the amplitudes of the unfolding traces is smaller, indicating a less pronounced deviation from two-state behaviour.

These results indicate that the N47A mutant is accumulating intermediate states different from the native and the unfolded states, which appear to be only accessible from the native state. These states appear to be silent in the standard kinetic experiments detected by intrinsic Trp fluorescence, since the kinetic traces fit well to single exponential decays and the chevron plots do not show any apparent deviation from the shape predicted by the two-state model.

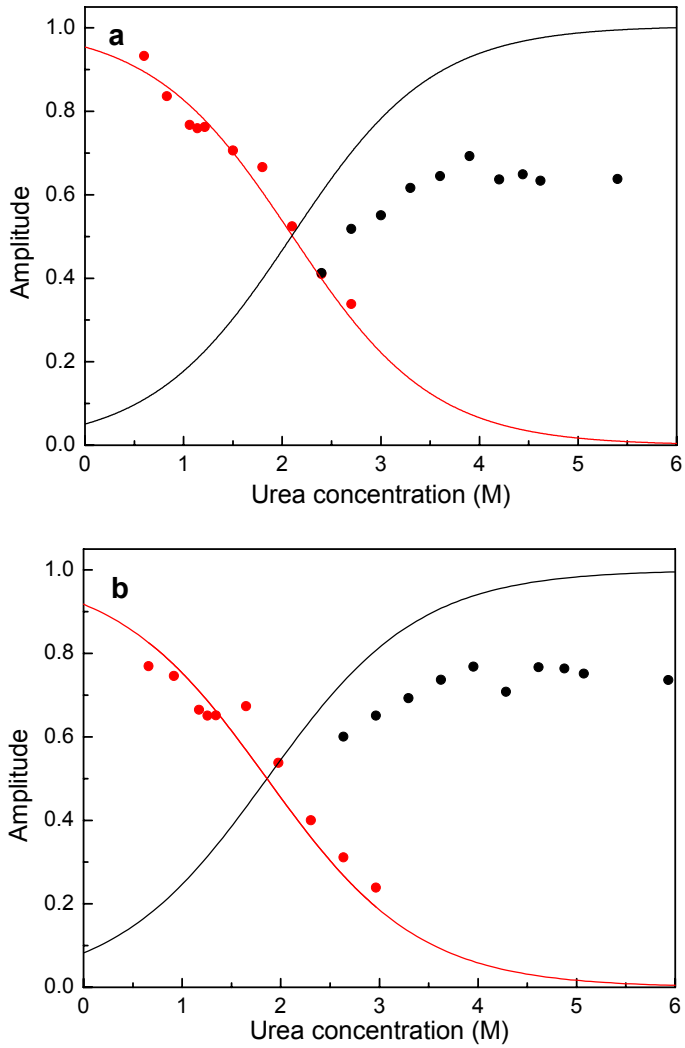

Figure 5.5. *Relative amplitudes of the folding and the unfolding kinetics of the N47A (a) and the WT (b) Spc-SH3 variants under the experimental conditions of Figure 5.4. The solid lines correspond to the predictions of the two-state model. In red, data of the refolding curves; in black, data of the unfolding curves.*

Once we obtained clear evidence of the presence of intermediate states during the unfolding kinetics of the N47A mutant, we tried to establish if these species are related to the enhanced propensity of the N47A mutant to amyloid fibril formation. We made additional folding and unfolding experiments under conditions that accelerate fibrillation,

i.e., a higher temperature of 37 ºC (Figure 5.6a) and a higher salt concentration of 200 mM (Figure 5.6b). These experiments were performed at low protein concentration to avoid significant aggregation during the kinetics.

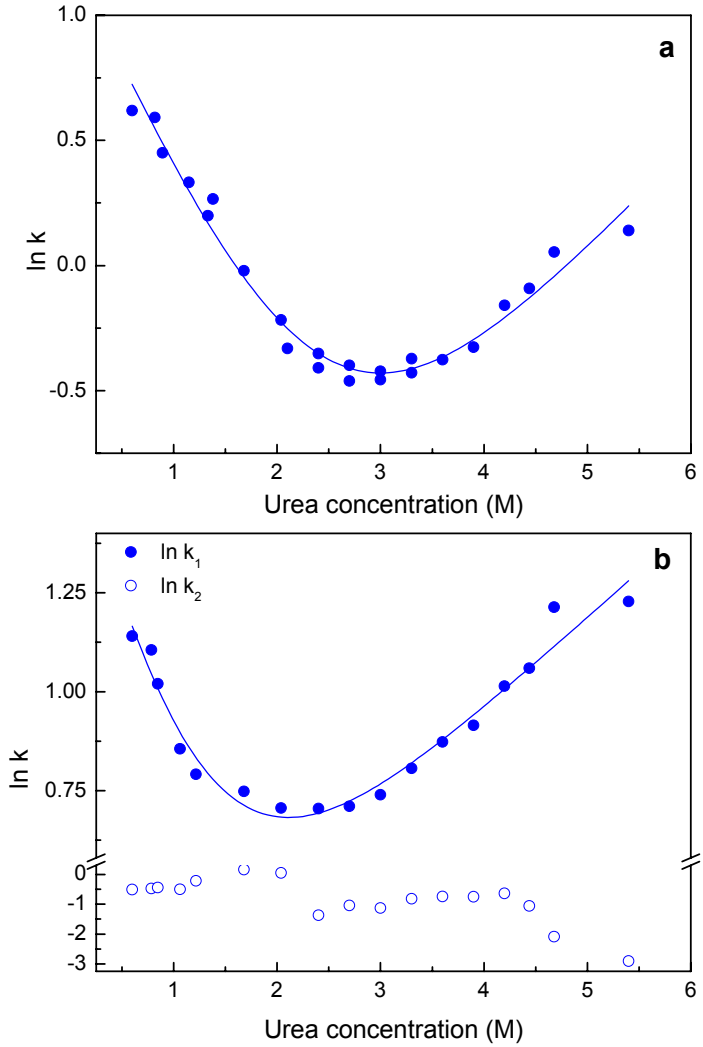

Figure 5.6. *Chevron plots for the folding and unfolding kinetics of the N47A Spc-SH3 mutant at 25 ºC in the presence of 200 mM NaCl (a) and at 37 ºC in the presence of 100 mM NaCl (b). The lines correspond to the best fit according to the two-state model. Protein concentration was 0.15 mg mL^{-1} in both cases and pH was 3.20. In panel b, the kinetic traces were fitted to a double exponential decay and only the data corresponding to the first exponential (filled circles) were fitted to a two-state model.*

In the presence of 200 mM NaCl at 25 ºC, the kinetics could also be well described by single exponential decays and the chevron plots were in apparent agreement with two-state behaviour (Figure 5.6a and Table 5.2) but the amplitudes of the unfolding traces decreased even more pronouncedly than at 100 mM NaCl (Figure 5.7a), indicating that the increase in salt concentration favours the early accumulation of partially unfolded species during the dead time of the unfolding kinetics.

Interestingly, both the folding and unfolding kinetics recorded at 37 ºC could only be fitted using a two exponential decay function. The chevron plot of the rate constants of the fast phase complied well with the V-shape expected for two-state folding (Figure 5.6b) and the amplitudes of this phase accounted for most part of the total amplitudes of the kinetics (see Figure 5.7b). This indicates that the fast phase corresponds to the folding and unfolding process of the majority of the protein. Nevertheless, as observed for the other conditions, the amplitudes of the unfolding traces were considerably smaller than that of the folding traces, due the presence of a burst phase.

The rate constants of the slow phase do not follow a V-shape in the chevron plot, suggesting a non-cooperative character for this event. This slow phase may be related to slow proline cis-trans isomerisation, as it has been described elsewhere [8], but we cannot discard from these data a different origin. The amplitude of the slow phase is very small, except at intermediate urea concentrations, where it is quite significant.

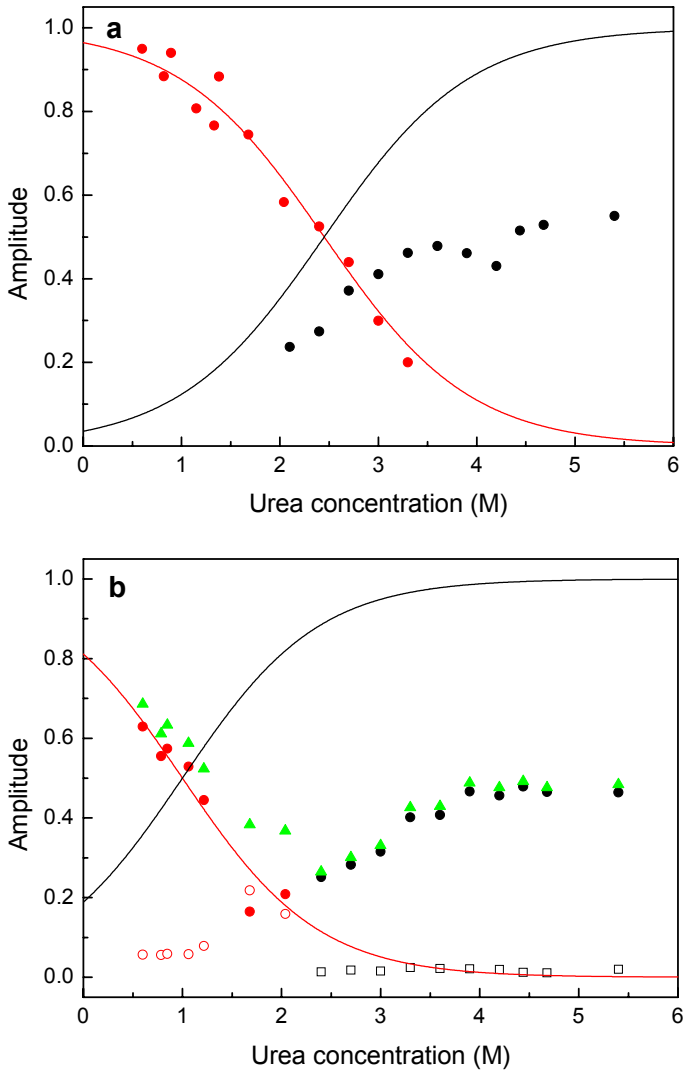

Figure 5.7. *Normalized amplitudes of the folding and unfolding kinetics of the N47A Spc-SH3 mutant at 200 mM NaCl at 25 ºC (a) and at 100 mM NaCl at 37 ºC (b). The solid lines correspond to the predictions of the two-state model. Protein concentration was 0.15 mg mL^{-1} in both cases and the pH was 3.20. In red, data of the refolding curves; in black, data of the unfolding curves. In panel b, filled symbols correspond to the amplitude of the first phase in the double exponential decay and open symbol correspond to that of the second phase. Green symbols corresponds to the sum of both amplitudes.*

These results confirm that the conditions that accelerate amyloid fibril formation augment the population of intermediate states during the dead time of the unfolding kinetics, which gives clear evidence of the relationship between these species and the trigger of the amyloid fibril formation.

5.3. FOLDING-UNFOLDING KINETICS IN THE PRESENCE OF ANS

The evidence obtained so far about the presence of partially-folded species accumulated during the dead time in the unfolding kinetics comes from deviations of the relative amplitudes of the kinetic traces from the predictions of the two-state folding-unfolding model. To attempt to directly detect these species, we acquired the folding and unfolding kinetics at 25 ºC in the presence of ANS by monitoring simultaneously the fluorescence of the dye and the intrinsic Trp fluorescence. To explore if the presence of ANS was affecting somehow the folding and unfolding kinetics, we repeated the experiments at three different ANS concentrations (30, 50 and 150 μM) (not shown) and compared the data with the kinetics obtained previously in the absence of ANS at the same urea concentrations. In these experiments we compared the N47A and the WT variants under identical stability conditions, i.e, 100 mM Glycine, 100 mM NaCl, pH 3.2 for N47A and pH 2.78 for WT.

Figure 5.8a and 5.8b shows some examples of the several kinetic traces obtained in the presence of 50 μM of ANS. It is interesting that the folding curves detected by ANS fluorescence show negligible amplitude, consistently with the absence of partially folded species during the folding process. In contrast, the unfolding curves showed a considerable ANS fluorescence decrease corresponding to the unfolding of species formed during the dead time of the kinetics.

We fitted the all curves to single exponential functions to obtain the kinetic parameters (Table 5.3).

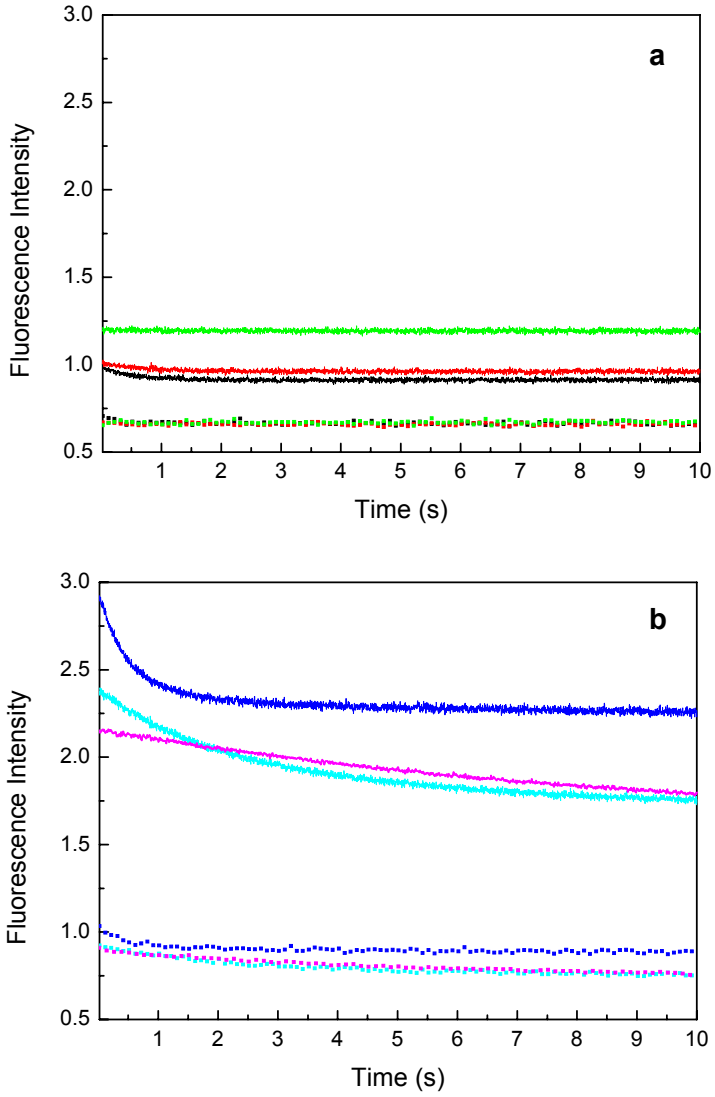

Figure 5.8. *Folding (a) and unfolding (b) kinetics measured by fluorescence of ANS at 485 nm for the N47A mutant (lines) and the WT Spc-SH3 (dots) at 25 ºC at 0.2 mg mL^{-1} in the presence of 50 μM ANS. The folding experiments were made at 0.6 M urea (black), 1.3 M urea (red) and 2.7 M urea (green). The unfolding experiments were made at 5.3 M urea (blue), 3.8 M urea (cyan) and 2.9 M urea (magenta).*

Table 5.3. *Kinetic parameters derived from fittings to single-exponential functions of the folding and unfolding kinetics of the WT and N47A variants followed by intrinsic fluorescence (k_{int}) at different ANS concentrations and followed by ANS fluorescence (k_{ANS}) in the case of the unfolding.*

Variant	Kinetic Process	Urea concentration (M)	ANS concentration (μM)	ln k_{int},	ln k_{ANS}
N47A	Folding	0.6	0	0.50	--
			30	0.56	--
			50	0.55	--
			150	0.59	--
		1.3	0	0.33	--
			30	0.31	--
			50	0.31	--
			150	0.36	--
		2.7	0	-0.22	--
			30	-0.34	--
			50	-0.31	--
			150	-0.31	--
	Unfolding	5.3	0	0.41	--
			30	0.46	0.33
			50	0.44	0.28
			150	0.47	0.29
		3.8	0	-0.21	--
			30	-0.14	-0.85
			50	-0.18	-1.10
			150	-0.10	-1.40
		2.9	0	-0.36	--
			30	-0.47	-2.21
			50	-0.46	-2.41
			150	-0.36	-2.53
WT	Holding	0.6	0	1.25	--
			30	1.31	--
			50	1.31	--
			150	1.36	--
		1.3	0	1.06	--
			30	1.09	--
			50	1.01	--
			150	1.02	--
		2.7	0	0.69	--
			30	0.58	--
			50	0.60	--
			150	0.67	--
	Unfolding	5.3	0	0.98	--
			30	1.02	0.39
			50	1.02	0.20
			150	1.04	0.31
		3.8	0	0.59	--
			30	0.54	-0.97
			50	0.58	-0.99
			150	0.60	-0.99
		2.9	0	0.37	--
			30	0.34	-2.21
			50	0.38	-2.12
			150	0.45	-2.41

The folding and unfolding kinetics of both variants followed by intrinsic Trp fluorescence in the presence of ANS are only slightly higher than those obtained in the absence of this dye and they do not depend on the ANS concentration (Table 5.3). This means that the presence of ANS is not affecting significantly the population distribution of the species present in solution during the experiment timescale.

The unfolding kinetics of the N47A mutant followed by ANS fluorescence corresponds to a process clearly different from the unfolding of the native protein that is observed by intrinsic fluorescence. The rate constants derived from the kinetic unfolding of these species are much lower than those obtained by intrinsic Trp fluorescence. This difference is more pronounced at low urea concentration. In fact, the ANS kinetic curves do not follow a monoexponential decay, by contrast the process seems to be affected by two different decays, the unfolding of the native protein and the unfolding of the intermediate states. We have studied the amplitude contribution of both processes by fitting ANS unfolding kinetics to a two exponential decay fixing the rate constant corresponding to the native protein unfolding as measured by intrinsic Trp fluorescence (Figure 5.9). At high urea concentration the process is dominated by the unfolding of the native protein, but when the urea concentration decreases the unfolding of the intermediate states is dominant.

The data are consistent with a rapid accumulation of ANS-binding species during the dead time of the experiment. These species unfold at much slower rate than the native protein, suggesting that they may constitute a kinetic trap for the unfolding pathway.

The WT protein showed similar results but the ANS intensity and the amplitude of the curves were considerably smaller, indicating a lower population of intermediate states than for the N47A mutant (Figure 5.8b and 5.9). It is interesting that the unfolding rate constants

derived from the ANS fluorescence kinetics are very similar for both variants, indicating that the intermediate species that we are observing in both cases have the same kinetic characteristics.

Accumulation of partially unfolded species is not evident during the folding process since the ANS fluorescence intensity is very small for both variants (Figure 5.8a).

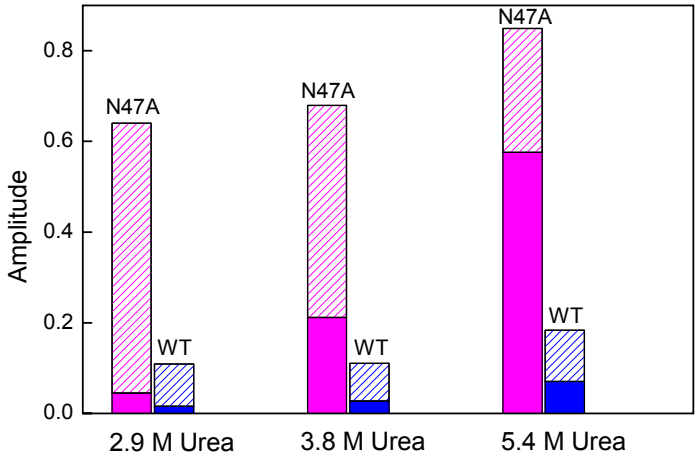

Figure 5.9. *Unfolding amplitudes of a two exponential decay fitting for the N47A and the WT Spc-SH3 variants in the presence of 50 μM ANS at urea concentrations indicated in the figure. In solid colour, the first phase that corresponds to the native species unfolding. In stripped colour, the second phase that corresponds to the unfolding of intermediate states.*

5.4. DISCUSSION

In this work we have tried to elucidate the molecular events that take place during the initial stages of the amyloid fibril formation of the Spc-SH3 domain and the factors that trigger the aggregation cascade. A comparative characterisation of the folding and unfolding kinetics of the N47A and WT Spc-SH3 domains under amyloidogenic conditions has provided evidence of the transient accumulation of partially unfolded species.

Most previous studies have indicated that the Spc-SH3 domain folds and unfolds following a two–state model [4], [5], [6], [9], [10],. However, more recent studies have demonstrated that the process can deviate from two-state behaviour and may involve intermediate states under specific conditions, i.e, high protein concentration [11] or physiological pH and isotonic concentration of salt [12]. Molecular dynamics simulations have also inferred the existence of low-populated intermediates during the folding of Spc-SH3 [13].

Although under conditions favouring amyloid fibril formation the thermal unfolding of the N47A mutant and the WT domain followed by intrinsic fluorescence showed a single two-state reversible transition, ANS fluorescence reveals a small and transient accumulation of partially unfolded species at temperatures around 60 ºC. Trapping intermediates occurring during the thermal unfolding pathway of proteins is in general difficult but has been described for some proteins such as the cardiotoxin-III all-beta-sheet protein [14] and the Bacilus subtilis lipase [15].

The kinetic experiments shown here demonstrate unequivocally that the unfolding process of the amyloidogenic N47A mutant of the Spc-SH3 deviates significantly from the two-state model, while this effect is less evident for the WT protein, even when studied under conditions where both variants have the same thermodynamic stability.

The observation of a burst phase in the unfolding kinetics of the N47A mutant followed by intrinsic Trp fluorescence suggested the formation during the dead time of the experiment of states of the protein different from the native and the unfolded ones. These states become favoured by the increase in protein concentration due to mass-action effect, indicating that they become stabilized by oligmerization.

Direct detection of these states was achieved in the unfolding kinetics when followed by ANS fluorescence. The fact that these species bind ANS implies that they expose hydrophobic clusters, consistently with a partially-unfolded or a collapsed conformation. ANS-binding of aggregation-prone intermediate states present during unfolding have been described for the marble brain syndrome-associated mutant H107Y of human carbonic anhydrase II [16].

Although these species were also present during the unfolding of the WT protein, the ANS intensity observed in the kinetics was smaller than for the N47A mutant, indicating a decreased population of intermediates under the same experimental conditions. This observation is in good correlation with a slower amyloid fibril formation of the WT domain compared to the N47A mutant [7] and suggests a direct relationship between the formation of these partially-unfolded species and the mechanism of amyloid fibrillation. This conclusion is further supported by the fact that increasing the salt concentration and the temperature also enhance the accumulation of partially-unfolded species and they also increase the rate of amyloid fibrillation (see Chapter 3.2). The presence of intermediate states populated during unfolding has been described in several amyloidogenic or aggregation prone proteins, such as the yeast prion protein Ure2 [17], alpha-amylase from mung beans [18] or the germ line human lambda6 light-chain protein [19].

In this study we never found significant evidence of the accumulation of these species during the folding processes, either in equilibrium (Figure 5.2) or kinetic folding experiments (Figure 5.8). This indicates that the partially-unfolded species are only kinetically accessible from the native state and never from the unfolded state. Furthermore, the low rate constants of unfolding for these species measured from the ANS-fluorescence kinetics suggest that they may

constitute kinetic traps for the unfolding process and therefore be off-pathway intermediates. Nevertheless, establishing unequivocally the position of these intermediates in the kinetic folding and unfolding pathway is a difficult task and needs a much more exhaustive investigation than that presented in this study.

5.5. BIBLIOGRAPHY

[1] Uversky, V.N. and Fink, A.L. (2004). Conformational constraints for amyloid fibrillation: the importance of being unfolded. Biochim Biophys Acta 1698, 131-53.

[2] Srinivasan, R., Jones, E.M., Liu, K., Ghiso, J., Marchant, R.E. and Zagorski, M.G. (2003). pH-dependent amyloid and protofibril formation by the ABri peptide of familial British dementia. J Mol Biol 333, 1003-23.

[3] Dumoulin, M. et al. (2005). Reduced global cooperativity is a common feature underlying the amyloidogenicity of pathogenic lysozyme mutations. J Mol Biol 346, 773-88.

[4] Viguera, A.R., Martinez, J.C., Filimonov, V.V., Mateo, P.L. and Serrano, L. (1994). Thermodynamic and kinetic analysis of the SH3 domain of spectrin shows a two-state folding transition. Biochemistry 33, 2142-50.

[5] Viguera, A.R., Blanco, F.J. and Serrano, L. (1995). The order of secondary structure elements does not determine the structure of a protein but does affect its folding kinetics. J Mol Biol 247, 670-81.

[6] Prieto, J., Wilmans, M., Jimenez, M.A., Rico, M. and Serrano, L. (1997). Non-native local interactions in protein folding and stability: introducing a helical tendency in the all beta-sheet alpha-spectrin SH3 domain. J Mol Biol 268, 760-78.

[7] Varela, L., Morel, B., Azuaga, A.I. and Conejero-Lara, F. (2009). A single mutation in an SH3 domain increases amyloid aggregation by accelerating nucleation, but not by destabilizing thermodynamically the native state. FEBS Lett 583, 801-6.

[8] Candel, A.M., Cobos, E.S., Conejero-Lara, F. and Martinez, J.C. (2009). Evaluation of folding co-operativity of a chimeric protein based on the molecular recognition between polyproline ligands and SH3 domains. Protein Eng Des Sel 22, 597-606.

[9] Sadqi, M., Casares, S., Lopez-Mayorga, O., Martinez, J.C. and Conejero-Lara, F. (2002). pH dependence of the hydrogen exchange in the SH3 domain of alpha-spectrin. FEBS Lett 514, 295-9.

[10] Cobos, E.S., Filimonov, V.V., Vega, M.C., Mateo, P.L., Serrano, L. and Martinez, J.C. (2003). A thermodynamic and kinetic analysis of the folding pathway of an SH3 domain entropically stabilised by a redesigned hydrophobic core. J Mol Biol 328, 221-33.

[11] Casares, S., Sadqi, M., Lopez-Mayorga, O., Conejero-Lara, F. and van Nuland, N.A. (2004). Detection and characterization of partially unfolded oligomers of the SH3 domain of alpha-spectrin. Biophys J 86, 2403-13.

[12] Petzold, K., Ohman, A. and Backman, L. (2008). Folding of the alphaII-spectrin SH3 domain under physiological salt conditions. Arch Biochem Biophys 474, 39-47.

[13] Periole, X., Vendruscolo, M. and Mark, A.E. (2007). Molecular dynamics simulations from putative transition states of alpha-spectrin SH3 domain. Proteins 69, 536-50.

[14] Jayaraman, G., Kumar, T.K., Sivaraman, T., Lin, W.Y., Chang, D.K. and Yu, C. (1996). Thermal denaturation of an all beta-sheet protein--identification of a stable partially structured intermediate at high temperature. Int J Biol Macromol 18, 303-6.

[15] Ahmad, S. and Rao, N.M. (2009). Thermally denatured state determines refolding in lipase: mutational analysis. Protein Sci 18, 1183-96.

[16] Almstedt, K., Lundqvist, M., Carlsson, J., Karlsson, M., Persson, B., Jonsson, B.H., Carlsson, U. and Hammarstrom, P. (2004). Unfolding a folding disease: folding, misfolding and aggregation of the marble brain syndrome-associated mutant H107Y of human carbonic anhydrase II. J Mol Biol 342, 619-33.

[17] Galani, D., Fersht, A.R. and Perrett, S. (2002). Folding of the yeast prion protein Ure2: kinetic evidence for folding and unfolding intermediates. J Mol Biol 315, 213-27.

[18] Tripathi, P., Hofmann, H., Kayastha, A.M. and Ulbrich-Hofmann, R. (2008). Conformational stability and integrity of alpha-amylase from mung beans: evidence of kinetic intermediate in GdmCl-induced unfolding. Biophys Chem 137, 95-9.

[19] Blancas-Mejia, L.M., Tellez, L.A., del Pozo-Yauner, L., Becerril, B., Sanchez-Ruiz, J.M. and Fernandez-Velasco, D.A. (2009). Thermodynamic and kinetic characterization of a germ line human lambda6 light-chain protein: the relation between unfolding and fibrillogenesis. J Mol Biol 386, 1153-66.

6.

MUTAGENIC ANALYSIS OF THE MECHANISM OF AMYLOID AGGREGATION OF SPC-SH3

6. MUTAGENIC ANALYSIS OF THE MECHANISM OF AMYLOID AGGREGATION OF SPC-SH3

As described in Chapter 2, we have found that the WT Spc-SH3 domain and several single mutants, in addition to the N47A mutant, can also form amyloid fibrils at acid pH, although at much slower rates when compared to the latter [1]. We have demonstrated that this difference is not due to a thermodynamic destabilization of the native state of the domain, but to an increase in the rate of the conformational processes that conduce to fibril nucleation.

Our results showed that mutations destabilizing the native state need not to be necessarily amyloidogenic but their effect on fibrillation may depend on how they influence the early conformational events during nucleation. These events consist of a conformational change implying partial unfolding of the protein immediately followed by formation of oligomeric species that appear to be critical in nucleating the fibrillation cascade.

Here we have employed a mutagenesis approach to analyse the mechanism of fibril formation. This approach has been widely used to investigate the molecular mechanism of protein folding [2].

We prepared a series of double-mutants using the single mutant N47A as our reference protein in this study (See chapter 8). Mutations have been made on selected positions of the polypeptide chain to probe every structural element of the protein (Table 6.1) (Figure 6.1).

Table 6.1. *Second mutations made on the N47A mutant and their location on the structural elements of the protein.*

MUTATION	POSITION
L10A	β strand 1
R21D	RT loop
K27A	Diverging turn
T32A	β strand 2
N38A	n-src loop
K43A	β strand 3
V46A	β strand 3
D48G	Distal turn
V53A	β strand 4
A56G	3_{10} helix
V58A	β strand 5

Figure 6.1. *Schematic ribbon drawing of the Spc-SH3 domain structure showing each place of mutation in magenta. N47A mutation is showed in blue.*

6.1. DSC ANALYSIS OF THE THERMODYNAMIC STABILITY OF THE DOUBLE MUTANTS

Our first step was to perform a set of DSC experiments to evaluate the changes in the stability of the native state produced by the mutations. The experiments were made in the buffer used in the aggregation experiments (100 mM Gly, 100 mM NaCl, pH 3.2) but at low protein concentration (1 mg mL^{-1} approximately) to avoid aggregation during the thermal unfolding (Figure 6.2). Under these conditions, the thermal unfolding of all mutants, except K43A, V53A and V58A, was highly reversible as we observed in the second heating scan (not shown). Mutants K43A, V53A and V58A did not show a clear unfolding transition, indicating that they are mostly unfolded under these experimental conditions, and therefore their DSC thermograms were not analyzed quantitatively. The thermograms of the rest of the mutants followed very well the two-state unfolding model, from which we obtained the thermodynamic parameters of the process (Table 6.2).

Mutations L10A, N38A, T32A, V46A, A56G and K27A had a significant destabilizing effect, whereas the R21D and D48G mutations stabilized the protein. Mutations K43A, V53A and V58A destabilized completely the native state.

A plot of the unfolding enthalpies, ΔH_u, versus the unfolding temperatures, Tm, measured for the different variants at pH 3.2, shows a single linear dependence (Figure 6.3). This indicates that the changes in enthalpy of unfolding were only due, within the experimental error, to its dependence with temperature due to the heat capacity change of unfolding, $\Delta Cp = d\Delta H/dT$, which appears to be common to all domain variants, 3.67 ± 0.15 kJ K^{-1} mol^{-1} [3]. This value is fully consistent with that shown in Chapter 2 and those previously

published for the Spc-SH3 domain [4, 5] and indicates that these mutations do not induce significant changes in the native structure.

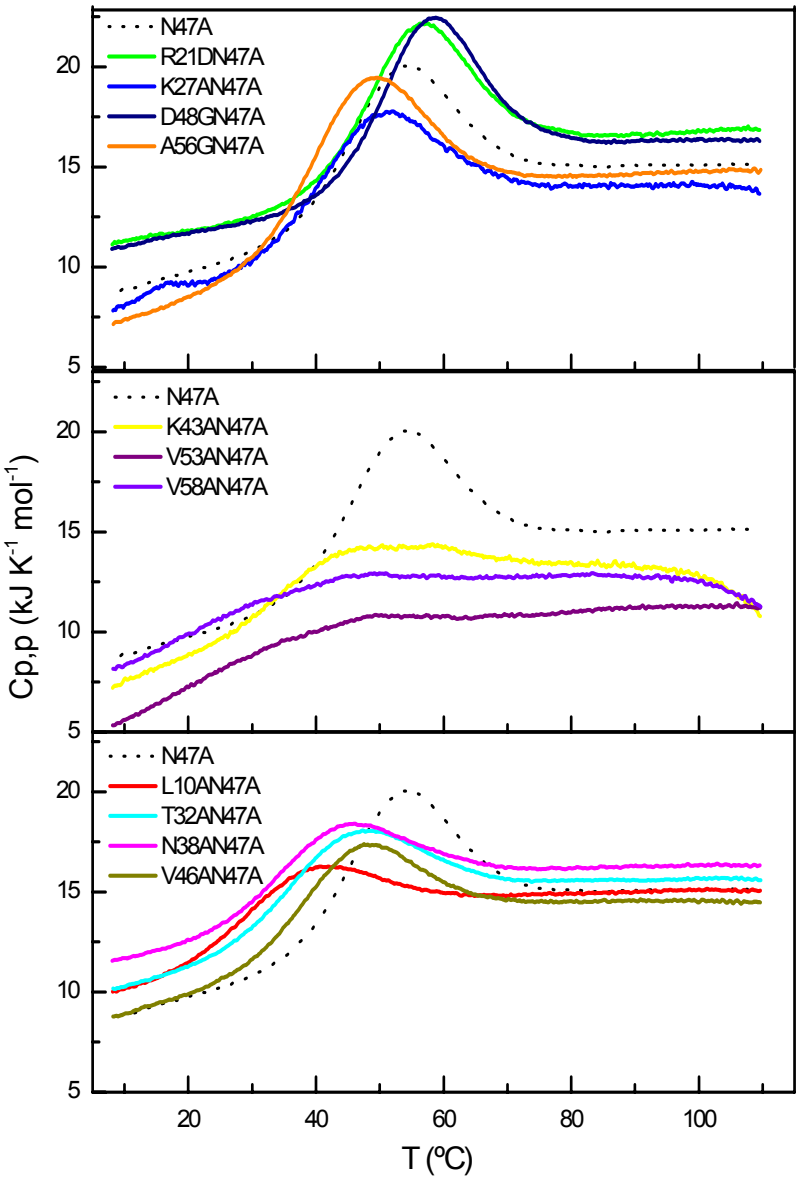

***Figure 6.2**. DSC experiments of the double mutants samples under fibrillation conditions at 0.8 mg mL^{-1} protein concentration. Scan rate was 2 ºC min^{-1} in all experiments.*

***Table 6.2**. Thermodynamic parameters of the equilibrium thermal unfolding of all the variants determined by DSC.*

VARIANT	Tm (ºC)	ΔH_u (Tm) (kJ mol^{-1})	ΔG_u (37 ºC) (kJ mol^{-1})[a]
N47A	50.9	149	5.28±0.4
N47A-L10A	30.3	77	-1.97±0.3
N47A-R21D	53.5	156	6.33±0.4
N47A-K27A	46.7	129	3.37±0.4
N47A-T32A	41.6	108	1.46±0.3
N47A-N38A	38.6	100	0.50±0.3
N47A-K43A	--	--	--
N47A-V46A	42.3	114	1.75±0.3
N47A-D48G	55.7	164	7.34±0.5
N47A-V53A	--	--	--
N47A-A56G	46.1	146	3.68±0.4
N47A-V58A	--	--	--

[a] Unfolding Gibbs energy at 37 ºC of each double mutant calculated by using a common heat capacity change of unfolding, $\Delta C_{p,u}$ of 3.67±0.15 kJ K^{-1} mol^{-1} that was determined by linear regression to all the ΔH_u (Tm) vs Tm data.

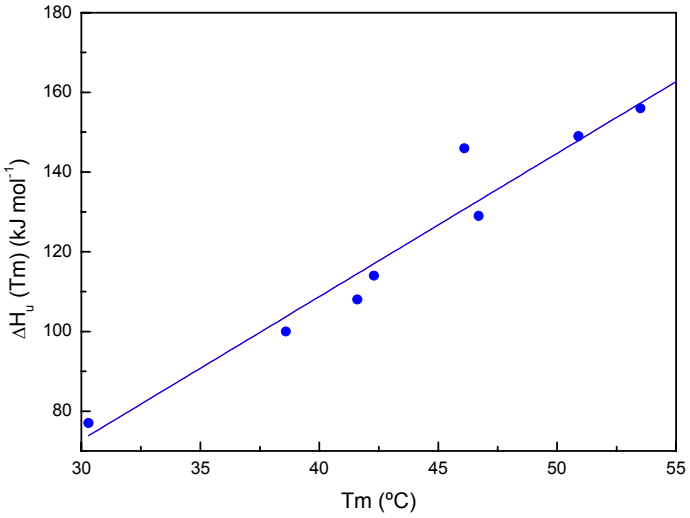

***Figure 6.3**. Plot of the enthalpy change of unfolding, ΔH_u, versus the unfolding temperature, Tm, for all the mutants obtained from the fittings of the DSC traces using two-state model. The line corresponds to the linear regression (Adj. R-Square=0.95) to all data from which a heat capacity change of unfolding (slope of the plot) of 3.67 ± 0.15 kJ K^{-1} mol^{-1} is derived.*

6.2. STRUCTURAL CHANGES INDUCED BY THE MUTATIONS.

To check if the second mutations produced important structural effects in the domain, we acquired the far-UV CD spectra of the double mutants. Spectra were registered in the aggregation buffer (100 mM Gly, 100 mM NaCl, pH 3.2) at low protein concentration (0.3 mg mL^{-1} approximately) at 25 ºC and at the temperature of the aggregation experiments (37 ºC) (Figure 6.4). The spectra of the K43A mutant could not be recorded due to lack of sample.

At 25 ºC all the mutants, except V53A and V58A, showed spectra typical of native Spc-SH3 (as in the case of the single N47A mutant) domain. At 37 ºC, the changes in the CD spectra produced by the mutations rank approximately according to their relative stability,

indicating that at this temperature a significant fraction of protein is unfolded depending on the Tm of the transition. V53A and V58A presented CD spectra at both temperatures very similar to that observed for the unfolded Spc-SH3 domain [4]. These data are therefore fully consistent with the thermodynamic parameters obtained from the DSC analysis.

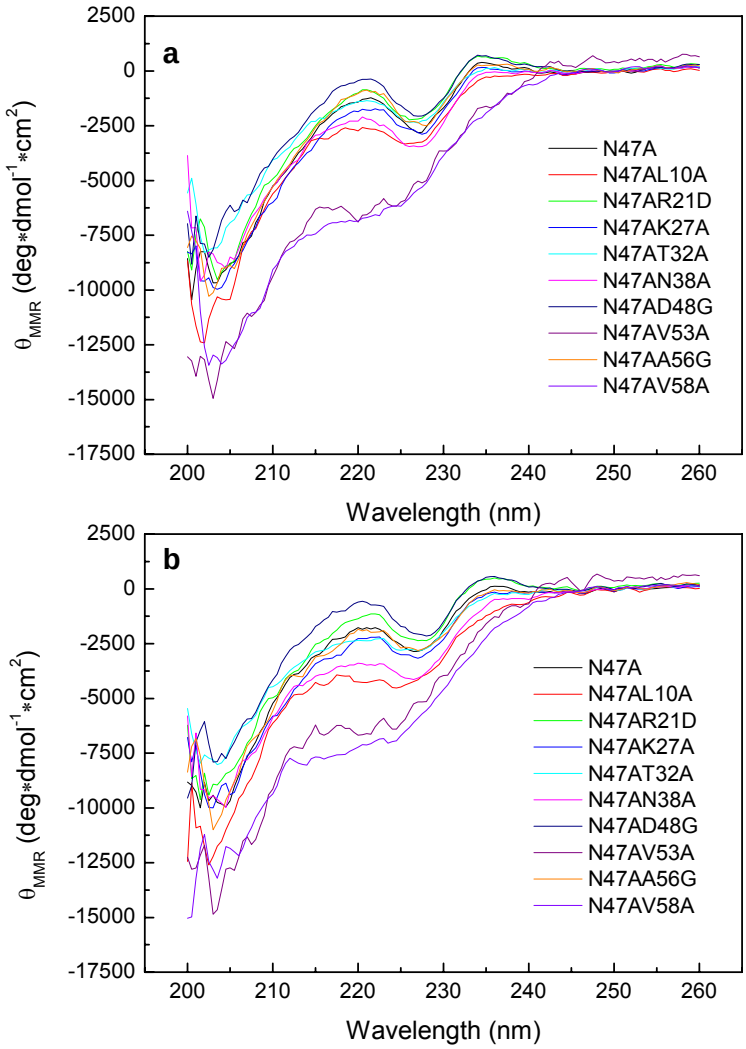

Figure 6.4. *Far-UV CD spectra for N47A and the double mutants in the aggregation buffer at a protein concentration of 0.3 mg mL^{-1} in a 0.1 cm path length CD cuvette at (a) 25 ºC and (b) 37 ºC.*

6.4. KINETICS OF AMYLOID FIBRILLATION OF THE DOUBLE MUTANTS

The kinetics of formation of amyloid fibrils of the double mutants was analyzed by ThT fluorescence under the conditions described previously for the N47A mutant [6], i.e., at 37 ºC in 100 mM glycine buffer pH 3.2, in the presence of 100 mM NaCl and a protein concentration of 8.2 mg mL^{-1} (Figure 6.5).

All variants except the L10A and D48G mutants formed amyloid fibrils to different extents when incubated at 37 ºC for long periods. The time dependence of the ThT fluorescence signal could be fitted to an exponential phase plus a second slower exponential or linear phase [6].

As discussed in Chapter 3, under these fibrillation conditions the rate limiting step of early fibrillation is a conformational change of the protein that leads to the rapid formation of aggregation nuclei and subsequently to fibrils. This explains the lack of a significant lag phase in the ThT kinetics.

From these fittings we obtained the apparent first-order rate constant (k) and the amplitude (A) of the nucleation process. The amplitude of the nucleation phase would be approximately proportional to the amount of fibrillation nuclei formed after this phase, since the ThT fluorescence is considered proportional to the mass amount of fibrils [7]. The slope of the second phase gives information about the rate of fibril growth after nucleation (Figure 6.6a, 6.6b).

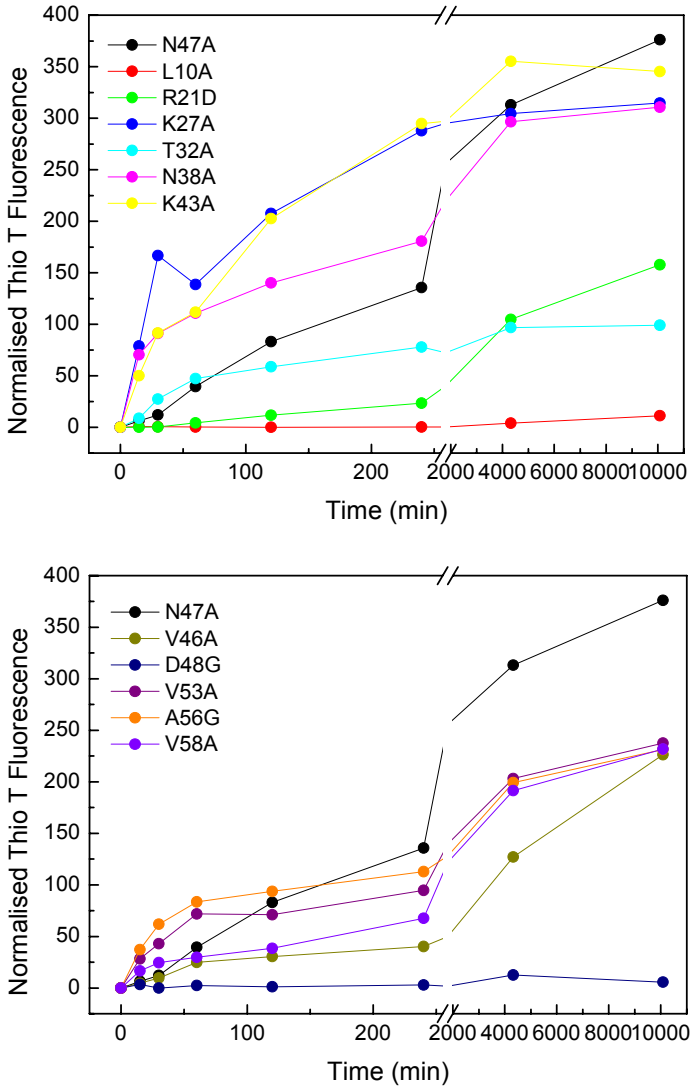

***Figure 6.5**. Kinetics of amyloid fibril growth of N47A and the double mutants of Spc-SH3 measured by ThT fluorescence. Aggregation was followed at 37 ºC in 100 mM glycine buffer pH 3.2, with 100 mM NaCl, at an equal protein concentration of 8.2 mg mL^{-1}.*

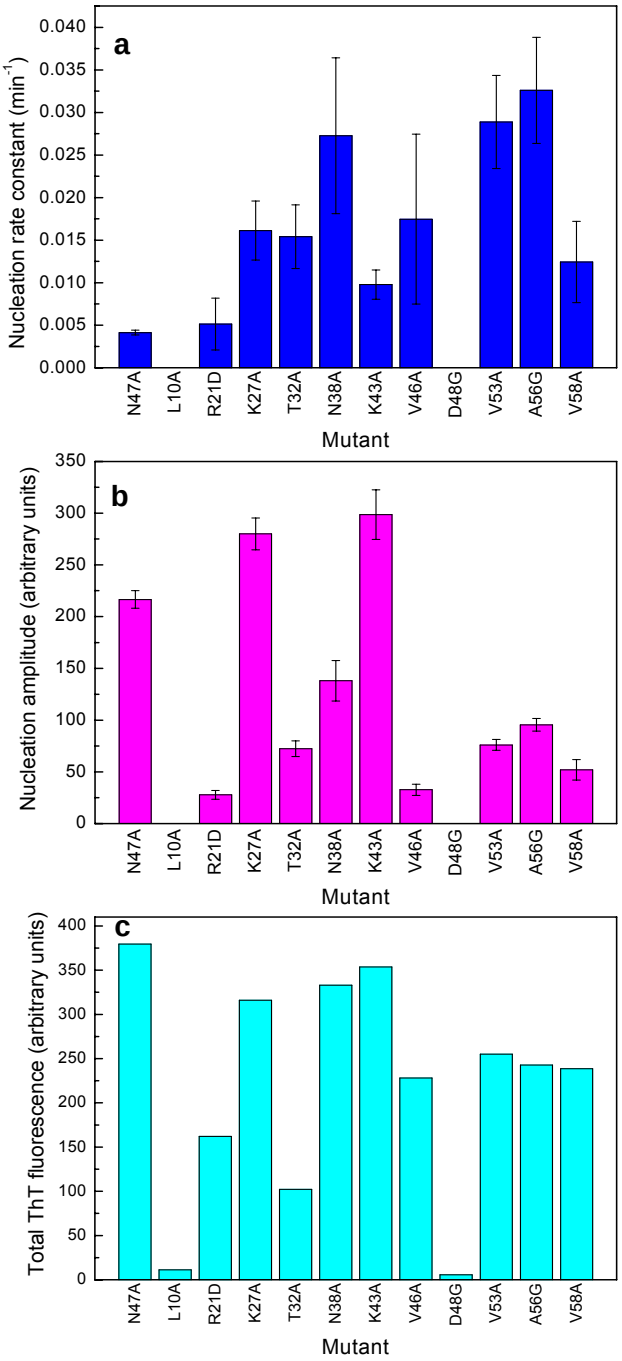

***Figure 6.6**. Kinetic parameters of the fibrillation of the set of double mutants and N47A obtained by fitting the ThT fluorescence profiles using a monoexponential growth (nucleation stage) plus an exponential or linear slower phase (elongation stage). a) Nucleation rate constant. b) Nucleation amplitude. c) Total ThT fluorescence at the end of the experiment*

We observed that the thermodynamic parameters (Table 6.2) do not correlate whatsoever with the fibrillation propensities of the double mutants, as we demonstrated before for a set of single mutants (Chapter 2) [1]. For instance, the strongly destabilizing mutation L10A inhibits almost completely amyloid formation, whereas mutations N38A and K27A, which destabilize less the native state, increased considerably the nucleation rate relative to the N47A mutant, but reduced significantly the total amount of fibrils. Likewise, mutations that fully destabilized the native state (K43A, V53A and V58A) had a dissimilar effect upon the fibrillation kinetics. To determine if the different fibrillation propensities of the mutants are related with the effect of the each mutation on the intrinsic propensity of the polypeptide chain to aggregate, we calculated the theoretical aggregation rate of every mutant as described elsewhere [8]. The equation used to predict these values was equation 6.1.

$$\log(k) = \alpha 0 + \alpha hydr \times I^{hydr} + \alpha pat \times I^{pat} + \alpha_{ch} \times I^{ch} + \alpha_{pH} \times E^{pH} + \alpha_{ionic} \times E^{ionic} + \alpha_{conc} \times E^{conc} \qquad (6.1)$$

where log(k) is the logarithm to base 10 of the aggregation rate constant k, in units of s^{-1}. Factors intrinsic to the amino acid sequence are denoted as I, while extrinsic, condition-dependent, factors are denoted as E. I^{hydr} represents the hydrophobicity of the sequence, calculated as the sum of the hydrophobic contributions of each residue, normalized by the number of amino acid residues in the sequence, N. The Roseman scale of hydrophobicity was used to estimate these propensities at neutral pH, using the data from Cowan and co-workers to adjust the changes in hydrophobicity experienced by amino acid residues at different pH values [9, 10]. I^{pat} takes into account the existence of patterns of alternating hydrophobic–

hydrophilic residues; a factor of +1 was assigned for each pattern of five consecutive alternating hydrophobic and hydrophilic residues in the sequence [11]. I^{ch} is the absolute value of the net charge of the sequence. E^{pH} accounts for the pH of the solution in which aggregation occurs and E^{ionic} defines the ionic strength of the solution, given in millimolar units. Finally, E^{conc} refers to the polypeptide concentration C (in millimolar units) in the solution, represented here as log(C + 1), an always positive term for any value of C.

We corrected these values with a stability factor that gives the fraction of protein that is unfolded at the aggregation temperature. This factor takes into account that the intrinsic aggregation rates are calculated for unstructured polypeptide chains. In fact, most of the predicted changes in aggregation rates are due to this stability factor, whereas the sequence changes have a very small effect.

Figure 6.7 compares the changes in fibrillation rates predicted by this calculation relative to the N47A with those observed experimentally. We have found that the relative changes in nucleation rates for many of the mutants are similar to those predicted theoretically, whereas for few mutants the predictions cannot explain the experimental data. No correlation is observed however with the effects on the amplitudes of the nucleation phase or with the variations in the total amount of aggregates (Figure 6.6b and 6.6c). These results are consistent with our conclusions derived from the analysis of single mutants presented above (chapter 2), [1].

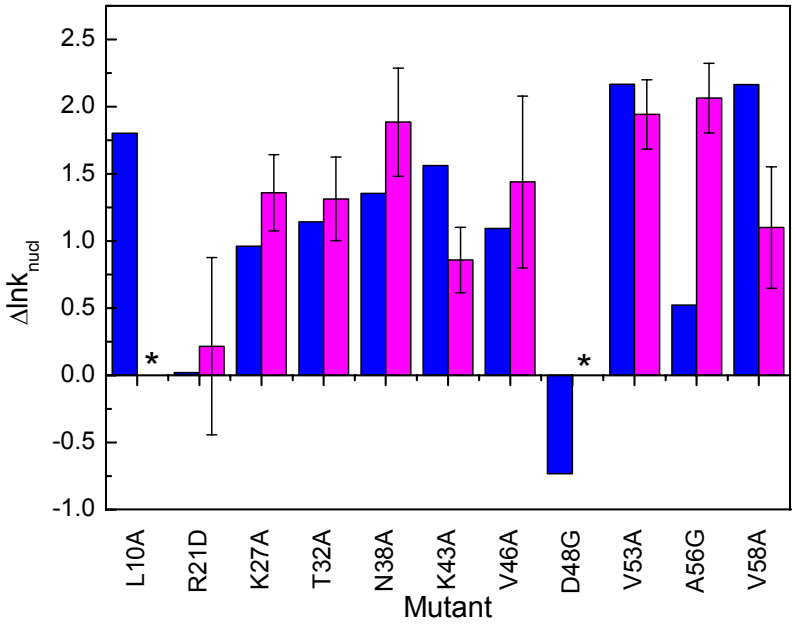

Figure 6.7. *Comparison between changes produced by mutations on the experimental rate constants of the nucleation stage (magenta) and the theoretical aggregation propensities corrected by a stability factor of the mutants (blue). The asterisks indicate no fibrillation for the corresponding mutants.*

According to these results, the effect of mutations on the rates of fibril nucleation of Spc-SH3 cannot be rationalized solely as the result of either the changes in native state stability or the changes in the intrinsic aggregation rate of the polypeptide chains. There must be therefore additional factors contributing to the observed effects on fibrillation.

6.4. AGGREGATION STAGES OF THE DOUBLE MUTANTS FOLLOWED BY DLS

The results presented here and our previous conclusions derived from the analysis of single mutants indicated that mutations alter the fibrillation propensity due to their effect on the rate of the fibril

nucleation phase. To understand better this event, we followed by DLS the early stages of aggregation of the double mutants at 37 ºC.

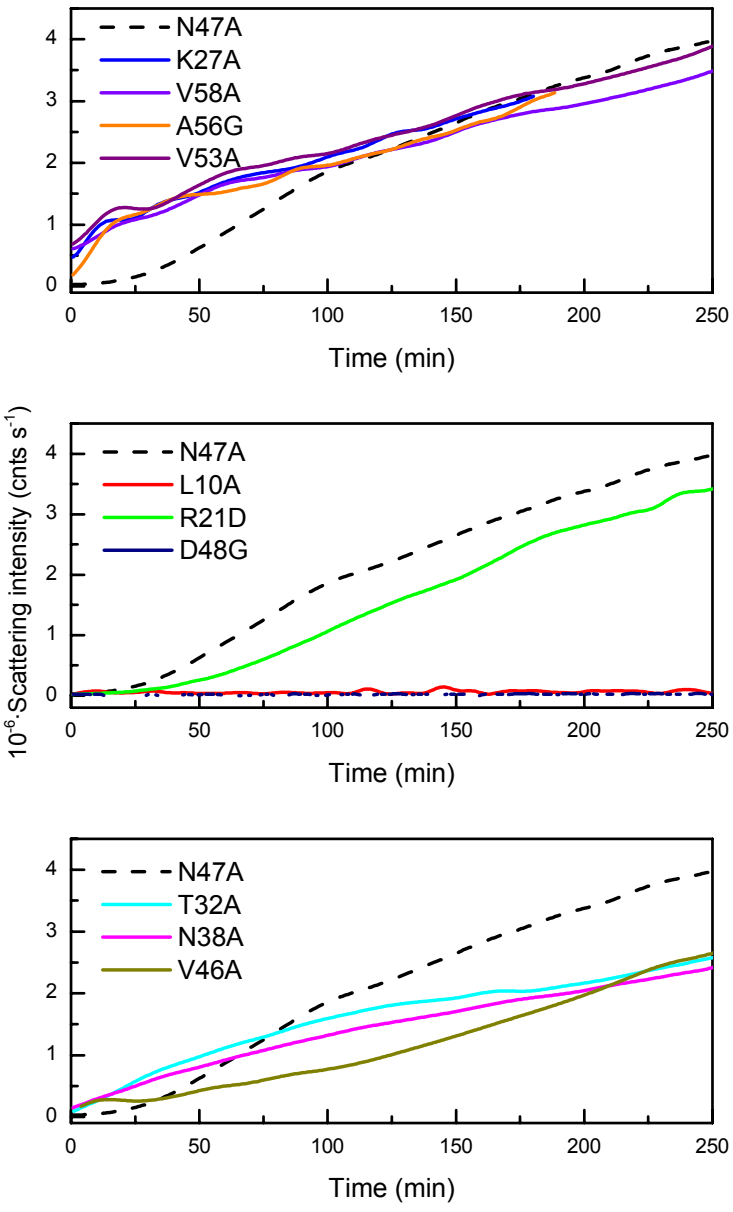

Figure 6.8. *Aggregation kinetics at 37 ºC of the double mutants and the N47A mutant followed by monitoring the scattering intensity. Experimental conditions are identical to those of Figure 6.5.*

The rates of growth of the scattering signal were quite consistent with the ThT fluorescence kinetics (Figure 6.5). Mutants L10A and D48G did not show a significant growth in scattering intensity indicating the absence of aggregate particles during the first 250 min. The rest of the mutants showed a considerable scattering increase but differed in the presence or absence of a significant lag phase. The R21D mutant in addition to the single mutant N47A had a significant lag, indicating a delay in the appearance of aggregate particles in the mixture. For the rest of mutants, no lag phase was observed, consistently with the ThT fluorescence data.

From the DLS data we calculated the size distributions of particles in the aggregation mixtures as a function of the incubation time. The time evolution of the apparent hydrodynamic radius, R_h, for the two first peaks observed in the distributions are represented in Figure 6.9.

At the start of the incubation, the size distributions of the N47A mutant presented only one peak with an apparent R_h of approximately 1.7 nm, consistently with the value reports for native Spc-SH3 [12]. The R_h of this peak expanded to approximately 3.2 nm at around 100 minutes of incubation. This event was interpreted previously as indicative of oligomerisation following an initial conformational change in the protein [6]. After about 10 minutes from the start of the incubation additional species appeared with an apparent R_h starting at approximately 7–9 nm and increasing progressively with the incubation time up to approximately 40 nm at 150 min. These particles were identified previously as small protofilaments of 6–7 nm in diameter elongating as the aggregation progresses. The apparent R_h of the fibrils stops increasing because of the lack of linear persistence of the fibrils. This apparent R_h would correspond to fibril lengths of about 250–500 nm. Finally, at long incubation times larger particles with

apparent R_h reaching up to several micrometers (not shown) became developed corresponding to long amyloid fibrils.

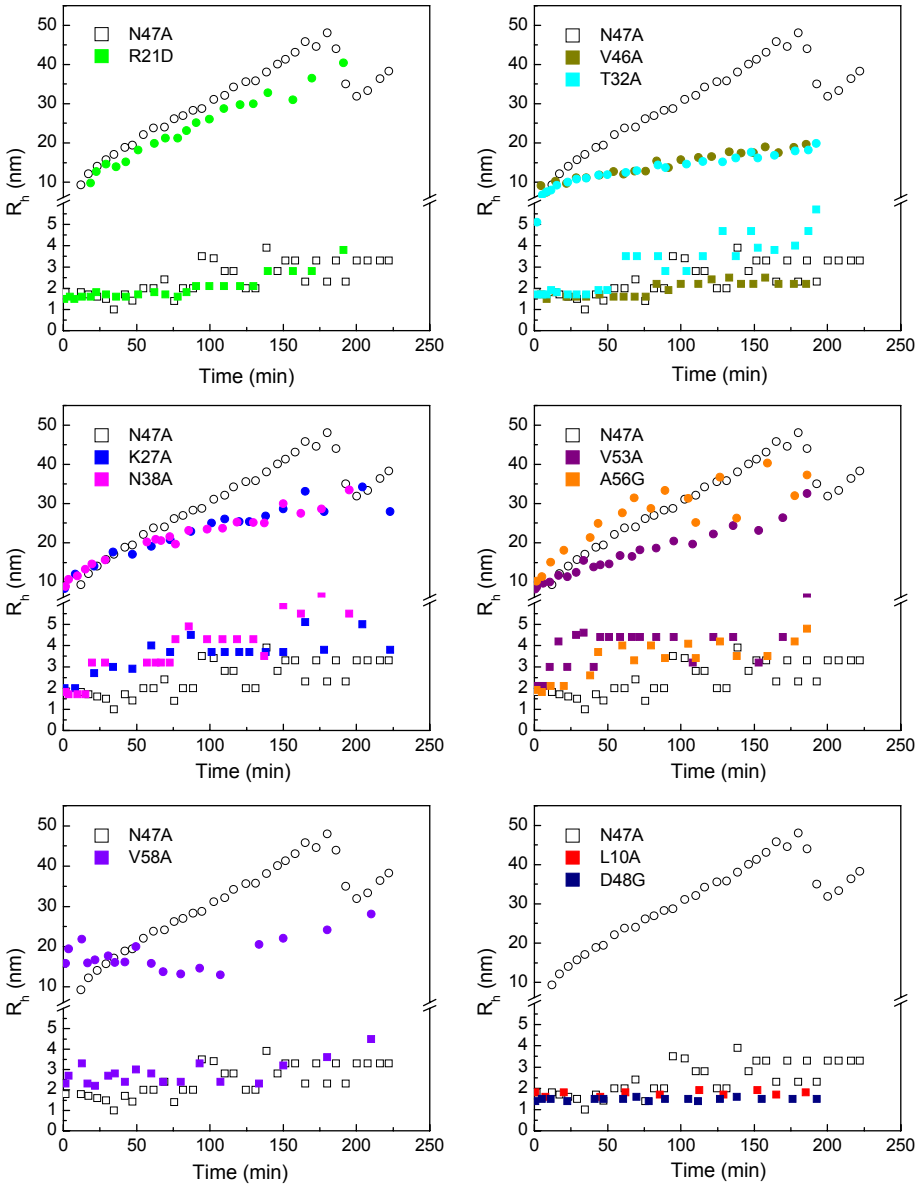

***Figure 6.9**. Time evolution of the apparent hydrodynamic radii (R_h) for the two smallest peaks in the particle size distributions measured by DLS during the course of fibrillation of the double mutants.*

The behaviour of the size distributions for the double mutants was markedly different depending on every mutant. For instance, mutants L10A and D48G presented only particles with an apparent R_h of 2 nm and 1.6 nm respectively during all the course of the experiment (not shown), in agreement with their lack of aggregation. These radii were consistent with that of the native monomer for D48G and with a mixture of native and unfolded monomers for L10A, which is in good agreement with the DSC and CD data for these mutants.

The R21D mutant presented a very similar behaviour to the N47A single mutant but the events occurred at a slower pace, with native particles at the beginning of the incubation that expand to about 3.2 nm at about 150 minutes of incubation. The appearance and growth of protofilaments was also delayed for a few minutes relative to the N47A mutant, consistently with a longer lag phase in the fibrillation kinetics observed by ThT fluorescence.

For a subset of mutants (K27A, N38A, V53A, A56G) the size expansion of the peak corresponding to monomeric particles occurred considerably faster than for N47A, in agreement with their faster nucleation rates and the absence of lag phase in the fibrillation kinetics, as described above. Protofibrillar aggregates of about 7-9 nm appeared in the mixtures from the very beginning of the incubation for these mutants although their growth is in general slower than for N47A.

Mutants V46A and T32A underwent a relatively slow expansion of the apparent R_h of the native particles, similar to that of N47A, and their protofibrils grew also at lower rates than the N47A mutant. Of note is the natively unfolded V58A mutant, which shows from the beginning of the incubation particles of about 2.5 nm, likely unfolded monomers, and particles of about 15-20 nm. These particle sizes

remain invariant for about 150 min but then oligomerisation and fibril growth appear to start simultaneously.

Taken together, these results show that the fibril nucleation process is the result of a subtle balance between a series of events, in which the proteins need to undergo conformational changes and oligomerisation prior to their further assembly into larger fibrillar aggregates. This balance is modulated considerably by the mutations, which act differentially on each of these steps resulting in considerable changes in the fibrillation efficiency.

6.5. MORPHOLOGY OF THE AGGREGATES FORMED BY THE DOUBLE MUTANTS.

To explore the morphology of the aggregate particles appearing during the fibrillation process, we analyzed by TEM samples of all the double mutants during the time course of aggregation. As described previously [1, 6] (see chapter 2) at early times of incubation (30 min) the N47A mutant formed protofibrillar and amorphous aggregates, which quickly reorganized after only 60 min of incubation into small curly fibrils with diameter of 6–7 nm and lengths ranging between few tenths and several hundreds of nanometres. These fibrils elongated further for longer incubation times.

Similar events occurred for the R21D mutant, which showed a longer lag phase in the fibrillation kinetics. At 30 min of incubation only few small globular and amorphous aggregates were visible in the TEM images (not shown) but a variety of irregular aggregate clusters and small fibrillar structures were sparsely visible at 60 min of incubation, which became reorganized later to form fibrils, as observed at 240 min of incubation (Figure 6.10a-c).

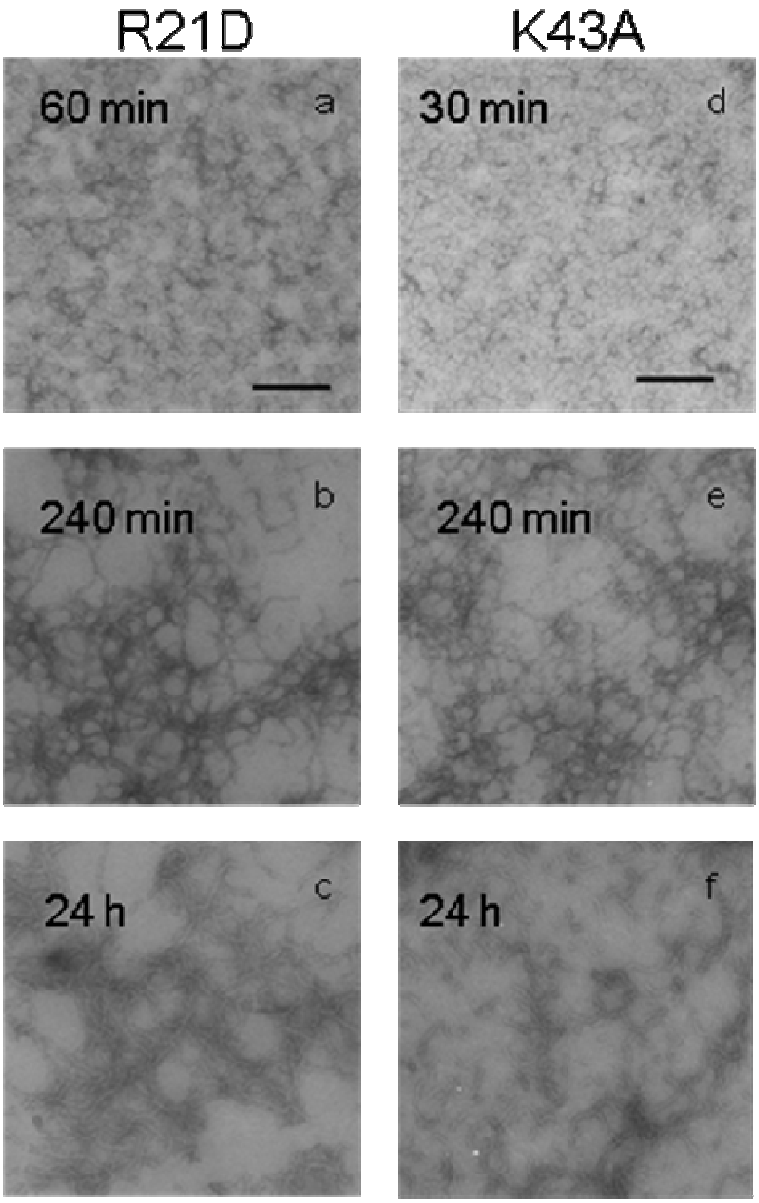

Figure 6.10. *Electron microscopy images of aggregated R21D (panels a-c) and K43A (panel d-f) double mutants after different times of incubation at 37 ºC as indicated in each image. Incubation conditions are identical to those of Figure 6.5 for each variant.*

For those mutants without any lag phase in the fibrillation kinetics, such as K43A mutant, small fibrils were already observable even after 30 minutes of incubation (Figure 6.10d). After long incubation times, all variants, except L10A and D48G, presented a tangle of amyloid fibrils with similar apparent curly morphology and diameter independently of the initial state and stability of the mutant. It appears that for all protein variants amyloid fibril formation involves similar early events, i.e., an initial formation of amorphous prefibrillar aggregates and a subsequent reorganization of these aggregates into fibrils, but these events occur at different speeds depending on the mutant.

6.6. DISCUSSION

In this study, we have made a series of mutations placed at every secondary structure element of the N47A Spc-SH3 domain. These mutations changed to different extents the thermodynamic stability of the native state as well as the intrinsic propensity of the polypeptide chain to aggregate but these effects did not correlate in general with the changes in the rates of amyloid fibril formation.

Our results may appear in conflict with previous studies which have found a significant inverse correlation between native stability and the propensity to form amyloids [13, 14, 15, 16, 17]. For instance, mutations L10A and D48G, which are destabilizing and stabilizing respectively (see Table 6.2), both inhibited amyloid fibril formation.

Previous studies have described that a key requirement for fibril formation is an increase in the population of partially folded conformations that become favoured by destabilizing the native state. This was observed in GAL and BIF monoclonal light chains [14], whose fibril formation is predominantly controlled by thermodynamic stability. The results allowed a rational strategy to inhibit amyloidosis based on the design of high affinity ligands stabilizing the native

protein. A similar tendency was also observed in mutational analysis of Acylphosphatase [13, 16], where all stabilizing mutations decreased the amyloid fibril rate and *vice versa*. It was concluded that the stability of the native state of globular proteins is a major factor preventing the *in vivo* conversion of natural proteins into amyloid fibrils.

On the other hand, a mutational analysis of the fibrillation of the thermophilic protein S6 revealed no correlation whatsoever between native stability and fibril formation [18]. Instead, the unfolding rates correlated directly with the lag phases of amyloid aggregation suggesting that the nucleation occurs from a quasi-native state. Additional evidence supporting the importance of local effects has been provided by the study of two amyloidogenic variants of human lysozyme [19], in which transient unfolding of a specific region of the protein including the beta domain and the C-helix is favoured by the mutations.

Some other studies have supported that the propensity of a protein to form amyloid fibrils has a significant dependence on the polypeptide chain sequence as is the case of Acylphosphatase (AcP) and its mutants [16, 20]. In these studies it was described that amyloid fibril formation is modulated by aminoacid hydrophobicity, β-sheet propensity and the total net charge of the protein. In a subsequent work [8] an approach was described to predict from the amino acid sequence the *in vitro* aggregation rates of a wide range of unstructured peptides and proteins considering a set of simple physicochemical parameters of the polypeptide chains and their environment. As we have described above, we used this approach to predict the effects of the mutations on the aggregation rates and corrected the obtained values by the contribution of the stability of every mutant (see Figure 6.7). Although the predictions were in agreement with the observed effects for some of the double mutants, they failed to explain other

changes. It is remarkable the case of the L10A mutation, which was predicted to produce one of the highest intrinsic aggregation propensities but inhibited completely amyloid fibril formation.

Our results indicate that the inhibitory or potentiating effect of amyloid formation exerted by the mutations occurs mainly at the stage of the conformational events leading to nucleation or at the nucleation step itself. In fact, our analysis by DLS clearly shows that formation of early oligomers occurred earlier for the mutants having a faster and a more efficient nucleation such as K27A, N38A, V53A and A56G, leading generally to a more extensive fibrillation. In contrast, oligomerisation never occurred for L10A and D48G, none of which form amyloid fibrils in spite of their different stabilities. It appears therefore that oligomerisation following a conformational change of the protein is crucial in the development of fibrillar aggregates, thus conditioning all the subsequent fibrillation process. This is in agreement with the fact that in all mutants studied here the duration of the lag phase in fibril formation is very similar to that of formation of oligomers (see Figures 6.8 and 6.9). This suggests that these oligomeric species may be the competent species of fibril nucleation or may even constitute themselves the aggregation nuclei.

The presence of oligomeric species in rapid equilibrium with the monomeric form has also been reported as critical for fibril nucleation as for example in Abeta [21] or yeast prion Sup35p [22] and the importance of their characterisation is emphasized by their implication in a number of neurotoxic processes [23].

This and our previous studies [1, 6] support the view that fibril nucleation is preceded by an initial conformational change followed by or concomitant to rapid formation of soluble oligomers, which nucleate the fibrillation process. Indeed, it has been described in a wide variety of protein systems, such as the B1 lg-binding domain of protein G (β1)

[15], several lysozyme variants [24] and transthyretin (TTR) [25], that the key requirement for fibril formation is to choose conditions where the population of certain partially folded intermediate conformations is maximized. The apparent rate constant of the first exponential phase could be then associated to the rate limiting step of the nucleation reaction and the amplitude of the first phase would be proportional to the relative amount of fibrillation nuclei.

Double mutants containing the N47A mutation (our reference in this study) were designed to produce stability changes in the protein by alteration of specific interactions at the different structural elements. Since the changes in stability produced by the mutations were evaluated by DSC as changes in the Gibbs energy of unfolding, ΔG_u, measuring the changes in the nucleation kinetics we could perform an analysis similar to the 'phi' analysis of protein folding rates by site-directed mutagenesis [26].

Using simple transition-state theory, the rate constant of the rate-limiting step of nucleation, k_{agg}, would be related to the height of the energy barrier according to the following equation:

$$\ln k_{agg} = \ln\left(\frac{k_B T}{h}\right) - \frac{\Delta G^{\neq}_{agg}}{RT} \qquad (6.2)$$

where $\Delta G^{\neq}_{agg}$ is the activation Gibbs energy of the nucleation process.

Assuming that under the aggregation conditions the native and the unfolded state are in rapid equilibrium and taking the fully unfolded state as the energy reference for all mutants, each mutation will change the average Gibbs energy of the monomeric species (the bottom of the energy barrier) as:

$$\left\langle \Delta\Delta G \right\rangle^{mut} = \Delta G_U^{mut} \cdot x_N^{mut} - \Delta G_U^{wt} \cdot x_N^{wt} = \frac{\Delta G_U^{mut}}{1 + K_U^{mut}} - \frac{\Delta G_U^{wt}}{1 + K_U^{wt}} \quad (6.3)$$

where *'wt'* refers here to our reference protein, i.e., the N47A single mutant, and *'mut'* refers to each double mutant. $\left\langle \Delta\Delta G \right\rangle^{mut}$ can be evaluated for each double mutant from the stability measurements made by DSC at low concentrations (see Table 6.2).

For those mutations that fully destabilize the protein, the mutants will fibrillate directly from the unfolded state. The fraction of native state x_N^{mut} will be then equal to 0 and the average Gibbs energy change will be equal to:

$$\left\langle \Delta\Delta G \right\rangle^{mut} = -\frac{\Delta G_U^{wt}}{1 + K_U^{wt}} \quad (6.4)$$

The height of the activation barrier would change with each mutation according to its relative effect on the $\left\langle \Delta\Delta G \right\rangle^{mut}$ value and upon the energy the transition state of nucleation.

$$\Delta \ln k_{agg} = \ln k_{agg}^{mut} - \ln k_{agg}^{WT} = -\frac{\Delta G_{agg}^{\neq,mut} - \Delta G_{agg}^{\neq,wt}}{RT} \quad (6.5)$$

Using to these equations, a specific mutation may be classified into different limiting classes, as follows:

Class 1: $\Delta \ln k_{agg} \approx -\frac{\langle \Delta\Delta G \rangle^{mut}}{RT}$

These mutations would affect native interactions that are not longer present in the transition state structure. Then the change in the rate-limiting step of fibrillation will reflect principally the change in stability of the native state due to the mutation.

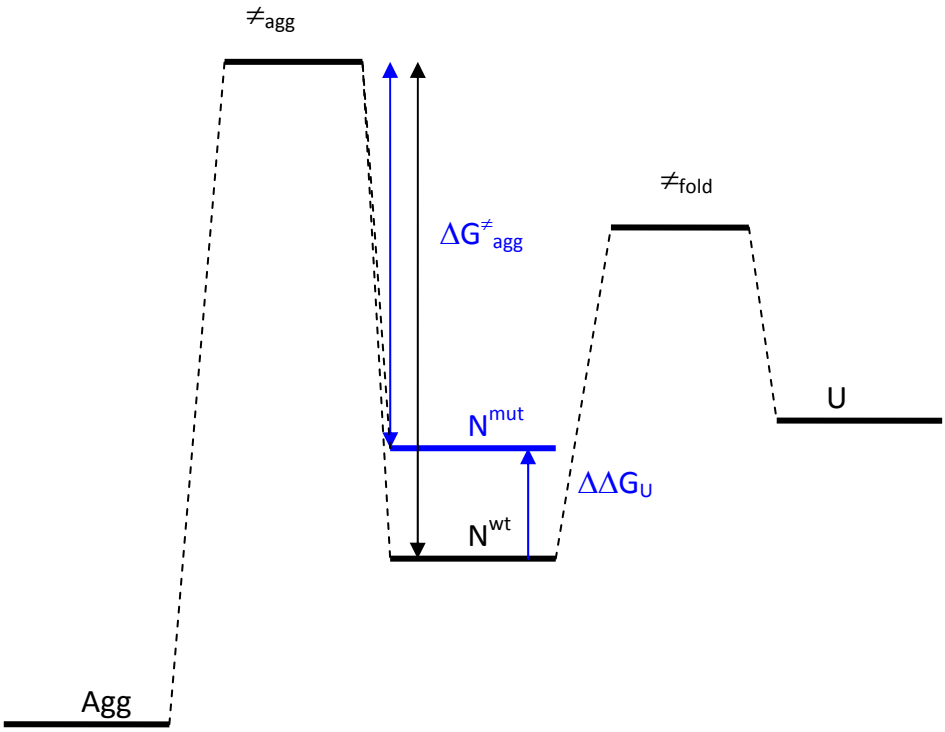

Class 2: $\Delta \ln k_{agg} \approx 0$

These mutations change the stability of the transition state similarly to that of the native state. This would be the case if the transition state had native-like structure at the place of the mutation. Then, the net change in energy barrier for the conformational change would be zero, and the rate constant would not change even if the native state stability were affected.

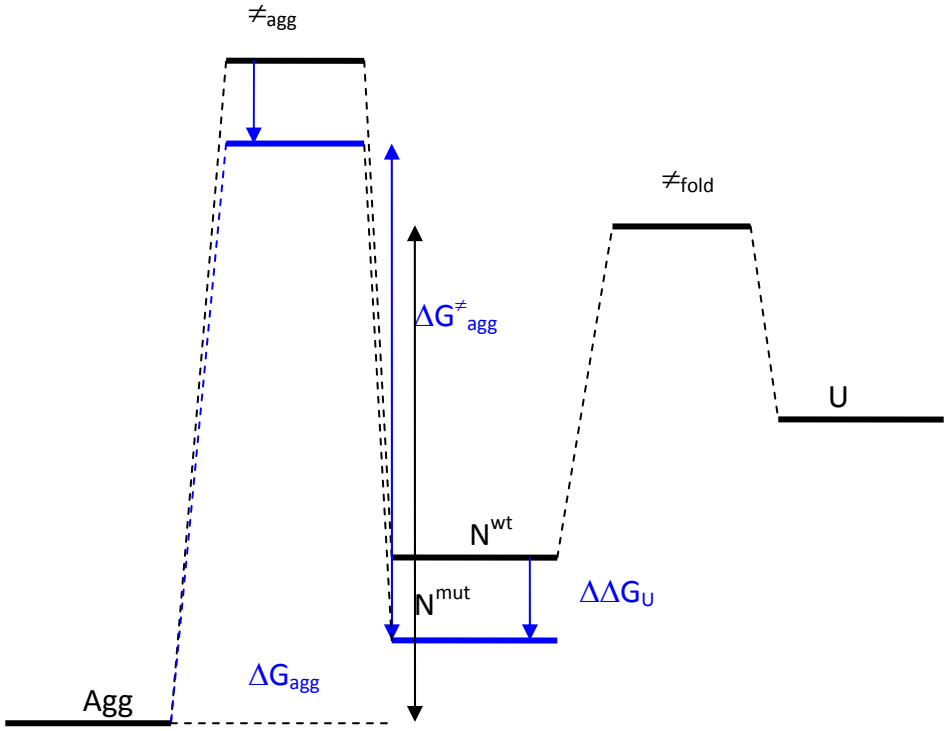

Class 3: $\Delta \ln k_{agg} > -\frac{\langle \Delta\Delta G \rangle^{mut}}{RT}$

These mutations change the stability of the transition state oppositely to that of the native state. This situation would occur if the mutation modifies a non-native interaction present in the transition state. A mutation destabilizing the native state but stabilizing the transition state results in a change in the activation barrier of nucleation of the same sign but of a larger magnitude than $\langle \Delta\Delta G \rangle^{mut}$. On the other hand, a mutation stabilizing the native state but destabilizing the transition state yields a change in the barrier opposite to the sign of $\langle \Delta\Delta G \rangle^{mut}$.

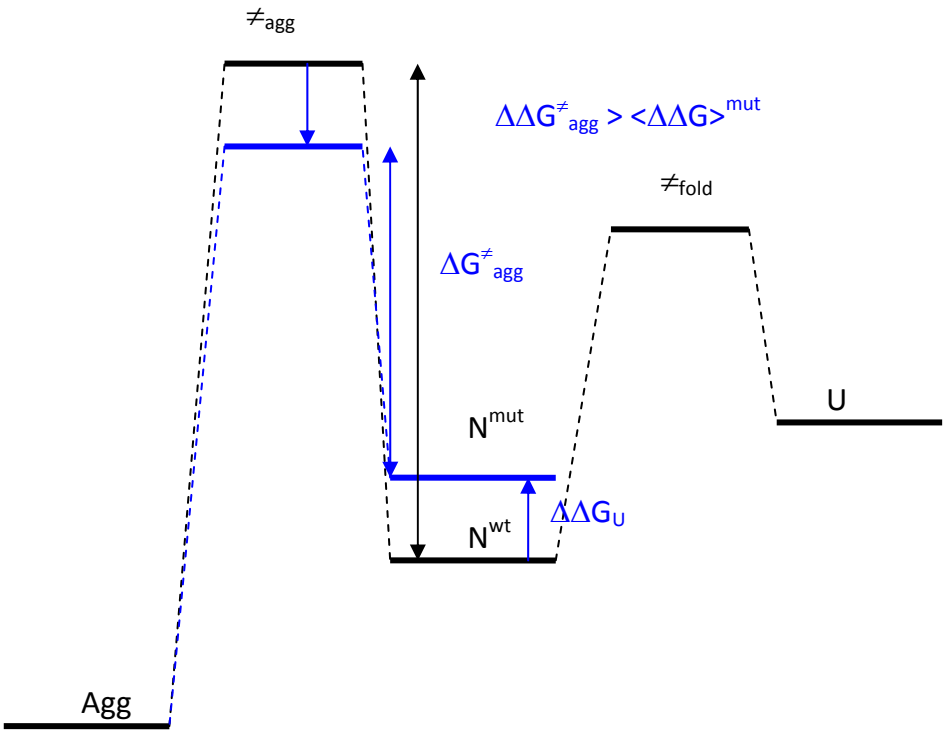

Table 6.3 summarizes the effects of the mutations on the nucleation rate constants and on folding stability and classifies the mutants under each class.

Table 6.3. *Effect of second mutations additional to N47A on the native state stability and activation energy barrier of fibril nucleation.*

Mutation to N47A	Structural element	$\Delta\ln(k_{agg}/min^{-1})$[a]	ΔG_u^{mut} [b] (kJ mol^{-1})	$-\langle\Delta\Delta G\rangle^{mut}/RT$ [c] (kJ mol^{-1})	Class[d]
L10A	β strand 1	--	-1.97±0.3	2.04±0.3	(inh)
R21D	RT loop	0.2 ± 0.6	6.33±0.4	-0.45±0.3	2
K27A	Diverging turn	1.4 ± 0.3	3.37±0.4	0.77±0.3	3
T32A	β strand 2	1.3 ± 0.3	1.46±0.3	1.44±0.3	1
N38A	n-src loop	1.9 ± 0.4	0.50±0.3	1.69±0.3	1
K43A	β strand 3	0.86 ± 0.24	(unf)	2.04±0.4	1-2
V46A	β strand 3	1.4 ± 0.6	1.75±0.3	1.35±0.3	1
D48G	Distal turn	--	7.34±0.5	-0.87±0.4	(inh)
V53A	β strand 4	1.9 ± 0.3	(unf)	2.04±0.4	1
A56G	3_{10} helix	2.04 ± 0.25	3.68±0.4	0.66±0.3	3
V58A	β strand 5	1.1 ± 0.5	(unf)	2.04±0.4	1-2

[a] *Calculated by fitting of the aggregation kinetics followed by ThT fluorescence using a double exponential decay.*
[b] *Unfolding Gibbs energy at 37 ºC of each double mutant measured by DSC by using a common heat capacity change of unfolding, $\Delta C_{p,u}$ of 3.67±0.15 that was determined by linear regression to all the ΔH_u (Tm) vs Tm data (see Table 6.2). Double mutants labelled (unf) are fully unfolded under fibrillation conditions.*
[c] *Calculated using equations 6.3 or 6.4 and using an unfolding Gibbs energy change of 5.28 kJ mol^{-1} for the N47A single mutant.*
[d] *Mutations labelled (inh) inhibited completely fibrillation.*

Figure 6.11 shows a comparison of the changes produced in the stability of the domain by the mutations and the changes in the aggregation rate constants.

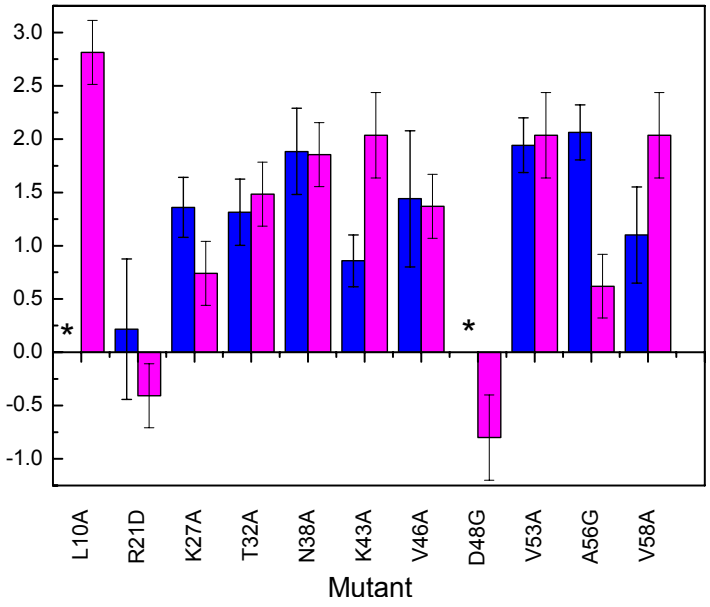

***Figure 6.11**. Changes in nucleation rate constants (∆ln(kagg/min^{-1}),blue) with the effects in native state stability (-<∆∆G>/RT, magenta).*

Figure 6.12 shows the location of mutated residues on a schematic ribbon representation of the Spc-SH3 structure. Each residue has been coloured according to its class. Class 1 mutations (T32A, N38A, V46A and V53A) and mutations classified as intermediate between class 1 and class 2 (K43A and V58A) are located in or near the core of the domain. According to our interpretation, these regions would be partially or completely unfolded in the transition state of fibril nucleation. Strikingly, these residues are in regions that have been described as part of the main structural motif of the folding transition state of the SH3 domain. In particular,

formation of the β3-β4-hairpin has been described as an obligatory step during folding of Spc-SH3 [27] and the central three-stranded β-sheet is largely folded in the transition state of Src-SH3 [28]. On the other hand, class 2 and 3 mutations, probing respectively native-like and non-native structure in the transition state of nucleation are located at the rest of structural elements, i.e., the long RT loop, the diverging turn and the 3_{10} helix. Most these regions have been shown to have low phi values (low structural order) in mutagenesis analysis of the folding transition state, whereas they would keep structural order in the transition state of fibril nucleation.

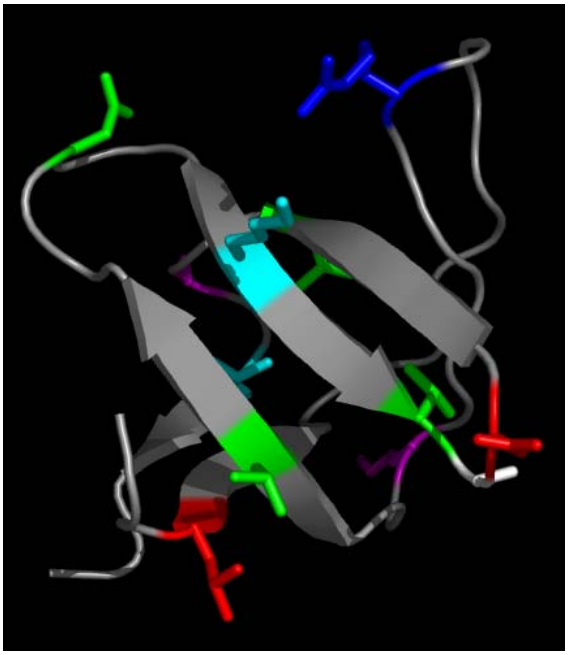

***Figure 6.12**. Schematic ribbon drawing of the Spc-SH3 domain structure showing each place of mutation coloured according to its class. Green, class 1; cyan, class 1-2; blue, class 2; magenta, class 3; red, inhibited fibrillation. N47A mutation is showed in white.*

It appears therefore that the transitions states of folding and fibrillation have markedly different structural features. While folding occurs by early formation of the distal β-hairpin followed by subsequent ordering of the rest of the structure around this motif, the conformational barrier leading to fibril nucleation does not follow the opposite but rather a completely different pathway, i.e., an unfolding of the central three-stranded β-sheet, while the other structural elements remain native-like or in non-native conformations. Accordingly, native folding and fibrillation of the Spc-SH3 domain take place on different regions of the conformational landscape.

This conclusion is of chief importance since it has been proposed that the sequences of native proteins have evolved to facilitate fast and efficient folding while setting high energy barriers that avoid fibrillation [29].

Despite their markedly different effect on the stability of the native state, mutations L10A and D48G abolished completely fibrillation, precluding their classification. Their inhibitory effect of fibrillation could be due to a particularly dramatic destabilization of the aggregation nuclei, to a large increase in the activation energy barrier of fibril nucleation or to a combination of both effects.

Mutation D48G has been described previously as strongly stabilizing the native state due to its effect on releasing steric strain at the distal turn, which facilitates formation of the distal β-hairpin and results in an increased folding rate [30]. Since nucleating fibrillation requires the selective unfolding of the distal β-hairpin, part of the central β-sheet, it is not surprising that this mutation precludes aggregation.

The effect of mutation L10A is even more remarkable. This mutation renders the Spc-SH3 domain highly unstable and at the same time abolishes fibrillation completely. It is possible that the hydrophobic

leucine sidechain is crucial to stabilize the structure of the transition state leading to nucleation. Another possibility is that L10 may be essential in structure of the aggregation nuclei and removal of the hydrophobic leucine sidechain may render nucleation energetically unfavourable. In any case this result indicates that this region of the domain is implicated in the specific interactions that occur during the initial steps of nuclei formation that trigger the aggregation cascade. This is in agreement with some studies in which it has been described the existence of specific intramolecular interactions between certain parts of the domain in the initial stage of the fibrillation process [31], [32]. This also happens in S6 protein, where certain amino acid residues locally grouped in the structure were found to act as ‘‘gate keepers” inhibiting the access to specific states that trigger the aggregation cascade [18]. Also, in human β2-microglobulin the kinetics of fibril formation seems to be regulated by a few key residues, with the rest of the sequence providing a scaffold for encouraging profitable interactions [33].

Also remarkable is the case of three mutants, K43A, V53A and V58A, which are initially unfolded under aggregation conditions and show fibrillation processes similar to that of folded mutants resulting in the same final fibrillar structures. This is also observed in the protein human β2-microglobulin since the fibrils formed commencing from a highly denatured state or a native-like precursor are apparently indistinguishable, suggesting that their assembly pathways must converge to a similar fibrillar product. This could occur either by unfolding of native β2-microglobulin to allow reorganisation of the protein structure, or by refolding of the highly dynamic polypeptide chain to a more structurally ordered intermediate species [34].

Taken all together, this mutagenic analysis clarifies the molecular mechanism of amyloid fibril formation and provides information about

which regions of the polypeptide chain are directly involved in the aggregation process.

6.7 BIBLIOGRAPHY

[1] Varela, L., Morel, B., Azuaga, A.I. and Conejero-Lara, F. (2009). A single mutation in an SH3 domain increases amyloid aggregation by accelerating nucleation, but not by destabilizing thermodynamically the native state. FEBS Lett 583, 801-6.

[2] Fersht, A.R., Matouschek, A. and Serrano, L. (1992). The folding of an enzyme. I. Theory of protein engineering analysis of stability and pathway of protein folding. J Mol Biol 224, 771-82.

[3] Privalov, P.L. (1979). Stability of proteins: small globular proteins. Adv Protein Chem 33, 167-241.

[4] Viguera, A.R., Martinez, J.C., Filimonov, V.V., Mateo, P.L. and Serrano, L. (1994). Thermodynamic and kinetic analysis of the SH3 domain of spectrin shows a two-state folding transition. Biochemistry 33, 2142-50.

[5] Filimonov, V.V., Azuaga, A.I., Viguera, A.R., Serrano, L. and Mateo, P.L. (1999). A thermodynamic analysis of a family of small globular proteins: SH3 domains. Biophys Chem 77, 195-208.

[6] Morel, B., Casares, S. and Conejero-Lara, F. (2006). A single mutation induces amyloid aggregation in the alpha-spectrin SH3 domain: analysis of the early stages of fibril formation. J Mol Biol 356, 453-68.

[7] LeVine, H., 3rd. (1999). Quantification of beta-sheet amyloid fibril structures with thioflavin T. Methods Enzymol 309, 274-84.

[8] DuBay, K.F., Pawar, A.P., Chiti, F., Zurdo, J., Dobson, C.M. and Vendruscolo, M. (2004). Prediction of the absolute aggregation rates of amyloidogenic polypeptide chains. J Mol Biol 341, 1317-26.

[9] Roseman, M.A. (1988). Hydrophobicity of the peptide C=O...H-N hydrogen-bonded group. J Mol Biol 201, 621-3.

[10] Cowan, R. and Whittaker, R.G. (1990). Hydrophobicity indices for amino acid residues as determined by high-performance liquid chromatography. Pept Res 3, 75-80.

[11] Broome, B.M. and Hecht, M.H. (2000). Nature disfavors sequences of alternating polar and non-polar amino acids: implications for amyloidogenesis. J Mol Biol 296, 961-8.

[12] Casares, S., Sadqi, M., Lopez-Mayorga, O., Conejero-Lara, F. and van Nuland, N.A. (2004). Detection and characterization of partially unfolded oligomers of the SH3 domain of alpha-spectrin. Biophys J 86, 2403-13.

[13] Chiti, F., Taddei, N., Bucciantini, M., White, P., Ramponi, G. and Dobson, C.M. (2000). Mutational analysis of the propensity for amyloid formation by a globular protein. EMBO J 19, 1441-9.

[14] Kim, Y.S., Wall, J.S., Meyer, J., Murphy, C., Randolph, T.W., Manning, M.C., Solomon, A. and Carpenter, J.F. (2000). Thermodynamic modulation of light chain amyloid fibril formation. Journal of Biological Chemistry 275, 1570-1574.

[15] Ramirez-Alvarado, M., Merkel, J.S. and Regan, L. (2000). A systematic exploration of the influence of the protein stability on amyloid fibril formation in vitro. Proc Natl Acad Sci U S A 97, 8979-84.

[16] Chiti, F., Calamai, M., Taddei, N., Stefani, M., Ramponi, G. and Dobson, C.M. (2002). Studies of the aggregation of mutant proteins in vitro provide insights into the genetics of amyloid diseases. Proc Natl Acad Sci U S A 99 Suppl 4, 16419-26.

[17] Ramirez-Alvarado, M. and Regan, L. (2002). Does the location of a mutation determine the ability to form amyloid fibrils? J Mol Biol 323, 17-22.

[18] Pedersen, J.S., Christensen, G. and Otzen, D.E. (2004). Modulation of S6 fibrillation by unfolding rates and gatekeeper residues. J Mol Biol 341, 575-88.

[19] Dumoulin, M. et al. (2005). Reduced global cooperativity is a common feature underlying the amyloidogenicity of pathogenic lysozyme mutations. J Mol Biol 346, 773-88.

[20] Chiti, F., Stefani, M., Taddei, N., Ramponi, G. and Dobson, C.M. (2003). Rationalization of the effects of mutations on peptide and protein aggregation rates. Nature 424, 805-8.

[21] Bitan, G., Kirkitadze, M.D., Lomakin, A., Vollers, S.S., Benedek, G.B. and Teplow, D.B. (2003). Amyloid beta -protein (Abeta) assembly: Abeta 40 and Abeta 42 oligomerize through distinct pathways. Proc Natl Acad Sci U S A 100, 330-5.

[22] Serio, T.R., Cashikar, A.G., Kowal, A.S., Sawicki, G.J., Moslehi, J.J., Serpell, L., Arnsdorf, M.F. and Lindquist, S.L. (2000). Nucleated conformational conversion and the replication of conformational information by a prion determinant. Science 289, 1317-21.

[23] Haass, C. and Selkoe, D.J. (2007). Soluble protein oligomers in neurodegeneration: lessons from the Alzheimer's amyloid beta-peptide. Nat Rev Mol Cell Biol 8, 101-12.

[24] Booth, D.R. et al. (1997). Instability, unfolding and aggregation of human lysozyme variants underlying amyloid fibrillogenesis. Nature 385, 787-93.
[25] Lai, Z., Colon, W. and Kelly, J.W. (1996). The acid-mediated denaturation pathway of transthyretin yields a conformational intermediate that can self-assemble into amyloid. Biochemistry 35, 6470-82.
[26] Fersht, A.R., Matouschek, A., Sancho, J., Serrano, L. and Vuilleumier, S. (1992). Pathway of protein folding. Faraday Discuss, 183-93.
[27] Martinez, J.C., Pisabarro, M.T. and Serrano, L. (1998). Obligatory steps in protein folding and the conformational diversity of the transition state. Nat Struct Biol 5, 721-9.
[28] Grantcharova, V.P., Riddle, D.S. and Baker, D. (2000). Long-range order in the src SH3 folding transition state. Proceedings of the National Academy of Sciences of the United States of America 97, 7084-7089.
[29] Dobson, C.M. (2001). The structural basis of protein folding and its links with human disease. Philos Trans R Soc Lond B Biol Sci 356, 133-45.
[30] Martinez, J.C. and Serrano, L. (1999). The folding transition state between SH3 domains is conformationally restricted and evolutionarily conserved. Nat Struct Biol 6, 1010-6.
[31] Bemporad, F., Vannocci, T., Varela, L., Azuaga, A.I. and Chiti, F. (2008). A model for the aggregation of the acylphosphatase from Sulfolobus solfataricus in its native-like state. Biochim Biophys Acta 1784, 1986-96.
[32] Bousset, L., Thomson, N.H., Radford, S.E. and Melki, R. (2002). The yeast prion Ure2p retains its native alpha-helical conformation upon assembly into protein fibrils in vitro. EMBO J 21, 2903-11.
[33] Routledge, K.E., Tartaglia, G.G., Platt, G.W., Vendruscolo, M. and Radford, S.E. (2009). Competition between intramolecular and intermolecular interactions in an amyloid-forming protein. J Mol Biol 389, 776-86.
[34] Platt, G.W. and Radford, S.E. (2009). Glimpses of the molecular mechanisms of beta2-microglobulin fibril formation in vitro: aggregation on a complex energy landscape. FEBS Lett 583, 2623-9.

7.

STRUCTURAL ANALYSIS OF AMYLOID FIBRILS

7. STRUCTURAL ANALYSIS OF AMYLOID FIBRILS

Nowadays there is a lack of detailed information on the relationship between structure and stability of amyloid fibrils that may shed light about the determinants of their formation.

In our preliminary results of monitoring fibrillation of Spc-SH3 by high-resolution NMR, only signals corresponding to the native protein were observed to gradually disappear during the course of aggregation and no other signals were observed, possibly due to extensive line broadening (chapter 3). This indicates that during the fibrillation pathway the native protein is incorporated into large species that cannot be observed by solution NMR.

H/D amide exchange combined with NMR spectroscopy constitutes a powerful technique to probe which regions of proteins are involved in stable structure at single-residue resolution. Recent applications of this approach to amyloid fibrils have shown that valuable structural information can be obtained about which regions of the polypeptide chain are involved in persistent hydrogen-bonded structure or excluded from solvent, providing a way to map the core structure of fibrillar assemblies.

Amyloid fibrils can be isolated from soluble material by centrifugation and resuspended in deuterated buffer allowing H/D exchange to occur. At several time points the exchange process can be quenched by freezing followed by lyophilization. The fibrils are then dissolved in d_6-DMSO, where H/D exchange is very slow and proton occupancy for each residue can then be measured in a 2D-HSQC NMR spectrum. The degree of protection against exchange compared with that of the fully disordered polypeptide chain informs about the residues involved in stable interactions within the fibrils. This procedure has been successfully used to characterize the regions of the protein chain involved in the amyloid fibril structures of several proteins [1, 2, 3, 4].

In an attempt to obtain structural information about the amyloid fibril core of the N47A Spc-SH3 domain, we have applied the methodology described above (see chapter 8 for details). We have analyzed the degree of protection against H/D amide exchange of amyloid fibrils preformed at different incubation times under our standard fibrillation conditions. We have compared the exchange profiles per residue of the polypeptide chain with those measured for the native state under the same experimental conditions (see Chapter 4).

7.1. ASSIGNMENT OF THE BACKBONE NMR RESONANCES OF THE DMSO-UNFOLDED PROTEIN

Prior to the H/D exchange experiment itself, it was necessary to assign the amide ^{1}H and ^{15}N NMR resonances in the DMSO-unfolded protein (see chapter 8). To achieve this goal, we prepared a 8 mg mL^{-1} sample of N47A Spc-SH3 in 95 % d_6-DMSO and 5 % H_2O at pH* 5.3 (direct pH-meter reading) and recorded an ^{1}H-^{15}N HSQC spectrum at 25 ºC. All backbone resonances in this spectrum are located in a quite limited range of HN chemical shifts from 7.7 to 8.9 ppm, suggesting that the protein was highly denatured (Figure 7.1).

We unambiguously assigned the backbone resonances of the 62 residues in the HSQC spectrum by using a set of triple resonance experiments (see chapter 8 for details). This task was achieved with the valuable help of Dr. Nico van Nuland and of Jose Luis Ortega Roldán. There is considerable overlapping between peaks in the HSQC spectrum, which precluded the measurement of the H/D exchange protection for a significant number of residues.

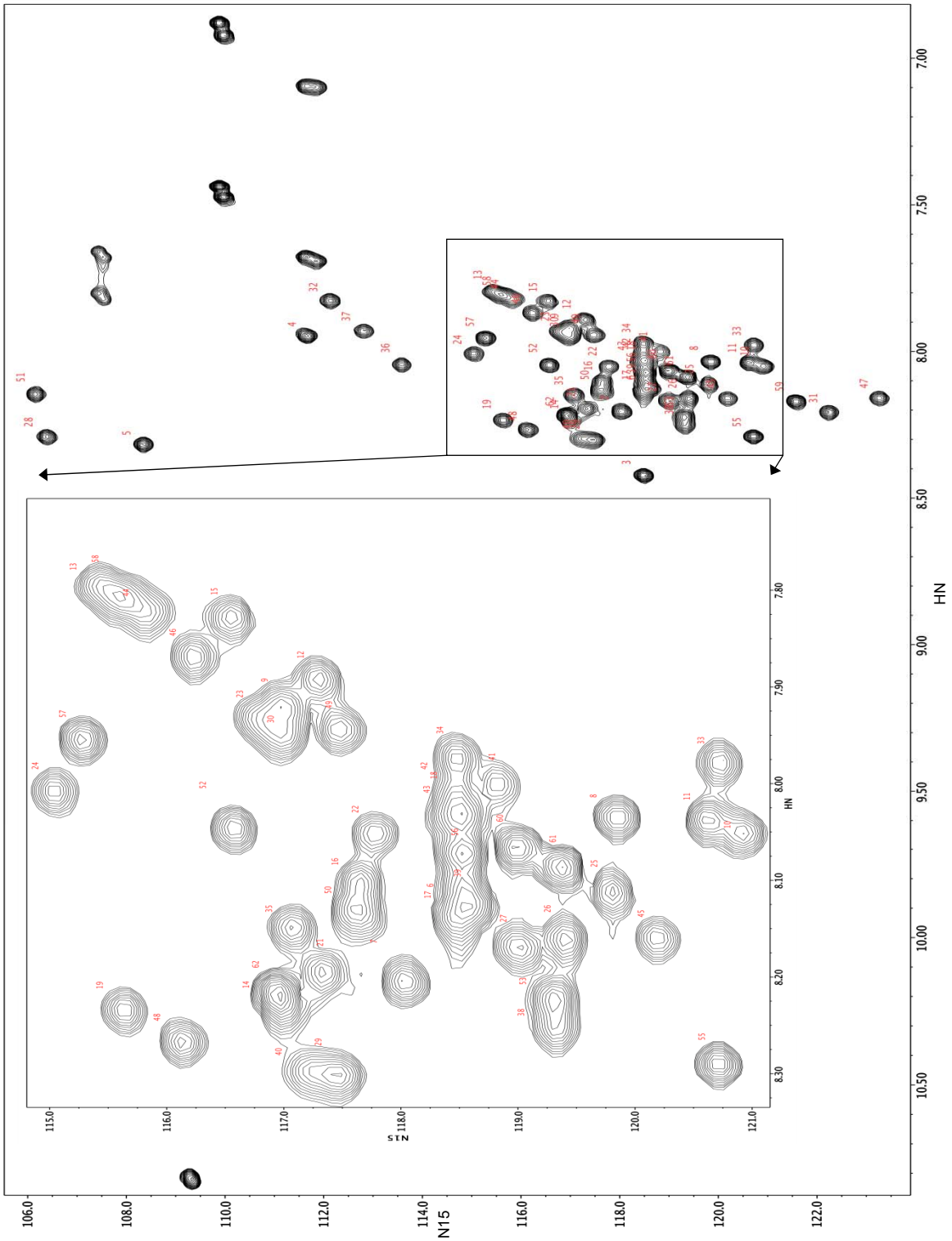

Figure 7.1. *^{1}H-^{15}N HSQC spectrum of N47A Spc-SH3 in 95% d_6-DMSO, 5% H_2O at pH 5.3 and 25ºC. The assignment of each backbone resonance is indicated by the residue number.*

7.2. HYDROGEN-DEUTERIUM EXCHANGE ANALYSIS OF N47A SPC-SH3 AMYLOID FIBRILS.

We prepared amyloid fibrils by incubation of two identical 8 mg mL^{-1} fresh protein samples of ^{15}N-labelled N47A Spc-SH3 during 10 days and during 1 month at 37 ºC [5]. The experimental conditions of fibril formation were 100 mM glycine buffer pH 3.2 and 100 mM NaCl. After incubation the fibrils were isolated by ultracentrifugation at 4 ºC and resuspended in ice-cold deuterated buffer and then the H/D exchange process was left to occur at 25 ºC for 7 days and 15 days. At time zero of exchange an identical sample aliquot was taken a reference sample. Exchange was stopped by freezing in liquid N_2 and lyophilization. Samples were redissolved in d_6-DMSO and the amide proton occupancy for each residue was measured by acquiring a series of ^{1}H-^{15}N-HSQC spectra, as described in Chapter 8. The proton occupancies at each time of exchange were compared with those of the reference sample in which no exchange was left to occur. The degrees of protection against H/D exchange of every residue at the two times of exchange have been plotted in Figure 7.2. The protection profiles have also been represented in colour code on ribbon representations of the native structure of the Spc-SH3 (Figure 7.3).

For the sake of clarity, Figure 7.4 shows TEM images of the amyloid fibrils formed at the two incubation times evaluated in this study, i.e. 10 days and 1 month, in order to relate the amyloid fibril morphology and the structural observations obtained with the H/D exchange method. As described in Chapter 3, fibrils incubated for 10 days are mainly curly and have low degree of order and low linear persistence, whereas fibril samples incubated during 1 month are mostly composed of well-ordered, straight and twisted amyloid fibrils.

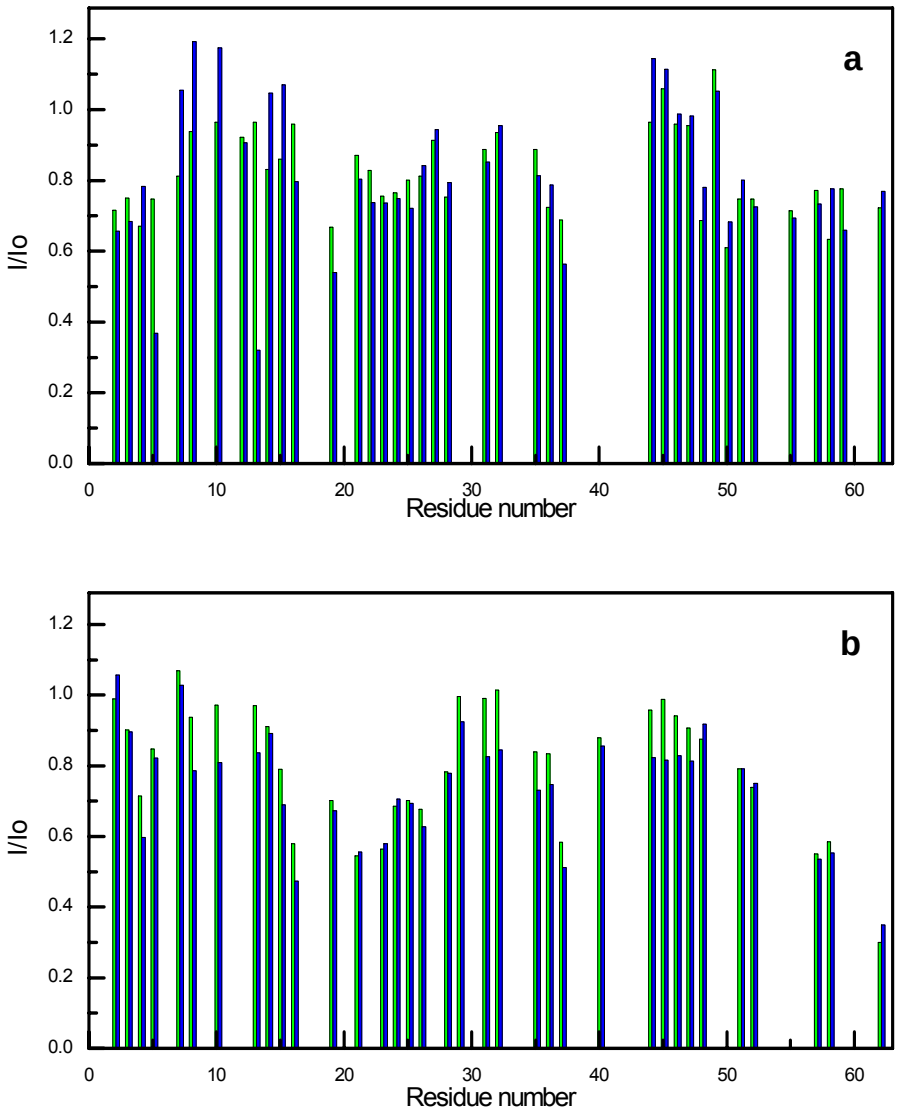

Figure 7.2. *Patterns of protection against H/D exchange of amyloid fibrils of N47A Spc-SH3 incubated during 10 days (A) and 1 month (B). Proton occupancies per residue relative to a non-exchanged fibril sample correspond to 7 days of H/D exchange (green) and 15 days (blue). Missing proton occupancies correspond to residues for which peaks in the HSQC spectrum measured in d_6-DMSO were overlapping.*

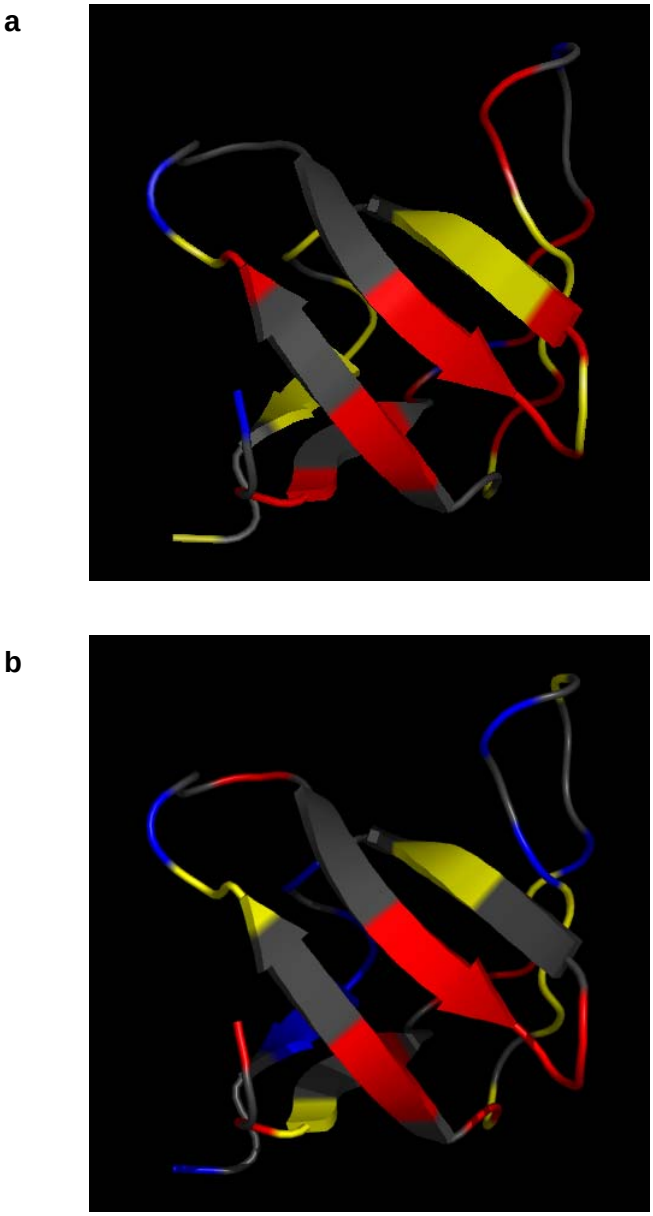

Figure 7.3. *Schematic representation of the N47A Spc-SH3 structure showing the proton occupancy of each residue in the amyloid fibrils atfer 15 days of H/D exchange. The thresholds of proton occupancy used for residue coloring are: red, $I/I_0 \geq 0.8$; yellow, $0.8 \geq I/I_0 \geq 0.6$; and blue, $I/I_0 \leq 0.6$. H/D exchange could not be measured for residues coloured in gray due to peak overlapping in the HSQC spectrum measured in d_6-DMSO. a) refers to 10 days incubation fibrils and b) refers to 1 month incubation fibrils.*

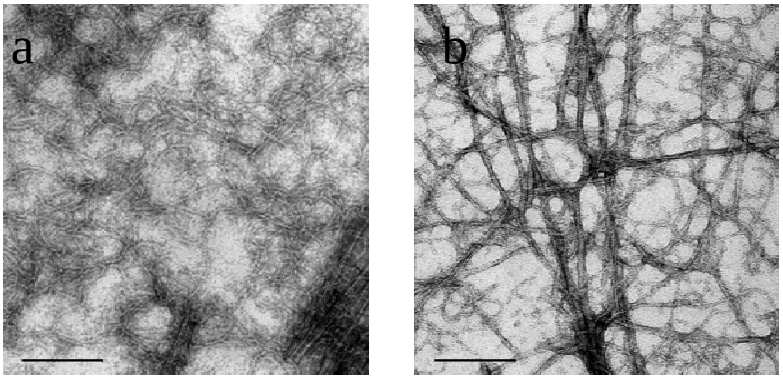

Figure 7.4. *Electron microscopy images of amyloid fibrils prepared by 10 days of incubation (a) and 1 month of incunbation (b). The scale bar represents 140 nm.*

Figure 7.2 shows the H/D exchange profiles for the two types of fibrils analyzed at 7 and 15 days of exchange. For a few residues the proton occupancies are higher than 1, suggesting some systematic errors in the measurement of the intensities of the NMR spectra. This is due to the intrinsic difficulty of these experiments, which required extensive sample manipulation. Nevertheless, it is immediately evident that the degree of protection against H/D exchange for the protein backbone within the fibrils is very high. In addition the protection patterns of the two fibril types are different, which is suggestive of a different internal structure.

In the case of fibrils incubated for 10 days the pattern of protection is relatively homogeneous and barely changed between 7 and 15 days of exchange. For a large subset of residues the proton occupancy ranges between 0.6 and 0.8, except for four residues (Gly5, Tyr13 and to less extent Ser19 and Thr37) that have decreased occupancies after 15 days of exchange. On the other hand, there are some stretches of residues showing a high protection, with proton occupancies near 1. These residues are located in region 7-16, corresponding in the native structure to the β_1-strand and the

beginning of the RT-loop, region 44-49, at the end of the β_3-strand and at the distal turn, and few residues near the diverging turn and the first part β_2-strand.

The H/D exchange pattern of amyloid fibrils incubated for 1 month is different to some extent. After 7 days of exchange, the regions of the protein backbone that remained fully protected against the exchange overlap partially with those observed in 10-days-old fibrils. These regions are residues 8-14, corresponding to the β_1-strand and the initial residues of the RT-loop, residues 29-32, located at the diverging turn and the first half of β_2-strand, and residues 44-48, corresponding to the end of β_3 strand and the distal turn. In addition, there is high protection at the N-terminus (residues 2-7) plus residue 40 at the n-src loop. Other regions show considerably less protection than in fibrils incubated for 10 days. In particular, part of the RT-loop, the 3_{10} helix and the β_4 and β_5 strands. After 15 days of exchange the proton occupancy of few of the most protected residues decreased to about 0.8, but for the rest it changes little in general.

7.3. DISCUSSION

Here we have obtained a first direct observation of the residues involved in the structure in two different types of fibrillar states of the Spc-SH3 domain. The results reveal that the protection against H/D exchange of the protein backbone in the fibrils is dramatically different from that of the native Spc-SH3 domain under similar experimental conditions (see chapter 4).

In the soluble native protein the H/D exchange occurs through an EX2 mechanism, with exponential decays of proton occupancies in all residues taking place within few days at 25ºC (see chapter 4 and [6]). In contrast, in the fibrillar state the proton occupancy of most residues remained relatively high and quite stable for more than two weeks.

The patterns of H/D exchange protection are also highly different between the native protein and the fibrillar state. In the native protein, residues 1-7 at the unstructured N-terminus exchanged completely within the dead time of the experiment. Fast exchange also occurred for unprotected residues 47 and 48 at the distal turn and the other loops and C-terminal end, whereas residues involved in stable secondary structures showed the highest protection degree. In contrast to this, in both types of fibrils the N-terminus and the residues at the distal turn were highly protected, indicating their participation in the fibril structure. Other residues with low or no protection in the native protein were also protected considerably in the fibrils. Accordingly, the regions of the N47A Spc-SH3 chain participating in the structure of the fibrillar states are markedly different to those in the native state.

Similar differences between the H/D mechanism of the soluble protein and the fibrillar state has been observed in Aβ peptides [7]. In this case all backbone amide hydrogens of the monomeric state undergo very rapid H/D exchange, consistent with the absence of protective structure within the molecule. On the other hand, Aβ incorporated into fibrils undergoes much slower exchange with complex kinetics having at least three classes of backbone amides in fibrils: those that exchange as rapidly as the backbone amide hydrogens of the monomer, those that exchange at intermediate rates, and those that do not exchange even after long times of exposure to D_2O, being about 50 % of the Aβ peptide backbone residues in this highly protected, rigid core structure of the fibrils.

A similar conclusion has been described in a H/D exchange study of β_2-microglobulin, in which most residues in the middle region of the molecule, even in the loop regions in the native form, were strongly protected from the H/D exchange [1]. Using a similar method to study transthyretin amyloid fibrils a model of the fibril core was proposed, in

which some of the β strands in the native structure are preserved from exchange whereas some loops, connecting parts and the rest of the β strands are exposed [8].

In the case of mature amyloid fibrils of the PI3-SH3 the pattern of H/D exchange measured at pH 1.6 suggested that the protected region of the amyloid fibrils encompasses much of the protein sequence (Ala 5 to Tyr 78) except few residues at the N- and the C-termini [2], even though previous models of the PI3-SH3 fibrils indicated that about 40% of the protein sequence is contained within the fibril β-sheet core. These observations bear some resemblance with our results. To explain the relatively homogeneous exchange pattern and the complex kinetics of H/D exchange in the amyloid fibrils of the PI3-SH3 domain, Dobson and coworkers proposed a molecular recycling mechanism of H/D exchange [2], in which the ensemble of molecules within the fibrils is in dynamic equilibrium with a pool of soluble protein molecules. Under these conditions, most of the amide hydrogens in the protein monomer are protected by their packing in the fibril structure but they fully exchange with the solvent upon monomer dissociation from the fibril ends. This dissociation-exchange-reassociation mechanism would then result in a slow and homogeneous change in the distribution of the proton occupancies within the fibril, as observed experimentally.

Our results with N47A Spc-SH3 amyloid fibrils also show H/D exchange patterns with a large part of the protein chain showing proton occupancies between 0.6 and 0.8, which suggest that the molecular recycling mechanism described for the PI3-SH3 domain may at least partially influence the exchange in these fibrils. Nevertheless, there are sequence regions with almost full protection even for long times of exchange, indicating that they are involved in highly persistent structure. In addition, significant differences between the exchange patterns observed for the two types of fibrils may be related with their morphological differences.

Both types of fibrils share similar regions in their persistent core structures, including the β_1-strand and the initial residues of the RT-loop, the diverging turn and first half of β_2-strand, and the end of β_3 strand and the distal turn. The 1-month-old mature fibrils incorporate additionally the N-terminal residues to the persistent core, whereas the two C-terminal β-strands become more solvent exposed. This shift in the fibril core structure is clearly manifested in the structural order and morphology of the fibrils.

In a very recent study using a pulsed-labelling H/D exchange method combined with electrospray-ionization mass spectrometry, Dobson and coworkers have obtained significant detail about the protected structure of amyloid fibrils of the PI3-SH3 domain formed by different conditions, favouring either protofibrillar or amorphous intermediates [9]. Despite the different mechanism of assembly, the two types of fibrils also share a considerable similarity in the protected core structure as we observe here. In the PI3-SH3 fibrils the most protected residues are at the RT-loop and the diverging turn and other regions have partial protection. Small differences between the fibrils were observed such as a higher protection at the N-terminus in one of them, as we observed here for the 1-month-old mature fibrils. These authors explained this additional protection by differences in the way the protofilaments interact within the higher-order structure of the mature fibrils.

7.4. BIBLIOGRAPHY

[1] Hoshino, M., Katou, H., Hagihara, Y., Hasegawa, K., Naiki, H. and Goto, Y. (2002). Mapping the core of the beta(2)-microglobulin amyloid fibril by H/D exchange. Nat Struct Biol 9, 332-6.

[2] Carulla, N. et al. (2005). Molecular recycling within amyloid fibrils. Nature 436, 554-8.

[3] Whittemore, N.A., Mishra, R., Kheterpal, I., Williams, A.D., Wetzel, R. and Serpersu, E.H. (2005). Hydrogen-deuterium (H/D) exchange mapping of Abeta 1-40 amyloid fibril secondary structure using nuclear magnetic resonance spectroscopy. Biochemistry 44, 4434-41.

[4] Vilar, M. et al. (2008). The fold of alpha-synuclein fibrils. Proc Natl Acad Sci U S A 105, 8637-42.

[5] Morel, B., Casares, S. and Conejero-Lara, F. (2006). A single mutation induces amyloid aggregation in the alpha-spectrin SH3 domain: analysis of the early stages of fibril formation. J Mol Biol 356, 453-68.

[6] Casares, S., Sadqi, M., Lopez-Mayorga, O., Martinez, J.C. and Conejero-Lara, F. (2003). Structural cooperativity in the SH3 domain studied by site-directed mutagenesis and amide hydrogen exchange. FEBS Lett 539, 125-30.

[7] Kheterpal, I., Zhou, S., Cook, K.D. and Wetzel, R. (2000). Abeta amyloid fibrils possess a core structure highly resistant to hydrogen exchange. Proc Natl Acad Sci U S A 97, 13597-601.

[8] Olofsson, A., Ippel, J.H., Wijmenga, S.S., Lundgren, E. and Ohman, A. (2004). Probing solvent accessibility of transthyretin amyloid by solution NMR spectroscopy. J Biol Chem 279, 5699-707.

[9] Carulla, N., Zhou, M., Arimon, M., Gairi, M., Giralt, E., Robinson, C.V. and Dobson, C.M. (2009). Experimental characterization of disordered and ordered aggregates populated during the process of amyloid fibril formation. Proc Natl Acad Sci U S A 106, 7828-33.

8.

MATERIALS AND METHODS

8. MATERIALS AND METHODS

8.1. PREPARATION OF PROTEIN SAMPLES

Large quantities of protein were required for the proposed research due to the high concentrations necessary for the aggregation experiments and the impossibility to recover most of the samples used.

The plasmids with the DNA encoding the WT Spc-SH3 and the N47A Spc-SH3 domains were kindly provided by Dr. Luis Serrano and Dr. Jose C. Martínez respectively whereas the DNA of all the double mutants was obtained using a QuickChange Site-Directed Mutagenesis kit (Stratagene) using primers designed to insert the desired mutations in the DNA of the N47A Spc-SH3 mutant, which was used as template (Table 8.1). The PCR program used is described in Table 8.2.

The melting temperature of the primers (T_{ml}) was calculated with the equation described in the QuickChange Site-Directed Mutagenesis kit instruction manual (Equation 8.1).

$$T_{ml} = 81.5 + 0.41 \times (\%GC) - 675 / N - \%mismatch \qquad (8.1)$$

Where %GC is the total percentage of guanidines and cytosines in the primer; N is the number of nucleotides of the primer and %mismatch is the percentage of nucleotides of the primer differing from the original DNA.

The DNAs obtained were inserted into pET3d plasmids for WT Spc-SH3 and pBAT4 plasmids for the rest of the mutants [1], all containing the ampicillin resistance gene. *E. coli* XL10-GOLD cells (Novagen) were transformed with the plasmids to amplify the DNAs. The plasmidic DNAs were then purified using a kit from Qiagen and sequenced at the sequencing facility of the Institute “López Neyra”

(CSIC, Granada). Once checked, the plasmids were then inserted into *E. coli* BL21/DE3 cells (Novagen) to over express the proteins.

Table 8.1. *Forward and reverse primer sequences used for site-directed mutagenesis upon the N47A mutant.*

Mutant	Primers	Primer melting temperature, T_{ml} (ºC)
L10A	5'-GAGCTTGTGGCAGCACTCTATGATTACC-3' 3'-GGTAATCATAGAGTGCTGCCACAAGCTC-5'	69.70
R21D	5'-CAAGAGAAGAGTCCTGACGAGGTGACTATGAAG-3' 3'-CTTCATAGTCACCTCGTCAGGACTCTTCTCTTG-5'	72.00
K27A	5'-GGTGACTATGAAGGCAGGAGATATTCTAACCC-3' 3'-GGGTTAGAATATCTCCTGCCTTCATAGTCACC-5'	71.80
T32A	5'-GGAGATATTCTAGCCCTGCTCAACAGC-3' 3'-GCTGTTGAGCAGGGCTAGAATATCTCC-5'	74.00
N38A	5'-GCTCAACAGCACCGCCAAGGACTGGTGG-3' 3'-CCACCAGTCCTTGGCGGTGCTGTTGAGC-5'	76.60
K43A	5'-CAAGGACTGGTGGGCGGTTGAAGTTGCC-3' 3'-GGCAACTTCAACCGCCCACCAGTCCTTG-5'	75.14
V46A	5'-GGAAGGTTGAAGCTGCCGATCGTCAGGG-3' 3'-CCCTGACGATCGGCAGCTTCAACCTTCC-5'	77.00
D48G	5'-GTTGAAGTTGCCGGTCGTCAGGGCTTTG-3' 3'-CAAAGCCCTGACGACCGGCAACTTCAAC-5'	77.25
V53A	5'-GTCAGGGCTTTGCACCAGCTGCCTATG-3' 3'-CATAGGCAGCTGGTGCAAAGCCCTGAC-5'	77.00
A56G	5'-GCTTTGTACCAGCTGGCTATGTGAAAAAAC-3' 3'-GTTTTTTCACATAGCCAGCTGGTACAAAGC-5'	73.43
V58A	5'-CCAGCTGCCTATGCGAAAAAACTAGATTAG-3' 3'-CTAATCTAGTTTTTTCGCATAGGCAGCTGG-5'	73.44

Table 8.2. *PCR program used for mutagenesis.*

Process	Time	Temperature (ºC)	Cycles
Initial DNA denaturation	30 sec	95	1
DNA denaturation	30 sec	95	20
Primers annealing	1 sec	$T=T_{ml}-5$	
DNA chain extension	10 min	68	
DNA elongation completion	3 min	68	1
Storage	End	4	1

Prior to overexpression of the proteins, the optimal conditions were checked for all the double mutants doing expression tests at different temperatures and using different IPTG induction times. The expression conditions used for WT and N47A Spc-SH3 domains were those already tested by Dr. Ana R. Viguera in her previous research [2] (Table 8.3). In all cases the optimal incubation temperature was 37 ºC.

The unlabelled proteins were expressed in cell cultures using standard LB medium and purified as described elsewhere [3]. The ^{15}N-labelled and the ^{15}N-^{13}C-doubly labelled proteins were expressed in cultures grown in minimal media M9 and purified as described elsewhere [4].

Prior to experiments at low protein concentration, the samples were thoroughly dialyzed against the appropriate buffer using dyalisis membranes with a 3500 Da MW-cutoff (Spectra/Por), whereas for aggregation experiments the lyophilized protein was directly dissolved in the buffer and the pH was checked after dissolution. In all cases the protein samples were centrifuged for 2 minutes at 14440 g in a micro-centrifuge (Hettich) and filtered through a 0.2 μm filter (Millipore).

Table 8.3. *Optimal expression conditions for the Spc-SH3 variants.*

Spc-SH3 Variant	Optimal expression conditions
WT	IPTG addition when O.D = 0.7, cell cultures collection after 14 hours of the IPTG addition.
N47A	IPTG addition at the beginning, cell cultures collection after 24 hours of the IPTG addition.
N47A L10A	IPTG addition when O.D = 0.7, cell cultures collection after 3 hours of the IPTG addition.
N47A R21D	IPTG addition when O.D = 0.7, cell cultures collection after 14 hours of the IPTG addition.
N47A K27A	IPTG addition at the beginning, cell cultures collection after 24 hours of the IPTG addition.
N47A T32A	IPTG addition when O.D = 0.7, cell cultures collection after 3 hours of the IPTG addition.
N47A N38A	IPTG addition when O.D = 0.7, cell cultures collection after 3 hours of the IPTG addition.
N47A K43A	IPTG addition when O.D = 0.7, cell cultures collection after 3 hours of the IPTG addition.
N47A V46A	IPTG addition when O.D = 0.7, cell cultures collection after 3 hours of the IPTG addition.
N47A D48G	IPTG addition when O.D = 0.7, cell cultures collection after 3 hours of the IPTG addition.
N47A V53A	IPTG addition when O.D = 0.7, cell cultures collection after 3 hours of the IPTG addition.
N47A A56G	IPTG addition when O.D = 0.7, cell cultures collection after 14 hours of the IPTG addition.
N47A V58A	IPTG addition when O.D = 0.7, cell cultures collection after 3 hours of the IPTG addition.

The protein concentration was determined by measurement of absorbance at 280 nm in a Lambda-25 (Perkin-Elmer) or Cary-50-Bio (Varian) spectrophotometer using extinction coefficients, ε_{280} = 15512.0

M^{-1} cm^{-1} and ε_{280} = 15220.2 M^{-1} cm^{-1}, for the WT and the N47A variants respectively, previously determined by other group members using the method of Gill and von Hippel [5]. For the double mutants the extinction coefficient of the N47A mutant was used without correction since any of the mutants imply change in the aromatic aminoacids.

8.2. FLUORESCENCE SPECTROSCOPY

Fluorescence consists in a photon emission that occurs when species excited by absorption of electromagnetic radiation decay to the ground level. The aromatic side chains of phenylalanine, tyrosine and tryptophan contribute to the intrinsic fluorescence emission of proteins in the UV-visible spectrum region [6-9]. Among these aromatic aminoacids, tryptophan presents the highest fluorescence intensity and its emission spectrum is the most sensitive to changes in its close environment. This allows the observation of changes in the tryptophan fluorescence emission spectra as a result of conformational processes in proteins (subunit association, ligand binding processes, or protein folding-unfolding). These changes can be observed as a wavelength shift of the fluorescent emission band and/or as a change in the intensity of fluorescence [10].

Apart from the intrinsic fluorescence of proteins, it is possible to study conformational changes in proteins by monitoring the fluorescence of dyes or fluorescent compounds that interact specifically with certain states or conformations of the protein. In this study we have used two of these compounds, i.e., Thioflavine T (ThT) (Sigma), which interacts specifically with amyloid aggregates increasing strongly its fluorescence [11], and 8-Anilino-naphthalene-1-sulfonic acid (ANS) (Fluka), which is an aromatic compound that specifically interacts with solvent-exposed hydrophobic patches in proteins with a strong fluorescence enhancement. ANS is commonly used to identify and characterize partially folded states in proteins [12].

8.2.1. Folding-unfolding kinetics

The folding and unfolding reactions of small globular proteins take place in a time scale that typically varies between a few milliseconds and a few seconds. The folding kinetic curves of single domain proteins usually follow a single exponential decay, which means that a unique activation energy barrier exists separating the native and the unfolded states. Proteins formed by several domains or with alternative conformations during the processes, can display more complicated kinetic mechanisms.

The observation of fast conformational events occurring in the time-scale of milliseconds to seconds, leading to the formation of partially-unfolded species and early aggregation precursors needs the use of fast techniques, such as stopped-flow spectroscopy and rapid mixing methods.

In this work we used either an Applied Photophysics SX.18MV-R or a Bio-Logic (Claix, France) SFM-3 stopped-flow spectrometers, both equipped with fluorescence detection (Figure 8.1).

Under drive activation, the two small volumes of solutions are driven from high performance syringes through a high efficiency mixer. The resultant mixture passes through a measurement flow cell and into a stopping syringe. As the solution fills the stopping syringe, the plunger hits a block, causing the flow to be stopped instantaneously. Using appropriate techniques, the kinetics of the reaction can be measured in the cell.

In these experiments the protein folding or unfolding process starts after the rapid mixing of an unfolded or a native protein solution, respectively, with an excess volume (usually 10–fold) of buffer containing different concentrations of denaturant (urea). After this event the fluorescence signal is registered during the time course of the process. The dead time of the stopped-flow instruments was estimated to be in the range of 3-4 ms.

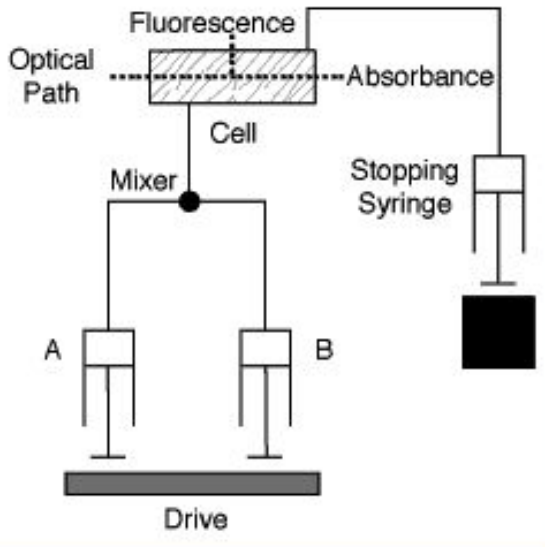

Figure 8.1. *Schematic representation of a stopped-flow device.*

The native protein samples were dissolved in the proper buffer, whereas the unfolded protein samples were dissolved in the same buffer containing a urea concentration of around 8 M. The different urea concentration samples were prepared by mixing different amounts of buffer and urea solution. The final urea concentration in all the solutions was determined by measurement of the refractive index with an Abbe refractometer (Atago) using Equation 8.2 [13]:

$$[\text{urea}] = 117.66 \times \Delta n + 29.753 \times (\Delta n)^2 + 185.56 \times (\Delta n)^3 \qquad (8.2)$$

where Δn is the difference between the refraction index of the urea solution and that of the pure buffer.

All the solutions were filtered and thermostatized at the proper temperature prior to each experiment.

The changes in the intrinsic tryptophan fluorescence were followed by monitoring the total fluorescence above 320 nm (using a cut-off filter), with excitation at 295 nm (8 nm bandwidth). The changes in the fluorescence of ANS were followed by measuring the total fluorescence above 420 nm, with excitation at 370 nm. The time scales were adjusted depending on the duration of the folding and unfolding kinetics. The photomultiplier voltage was set to a constant value for each set of experiments made to be compared. Typically, an unfolding or refolding kinetic trace was obtained by averaging 5 shots under identical conditions.

Unless stated, the averaged kinetics was fitted to an exponential decay function to obtain the kinetic parameters (rate constant, amplitude, starting and ending point). To obtain a 'Chevron' plot, the neperian logarithm of the apparent kinetic constants (k_{urea}) was represented against the urea concentration (Equation 8.3) and the curve was analyzed with Origin software (OriginLab, Northampton, MA) according to the two-state model to obtain different magnitudes of the folding-unfolding reaction (folding and unfolding rate constants in the absence of urea ($k_{\mp\text{-}D}$ and $k_{\mp\text{-}N}$), folding and unfolding branch slopes ($m_{\mp\text{-}D}$ and $m_{\mp\text{-}N}$), urea concentration at the transition midpoint, unfolding Gibbs energy, etc.) [14].

$$\ln k_{urea} = \ln\left[\left(k_{\mp\text{-}D}\times\exp\left(m_{\mp\text{-}D}\times[urea]\right)\right)+\left(k_{\mp\text{-}N}\times\exp\left(m_{\mp\text{-}N}\times[urea]\right)\right)\right] \qquad (8.3)$$

8.2.2. Thioflavin T binding assay

ThT binding assays were performed to monitor the kinetics of amyloid fibril aggregation [15]. The ThT fluorescence is considered as approximately proportional to the mass of amyloid aggregates and is one of the most extended probes in the study of the kinetics of amyloid formation [11].

These fluorescence experiments were performed using a Perkin Elmer LS-55 spectrofluorimeter (Perkin Elmer, Shelton, CT, USA) and a Cary Eclipse spectrofluorimeter (Varian Inc.).

A typical fluorimeter includes a light source, a specimen chamber with integrated optical components, and high sensitivity detectors. The most common light sources for fluorimeters are lamp sources, such as xenon arc lamps. These lamps provide a relatively uniform intensity over a broad spectral range from the ultraviolet to the near infrared. The optical paths of the excitation and the detection light paths are along the orthogonal axis. The orthogonal arrangement ensures minimal leakage of excitation light into the detection side. High sensitivity photodetectors such as photomultipliers or charge coupled device cameras are commonly used. For spectral measurement, monochromators or bandpass filters are placed in the excitation and emission light paths to select a specific spectral band.

To perform studies of aggregation kinetics, a 1.1 mM (8 mg/mL) protein sample was incubated at 37 ºC in the appropriate buffer to form amyloid fibrils [16]. At different incubation times aliquots of 10 μL were taken from the solution and rapidly frozen in liquid nitrogen. A 250 μM stock solution of ThT was freshly prepared in 25 mM potassium phosphate buffer (pH 6.0). Protein aliquots (10 μL) were diluted into 25 mM phosphate buffer at pH 6.0 (940 μL) and 50 μL of ThT solution were added obtaining a final volume of 1 mL. The fluorescence emission spectra were recorded between 450 and 600 nm (5 nm band width) at 25 ºC in a 10 mm path-length cuvette using an excitation wavelength of 440 nm (2.5 nm band width). The ThT fluorescence intensity was evaluated from the emission spectra by integration of the area under the spectrum curve.

8.2.3. Equilibrium urea-induced unfolding experiments

Intrinsic and ANS fluorescence measurements were performed to follow the unfolding of the protein under equilibrium. Protein samples (30 μM) were prepared with different concentrations of urea (0–8 M) in the appropriate buffer and equilibrated at 25 ºC overnight. To measure ANS fluorescence the solutions contained 25 μM of ANS.

Tryptophan fluorescence measurements were performed at 25 ºC recording the emission spectra from 300 to 400 nm (2.5 nm band width) with an excitation wavelength of 295 nm (5 nm band width). ANS fluorescence emission spectra were recorded from 400 to 600 nm (5.5 nm band width) using an excitation wavelength of 370 nm (7.5 nm band width). Relative fluorescence intensity values were evaluated from the area under the spectra and plotted against molar concentration of urea.

8.2.4. Equilibrium thermal unfolding experiments

Intrinsic and ANS fluorescence measurements were performed to follow the thermal unfolding of the protein. These fluorescence experiments were performed using a Cary Eclipse spectrofluorimeter equipped with a temperature controller Peltier system (Varian Inc.).

Protein samples at concentrations sufficiently low to avoid aggregation were prepared in the proper buffer containing 50 μM of ANS. Both intrinsic fluorescence at 350 nm and ANS fluorescence at 480 nm were simultaneously measured during the temperature scans (from 10 ºC to 100 ºC). Excitation wavelengths were 295 nm and 370 nm for intrinsic and ANS fluorescence respectively.

8.3. DYNAMIC LIGHT SCATTERING

Dynamic light scattering (DLS) gives information about the molecular size of the particles present in a solution. The intensity of the light dispersed by a small volume of a particles solution is not constant

but it rapidly fluctuates with time. These fluctuations are due to the thermal Brownian motions of the particles that produce variations in the distance between them. Interferences between the light waves dispersed by neighbour particles give rise to the intensity fluctuations in the plane of detection, containing information about these movements. Analysing the relationship between the intensity fluctuations and time allows us obtaining the translational diffusion coefficient of the particles, D. Using the Stokes-Einstein equation (Equation 8.4) it is possible to calculate the apparent hydrodynamic radius of the particles, supposed these approximately spherical.

$$D = \frac{k_B \times T}{6 \times \pi \times \eta \times R} \tag{8.4}$$

k_B is the Boltzmann constant, T is the absolute temperature, η is the viscosity of the solution and R is the ideal gases constant.

A DLS instrument provides the correlation function of the dispersed light intensity during a period of time. This function is obtained by measuring the similitude between a signal acquired at a time and the same signal measured after a delay. The correlation function expresses the fluctuation rate of the dispersed light intensity due to the Brownian movements of the particles.

In DLS there are two correlation functions of two properties of the particle solution. The first one is obtained from the photon flow (Equation 8.5) and the second one from the magnetic field that comes from the light spectrum Fourier transformed (Equation 8.6). These two correlation functions are then combined to give the final correlation function, which takes into account the phase similitude between them [17, 18].

$$G^2(\tau) =< i(t)i(t+\tau) >= \int_0^\infty i(t)i(t+\tau)dt \quad (8.5)$$

$$G^1(\tau) =< B(t)B^*(t+\tau) > \quad (8.6)$$

G^1 and G^2 represent the two correlation functions, i represents the photon flow, B is the magnetic field and τ is the lag time between the acquisitions of both properties (i and B) at two different times.

When $\tau = 0$, G^2 and G^1 are completely in phase so the final correlation function is big. When τ increases, G^2 and G^1 become out of phase so the final correlation function decreases. This correlation function is a single exponential decay if there is a unique particle size in the solution or a multiple exponential decay for more complicated mixtures.

DLS measurements were performed with a DynaPro MS-X instrument (Wyatt Technology Corporation, Santa Barbara, CA, USA) equipped with Peltier temperature control of the sample (Figure 8.2).

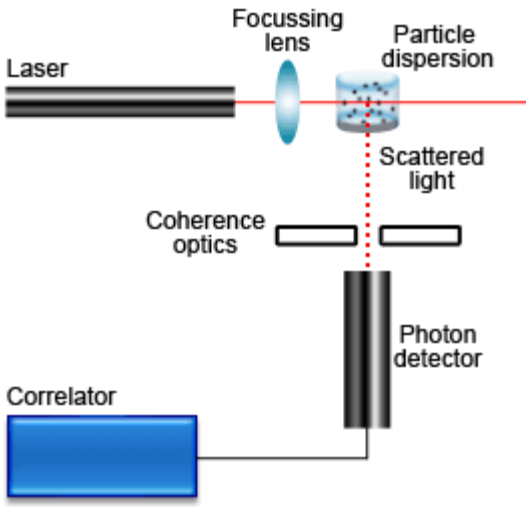

Figure 8.2. *Schematic representation of a DLS instrument.*

A dynamic light scattering instrument contains a light source that is a laser, a spectrometer containing the optical components, a detector that is usually a photomultiplier, a signal analyzer and a computer with software for analysis.

The protein solutions and the buffers were centrifuged and filtered through 0.02 μL Anotop filters (Whatman plc, Brentford, Middlesex, UK) immediately before the measurements. DLS measurements were made using a 30 μL quartz sample cuvette at constant temperature (typically 37 ºC in the aggregation kinetic experiments). DLS data were acquired during 5 seconds and averaged every 45 seconds. Data were recorded as a function of time until saturation of the scattering signal. Prior to the start of the experiment the laser power was adapted to the sample characteristics to avoid early saturation of the instrument. Dynamics software (Wyatt Technology Corporation, Santa Barbara, CA, USA) was used in data collection and processing to obtain the distributions of hydrodynamic radii in the solution during the aggregation process. Hydrodynamic radius, scattering intensity and mass percentage of all the species in the solution were plotted against the incubation time.

8.4. CIRCULAR DICHROISM

Circular dichroism spectroscopy (CD) measures the wavelength dependence of the differential absorption of the left and right-handed circularly polarized light. The left- and right-handed components of a polarized beam of light interact differently with the chiral centres of an optically active chromophore. This interaction results in a decrease of the velocity of wave propagation and its absorption, which depends on the wavelength (Equation 8.7 and 8.8).

$$\Delta Abs\ (\lambda) = AbsL\ (\lambda) - AbsR\ (\lambda) = [\varepsilon L\ (\lambda) - \varepsilon R\ (\lambda)] \times c \times l \quad (8.7)$$

$$\Delta Abs\ (\lambda) = \Delta\varepsilon \times c \times l \quad (8.8)$$

being AbsL(λ) and AbsR(λ) the absorbances of the sample of the left- and right-handed circularly polarized light respectively, c the sample concentration in molar, l is the light path length in cm and εL(λ) and εR(λ) the molar extinction coefficients for every type of light in L mol^{-1} cm^{-1}. This phenomenon results in a difference in amplitude and phase between the two components of the polarized light so that the vector sum of the two components rotates following an elliptical helical path proportional to the ΔAbs(λ) that is measured in ellipticity units (θ) (degrees). The normalized CD spectra are expressed as molar ellipticity [θ] in degree cm^2 $dmol^{-1}$.

Circular dichroism is a useful technique to study protein and nucleic acids conformational properties in solution [19]. The CD bands observed in proteins are situated in two regions of the electromagnetic spectrum, in the far-UV, between 170 and 250 nm, where most contributions absorption bands come from the peptide bonds, and in the near-UV, between 250 and 320 nm, where the bands arise from the aminoacids with aromatic groups in their side chains. Each region gives different and complementary information about protein structure. The far-UV CD spectroscopy has high sensitivity to changes in the different secondary structure elements in proteins: α-helix, β-sheets, β-turns, random coils [20] (Figure 8.3), whereas the near-UV CD spectroscopy gives information about changes in the tertiary structure of the protein.

CD experiments were performed on a Jasco J-715 (Tokyo, Japan) spectropolarimeter equipped with a Peltier-thermostated cell holder (Figure 8.4).

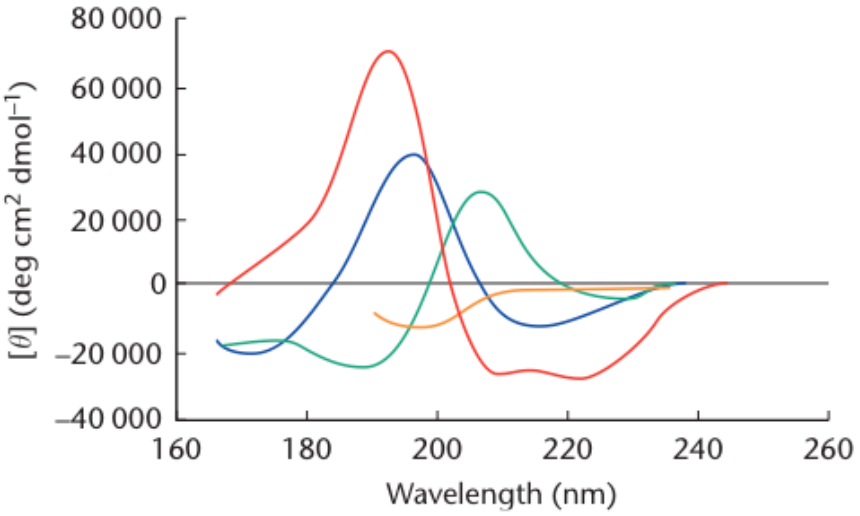

***Figure 8.3**. Typical CD spectra of pure secondary structure elements in proteins and polypeptides. Red, α-helix; blue, antiparallel β-sheet; green, type I β-turn and orange, random coil.*

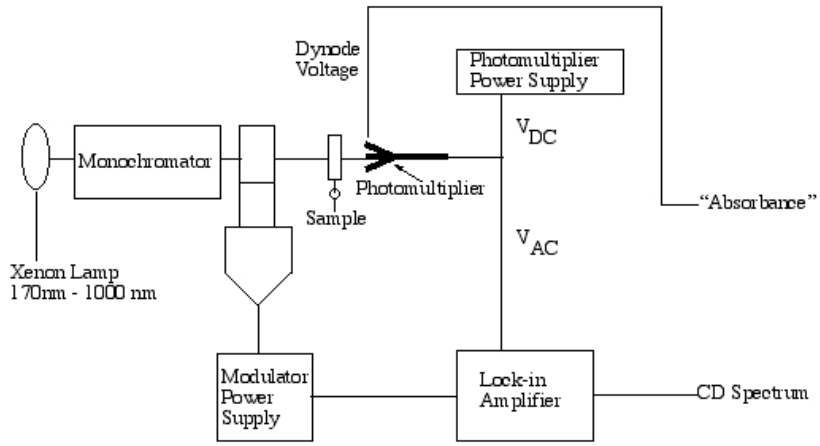

***Figure 8.4.** Schematic diagram of the components of a CD instrument.*

A CD instrument produce a periodic variation in the polarization of the light beam induced by the polarization modulator through all

ellipticities from left circular through elliptical, unchanged linear and elliptical to right circular. This polarized light passes through the sample to a photomultiplier detector.

Measurements of the far-UV CD spectra (260–190 nm) were made using a 0.1 mm path length quartz cuvette. The resulting spectrum was the average of eight scans at 100 nm/min, 0.5 nm step resolution, 1 second of response and 0.5 nm of band width. A nitrogen flow of 9 L/min was used to purge and refrigerate the system.

To monitor the time course of aggregation, 70 μL of freshly prepared protein sample were introduced in the cuvette and incubated at constant temperature (37 ºC). The CD signal at 215 nm was measured as a function of time with 20 seconds step resolution, 4 seconds of response and 1.0 nm of band width**.**

8.5. TRANSMISSION ELECTRON MICROSCOPY

Transmission electron microscopy (TEM) uses an electron beam to visualize objects with sizes in the range of nm to μm. This technique is widely used to obtain morphological information about the aggregates formed during the amyloid fibrillation process.

TEM measurements were made in a Zeiss 902 electron microscope was used operating at 80 kV (Figure 8.5). The main parts of an electron microscope are: the electron gun that provides the electron beam that interacts with the specimen and becomes dispersed creating an augmented image; the magnetic lenses that direct and focus the electron beam, a high vacuum system that prevents the dispersion of electrons by the air molecules; an image recording system consisting in a photographic film or a electronic sensor interfaced to a computer.

To prepare samples for TEM observation during the aggregation process, 20 μL aliquots were taken from the aggregating sample and rapidly frozen in liquid nitrogen. Just before measurement the samples

were diluted 10-fold with buffer and 15 μL aliquots were placed on top of a formvar (polyvinyl formal polymer for support films) coated grid and left for 4 min. The grid was then washed twice with distilled water and stained with 1 % (w/v) uranyl acetate (a powerful electron dispersion dye) during 1 min. The samples were dried during 6 minutes at 40 ºC and then observed in the microscope. The negatives images were digitalized to follow the morphological changes of the aggregates during the fibrillation kinetics.

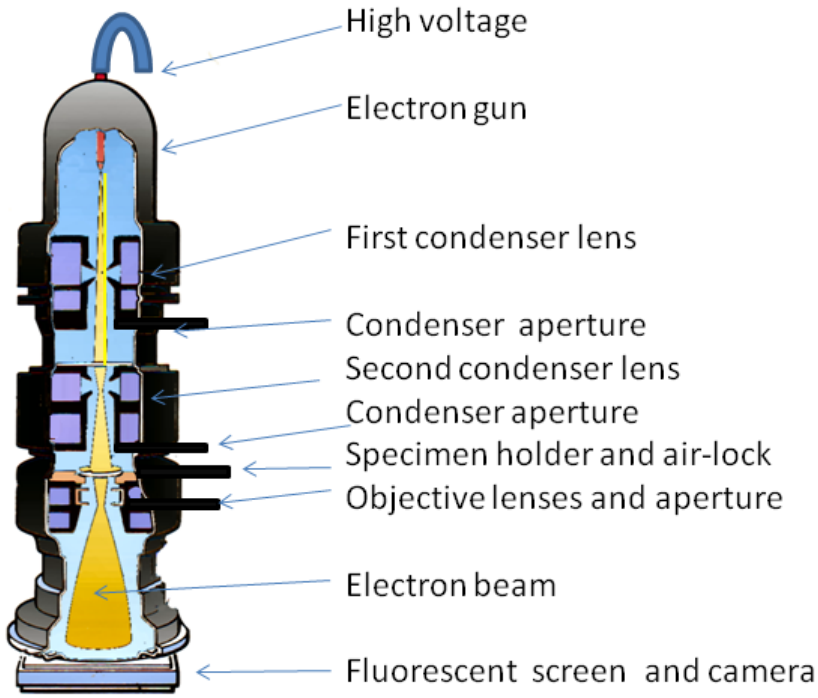

Figure 8.5. *Scheme of a transmission electron microscope.*

8.6. NUCLEAR MAGNETIC RESONANCE

The conformational changes of the soluble states of the protein (native state and low-order oligomers) may be characterized in real time by NMR at high resolution under favourable conditions. ^{1}H and ^{15}N chemical shift changes can be easily measured for the backbone

with 2D ^{1}H-^{15}N HSQC (*Heteronuclear Single-Quantum Correlation)* spectra [21], constituting a very sensitive probe of the conformation of the protein in solution.

For fast time-resolved measurements, 2D ^{1}H-^{15}N SOFAST-HMQC (*band-Selected Optimized Flip-Angle Short Transient Heteronuclear Multiple-Quantum Correlation*) spectra [22] can be measured within a few seconds providing similar information as the standard 2D HSQC experiment but a much higher time resolution. Chemical shift displacements produced by added agents, changes in environmental conditions or during the course of aggregation may allow the structural characterization of partially or fully unfolded species, if sufficiently populated in solution.

Solution NMR spectroscopy suffers however of extraordinary line broadenings when analyzing large molecules and especially protein aggregates due to their fast relaxation, making it useless to study these systems directly in solution. Nevertheless, there are some powerful NMR-based methods to circumvent this problem, in particular those based on hydrogen-deuterium exchange, as described below.

To perform all the NMR experiments we used singly labelled (^{15}N) or doubly labelled (^{15}N and ^{13}C) protein. The NMR spectra were acquired in a Varian NMR Direct-Drive Systems 600 MHz spectrometer (^{1}H resonance frequency of 600.25 MHz) equipped with a triple resonance probe with XYZ-pulsed field gradients. The spectra were processed with NMRPipe [23] and analyzed with NMRview [24].

8.6.1. Amyloid fibril formation monitored by two-dimensional NMR.

To follow the amyloid fibril aggregation by two-dimensional NMR in real time, 4 mg of ^{15}N-labelled protein was dissolved in 500 μL of cold aggregation buffer (100 mM Gly, 100 mM NaCl, pH 3.2) containing 10 % D_2O and placed into the NMR tube. The final protein concentration

was 1.1 mM (8 mg/mL). The temperature in the probe was set to 37 ºC and immediately after temperature equilibration a series of ^{1}H-^{15}N HSQCs were acquired during the time course of aggregation. Spectra of 512x32 complex points were recorded using a relaxation delay of 1 second resulting in a total experiment time of 2 minutes and 28 seconds. The spectral widths were 12.04 ppm for ^{1}H and 30.00 ppm for ^{15}N.

The assignment of the ^{1}H-^{15}N crosspeaks of the HSQC spectrum of the N47A Spc-SH3 domain was performed using as a reference the previously published assignment of the WT Spc-SH3 domain [25].

To obtain the aggregation kinetics, the signal intensities were evaluated using NMRview and represented against incubation time.

8.6.2. Native-state amide hydrogen/deuterium exchange followed by NMR spectroscopy.

Proteins and peptides in aqueous solution have the ability to exchange their labile hydrogens with hydrogens of the solvent [26]. The speed of the hydrogen exchange depends on the solution conditions (pH, temperature, ionic strength, etc.) as well as the chemical nature and the local environment of each hydrogen. Hydrogen exchange rates give therefore information about conformational properties of proteins.

In proteins there are three different kinds of hydrogens depending on the speed of exchange with the solvent:

- Hydrogens covalently bonded to carbon exchange too slowly to be observable.
- Hydrogens bonded to oxygen or nitrogen in side chains exchange very fast and are usually not observable.
- Hydrogens bonded to the amide nitrogen in the peptide bonds exchange with intermediate speed depending on the local

environment of the hydrogen. This exchange is usually observable by NMR.

The amide hydrogen-deuterium exchange method (H/D exchange) measures the exchange of the third kind of hydrogens by the deuteriums from the solvent. A typical H/D exchange experiment is usually made by rapid dissolution of the polypeptide or protein into deuterated buffer immediate followed by observation of the rate of disappearance of the amide proton signals by NMR. The rate of exchange of a particular amide hydrogen is well described by the following first-order rate equation, equation 8.9:

$$-\frac{d[H]}{dt} = k_{obs}[H] \qquad (8.9)$$

where k_{obs} is the observed first-order rate constant of exchange and [H] is the concentration of unexchanged hydrogens in the sample.

The exchange rate constants in fully unstructured polypeptides chains have been previously calibrated using model peptides by Englander and coworkers [27], allowing the calculation of the so-called “intrinsic rate constants”, k_{int}, for a known polypeptide sequence under specific solution conditions [28].

Any kind of structure in a polypeptide chain will affect the H/D exchange of the amide hydrogen of each residue. For instance, in a structured protein many amide hydrogens are occluded from the solvent in the protein interior, hindering the access of the solvent to the amide hydrogen locus. Nevertheless, the most important factor slowing-down hydrogen exchange is the involvement in hydrogen bonds [29, 30]. Most slowly-exchanging hydrogens in proteins have been found to participate in hydrogen bonds even at the protein surface.

The protective effect of structure on the H/D exchange rates can be evaluated as a protection factor, PF, which is given by the ratio between k_{int} and the experimental rate constant, k_{obs}, observed for this residue (Equation 8.10).

$$PF = \frac{k_{int}}{k_{obs}} \tag{8.10}$$

When interpreting the protection factors, one has to take into account the dynamics of the conformational processes that render an amide hydrogen accessible to solvent for exchange [31]. If the conformational fluctuations are much faster than the intrinsic exchange (mechanism EX2), the observed exchange rate is given by equation 8.11 [32]:

$$k_{obs} = K_{op} \times k_{int} \tag{8.11}$$

where K_{op} is the "opening" equilibrium constant for the conformational process. This scenario is the most frequent for globular proteins of rapid folding if the intrinsic exchange rate constants are not too high (not very high pH). In this situation the PF values provide thermodynamic information about the dynamic conformational processes of the protein (equation 8.12).

The opposite limit (EX1) occurs when the intrinsic exchange is much faster than the conformational processes, and then the exchange rate constant observed is equal to the rate of opening or unfolding process that exposes the hydrogen to the solvent.

$$\Delta G_{op} = -RT \times \ln(K_{op}) = -RT \times \ln\left(\frac{k_{obs}}{k_{int}}\right) = RT \times \ln PF \tag{8.12}$$

In this work, the H/D exchange measurements have been made under conditions where the EX2 mechanism is fully applicable [28,33]. The H/D exchange rate constants were measured under native conditions dissolving approximately 0.5 mg of protein in 500 μL of buffer with 100 mM d_5-glycine, at pH* 3.2 and 30 ºC at different salt concentrations. The final protein concentration was about 0.15 mM. Immediately after, the sample was filtered through a 0.45 μm filter, placed in a NMR tube and this inside the NMR probe, previously set at the desired temperature. After temperature equilibration (approximately 7 minutes after sample dissolution) a series of two-dimensional ^{1}H-^{15}N SOFAST-HMQCs were recorded. Spectra of 1700x32 complex points were recorded using a relaxation delay of 0.3 seconds resulting in a total experiment time varying from 11 minutes and 4 seconds to 43 minutes and 47 seconds, depending on the number of acquisitions per increment. The spectral width was 14.20 ppm for ^{1}H and 28.00 ppm for ^{15}N.

The equilibrium constants (K_{op}) for the conformational opening process, rendering the amide hydrogen of each particular residue susceptible to exchange, was calculated using Equation 8.11, and the apparent Gibbs energy of H/D exchange was obtained by Equation 8.12.

8.6.3. Amide hydrogen/deuterium exchange in the amyloid fibrils.

Amide H/D EXCHANGE combined with NMR spectroscopy has also been used to characterize the structure of amyloid fibrils and to extract valuable structural information about regions of the polypeptide chains that are involved in persistent hydrogen-bonded structure or are excluded from solvent, providing a way to map the core structure of fibrillar assemblies [34,35].

To perform these experiments it is necessary to prepare amyloid fibrils in the usual protonated aggregation buffer and isolate them from the soluble material. Then the fibrils are resuspended it in fully deuterated aggregation buffer allowing the H/D exchange process to occur. At certain time points, a sample aliquot is frozen in liquid nitrogen and lyophilized to stop exchange and remove the solvent.

To evaluate the progress of exchange by NMR the lyophilized sample aliquot has to be dissolved in a solvent able to disaggregate the amyloid fibrils into protein monomers. In addition, the solvent must slow down the exchange process to allow NMR measurement of the proton occupancy of each amide group. DMSO is exceptionally useful for these H/D exchange experiments with amyloid fibrils for the following reasons. First, DMSO effectively dissolves amyloid fibrils into the monomeric unfolded form, which is amenable to NMR analysis [36]. Second, DMSO has no exchangeable protons. In the presence of >90 % (v/v) DMSO, the base-catalyzed H/D exchange is substantially suppressed, resulting in a ≈ 100-fold reduction of intrinsic exchange rate [37]. These two properties thus make monitoring the H/D exchange kinetics of amyloid fibrils possible.

The drawback of this approach is the need of assigning the NMR signals of the amide protons in the DMSO-unfolded state of the protein. This procedure is described below. Once this assignment is available the proton occupancy of each residue can be evaluated by measuring the cross peak intensity in a HSQC spectrum. Since H/D exchange is not fully suppressed in DMSO, a series of consecutive HSQC spectra need to be acquired to correct for the slow exchange that occurs during measurements.

Amyloid fibrils were prepared as described [16] by incubating an 8 mg/mL fresh sample of ^{15}N,^{13}C-labelled N47A Spc-SH3 at 37 ºC during 10 days and 1 month. The fibrils were separated from the soluble protein by centrifugation of the fibril solution at 104444 at 4 ºC during 3

hours. The pelleted fibrils were resuspended in double volume of deuterated buffer (100 mM NaCl, 100 mM Gly, pD* 3.2, 100 % D_2O) and agitated vigorously using a magnetic stirrer during 12 hours at 4 ºC. Once the fibril suspension was homogeneous, the H/D exchange reaction was initiated by raising the temperature of the solution to 25 ºC.

At several times of H/D exchange (3 days; 7 days; and 15 days), fibril sample aliquots of approximately 4 mg were frozen in liquid nitrogen, immediately lyophilized and kept at -80 ºC until measurement. For H/D exchange measurement the lyophilized samples were dissolved in 95 % (v/v) d_6-dimethyl sulfoxide, 5 % D_2O, pD* 5.3 [34]. After dissolution and pD* readjustment (10 minutes), the sample solution was filtered and immediately loaded into a NMR tube and it was performed the equilibration (30 minutes). A set of 7 or 8 consecutive HSQCs were recorded at 25 ºC. Spectra of 2048x64 complex points were recorded using a relaxation delay of 1 second resulting in a total experiment time of 20 minutes and 2 seconds. The spectral width was 14.20 ppm for ^{1}H and 22.00 ppm for ^{15}N. A reference spectrum was acquired with a sample, for which the H/D exchange process was omitted.

The intensities of every peak of the HSQC series were extrapolated to time zero to obtain the intensity of every peak at the moment of the dissolution of the fibrils in DMSO. The corrected intensities were referred to those measured for the sample in which exchange was omitted. This procedure provided us with the proton occupancy for each residue of the protein in the fibrils at each time of H/D exchange. H/D exchange could not be measured for some residues due to peak overlapping in the HSQC spectrum measured in DMSO.

8.6.4. Assignment of the amide ^{1}H and ^{15}N NMR resonances in DMSO-unfolded state.

The assignment of the amide ^{1}H and ^{15}N NMR resonances in the DMSO-unfolded protein was carried out using a set of triple resonance experiments (HNCACB, CBCA(CO)NH, HNCO, HNCACO, CC-TOCSY) with the valuable assistance of Dr. Nico van Nuland and of José Luis Ortega Roldán. ^{1}H chemical shifts were referenced with respect to the 2.5 ppm methyl signal of d_6-DMSO.

A modified version of SmartNotebook 3.2 [38] tool integrated in NMRView was used to semi-automatically assign the protein backbone in DMSO. The SmartNotebook module allows visual inspection of backbone sequential connectivities between residues and provides a tool to assign these residues to segments of the primary sequence based on the characteristic random coil carbon chemical shifts of each aminoacid [39]. Peak lists containing ^{13}CO, $^{13}C\alpha$ and $^{13}C\beta$ frequencies taken from the HNCO, HNCACO, HNCACB and CBCA(CO)NH spectra at the ^{1}H,^{15}N frequency pair of every peak in the HSQC spectrum were used as input for SmartNotebook, which then creates automatically connections between the ^{1}H,^{15}N pairs [4]. Due to the high overlap present in the HSQC spectrum, the CC-TOCSY spectrum was used to visually inspect the correctness of the assignment.

8.7. DIFFERENTIAL SCANNING CALORIMETRY

DSC is the most powerful technique to directly measure the energetic changes occurring during conformational processes in proteins [40]. This technique measures the heat capacity of the protein solution as a function of temperature and is the only technique capable of a complete thermodynamic characterization of the folding-unfolding equilibrium of a protein providing information about the mechanism and cooperativity of the process.

For the unfolding of a typical globular protein, the usual output of a DSC experiment is a thermogram with a heat absorption peak that indicates an endothermic process induced by the temperature increment. Once the thermogram is analyzed and if the unfolding process takes place under equilibrium (it is reversible and not scan rate dependent), it is possible to determine all thermodynamic parameters associated with the transition such as the enthalpy, ΔH, the entropy, ΔS, the Gibbs energy, ΔG and the heat capacity, ΔC_p.

In this work the DSC experiments were carried out with an automatic VP-DSC (Valery-Plotnikov differential scanning calorimeter) capillary-cell microcalorimeter instrument from MicroCal (Northampton, MA) [41] (Figure 8.6).

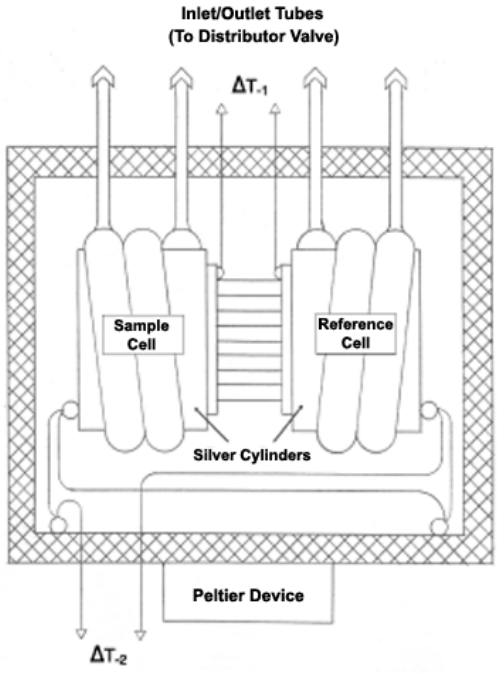

Figure 8.6. *VP-DSC capillary calorimeter diagram.*

This calorimeter works adiabatically and measures the difference in heat capacity between two almost identical cells. The temperature

scan can be performed by increasing and decreasing the temperature in a continuously, constant and limited way to allow the sample to be in equilibrium during the complete scan. The DSC experiments were carried out at scan rates of 120 °C/h or 90 ºC/h. Calorimetric cells (operating volume 0.135 mL) were kept under an excess pressure of 60 psi to prevent degassing during the scan and also to permit the scans to be extended up to a temperature of 125 °C without boiling.

DSC was used to measure the thermodynamic magnitudes characterizing the native-state stability of the Spc-SH3 domain and the mutants under study [42]. DSC thermograms were also acquired during thermally-induced fibrillation to measure the energetic changes involved during this process. In addition, since amyloid fibrils can be melted and dissociated at high temperatures [16], we also used DSC to monitor this process and determine the energetic changes involved in fibril dissociation.

Protein solutions for the calorimetric experiments under native conditions were prepared by exhaustive dialysis against the proper buffer, and the buffer from the last dialysis step was used in the reference cell of the calorimeter. For the calorimetric experiments directed to monitor thermally-induced aggregation, fresh lyophilized protein was dissolved in the proper buffer. For experiments with preformed amyloid fibrils, fibrils were prepared as described before [16] and centrifugated at 104444 g at 4 ºC for 3 hours. The pellets were resuspended in the same buffer.

Several baselines with buffer in both cells were obtained before each run in order to ascertain an appropriate equilibration of the instrument. Reheating runs were carried out to determine the calorimetric reversibility of the denaturation processes. After baseline subtraction, the temperature dependence of the partial molar heat capacity (Cp) was calculated from the DSC thermograms using Origin (OriginLab, Northampton, MA) as described elsewhere [40]. Firstly, the

calorimeter signal (mV) was converted into molar heat capacity units (kJ K^{-1} mol^{-1}) taking into account the instrument dynamic correction and response, the scan speed, the cell volume, the protein concentration and the protein partial specific volume (supposed 0.73 mL/g for all globular protein [43]). The Cp curves were fitted according to the two-state unfolding model when possible, as described elsewhere [2] using a quadratic function (equation 8.13) to describe the molar heat capacity of the unfolded state ($C_{p,u}$), which was calculated for every protein variant as described elsewhere [43] (Table 8.4).

$$C_{p,u} = a0 + b0 \times T + c0 \times T^2 \qquad (8.13)$$

Table 8.4. *Parameter to determine the $C_{p,u}$ function*

.

Variant	b0	c0
WT	0.11242	-0.000140
N47A	0.11013	-0.000140
N47AL10A	0.11100	-0.000144
N47AR21D	0.10941	-0.000140
N47AK27A	0.11254	-0.000146
N47AT32A	0.11340	-0.000148
N47AN38A	0.10800	-0.000140
N47AK43A	0.11249	-0.000146
N47AV46A	0.10964	-0.000141
N47AD48G	0.10910	-0.000142
N47AV53A	0.10960	-0.000141
N47AA56G	0.11100	-0.000142
N47AV58A	0.10960	-0.000141

The intercept in the quadratic equation, a0, was determined independently in every DSC experiment and b0 and c0 are kept constant during the fitting.

8.8. BIBLIOGRAPHY

[1] Peranen, J., Rikkonen, M., Hyvonen, M. and Kaariainen, L. (1996). T7 vectors with modified T7lac promoter for expression of proteins in Escherichia coli. Anal Biochem 236, 371-3.

[2] Viguera, A.R., Martinez, J.C., Filimonov, V.V., Mateo, P.L. and Serrano, L. (1994). Thermodynamic and kinetic analysis of the SH3 domain of spectrin shows a two-state folding transition. Biochemistry 33, 2142-50.

[3] Sadqi, M., Casares, S., Abril, M.A., Lopez-Mayorga, O., Conejero-Lara, F. and Freire, E. (1999). The native state conformational ensemble of the SH3 domain from alpha-spectrin. Biochemistry 38, 8899-906.

[4] Ortega Roldan, J.L., Romero Romero, M.L., Ora, A., Ab, E., Lopez Mayorga, O., Azuaga, A.I. and van Nuland, N.A. (2007). The high resolution NMR structure of the third SH3 domain of CD2AP. J Biomol NMR 39, 331-6.

[5] Gill, S.C. and von Hippel, P.H. (1989). Calculation of protein extinction coefficients from amino acid sequence data. Anal Biochem 182, 319-26.

[6] Demchenko, A.P. (1981). Ultraviolet spectroscopy of proteins. Springer-Verlag, New York (USA)

[7] Konev, S.V. (1967). Fluorescence and phosphorescence of proteins and nucleic acids. Plenum Press, New York (USA)

[8] Permyakov, E.A. (1993). Luminiscent spectroscopy of proteins. CRC Press, Boca Raton (Florida, USA)

[9] Weinryb, I.S., R.F. (1971). The luminiscence of aromatic amino acids. In Excited States of Proteins and Nucleic Acids. Plenum Press, New York (USA), 277-318.

[10] Royer, C.A. (2006). Probing protein folding and conformational transitions with fluorescence. Chem Rev 106, 1769-84.

[11] LeVine, H., 3rd. (1999). Quantification of beta-sheet amyloid fibril structures with thioflavin T. Methods Enzymol 309, 274-84.

[12] Azuaga, A.I., Dobson, C.M., Mateo, P.L. and Conejero-Lara, F. (2002). Unfolding and aggregation during the thermal denaturation of streptokinase. Eur J Biochem 269, 4121-33.

[13] Warren, J.R. (1966). On the refractive indices of aqueous solutions of urea. J Phys Chem A 70, 297-300.

[14] Martinez, J.C. and Serrano, L. (1999). The folding transition state between SH3 domains is conformationally restricted and evolutionarily conserved. Nat Struct Biol 6, 1010-6.
[15] Nilsson, M.R. (2004). Techniques to study amyloid fibril formation in vitro. Methods 34, 151-160.
[16] Morel, B., Casares, S. and Conejero-Lara, F. (2006). A single mutation induces amyloid aggregation in the alpha-spectrin SH3 domain: analysis of the early stages of fibril formation. J Mol Biol 356, 453-68.
[17] Hiemenz, P., C. (1984). Light Scattering by Polymer Solutions. Polymer Chemistry: The Basic Concepts, 659-722.
[18] Pecora, R. (1985). Dynamic Light Scattering: Applications of Photon Correlation Spectroscopy. Plenum Press.
[19] Johnson, W.C., Jr. (1990). Protein secondary structure and circular dichroism: a practical guide. Proteins 7, 205-14.
[20] Compton, L.A. and Johnson, W.C., Jr. (1986). Analysis of protein circular dichroism spectra for secondary structure using a simple matrix multiplication. Anal Biochem 155, 155-67.
[21] Palmer, A.G., 3rd, Fairbrother, W.J., Cavanagh, J., Wright, P.E. and Rance, M. (1992). Improved resolution in three-dimensional constant-time triple resonance NMR spectroscopy of proteins. J Biomol NMR 2, 103-8.
[22] Schanda, P., Kupce, E. and Brutscher, B. (2005). SOFAST-HMQC experiments for recording two-dimensional heteronuclear correlation spectra of proteins within a few seconds. J Biomol NMR 33, 199-211.
[23] Delaglio, F., Grzesiek, S., Vuister, G.W., Zhu, G., Pfeifer, J. and Bax, A. (1995). NMRPipe: a multidimensional spectral processing system based on UNIX pipes. J Biomol NMR 6, 277-93.
[24] Johnson, B.A., Stevens, S.P. and Williamson, J.M. (1994). Determination of the three-dimensional structure of margatoxin by 1H, 13C, 15N triple-resonance nuclear magnetic resonance spectroscopy. Biochemistry 33, 15061-70.
[25] Blanco, F.J., Ortiz, A.R. and Serrano, L. (1997). 1H and 15N NMR assignment and solution structure of the SH3 domain of spectrin: comparison of unrefined and refined structure sets with the crystal structure. J Biomol NMR 9, 347-57.
[26] Linderstrom-Lang, K. (1955). The pH-dependence of the deuterium exchange of insulin. Biochim Biophys Acta 18, 308.
[27] Bai, Y., Milne, J.S., Mayne, L. and Englander, S.W. (1993). Primary structure effects on peptide group hydrogen exchange. Proteins 17, 75-86.

[28] Sadqi, M., Casares, S., Lopez-Mayorga, O., Martinez, J.C. and Conejero-Lara, F. (2002). pH dependence of the hydrogen exchange in the SH3 domain of alpha-spectrin. FEBS Lett 514, 295-9.

[29] Englander, S.W. and Kallenbach, N.R. (1983). Hydrogen exchange and structural dynamics of proteins and nucleic acids. Q Rev Biophys 16, 521-655.

[30] Tuchsen, E. and Woodward, C. (1985). Mechanism of surface peptide proton exchange in bovine pancreatic trypsin inhibitor. Salt effects and O-protonation. J Mol Biol 185, 421-30.

[31] Woodward, C., Simon, I. and Tuchsen, E. (1982). Hydrogen exchange and the dynamic structure of proteins. Mol Cell Biochem 48, 135-60.

[32] Hvidt, A. and Nielsen, S.O. (1966). Hydrogen exchange in proteins. Adv Protein Chem 21, 287-386.

[33] Radford, S.E., Buck, M., Topping, K.D., Dobson, C.M. and Evans, P.A. (1992). Hydrogen exchange in native and denatured states of hen egg-white lysozyme. Proteins 14, 237-48.

[34] Hoshino, M., Katou, H., Hagihara, Y., Hasegawa, K., Naiki, H. and Goto, Y. (2002). Mapping the core of the beta(2)-microglobulin amyloid fibril by H/D exchange. Nat Struct Biol 9, 332-6.

[35] Carulla, N., Caddy, G.L., Hall, D.R., Zurdo, J., Gairí, M., Feliz, M., Giralt, E., Robinson, C.V., Dobson, C.M. (2005). Molecular recycling within amyloid fibrils. Nature 436, 554-8.

[36] Nurmi, M.J., Ekfors, T.O., Rajala, P.O. and Puntala, P.V. (1990). Intravesical dimethyl sulfoxide instillations in the treatment of secondary amyloidosis of the bladder. J Urol 143, 808-10.

[37] Zhang, Y.Z., Paterson, Y. and Roder, H. (1995). Rapid amide proton exchange rates in peptides and proteins measured by solvent quenching and two-dimensional NMR. Protein Sci 4, 804-14.

[38] Slupsky, C.M., Boyko, R.F., Booth, V.K. and Sykes, B.D. (2003). Smartnotebook: a semi-automated approach to protein sequential NMR resonance assignments. J Biomol NMR 27, 313-21.

[39] Wishart, D.S. and Sykes, B.D. (1994). The 13C chemical-shift index: a simple method for the identification of protein secondary structure using 13C chemical-shift data. J Biomol NMR 4, 171-80.

[40] Privalov, P.L. and Potekhin, S.A. (1986). Scanning microcalorimetry in studying temperature-induced changes in proteins. Methods Enzymol 131, 4-51.

[41] Plotnikov, V.V., Brandts, J.M., Lin, L.N. and Brandts, J.F. (1997). A new ultrasensitive scanning calorimeter. Anal Biochem 250, 237-44.

[42] Varela, L., Morel, B., Azuaga, A.I. and Conejero-Lara, F. (2009). A single mutation in an SH3 domain increases amyloid aggregation by accelerating nucleation, but not by destabilizing thermodynamically the native state. FEBS Lett 583, 801-6.

[43] Makhatadze, G.I. and Privalov, P.L. (1990). Heat capacity of proteins. I. Partial molar heat capacity of individual amino acid residues in aqueous solution: hydration effect. J Mol Biol 213, 375-84.

9.

SUMMARY AND CONCLUSIONS / RESUMEN Y CONCLUSIONES

9. SUMMARY AND CONCLUSIONS / RESUMEN Y CONCLUSIONES

9.1. SUMMARY OF RESULTS

In this Thesis project we have presented an investigation of the mechanism of amyloid fibril formation of a small globular domain, the α-spectrin SH3 domain. The combined use of a wide variety of biophysical techniques and methods has allowed us: i) To dissect the overall process into different kinetic stages, and to describe how environmental factors affect them. ii) To obtain a quite detailed picture of the molecular events taking place during each step. iii) To detect key intermediates accumulating during the fibrillation process. vi) To characterize the morphology and structure of the amyloid fibrils finally formed.

In this chapter we summarize the main achievements of this work and relate the different types of information to obtain an overall picture of the fibrillation process and the main factors governing it.

This study was based upon a previous work of our group [1], in which we discovered that the N47A mutation induced the rapid formation of amyloid fibrils of the Spc-SH3 under mild acid conditions, an observation that had passed unnoticed so far in previous studies.

On the basis of these results, we undertook a comparative analysis of the thermodynamic stability and the fibrillation propensity of the N47A mutant and the WT Spc-SH3, together with a few other single mutants (Chapter 2). We demonstrated that, in contrast with other studies with several amyloid forming proteins, the destabilization of the native state produced by the N47A mutation is not the main factor favouring fibril formation by this small domain. We showed that the amyloidogenic effect of the mutation is due to its effect in accelerating the conformational events previous to nucleation or at the nucleation step itself. In particular, the N47A mutation favours an

extensive conformational change of the protein and the subsequent or concomitant formation of early oligomers.

Small oligomeric states, generally soluble and with a low degree of structural order are common in early stages of fibril formation of other proteins. The assembly and structural reorganization of these species leads to the formation of protofibrils. For example, the 40- or 42-residue forms of Abeta give rise to different oligomeric species with a relatively disordered structure in rapid equilibrium with the monomeric forms [2,3]. Likewise, similar oligomers featuring dynamic structures have been identified during amyloid fibril formation of the yeast prion Sup35p, phosphoglycerate kinase or the PI3K-SH3 domain [4-6]. Transient oligomeric intermediates have also been detected for example during the lag phases of fibrillation of alpha-synuclein [7,8], mouse prion protein [9] and human insulin [10]. These oligomers promote the nucleation stage that results in the formation of amyloid fibrils efficiently, reducing the lag phase of aggregation, as we also observed here for the effect of oligomers of N47A Spc-SH3 on the fibrillation of the WT form. It appears therefore that formation of early oligomeric species is a crucial step in the amyloid cascade.

An exhaustive study of the effect of environmental conditions on these early fibrillation stages of the N47A Spc-SH3 has been described in Chapter 3. We explored the effect of NaCl concentration, pH, temperature, and protein concentration on the fibrillation kinetics. We showed that the NaCl concentration influences very strongly the early fibrillation steps in contrast to pH, which has an only moderate effect. An increase of salt concentration strongly accelerates the conformational conversion and the appearance of oligomers, which results in an enhancement of the fibril nucleation, a reduction of the lag phase and a faster fibril growth. Importantly, the effect of salt is not limited to an increase in fibril nucleation velocity but it also has an effect on the final morphology and structure of the fibrils. Fibrils formed

at low salt concentration are initially curly but they turn into well-ordered, twisted amyloid fibrils after long incubation times, whereas curly fibrils assembled at high salt concentrations are thinner and they cannot evolve to ordered fibrils. These observations suggested that the protein monomers are arranged in a different way within the fibril structure and that this organization is determined by the environmental conditions at the early stages of the fibrillation process.

The study of the effect of temperature on the initial conformational change of the protein allowed us measuring apparent activation energies of the process at different salt concentrations. The activation enthalpy decreases with the concentration of salt indicating a reduction in the net balance of interactions involved in the activation barrier leading to fibril nucleation.

An enhancement of intermolecular association by screening of charge-charge repulsion would not appear to be crucial in triggering fibrillation, in agreement with the observation that increasing the net positive charge of the protein by lowering pH does not result in less aggregation but in the opposite effect. We hypothesized that salt may profoundly affect the energy landscape accessible to the protein due to the influence of salt ions upon the protein hydration shell. This effect may promote alternative unfolding pathways accessible to the polypeptide chain, leading to diverse amyloidogenic species as we observed in this work.

In support of this hypothesis are the results presented in Chapter 4, where we analyzed the conformational ensemble of the Spc-SH3 domain by NMR-detected H/D exchange under conditions near those of fibrillation. We found that for many residues there is significant super protection, i.e., they exchange with apparent Gibbs energies that are higher than those of global unfolding, which is suggestive of residual structure in the unfolded ensemble. This effect is enhanced by amyloidogenic factors, i.e., the N47A mutation and the increase in salt

concentration. We concluded therefore that amyloid-enhancing factors favour more compact denatured states with the presence of residual structure that may be prone to intermolecular association. In fact, the size of early oligomers formed during fibrillation is increased by salt and temperature as shown by DLS in Chapter 3. Since the Spc-SH3 domain has a significant probability of sampling these conformations under mild acid conditions [11], at high protein concentrations even a low relative population of compact denatured states might be enough to trigger the amyloid cascade. Similar compact denatured states have been related to amyloid formation by native proteins at acid pH [12, 13], including the PI3-SH3 domain [14].

On the basis of these results, we attempted to directly detect the presence of compact partially folded species during equilibrium and kinetic folding unfolding experiments using ANS as a probe (Chapter 5). Although ANS-binding species were detected at intermediate temperatures in thermal unfolding experiments, they are very low populated in equilibrium measurements. Nevertheless, a comparative analysis of the folding-unfolding kinetics of the N47A mutant and the WT domain provided evidence of the presence of partially-folded species accumulating rapidly during the dead time of the unfolding kinetics, although they were not detectable during the folding kinetics. This indicates that these species are not kinetically accessible from the unfolded state during these experiments. In addition, these species interact with ANS and unfold more slowly than the native state, suggesting that they may constitute a kinetic trap during the unfolding process. Once more, the observation that aggregation-enhancing factors (protein and salt concentration and temperature increase) augment the population of these partially-folded states implies that they may play a key role in the initial conformational events of the nucleation of fibrils, as observed for other proteins [15-17].

The results of chapter 4 and 5 indicate that the series of conformational events leading to nucleation of the amyloid fibrils is initiated by accumulation of compact partially-unfolded species with high tendency to oligomerize. These dynamic oligomers may be prone to undergo a structural transition to form more stable protofibrillar species, which further nucleate the fibril growth process.

To structurally characterize the conformational events leading to fibril nucleation, we undertook a mutagenesis analysis of the aggregation kinetics of the Spc-SH3 domain (Chapter 6). A series of second mutations made on the N47A mutant covering all the structural elements of the protein corroborated the lack of correlation between the thermodynamic stability of the native state and the amyloid formation propensity. Our results indicated that the inhibitory or potentiating effect of amyloid formation exerted by the mutations is also related to the efficiency in the formation of early oligomers, which occurs earlier for the mutants having a faster and a more efficient fibril nucleation, in agreement with the results of previous Chapters.

An analysis of the apparent rates of the fibril nucleation process of the mutants measured by ThT fluorescence has allowed us to map structurally the transition state of the nucleation process. It appears that the conformational transition occurring during fibril nucleation follows a completely different pathway to that of the folding-unfolding process and involves partial unfolding of the domain core, while some native-like and non-native structure remains at regions that fold late during normal two-state native folding. This conclusion is of chief importance since it has been proposed that the sequences of native proteins have evolved to facilitate fast and efficient folding while setting high energy barriers that avoid fibrillation [18]. This result is also in accordance with a kinetic inaccessibility from the unfolded state of the partially folded species described in Chapter 5, which supports our

conclusion that unfolding and amyloid nucleation follow diverging pathways in the conformational landscape of the protein.

Finally, in Chapter 7 we describe a structural study of amyloid fibrils using H/D exchange detected by NMR. It turned out that the fibrils are much more resistant than the native protein against exchange as described in similar studies with other proteins [19-22]. Furthermore, highly protected regions in the fibrils encompass sequence segments that are fully unprotected in the native protein, such as the 7 N-terminal residues or residues 47 and 48 at the distal turn. This indicates a completely different arrangement of the polypeptide chain in the fibrillar state compared to the native state, consistent with each state being an end point of diverging routes in the conformational landscape.

In addition, fibril samples prepared for long incubation times and composed mainly of twisted and ordered amyloid fibrils show a different pattern of protection than samples obtained at short incubation times and made of predominantly curly fibrils. There is a significant shift in the regions of the polypeptide chain that form the core of the fibril structure, supporting our conclusion that the two types of fibrils are assembled by diverging pathways possibly involving different oligomers and protofibrillar species, as discussed in Chapter 4 and elsewhere [23].

9.2. OVERALL DISCUSSION

The variety and abundance of experimental data accumulated in this study has allowed us to describe a mechanism for the assembly of the amyloid fibrils of the Spc-SH3 domain (Figure 9.1). As described elsewhere [11], [24], at mild acid pH the most populated state is the native state but the protein is quite dynamic and undergoes a wide variety of conformational changes ranging from local fluctuations to extensive unfolding.

Our results suggest that not all conformational excursions occur along the same pathway but different states in the conformational ensemble could be favoured by the influence of environmental conditions (salt concentration, temperature, pH) or by specific mutations (for instance the N47A mutation).

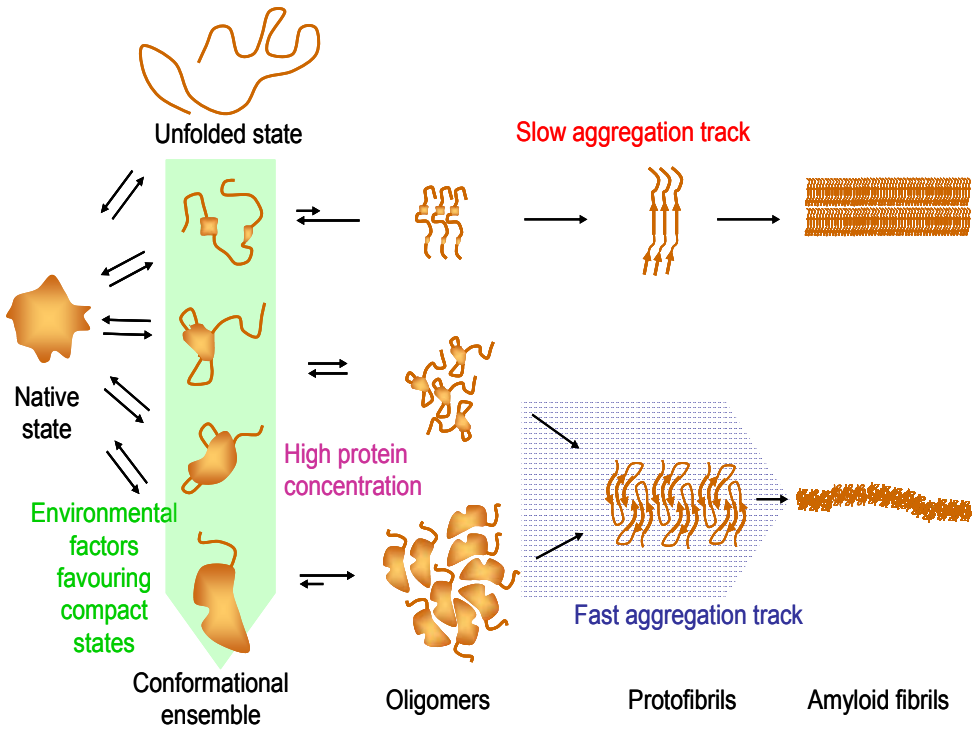

Figure 9.1. *Schematic drawing illustrating the different stages and pathways of amyloid fibril fibrillation of the Spc-SH3 domain derived from the results of this work. The pictures of each state do not intend to describe the actual structures but be only mere representations of their main features. The black arrows indicate possible pathways.*

High salt concentration appears to alter the energy landscape to favour the population of more compact partially folded states, in which the domain core may become transiently unstructured, whereas low salt appears to privilege the typical folding-unfolding route of the SH3 domain, which is conformationally quite constrained [25]. Similarly, specific mutations, such as the N47A mutation, can destabilize the

transition state of normal folding-unfolding, thus favouring alternative states.

If the concentration of the protein is high enough, the absolute concentration of partially folded states prone to intermolecular association may be sufficient for these species to oligomerize, even if their population is low in relative terms. Our results also indicate the size distribution of these oligomers depends of the conditions as we have observed at different salt concentrations or temperatures. It is likely that the oligomer structure is quite dynamic and it may depend of the nature of the oligomerizing species. These oligomers appear to be the critical nuclei in triggering the amyloid cascade since we have found a direct correlation between the rate of formation of oligomers and the rate of fibrillation.

At certain point, a structural conversion of the dynamic oligomers into more stable fibrils must take place and once protofibrils are nucleated they elongate by incorporation of additional partially folded protein molecules giving rise to curly fibrils. Under conditions that favour efficient oligomerization (high temperature, high salt and protein concentration), their structural conversion leading to protofibrillar structures is faster and so it is also fibril growth, but the resulting fibrils are more disordered possibly because of the structural constraints imposed by a more compact arrangement in the preceding structures. On the other hand, conditions that promote less compact structures and smaller, less stable oligomers conduct to a slower formation of protofibrils, with the presence of a long lag phase, but the final amyloid fibrils can achieve a higher structural order. We have also found that curly fibrils are not unique, as shown in Chapter 3, but their structure may also be directed by nucleation conditions, and there must be some pivotal states connecting the diverging fibrillation pathways.

In summary, we have shown that the fibrils formation mechanism is very complex molecular process finely modulated by a number of

intrinsic or environmental factors that direct the subsequent aggregation cascade from the very early conformational events.

9.3. CONCLUSIONS

Finally, we summarize here the main conclusions of this Thesis project:

- In the small Spc-SH3 domain not all mutations destabilizing the native state are intrinsically amyloidogenic. Amyloidogenic mutations must produce a particular redistribution of the conformational ensemble of the protein leading specifically to a significant reduction in the energy barrier of nucleation of the fibrillation process.
- The existence of transiently accumulated partially folded species detected during the unfolding of the protein can be related with the triggering of the amyloid fibril cascade.
- Environmental conditions of aggregation such as salt concentration, pH, protein concentration and temperature act by altering the conformational landscape and favouring compact partially folded states with different propensities to oligomerize and this determines the rate and the subsequent pathway of fibrillation.
- It is likely that the role of salt in enhancing fibrillation is related to its influence upon the cooperativity of the protein hydration shell due to a direct interaction of salt ions with the protein groups or with the water of the first hydration layer. This results in more compact partially unfolded states accessible to the protein ensemble.
- The two-state folding-unfolding process and the fibril nucleation process of the Spc-SH3 domain follow diverging pathways in the conformational landscape.

- The fibril morphology and structure is determined by environmental conditions at the early conformational events leading to fibril nucleation.
- The structure of the amyloid fibril core is formed by several regions of the polypeptide chain including segments that are fully unstructured or form loops in the native protein, indicating a profound structural conversion during the amyloid cascade.

9.4. COMPLEMENTARY TRAINING ACTIVITIES AND PUBLICATIONS

As complementary activities carried out during this predoctoral period, it has been performed a study of the aggregation mechanism of the acylphosphatase from Sulfolobus solfataricus (Sso AcP) during a three-month stay from September to December 2007 in the laboratory of Prof. Fabrizio Chiti. This work led to the publication of an article in Biochimica et Biophysica Acta [26].

In addition, it has been developed a study by DSC of the thermally-induced unfolding of amyloid fibrils of the N47A Spc-SH3 mutant in collaboration with other member of the group. In this work, a mathematical model for the quantitative interpretation of the DSC data of amyloid fibrils has been derived. The work has been recently accepted for publication in the Journal of Physical Chemistry B [27].

Finally, the results presented in Chapter 3 have been published in FEBS letters [28].

Reprints of these 3 articles are included at the end of this project.

9.5. RESUMEN Y CONCLUSIONES

Resumen de resultados

En esta Memoria se presenta el trabajo de investigación sobre el mecanismo de formación de fibras amiloides por un pequeño dominio globular proteico, el dominio SH3 de α-espectrina. El uso combinado de una gran variedad de métodos y técnicas biofísicas nos ha permitido: i) Diseccionar el proceso global en diferentes etapas cinéticas y describir cómo éstas se ven afectadas por las condiciones ambientales. ii) Obtener una visión detallada de los procesos moleculares que tienen lugar durante cada etapa. iii) Detectar intermedios clave que se acumulan durante el proceso de fibrilación. iv) Caracterizar la morfología y estructura de las fibras amiloides formadas al final del proceso de agregación.

En este capítulo se resumen los principales resultados obtenidos con este trabajo de investigación y se relaciona la información obtenida para conseguir de esta forma una visión global del proceso de fibrilación y los principales factores que lo gobiernan.

Este estudio se ha basado en un trabajo previo de nuestro grupo de investigación [1], en el que se observó que la mutación N47A inducía la formación rápida de fibras amiloides por el dominio Spc-SH3 en condiciones de pH moderadamente ácido. Esta observación había pasado desapercibida hasta el momento en previos estudios de investigación.

Basándonos en esos resultados, se llevó a cabo un análisis comparativo de la estabilidad termodinámica y la propensión a la agregación del mutante N47A y de la forma WT del dominio Spc-SH3, junto con una serie de mutantes simples (Capítulo 2). Se demostró que, al contrario de lo apuntado por numerosos estudios realizados sobre diferentes proteínas amiloidogénicas, la desestabilización del estado nativo producida por la mutación N47A no es el factor principal

que favorece la formación de fibras por este pequeño dominio. Se comprobó que el efecto amiloidogénico de la mutación se debe a la aceleración que produce sobre los procesos conformacionales previos al proceso de nucleación o sobre la propia etapa de nucleación. En concreto, la mutación N47A favorece un extenso cambio conformacional de la proteína y la subsiguiente o simultánea formación de oligómeros iniciales en el proceso de agregación.

La presencia de pequeños oligómeros, generalmente solubles y sin estructura definida, es común en las etapas iniciales de la formación de fibras amiloides de numerosas proteínas. La reorganización estructural y la unión de estas especies permiten la formación de protofibras. Por ejemplo, las variantes de 40 y de 42 residuos del péptido Abeta forman especies oligoméricas diferentes con estructuras relativamente desordenadas que se encuentran en equilibrio rápido con las especies monoméricas [2, 3]. Del mismo modo, se han identificado durante la formación de fibras amiloides oligómeros similares con estructuras dinámicas en el prion de la levadura de Sup35p, en la fosfoglicerato quinasa y en el dominio PI3K-SH3 [4-6]. También se han detectado intermedios oligoméricos transitorios durante las fases de retardo de la fibrilación de la alfa-sinucleína [7,8], de la proteína prion de ratón [9] y de la insulina humana [10]. Estos oligómeros actúan eficientemente como núcleos de la etapa inicial de formación de fibras amiloides, reduciendo la fase de retardo de la agregación, tal y como hemos observado en nuestro caso al añadir oligómeros de N47A Spc-SH3 durante la fibrilación de la forma WT. Parece por tanto, que la formación inicial de especies oligoméricas constituye una etapa crucial en el desencadenamiento de la cascada de agregación amiloide.

En el Capítulo 3 se describe un estudio exhaustivo del efecto de las condiciones ambientales sobre dichas etapas iniciales de la agregación de N47A Spc-SH3. Se exploraron los efectos de la

concentración de NaCl, del pH, de la temperatura y de la concentración de proteína sobre las cinéticas de fibrilación. Se demostró que la concentración de NaCl afecta enormemente las etapas iniciales de la fibrilación, al contrario que el pH, que sólo tiene un efecto moderado. El aumento de la concentración de sal acelera fuertemente la conversión conformacional y la aparición de oligómeros, lo que resulta en un incremento del grado de nucleación en el proceso de fibrilación, una reducción de la fase de retardo y un crecimiento de fibras más rápido. Es destacable el hecho de que el efecto de la sal no se limita a un aumento de la velocidad de nucleación sino que también afecta a la morfología y la estructura final de las fibras. Las fibras formadas a baja concentración de sal son inicialmente rizadas pero tras largos periodos de incubación se convierten en fibras amiloides rectas, ordenadas y formadas por filamentos enrollados. En cambio, las fibras formadas a altas concentraciones de sal son finas y rizadas y no se transforman en fibras ordenadas. Estas observaciones sugieren que la proteína monomérica se reorganiza de forma diferente en la estructura fibrilar siendo esta organización determinada por las condiciones ambientales en las etapas iniciales del proceso de fibrilación.

El estudio del efecto de temperatura sobre el cambio conformacional inicial de la proteína, nos permitió determinar las energías de activación aparentes del proceso a diferentes concentraciones de sal. La entalpía de activación disminuye con el aumento de la concentración de sal, lo que indica una reducción en el balance de interacciones implicadas en la barrera de activación que tiene lugar en la etapa de nucleación del proceso de agregación.

El favorecimiento de la asociación intermolecular a través del apantallamiento de las repulsiones carga-carga mediado por la sal no parece ser crucial en el desencadenamiento del proceso de fibrilación. Esto está de acuerdo con el hecho de que el aumento de la carga neta

positiva de la proteína por la disminución del pH resulta en un aumento de la agregación y no al contrario. Nuestra hipótesis consiste en que la sal podría afectar profundamente el paisaje de energía accesible a la proteína, debido a la influencia de los iones salinos sobre la superficie de hidratación de la proteína. Este efecto puede promover rutas de desplegamiento alternativas accesibles a la cadena polipeptídica, que dan lugar a la formación de diversas especies amiloidogénicas, como se observó en este trabajo de investigación.

Los resultados mostrados en el Capítulo 4 apoyan la hipótesis anterior. Se analizó el equilibrio conformacional del dominio Spc-SH3 mediante el uso de intercambio H/D detectado por RMN (Resonancia Magnética Nuclear) en condiciones cercanas a las de fibrilación. Se encontró una significativa superprotección para numerosos residuos, lo que implica que la energía de Gibbs aparente de intercambio H/D es mayor que la que se obtiene para el proceso de desplegamiento global, lo cual sugiriere la existencia de estructura residual en el estado desplegado. Este efecto se ve incrementado por los factores que favorecen la agregación, es decir, la mutación N47A y el aumento de la concentración de sal. Se concluyó de este modo que los factores que favorecen la formación de amiloides favorecen a su vez estados desplegados más compactos en los que existe estructura residual y que tienen tendencia a la asociación intermolecular. De hecho, el tamaño de los oligómeros iniciales formados durante el proceso de fibrilación aumenta al aumentar la concentración de sal y la temperatura como se describe mediante el estudio de DLS (Dispersión Dinámica de luz) en el Capítulo 3. Teniendo en cuenta que el dominio Spc-SH3 presenta una probabilidad significativa de adoptar estas conformaciones en condiciones de pH moderadamente ácido [11], cuando la concentración de proteína es alta se podría desencadenar la cascada de agregación amiloide incluso con una población relativamente baja de dichos estados desplegados compactos.

Estados desplegados compactos similares se han relacionado con la formación de amiloides en proteínas nativas a pH ácido [12, 13], incluyendo el dominio PI3-SH3 [14].

Basándonos en estos resultados, se intentó detectar directamente la presencia de especies compactas parcialmente desplegadas durante experimentos de plegamiento y desplegamiento en equilibrio y cinéticos usando como sonda el ANS (Capítulo 5). Se detectaron especies que se unen a ANS a temperaturas intermedias durante el proceso de desplegamiento térmico, pero estas especies están muy poco pobladas en los experimentos de equilibrio. Por el contrario, tras realizar un análisis comparativo de las cinéticas de plegamiento y desplegamiento del mutante N47A y de la forma WT, se obtuvieron claras evidencias de la presencia de especies parcialmente desplegadas que se acumulan rápidamente durante el tiempo muerto de las cinéticas de desplegamiento, aunque no se observa durante el proceso de plegamiento. Esto indica que estas especies no son cinéticamente accesibles desde el estado desplegado. Además, estas especies se unen a ANS y se despliegan más lentamente que el estado nativo, lo que sugiere que podrían constituir una trampa cinética durante el proceso de desplegamiento. De nuevo, la observación de que los factores que favorecen la agregación (aumento de la concentración de sal y de proteína y aumento de temperatura) aumentan la población de estos estados parcialmente desplegados implica que dichas especies podrían desempeñar un papel clave en los procesos conformacionales iniciales del proceso de nucleación de las fibras. Esto se ha observado también para otras proteínas [15-17].

Los resultados descritos en los Capítulos 4 y 5 indican que los cambios conformacionales que dan lugar a la nucleación de la formación de fibras amiloides se inician por la acumulación de especies compactas parcialmente desplegadas con alta tendencia a la

oligomerización. Estos oligómeros dinámicos podrían sufrir una transición estructural para formar especies protofibrilares estables que actuarían posteriormente como núcleos de agregación durante el crecimiento de las fibras.

Se llevó a cabo un análisis de las cinéticas de agregación presentadas por una serie de mutantes del dominio Spc-SH3 con el fin de caracterizar estructuralmente los procesos conformacionales que dan lugar a la nucleación de las fibras (Capítulo 6). Las mutaciones se realizaron sobre el mutante N47A, abarcando todos los elementos estructurales de la proteína. El estudio de las cinéticas de agregación amiloide de todos estos dobles mutantes corroboró la ausencia de correlación entre la estabilidad termodinámica del estado nativo y la propensión a la formación de amiloides. Los resultados obtenidos indicaron que la aceleración o la inhibición del proceso de fibrilación producidas por las mutaciones están relacionadas con la eficiencia en la formación de los oligómeros iniciales, lo que ocurre con anterioridad en el caso de mutantes que presentan un proceso de nucleación de las fibras más eficiente. Esto está de acuerdo con los resultados de los capítulos anteriores.

Se realizó un análisis de las constantes de velocidad aparentes del proceso de nucleación de las fibras en los dobles mutantes a partir de las cinéticas de agregación medidas por fluorescencia de ThT. Esto nos permitió delimitar las regiones que participan en la estructura del estado de transición del proceso de nucleación. Presumiblemente, la transición conformacional que ocurre durante el proceso de nucleación de las fibras sigue una ruta completamente diferente a la del proceso de plegamiento o desplegamiento. Dicha transición implica el desplegamiento parcial del núcleo del dominio, mientras que aquellas regiones que se pliegan posteriormente durante el proceso usual de plegamiento nativo de dos estados mantienen una estructura similar a la nativa o adquieren una conformación no nativa. Esta conclusión es

de gran importancia puesto que comunmente aceptado que las secuencias de las proteínas ha evolucionado para favorecer el plegamiento rápido y eficientemente al estado nativo, mientras que aumentan de las barreras energéticas que favorecen la fibrilación [18]. Este resultado también está de acuerdo con el hecho de que las especies parcialmente desplegadas descritas en el Capítulo 5 son cinéticamente inaccesibles desde el estado desplegado. Esto apoya lnuestra conclusión de que el desplegamiento y el proceso de nucleación amiloide siguen rutas divergentes en el paisaje conformacional de la proteína.

Finalmente, en el Capítulo 7, se describe un estudio estructural de las fibras amiloides mediante el uso de intercambio H/D detectado por RMN. Se observó que las fibras amiloides son mucho más resistentes que la proteína nativa al proceso de intercambio, como se ha descrito en estudios similares con otras proteínas [19-22]. Además, segmentos de la secuencia que están completamente expuestos en la proteína nativa forman en cambio parte de regiones altamente protegidas en las fibras, como es el caso de los siete primeros residuos de la región N-terminal y los residuos 47 y 48 en el giro distal. Esto indica que la organización estructural de la cadena polipeptídica en los estados fibrilar y nativo es completamente diferente, lo que está de acuerdo con que cada uno de estos estados constituya el punto final de dos rutas divergentes en el paisaje conformacional.

Además, las fibras obtenidas tras largos periodos de incubación, que están formadas mayoritariamente por fibras amiloides ordenadas y enrolladas, presentan perfiles de protección frente al intercambio diferentes a los de fibras obtenidas tras periodos de incubación cortos (rizadas y desordenadas). Existe un cambio significativo de las regiones de la cadena polipeptídica que forman el núcleo de la estructura fibrilar, lo que apoya la conclusión de que se forman dos tipos de fibras distintas por rutas divergentes que implican

posiblemente oligómeros y especies protofibrilares diferentes, como se discutió en el Capítulo 4 y en bibliografía [23].

Discusión general

La abundancia y variedad de datos experimentales acumulados en este estudio nos ha permitido proponer un mecanismo molecular para la formación de fibras amiloides del dominio Spc-SH3 (Figura 9.1). Como se describe en bibliografía [11,22], el estado más poblado a valores de pH moderadamente ácido es el estado nativo, pero la estructura de la proteína es altamente dinámica y sufre una gran variedad de cambios conformacionales transitorios, que abarcan desde fluctuaciones locales hasta desplegamiento extenso. Nuestros resultados sugieren que no todos los cambios conformacionales ocurren a través de la misma ruta. Por el contrario, diferentes estados conformacionales pueden estar favorecidos por la influencia de factores ambientales (concentración de sal, temperatura, pH) o por mutaciones específicas (por ejemplo, la mutación N47A). El aumento de la concentración de sal parece afectar alterando el paisaje de energía que favorece la población de estados parcialmente desplegados compactos, en los que el núcleo del dominio podría estar transitoriamente desestructurado. Sin embargo, la disminución de la concentración de sal parece favorecer la típica ruta de plegamiento y desplegamiento del dominio SH3, que está bastante restringido conformacionalmente [25]. Análogamente, mutaciones específicas, como la mutación N47A, pueden desestabilizar el estado de transición del proceso normal de plegamiento y desplegamiento, lo que podría favorecer estados alternativos.

Si la concentración de proteína es suficientemente alta, la concentración absoluta de estados parcialmente desplegados con tendencia a la asociación intermolecular puede ser suficiente para que estas especies oligomericen, aun cuando su población sea baja en

términos relativos. Nuestros resultados también indican que la distribución de tamaños de estos oligómeros depende de las condiciones empleadas, como hemos observado en los estudios realizados a diferentes concentraciones de sal o a diferentes temperaturas. Existen indicios de que la estructura de los oligómeros es bastante dinámica y puede depender de la naturaleza de las especies que los forman. Estos oligómeros parecen ser núcleos críticos en el desencadenamiento de la cascada de agregación amiloide, ya que hemos encontrado una correlación directa entre el grado de formación de los oligómeros y la velocidad de fibrilación.

En cierto momento, debe tener lugar una conversión estructural de los oligómeros dinámicos en protofibras más estables, y una vez alcanzado el proceso de nucleación, comienza el proceso de elongación mediante la incorporación de moléculas de proteína parcialmente desplegadas que dan lugar a las fibras rizadas y desordenadas. En las condiciones que favorecen el proceso de oligomerización (alta temperatura y alta concentración de proteína y sal), la conversión estructural que da lugar a estructuras protofibrilares es más rápida y del mismo modo lo es el crecimiento fibrilar, pero las fibras resultantes son más desordenadas debido posiblemente a limitaciones estructurales impuestas por un ordenamiento más compacto en las estructuras precedentes. Por el contrario, las condiciones que favorecen estructuras menos compactas y oligómeros más pequeños conducen a la formación más lenta de protofibras, con la existencia de una larga fase de retardo, pero las fibras amiloides finales pueden sufrir una ordenación estructural mayor. También hemos encontrado que las fibras rizadas pueden ser de varios tipos, como se muestra en el Capítulo 3, pero su estructura puede también estar dirigida por las condiciones del proceso de nucleación y podrían existir algunos estados clave que conectan las diferentes rutas de fibrilación.

En resumen, hemos mostrado que el mecanismo de formación de fibras es un proceso molecular muy complejo que está estrictamente modulado por diversos factores intrínsecos o ambientales que dirigen la subsiguiente cascada de agregación desde los procesos conformacionales iniciales.

Conclusiones

Finalmente, aquí se resumen las conclusiones más relevantes de este proyecto de Tesis Doctoral:

- En el pequeño dominio Spc-SH3 no todas las mutaciones que desestabilizan el estado nativo son intrínsecamente amiloidogénicas. Las mutaciones amiloidogénicas pueden producir una redistribución concreta del conjunto de conformaciones de la proteína que da lugar a una reducción significativa específica de la barrera energética del proceso de nucleación de las fibras.
- La existencia de especies parcialmente desplegadas que se acumulan transitoriamente durante el proceso de desplegamiento de la proteína, pueden estar relacionadas con el desencadenamiento de la cascada de agregación amiloide.
- Las condiciones ambientales del proceso de agregación como la concentración de sal y proteína, la temperatura y el pH, actúan alterando el paisaje conformacional y favoreciendo estados parcialmente desplegados compactos con diferentes tendencias a la oligomerización, lo que determina la velocidad y la ruta del proceso de fibrilación.
- El aumento de la fibrilación producido por el incremento de la concentración de sal es muy probablemente debido a su influencia sobre la cooperatividad de la capa de hidratación superficial de la proteína debido a la interacción directa de los iones de la sal con los grupos de la proteína o con el agua de

dicha capa. Esto resulta en estados parcialmente desplegados más compactos accesibles al conjunto de la proteína.

- El proceso de plegamiento y desplegamiento de dos estados y el proceso de nucleación de las fibras en el dominio Spc-SH3 siguen rutas divergentes en el paisaje conformacional.
- La morfología y estructura de las fibras está gobernada por las condiciones ambientales en las etapas iniciales que dan lugar al proceso de nucleación de las fibras.
- La estructura del núcleo de las fibras está formado por diversas regiones de la cadena polipeptídica que incluyen segmentos que están totalmente desestructurados o formando lazos en la proteína nativa, lo que indica una profunda conversión estructural durante la cascada de agregación amiloide.

9.6. BIBLIOGRAPHY

[1] Morel, B., Casares, S. and Conejero-Lara, F. (2006). A single mutation induces amyloid aggregation in the alpha-spectrin SH3 domain: analysis of the early stages of fibril formation. J Mol Biol 356, 453-68.

[2] Bitan, G., Kirkitadze, M.D., Lomakin, A., Vollers, S.S., Benedek, G.B. and Teplow, D.B. (2003). Amyloid beta -protein (Abeta) assembly: Abeta 40 and Abeta 42 oligomerize through distinct pathways. Proc Natl Acad Sci U S A 100, 330-5.

[3] Teplow, D.B. et al. (2006). Elucidating Amyloid Î²-Protein Folding and Assembly: A Multidisciplinary Approach. Accounts of Chemical Research 39, 635-645.

[4] Serio, T.R., Cashikar, A.G., Kowal, A.S., Sawicki, G.J., Moslehi, J.J., Serpell, L., Arnsdorf, M.F. and Lindquist, S.L. (2000). Nucleated conformational conversion and the replication of conformational information by a prion determinant. Science 289, 1317-21.

[5] Modler, A.J., Gast, K., Lutsch, G. and Damaschun, G. (2003). Assembly of amyloid protofibrils via critical oligomers - A novel pathway of amyloid formation. Journal of Molecular Biology 325, 135-148.

[6] Bader, R., Bamford, R., Zurdo, J., Luisi, B.F. and Dobson, C.M. (2006). Probing the mechanism of amyloidogenesis through a tandem repeat of the PI3-SH3 domain suggests a generic model for protein aggregation and fibril formation. J Mol Biol 356, 189-208.

[7] Dusa, A., Kaylor, J., Edridge, S., Bodner, N., Hong, D.-P. and Fink, A.L. (2006). Characterization of Oligomers during Î±-Synuclein Aggregation Using Intrinsic Tryptophan Fluorescence. Biochemistry 45, 2752-2760.

[8] Kaylor, J., Bodner, N., Edridge, S., Yamin, G., Hong, D.-P. and Fink, A.L. (2005). Characterization of Oligomeric Intermediates in [alpha]-Synuclein Fibrillation: FRET Studies of Y125W/Y133F/Y136F [alpha]-Synuclein. Journal of Molecular Biology 353, 357-372.

[9] Jain, S. and Udgaonkar, J.B. (2008). Evidence for Stepwise Formation of Amyloid Fibrils by the Mouse Prion Protein. Journal of Molecular Biology 382, 1228-1241.

[10] Mirco Sorci, Robert A. Grassucci, Ingrid Hahn, Joachim Frank and Georges Belfort. (2009). Time-dependent insulin oligomer reaction pathway prior to fibril formation: Cooling and seeding. Proteins: Structure, Function, and Bioinformatics 9999, NA.

[11] Sadqi, M., Casares, S., Lopez-Mayorga, O., Martinez, J.C. and Conejero-Lara, F. (2002). pH dependence of the hydrogen exchange in the SH3 domain of alpha-spectrin. FEBS Lett 514, 295-9.

[12] Routledge, K.E., Tartaglia, G.G., Platt, G.W., Vendruscolo, M. and Radford, S.E. (2009). Competition between intramolecular and intermolecular interactions in an amyloid-forming protein. J Mol Biol 389, 776-86.

[13] Ohkuri, T., Yasumatsu, K., Shigemura, N., Yoshida, R. and Ninomiya, Y. (2006). Amiloride inhibition on NaCl responses of the chorda tympani nerve in two 129 substrains of mice, 129P3/J and 129X1/SvJ. Chem Senses 31, 565-72.

[14] Zurdo, J., Guijarro, J.I., Jimenez, J.L., Saibil, H.R. and Dobson, C.M. (2001). Dependence on solution conditions of aggregation and amyloid formation by an SH3 domain. J Mol Biol 311, 325-40.

[15] Galani, D., Fersht, A.R. and Perrett, S. (2002). Folding of the yeast prion protein Ure2: kinetic evidence for folding and unfolding intermediates. J Mol Biol 315, 213-27.

[16] Tripathi, P., Hofmann, H., Kayastha, A.M. and Ulbrich-Hofmann, R. (2008). Conformational stability and integrity of alpha-amylase from mung beans: evidence of kinetic intermediate in GdmCl-induced unfolding. Biophys Chem 137, 95-9.

[17] Blancas-Mejia, L.M., Tellez, L.A., del Pozo-Yauner, L., Becerril, B., Sanchez-Ruiz, J.M. and Fernandez-Velasco, D.A. (2009). Thermodynamic and kinetic characterization of a germ line human lambda6 light-chain protein: the relation between unfolding and fibrillogenesis. J Mol Biol 386, 1153-66.

[18] Dobson, C.M. (2001). The structural basis of protein folding and its links with human disease. Philos Trans R Soc Lond B Biol Sci 356, 133-45.

[19] Kheterpal, I., Zhou, S., Cook, K.D. and Wetzel, R. (2000). Abeta amyloid fibrils possess a core structure highly resistant to hydrogen exchange. Proc Natl Acad Sci U S A 97, 13597-601.

[20] Hoshino, M., Katou, H., Hagihara, Y., Hasegawa, K., Naiki, H. and Goto, Y. (2002). Mapping the core of the beta(2)-microglobulin amyloid fibril by H/D exchange. Nat Struct Biol 9, 332-6.

[21] Olofsson, A., Ippel, J.H., Wijmenga, S.S., Lundgren, E. and Ohman, A. (2004). Probing solvent accessibility of transthyretin amyloid by solution NMR spectroscopy. J Biol Chem 279, 5699-707.

[22] Carulla, N. et al. (2005). Molecular recycling within amyloid fibrils. Nature 436, 554-8.

[23] Gosal, W.S., Morten, I.J., Hewitt, E.W., Smith, D.A., Thomson, N.H. and Radford, S.E. (2005). Competing pathways determine fibril morphology in the self-assembly of beta2-microglobulin into amyloid. J Mol Biol 351, 850-64.

[24] Casares, S., Sadqi, M., Lopez-Mayorga, O., Martinez, J.C. and Conejero-Lara, F. (2003). Structural cooperativity in the SH3 domain studied by site-directed mutagenesis and amide hydrogen exchange. FEBS Lett 539, 125-30.

[25] Martinez, J.C., Viguera, A.R., Berisio, R., Wilmanns, M., Mateo, P.L., Filimonov, V.V. and Serrano, L. (1999). Thermodynamic analysis of alpha-spectrin SH3 and two of its circular permutants with different loop lengths: discerning the reasons for rapid folding in proteins. Biochemistry 38, 549-59.

[26] Bemporad, F., Vannocci, T., Varela, L., Azuaga, A.I. and Chiti, F. (2008). A model for the aggregation of the acylphosphatase from Sulfolobus solfataricus in its native-like state. Biochim Biophys Acta 1784, 1986-96.

[27] Morel, B., Varela, L., and Conejero-Lara, F. (2010). The thermodynamic stability of amyloid fibrils studied by differential scanning calorimetry. J. Phys. Chem. In press.

[28] Varela, L., Morel, B., Azuaga, A.I. and Conejero-Lara, F. (2009). A single mutation in an SH3 domain increases amyloid aggregation by accelerating nucleation, but not by destabilizing thermodynamically the native state. FEBS Lett 583, 801-6.

10.
APPENDIX

Biochimica et Biophysica Acta 1784 (2008) 1986–1996

Contents lists available at ScienceDirect

Biochimica et Biophysica Acta

journal homepage: www.elsevier.com/locate/bbapap

A model for the aggregation of the acylphosphatase from *Sulfolobus solfataricus* in its native-like state

Francesco Bemporad [a], Tommaso Vannocci [a], Lorena Varela [b], Ana I. Azuaga [b], Fabrizio Chiti [a,c,*]

[a] *Department of Biochemical Sciences, University of Florence, Viale Morgagni 50, Florence 50134, Italy*
[b] *Department of Physical Chemistry, University of Granada, Fuentenueva S/N, Granada 18071, Spain*
[c] *Consorzio interuniversitrio "Istituto Nazionale Biostrutture e Biosistemi" (I.N.B.B.), Viale delle Medaglie d'Oro, 305, Roma 00136, Italy*

ARTICLE INFO

Article history:
Received 9 May 2008
Received in revised form 19 August 2008
Accepted 21 August 2008
Available online 12 September 2008

Keywords:
Amyloid
Protofibrils
Native-like aggregation
Acylphosphatase
Early aggregates
Sulfolobus
Thioflavin

ABSTRACT

Evidence is accumulating that normally folded proteins retain a significant tendency to form amyloid fibrils through a direct assembly of monomers in their native-like conformation. However, the factors promoting such processes are not yet well understood. The acylphosphatase from *Sulfolobus solfataricus* (Sso AcP) aggregates under conditions in which a native-like state is initially populated and forms, as a first step, aggregates in which the monomers maintain their native-like topology. An unstructured N-terminal segment and an edge β-strand were previously shown to play a major role in the process. Using kinetic experiments on a set of Sso AcP variants we shall show that the major event of the first step is the establishment of an inter-molecular interaction between the unstructured segment of one Sso AcP molecule and the globular unit of another molecule. This interaction is determined by the primary sequence of the unstructured segment and not by its physico-chemical properties. Moreover, we shall show that the conversion of these initial aggregates into amyloid-like protofibrils is an intra-molecular process in which the Sso AcP molecules undergo conformational modifications. The obtained results allow the formulation of a model for the assembly of Sso AcP into amyloid-like aggregates at a molecular level.

© 2008 Elsevier B.V. All rights reserved.

1. Introduction

Amyloid aggregation is the conversion of proteins and peptides from their soluble state into fibrillar aggregates with well defined morphological, structural and tinctorial properties [1]. These include a long and unbranched shape when fibrils are analyzed with transmission electron microscopy (TEM) [2] or atomic force microscopy [3], the ability to bind specific dyes, such as Thioflavin T (ThT) [4] or Congo red (CR) [5] and a typical cross-β pattern when analyzed by X-ray fiber diffraction [2]. Such fibrillar species are generally referred to as amyloid fibrils, at least when they accumulate extracellularly and several pathological conditions are associated with their formation [1].

The propensity of normally folded proteins to form amyloid-like fibrils increases in conditions that favor the partial unfolding of the native state across the major unfolding energy barrier, such as at low pH, high temperature or in the presence of moderate concentrations of organic solvents [6–8]. However, increasing evidence is now accumulating that folded proteins retain a significant, albeit small, tendency to aggregate with no need of unfolding as a first necessary step [9–11]. Despite the identification of unfolding-independent aggregation pathways, the mechanisms and the structural and sequence determinants that promote aggregation from native-like states are not yet well understood.

In this work we have focused our attention on the acylphosphatase from *Sulfolobus solfataricus* (Sso AcP), a protein previously shown to aggregate into amyloid-like protofibrils through such a mechanism [11–13]. This 101-residue long protein is an enzyme, able to hydrolyze acylphosphates with formation of acyl groups and phosphate ions [14]. The structure of Sso AcP, recently determined by nuclear magnetic resonance (NMR) spectroscopy and X-ray crystallography [14], features the typical βαββαβ topology of the other acylphosphatases so far characterized and belonging to the ferredoxin-like fold [15–19]. By contrast to related proteins, however, Sso AcP contains an unstructured, 11-residue N-terminal segment as shown in Fig. 1 [14].

Aggregation of Sso AcP has been characterized in 50 mM acetate buffer at pH 5.5 and 25 °C, in the presence of 20% (v/v) 2,2,2-trifluoroethanol (TFE). Under these conditions Sso AcP folding is faster than unfolding and the protein displays enzymatic activity [11]; moreover, the near-UV and far-UV circular dichroism (CD) analyses performed before aggregation show that the protein has the same secondary structure content and the same packing around aromatic residues as the native protein in a buffer in which aggregation does not occur [13]. These lines of evidence indicate that Sso AcP adopts initially a native-like state under these conditions. Hydrogen/deuterium exchange monitored with mass-spectrometry indicate,

* Corresponding author. Department of Biochemical Science, University of Florence, Viale Morgagni 50, Florence 50134, Italy.
E-mail address: fabrizio.chiti@unifi.it (F. Chiti).

1570-9639/$ – see front matter © 2008 Elsevier B.V. All rights reserved.
doi:10.1016/j.bbapap.2008.08.021

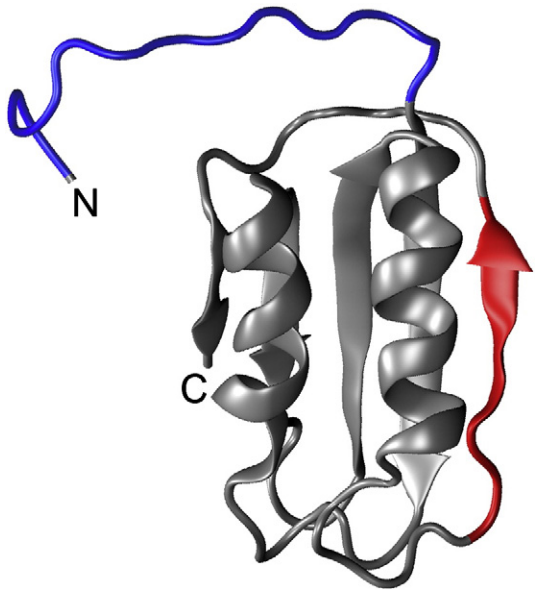

Fig. 1. Ribbon representation of the Sso AcP structure as determined using NMR [14]. The PDB entry is 1Y9O. The regions that were shown to be important in aggregation are highlighted [13]. These correspond to the 11-residue N-terminal segment (blue) and β-strand 4 (red). The figure has been drawn with VMD 1.8.3 for win32 [36].

however, that Sso AcP undergoes, under these conditions, structural fluctuations larger than those existing in solution media in which aggregation does not occur [13].

Aggregation occurs in two distinct phases. In a first phase, the protein converts, within one minute, from the initial native-like state into early aggregates [12]. Formation of early aggregates can be detected as an increase in static light scattering intensity and a significant change in mean residue ellipticity at 208 nm (at this wavelength the difference of far-UV signal between the native-like monomer and the early aggregates was the highest). The resulting aggregates retain, however, a native-like structure, as shown by far-UV CD and Fourier transform infrared (FTIR) spectroscopy and by the presence of enzymatic activity in the sample [12]. Such an activity disappears after centrifugation, confirming that it is due to the aggregates rather than to any residual non aggregated protein [12]. The early aggregates do not bind to ThT and CR and do not possess an extensive β-sheet structure as inferred from far-UV CD and FTIR [12].

In the second phase, the early aggregates convert, on the time scale of several minutes, into amyloid-like protofibrils having the ability to bind CR and ThT and a remarkable content in β-sheet structure, as inferred by FTIR spectroscopy and far-UV CD [11,12]. These species do not show enzymatic activity [12]. When analyzed with TEM, protofibrils appear as spherical oligomers, or chain-like structures, both having a diameter of 3–5 nm [12]. Kinetic tests indicate that conversion of the early aggregates into protofibrils occurs directly with no need of disassembly and re-aggregation [12]. Formation of protofibrils from the early aggregates can be detected by a further change in mean residue ellipticity at 208 nm and light scattering intensity and by a substantial increase in ThT fluorescence [12].

In a recent study the regions that promote aggregation of the Sso AcP native state have been investigated [13]. It was shown that a mutant lacking the unstructured N-terminal segment and consisting only of the globular part of Sso AcP (ΔN11 Sso AcP) is not able to aggregate in conditions that promote aggregation of the wild-type protein. This clearly suggests that the N-terminal segment plays a major role in promoting aggregation of Sso AcP (Fig. 1). However, this segment is not able to aggregate by itself when dissected from the globular domain, suggesting that aggregation of the full-length protein is not due to interactions between N-terminal segments of different Sso AcP molecules [13]. A protein engineering analysis, in which several residues of the Sso AcP sequence were mutated, showed that there is a significant inverse correlation between the rate of the first aggregation phase and the conformational stability of the investigated Sso AcP variants [13]. This confirms that formation of the early aggregates is facilitated by structural and cooperative fluctuations involving the entire Sso AcP molecule. However, mutations of residues positioned in the β-strand 4 were found to deviate from this correlation by over 2 standard deviations, suggesting a different role for this region [13]. Importantly, a limited proteolysis analysis showed that the β-strand 4 is flexible in the native-like state populated prior to aggregation [13]. Further support to a major role of this region in promoting Sso AcP aggregation comes from the recent observation that mutations designed to introduce structural protections in the β-strand 4 abrogate aggregation from the native state [20]. The Sso AcP variants bearing such mutations aggregate via an alternative mechanism that is independent of the transient formation of native-like aggregates [20].

Although the N-terminal segment and the β-strand 4 are recognized to play important roles in the first phase of Sso AcP self-assembly, the mechanism of aggregation of Sso AcP and the precise function of these two regions in the process are still unclear. In this work we shall investigate in detail the role of the N-terminal segment in order to identify the interactions that lead to the formation of the early aggregates and, more generally, to understand the driving forces promoting native-like aggregation. This will be achieved using a variety of strategies including the analysis of the behavior of Sso AcP variants and cross-linked dimers, experiments of co-aggregation of wild-type and ΔN11 Sso AcP and the study of the effect of peptides corresponding to the N-terminal segment of Sso AcP on the process. The collected data shall be used to propose a model for the aggregation of the protein that recapitulates all the experimental evidence observed to date on the aggregation of this system.

2. Materials and methods

2.1. Materials

Guanidine hydrochloride (GdnHCl), TFE, ThT and CR were purchased from Sigma. Synthetic peptides were purchased from Genscript Corporation (Piscataway, New Jersey) and had amidated C-termini. The purity of samples was in all cases >95%. Benzoyl phosphate (BP) was synthesized as previously described [21]. Oligonucleotides for site directed mutagenesis were purchased from MWG (Ebersberg, Germany).

2.2. Mutagenesis, protein expression and purification

Wild-type Sso AcP and ΔN11 Sso AcP were expressed and purified as previously described [13,22]. The genes encoding for C-tail Sso AcP, I72V–ΔN11, D6C and D85C Sso AcP were obtained starting from the pGEX-2T plasmid carrying the gene of ΔN11 or wild-type Sso AcP and using the Quick Change Site-Directed Mutagenesis Kit from Stratagene (La Jolla, California). In the case of C-tail Sso AcP three consecutive insertions were made in the gene encoding ΔN11 Sso AcP to reach the final insertion of 11 residues. The presence of the desired mutations was verified by DNA sequencing. The encoded proteins were expressed and purified as wild-type Sso AcP [22]. Purity of samples was checked by sodium dodecyl sulfate polyacrylamide gel electrophoresis (SDS-PAGE) and MALDI-TOF mass spectrometry.

2.3. Cross-linking

D6C and D85C Sso AcP were incubated separately for three hours at room temperature, under stirring at a concentration of 400 μM in a 100 mM TRIS buffer at pH 9.2 with 400 μM H_2O_2. Samples were

protected with aluminum foils. Presence of the desired homodimer stabilized by a disulphide bridge was assessed by MALDI-TOF mass spectrometry and by SDS-PAGE in the presence and in the absence of β-mercaptoethanol. No monomeric protein was detected at the end of the reaction.

2.4. Far-UV CD

Far-UV CD spectra were acquired at 25 °C with a Jasco J-810 spectropolarimeter (Tokyo, Japan) equipped with a thermostated cell holder attached to a C25P Thermo Haake water circulating bath (Karlsruhe, Germany) and a quartz cell of 1 mm path length. Spectra of native wild-type, ΔN11, C-tail, 6Dim and 85Dim Sso AcP were acquired at a protein concentration equal to 34 μM in a 10 mM TRIS buffer at pH 8.0 and 25 °C (protein concentration is always referred to monomer). Spectra of wild-type, C-tail, 6Dim and 85Dim Sso AcP during aggregation were also acquired at a protein concentration equal to 34 μM in 50 mM acetate buffer at pH 5.5 with 20% (v/v) TFE and 25 °C. In another set of experiments mean residue ellipticity at 208 nm over time was recorded, in a 1 mm cell using the J-810 instrument, for the following samples: (1) samples containing different amounts of wild-type Sso AcP ranging from 0.1 to 1.0 mg ml^{-1}; (2) samples containing different relative amounts of wild-type and ΔN11 Sso AcP (total protein concentration was 34 μM); (3) samples containing 34 μM wild-type Sso AcP in the presence of 4-fold molar excesses of N11, N14, scrambled-N11 and control peptide; (4) samples containing 34 μM C-tail Sso AcP; (5) samples containing 34 μM 6Dim or 85Dim Sso AcP. In all cases conditions were 50 mM acetate buffer at pH 5.5, 20 % (v/v) TFE, 25 °C. The recorded traces were analyzed using the following equation:

$$[\theta]_{208}(t) = A_1 \cdot e^{(-k_1 \cdot t)} + A_2 \cdot e^{(-k_2 \cdot t)} + q \quad (1)$$

where $[\theta]_{208}(t)$ represents the mean residue ellipticity at 208 nm as a function of time, q represents the plateau signal, A_1, A_2, k_1 and k_2 are amplitudes and rate constants of the first and second aggregation phases, respectively.

2.5. ThT fluorescence

Aggregation kinetics followed by ThT fluorescence were performed as previously reported [11–13]. Aggregation was carried out in 50 mM acetate buffer at pH 5.5 with 20% (v/v) TFE and 25 °C on the following samples: (1) 34 μM wild-type Sso AcP; (2) 34 μM C-tail Sso AcP; (3) 34 μM I72V-ΔN11 Sso AcP; (4) different relative amounts of wild-type and ΔN11 Sso AcP (total protein concentration was 34 μM); (5) 34 μM ΔN11 Sso AcP in the presence of the four peptides in molar excesses ranging from 1-fold to 25-fold; (6) 34 μM wild-type Sso AcP in the presence of 10 fold-molar excesses of the four peptides; (7) 34 μM 6Dim or 85Dim Sso AcP. At different times 60 μl of the tested sample were mixed with 440 μl of a solution containing 25 μM ThT, 25 mM phosphate buffer, pH 6.0. Fluorescence of the resulting sample was read in a 10×2 mm cuvette with a PerkinElmer LS 55 spectrofluorimeter (Wellesley, Massachusetts) equipped with a thermostated cell compartment. Excitation and emission wavelengths were 440 and 485 nm, respectively. Two different types of plots were produced. In Fig. 3B, 4B, 7C and 8B the ThT fluorescence intensity value in the absence of protein was subtracted from all the fluorescence measurements in the presence of the tested sample and the resulting values were normalized so that the final fluorescence intensity at the end of the kinetic trace was 100%. In Fig. 6B and 7A the ThT fluorescence intensity in the presence of the tested sample was directly reported as fold increase relative to signal in the absence of protein. The obtained plots were analyzed using the following equation:

$$F(t) = A \cdot e^{(-k_2 \cdot t)} + q \quad (2)$$

where $F(t)$ represents the fluorescence as a function of time, A is the amplitude of the observed phase, q is the fluorescence at the plateau and k_2 is the kinetic rate constant for the conversion of early aggregates into amyloid-like protofibrils.

2.6. Static light scattering

Formation of early aggregates by wild-type Sso AcP in the presence of N11, N14, scrambled-N11 and control peptide was followed with static light scattering at 208 nm in a Jasco V-630 spectrophotometer (Tokyo, Japan) with a 0.1 cm cell. Conditions were 34 μM Sso AcP in 50 mM acetate buffer at pH 5.5 with 20% (v/v) TFE at 25 °C, in the presence of a four-fold molar excess of the tested peptides. The obtained traces showed a linear decrease in signal after a rapid exponential phase, with the linear decrease corresponding to the beginning of the second exponential aggregation phase [13]. To simplify the visualization of the kinetic traces the data after the first exponential phase were fitted to a linear equation and the recorded traces were then normalized to the obtained straight line. The resulting plot was fitted to the following equation:

$$A(t) = A \cdot e^{(-k_1 \cdot t)} + q \quad (3)$$

where $A(t)$ is the absorbance as a function of time, A is the amplitude of the observed phase, k_1 is the rate constant for the formation of the early aggregates (first aggregation phase) and q is the apparent equilibrium value. The obtained rate constant k_1 did not vary significantly after normalization, suggesting that this correction does not affect the measurement of k_1.

2.7. Dynamic light scattering (DLS)

The hydrodynamic diameter was measured for wild-type, C-tail and ΔN11 Sso AcP in 10 mM TRIS buffer at pH 8.0 and 25 °C and for ΔN11 Sso AcP in the absence and presence of equimolar amounts of N11 and N14 peptides in 50 mM acetate buffer at pH 5.5, 20% (v/v) TFE, 25 °C. Size distributions by light scattering intensity were acquired with a Zetasizer Nano S DLS device from Malvern Instruments (Malvern, Worcestershire, UK). Low-volume 12.5×4.5 mm disposable cuvettes were used. A Peltier thermostating system maintained the temperature at 25 °C. The viscosity and refractive index parameters were set for each solution. The buffer and stock protein solutions were centrifuged (20,000 ×g, 5 min) and filtered with 0.02 μm Anotop 10 filters (Whatman, Maidstone, UK) before the measurements.

2.8. Equilibrium unfolding

28 samples of the tested protein variant (8.5 μM) were incubated for 1 h in 50 mM acetate buffer at pH 5.5, 37 °C, and different concentrations of GdnHCl ranging from 0 to 7.2 M. The values of mean residue ellipticity at 222 nm ($[\theta]_{222}$) of the samples were measured with the Jasco J-810 described above and a 1 mm path length cell. The plot of $[\theta]_{222}$ versus GdnHCl concentration was fitted to a two-state transition equation, as described [23], to determine the free energy change upon unfolding in the absence of denaturant ($\Delta G_{U-F}^{H_2O}$), the dependence of ΔG_{U-F} on GdnHCl concentration (m value), and the midpoint of unfolding (C_m).

2.9. Enzymatic activity measurements

Enzymatic activity was measured in a continuous optical test at 283 nm using BP as a substrate [24] with a Lambda 4V Perkin Elmer spectrophotometer (Wellesley, Massachusetts). Experimental conditions were 2.0 μg ml^{-1} Sso AcP, 5.0 mM BP, 50 mM acetate buffer at pH 5.5, 37 °C. BP was freshly dissolved before enzymatic activity measurements.

2.10. CR staining

Samples at the plateau of the ThT kinetics were tested for CR binding. Aliquots of 60 μl of each sample were mixed with 440 μl of solutions containing 20 μM CR, 5 mM phosphate buffer, 150 mM NaCl, pH 7.4, at 25 °C. After sample equilibration, optical absorption spectra were acquired from 400 to 700 nm with the Jasco spectrophotometer described above and a 5 mm path length cuvette. Solutions without protein and solutions without CR were used as controls.

3. Results

3.1. Sso AcP aggregates regardless of the position of the N-terminal segment

To get insight into the mechanism of amyloid-like aggregation of Sso AcP, we have first produced a mutant in which the 11-residue unstructured segment at the N-terminus has been moved to the C-terminus. In this mutant the sequence of both the segment, now at the C-terminus, and the globular part of Sso AcP have not changed. However, the N-terminus and C-terminus of the globular unit are far from each other (Fig. 1) and the different positioning of the unstructured segment in the mutant offers a unique opportunity to assess the possible importance of intra-molecular interactions between the unstructured segment and the globular part of Sso AcP. For example, if any intra-molecular interactions occurring prior to aggregation play a key role in the process, the aggregation will necessarily be affected by moving the segment from the N- to the C-terminus. We will refer to this mutant as C-tail Sso AcP.

Since the aggregation of Sso AcP starts from an ensemble of native-like conformations we have checked the effect of the mutation on the native state of the protein. Fig. 2A shows a comparison between far-UV CD spectra of wild-type and C-tail Sso AcP recorded in 10 mM TRIS buffer at pH 8.0 and 25 °C. The CD spectra are apparently identical. In a second experiment we have measured the hydrodynamic diameter of wild-type and C-tail Sso AcP under the same solution conditions (Fig. 2B). Both proteins show a peak at 3.7±0.1 nm. This value is consistent, within the experimental error, with the average diameter determined by ^{1}H-NMR for native Sso AcP [14]. The difference in the widths of the distributions arises from different experimental errors related to the different number of samples averaged in the graph (10 and 4 traces were averaged for wild-type and C-tail Sso AcP, respectively) and does not reflect a difference in the two protein samples. Then, we have measured the conformational stability of C-tail Sso AcP in an equilibrium unfolding experiment, using GdnHCl as a denaturant, in 50 mM acetate buffer at pH 5.5 and 37 °C (Fig. 2C). Unfolding of C-tail Sso AcP is reversible, as the protein recovers 97% of its activity following refolding (data not shown). Moreover, equilibrium unfolding of wild-type Sso AcP was previously shown to be characterized by a two-state cooperative and reversible transition [22]. Thus, the obtained plot has been analyzed with the method provided by Santoro and Bolen [23]. Results of this analysis show an m value equal to 11.4±0.5 kJ mol^{-1} M^{-1} for both wild-type and C-tail Sso AcP. The denaturant concentration at which protein is 50% unfolded (C_m) is 4.2±0.1 and 3.8±0.1 M for wild-type and C-tail Sso AcP, respectively. The free energy change upon unfolding in the absence of denaturant ($\Delta G_{U-F}^{H_2O}$) is 43.0±2.0 and 48.0±2.0 kJ mol^{-1} for C-tail and wild-type Sso AcP, respectively. This shows that moving the unstructured segment from the N-terminus to the C-terminus induces a slight destabilization of the native protein. Finally, we have measured the enzymatic activity of C-tail Sso AcP in 50 mM acetate buffer at pH 5.5 and 25 °C using benzoyl phosphate (BP) as a substrate. The obtained k_{CAT} values are 190±20 and 152±20 s^{-1} for wild-type and C-tail Sso AcP, respectively. This small decrease in enzymatic activity is probably due to a steric effect induced by moving the unstructured segment to the C-terminus, which is much closer to the catalytic site of Sso AcP than the N-terminus [14]. Taken together, these results show that moving the unstructured segment from the N- to the C-terminus does not significantly affect the secondary structure, compactness, conformational stability and enzymatic activity of Sso AcP.

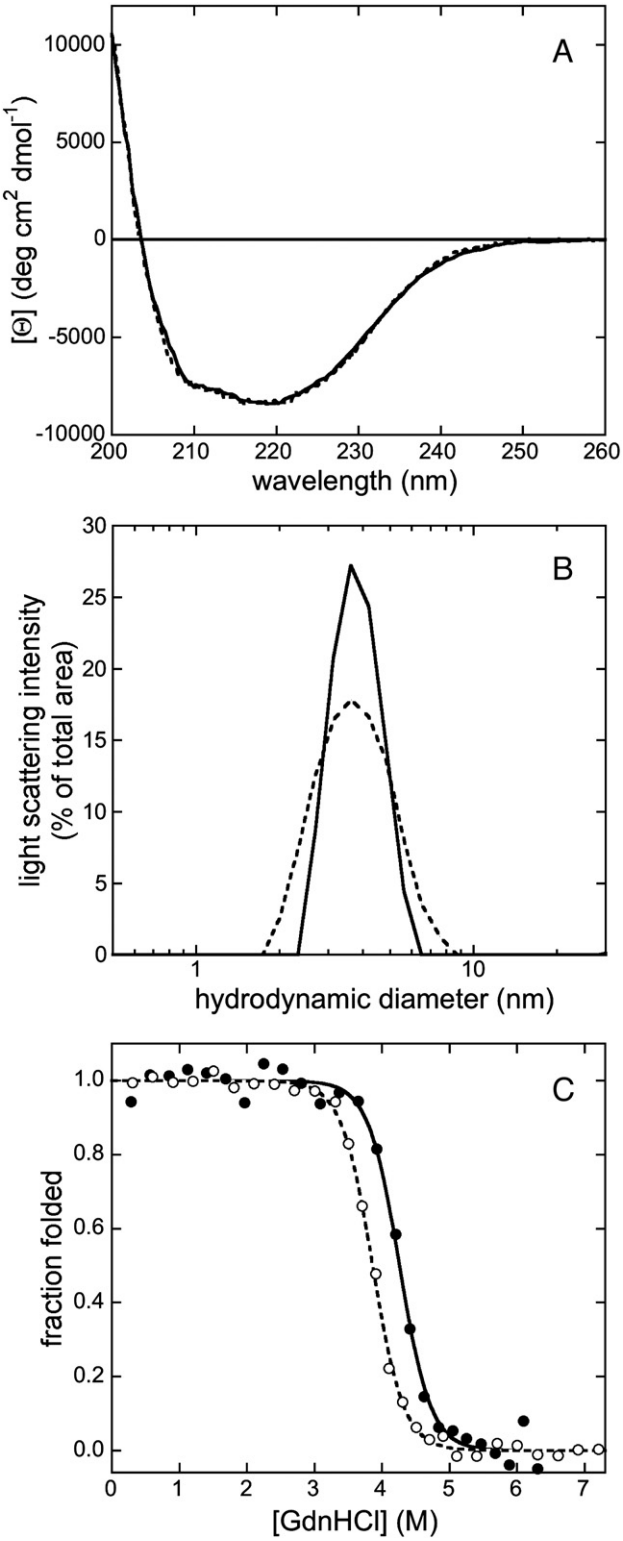

Fig. 2. (A) Far-UV CD spectra of wild-type (continuous line) and C-tail (dashed line) Sso AcP in 10 mM TRIS buffer at pH 8.0, 25 °C. The spectra are highly superimposable. (B) Size distributions of wild-type (continuous line) and C-tail (dashed line) Sso AcP in 10 mM TRIS buffer at pH 8.0, 25 °C determined using DLS. An apparent hydrodynamic diameter equal to 3.7±0.1 nm has been measured for both proteins. (C) Equilibrium unfolding curves of wild-type (●) and C-tail (○) Sso AcP carried out in 50 mM acetate buffer at pH 5.5, 37 °C. Continuous and dashed lines represent best fits of experimental data to the Santoro and Bolen model for wild-type and C-tail Sso AcP, respectively [23].

We have thus studied the behavior of C-tail Sso AcP under conditions that induce amyloid-like aggregation of the wild-type protein, that is 34 μM protein in 50 mM acetate buffer at pH 5.5, 20% (v/v) TFE, 25 °C (Fig. 3). The aggregation of C-tail Sso AcP has first been followed with far-UV CD at 208 nm. Similarly to the wild-type protein, recorded traces show two distinct phases (inset in Fig. 3A). The first phase corresponds to the formation of native-like aggregates. Aggregation rate constants for such phase, determined by best fits of experimental data to Eq. (1), are $(2.5\pm0.3)\cdot10^{-2}$ s^{-1} for wild-type Sso AcP and $(2.6\pm0.3)\cdot10^{-2}$ s^{-1} for C-tail Sso AcP. The second phase, corresponding to the conversion of native-like aggregates into amyloid-like protofibrils, has rate constants of $(3.0\pm0.4)\cdot10^{-3}$ s^{-1} for wild-type Sso AcP and $(2.9\pm0.3)\cdot10^{-3}$ s^{-1} for C-tail Sso AcP. The CD spectrum of the early aggregates formed by C-tail Sso AcP at the end of the first phase is similar to that recorded for the wild-type protein, with a single negative peak at about 224 nm (Fig. 3A). Moreover, no significant differences have been detected in the far-UV CD spectra measured for the protofibrils formed by the two protein variants at the end of the second phase (Fig. 3A).

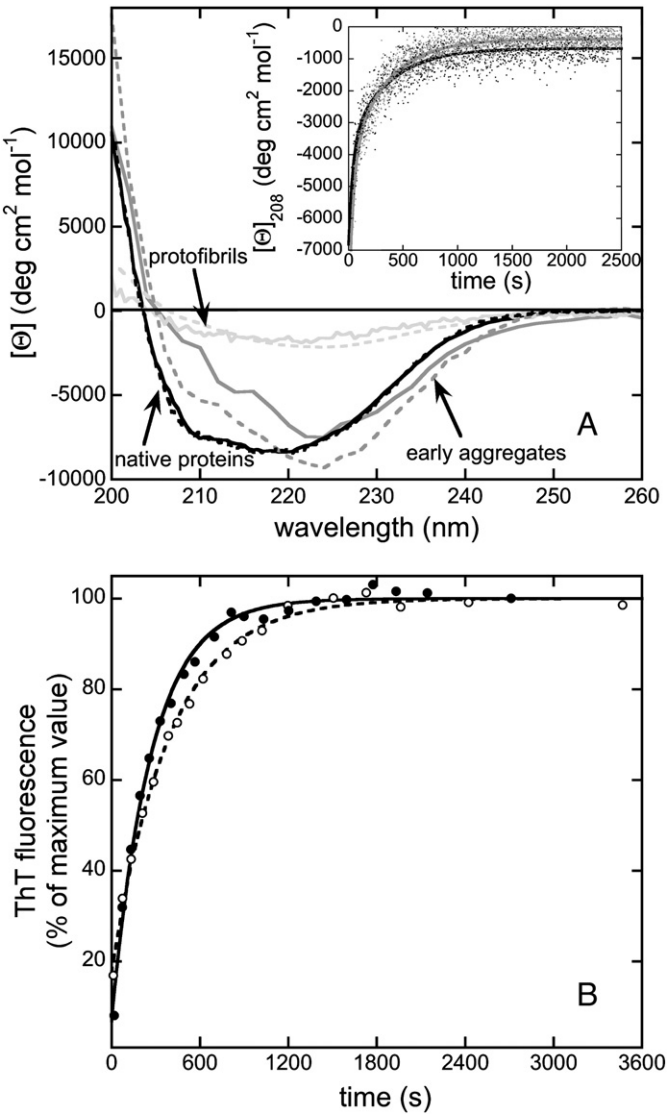

Fig. 3. (A) Far-UV CD spectra of wild-type (continuous lines) and C-tail (dashed lines) Sso AcP. Spectra are shown for native proteins (black) in 10 mM TRIS buffer at pH 8.0 and 25 °C, early aggregates (dark grey) and protofibrils (light grey) in 50 mM acetate buffer at pH 5.5, 20% (v/v) TFE, 25 °C. Early aggregates spectra have been extrapolated using Eq. (1) as reported in Materials and methods. The inset shows the change in mean residue ellipticity at 208 nm resulting from aggregation for wild-type (black) and C-tail (light grey) Sso AcP in 50 mM acetate buffer at pH 5.5, 20% (v/v) TFE, 25 °C. Continuous lines represent best fits of experimental data to Eq. (1). (B) ThT fluorescence during aggregation of wild-type (●) and C-tail (○) Sso AcP in 50 mM acetate buffer at pH 5.5, 20% (v/v) TFE, 25 °C. The ThT signal has been normalized to the plateau value. Lines represent best fits of experimental data to Eq. (2). Protein concentration was 34 μM in all experiments.

Aggregation has also been followed using ThT fluorescence, which allows the conversion of native-like aggregates into amyloid-like protofibrils to be monitored [11,12]. Similarly to the wild-type protein, C-tail Sso AcP induces a 12-fold increase in ThT emission. The rate constants of such increases, determined by best fits of experimental data to Eq. (2), are $(3.7\pm0.4)\cdot10^{-3}$ s^{-1} for wild-type Sso AcP and $(2.5\pm0.3)\cdot10^{-3}$ s^{-1} for C-tail Sso AcP (Fig. 3B), in good agreement with values determined from far-UV CD. The species populated by C-tail Sso AcP at the plateau of the ThT kinetic experiment binds to CR inducing, similarly to the wild-type protein [11], a shift in CR peak wavelength from 490 to 540 nm (data not shown).

Taken together, these data show that the positioning of the unstructured segment of Sso AcP does not affect the aggregation process. These observations rule out models for the aggregation mechanism of Sso AcP based on a specific intra-molecular interaction between the N-terminus and the globular part of the molecule that leads to the formation of an aggregation-prone monomer (see models 6, 12 and 17 in Supplementary Data). Indeed, the N- and C-termini are far from each other and moving the unstructured segment to the C-terminus necessarily affects any specific intra-molecular interaction of this type.

3.2. The N-terminal segment does not induce Sso AcP aggregation via a destabilizing effect

It was previously shown that the Sso AcP variant lacking the 11-residue N-terminal segment (ΔN11 Sso AcP) is characterized by a conformational stability slightly higher than wild-type Sso AcP [13]. At pH 5.5 and 37 °C $\Delta G_{U-F}^{H_2O}$ values are equal to 48.0±2.0 kJ mol^{-1} and 52.0±1.7 kJ mol^{-1} for wild-type and ΔN11 Sso AcP, respectively [13,22]. Since ΔN11 Sso AcP is not able to aggregate in conditions that promote aggregation of wild-type Sso AcP, the possibility exists that the role played by the unstructured segment in the aggregation process is related to its destabilizing effect. To assess this hypothesis, we have produced a mutant that lacks the N-terminal segment and has a conformational stability similar or lower than the wild-type protein. In particular, we have substituted an isoleucine located in the hydrophobic core of ΔN11 Sso AcP (Ile72) with a valine. We will refer to the obtained mutant as I72V–ΔN11 Sso AcP.

The equilibrium unfolding curve obtained in 50 mM acetate buffer at pH 5.5 and 37 °C on this mutant shows that the elimination of the methyl group at position 72 results in a significant destabilization of the protein (Fig. 4A). The $[\Delta G_{U-F}^{H_2O}]$ value is 43.1±1.6 kJ mol^{-1}. This value is 8.9 kJ mol^{-1} lower than that of the ΔN11 variant and 4.9 kJ mol^{-1} lower than that of the wild-type protein. Thus, I72V–ΔN11 Sso AcP is a variant without the unstructured segment and with a conformational stability slightly lower than the wild-type protein. The recovery of enzymatic activity following refolding shows that unfolding of I72V–ΔN11 Sso AcP is a reversible process (data not shown). The change in ThT fluorescence over time under conditions promoting aggregation is shown in Fig. 4B. This mutant induces the same change in fluorescence as the wild-type protein, but the process is three orders of magnitude slower, with a rate constant of $(8.1\pm0.8)\cdot10^{-6}$ s^{-1}.

As a further control we have used inorganic phosphate, a well known competitive inhibitor of acylphosphatases [25], to increase the conformational stability of wild-type Sso AcP to the ΔN11 value under aggregation conditions (see Supplementary Data). In these conditions wild-type Sso AcP aggregates with a rate constant higher than that of the I72V-ΔN11 variant in the absence of phosphate, confirming that the ability of the N-terminus to induce aggregation of Sso AcP cannot be explained only on the basis of its destabilizing effect

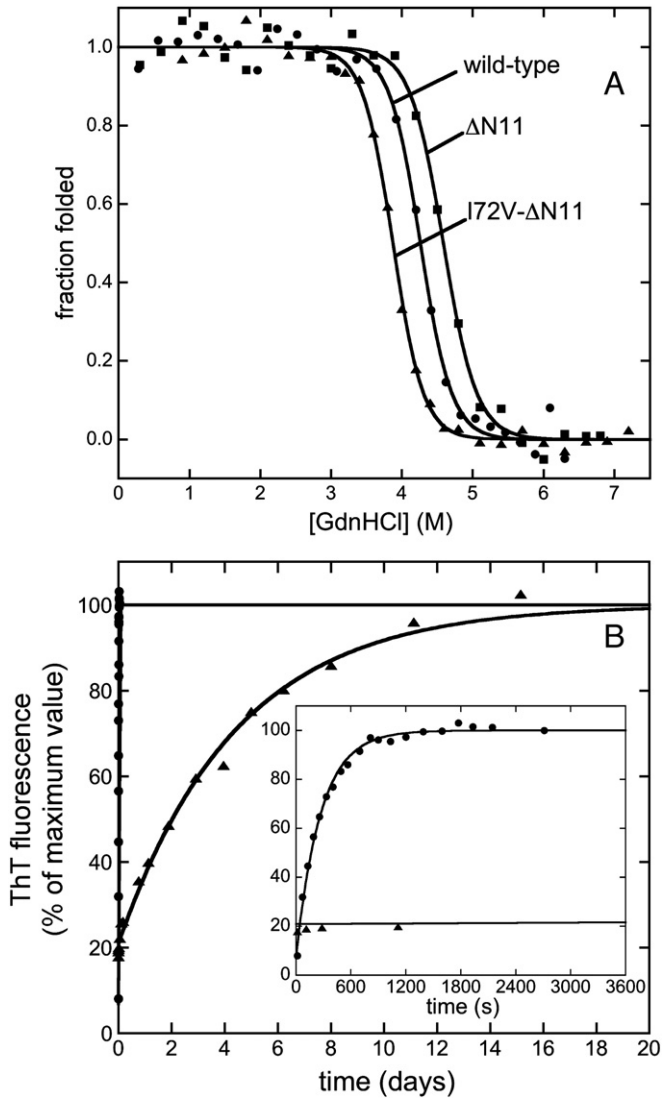

Fig. 4. (A) Equilibrium unfolding curves of wild-type (●), ΔN11 (■) and I72V-ΔN11 (▲) Sso AcP in 50 mM acetate buffer at pH 5.5, 37 °C. Continuous lines represent best fits of experimental data to the Santoro and Bolen model [23]. (B) ThT fluorescence during aggregation of 34 μM wild-type (●) and 34 μM I72V-ΔN11 (▲) Sso AcP in 50 mM acetate buffer at pH 5.5, 20% (v/v) TFE and 25 °C. The inset shows the first hour of recording. Continuous lines represent best fits of experimental data to Eq. (2).

(see Supplementary Data). These observations rule out models for the aggregation mechanism of the protein in which the fundamental force leading to the formation of early aggregates is the destabilization induced by the N-terminal unstructured segment on the globular part of Sso AcP (see models 11 and 14 in Supplementary Data).

3.3. Wild-type Sso AcP aggregation does not sequester ΔN11 Sso AcP into the aggregates

As a next step, we have studied the dependence of the rate constants of the two aggregation phases (k_1 and k_2) on protein concentration. The process has been followed by means of far-UV CD at 208 nm (data not shown) and the recorded traces have been analyzed with Eq. (1). The results show that k_2 does not change when protein concentration ranges from 0.1 to 1 mg ml^{-1} (Fig. 5). This finding is in agreement with the protein concentration independence of k_2 measured with ThT fluorescence, as previously reported [12]. Unlike k_2, the rate constant k_1 linearly increases with Sso AcP concentration (Fig. 5). The data reported here are in agreement with the previously proposed mechanism in which the first phase of aggregation (formation of early aggregates) is an inter-molecular process whose rate depends on the concentration of free molecules in the solution and the second phase of the process results from a structural reorganization of these species into protofibrils. Moreover, these data rule out models for Sso AcP aggregation in which small dimers or higher order oligomers form as transient on-pathway intermediates; in this case aggregation rate k_1 should depend at least on the second power of protein concentration (see model 15 in Supplementary Data).

To get insight into the specific role played by the N-terminal stretch of Sso AcP in the aggregation mechanism of the full length protein we have studied the behavior of wild-type Sso AcP in the presence of the ΔN11 variant. In these experiments the total Sso AcP concentration (wild-type+ΔN11) remains equal to 34 μM, but the relative amounts of the two protein variants vary, ranging from 0% to 100%. Fig. 6A shows aggregation kinetics followed by far-UV CD at 208 nm. The rate constant of formation of protofibrils (k_2), as determined by best fits of experimental data to Eq. (1), does not change with ΔN11 Sso AcP concentration. By contrast, a significant positive correlation is observed between the rate constant for the first aggregation phase (k_1) and wild-type content. The amount of protofibrils present at the end of the kinetic experiment, as inferred from the value reached at the plateau of the trace, increases linearly with the relative amount of wild-type Sso AcP in the sample (Fig. 6C).

Similar results have been obtained by monitoring the process using ThT fluorescence (Fig. 6B). The rate constant of the second phase (k_2), determined by best fits of experimental data to Eq. (2), does not show significant changes as the relative amounts of the protein variants change. However, an increase of the wild-type content in the sample results in a linear increase of fluorescence at the plateau of the experiment (Fig. 6C). These results show that the aggregates forming from wild-type Sso AcP are not able to co-aggregate ΔN11 Sso AcP into the initial aggregates and protofibrils. They also rule out models in which the globular part of an Sso AcP molecule establishes contacts through two distinct regions in the early aggregates (see models 3, 4 and 5 in Supplementary Data). Models based on domain swapping are also excluded (see model 14 in Supplementary Data).

3.4. A specific inter-molecular interaction between N-terminal segment and the globular part induces aggregation

Next, we have studied the effect of the four following peptides on the aggregation of both wild-type and ΔN11 Sso AcP: (1) an 11-residue

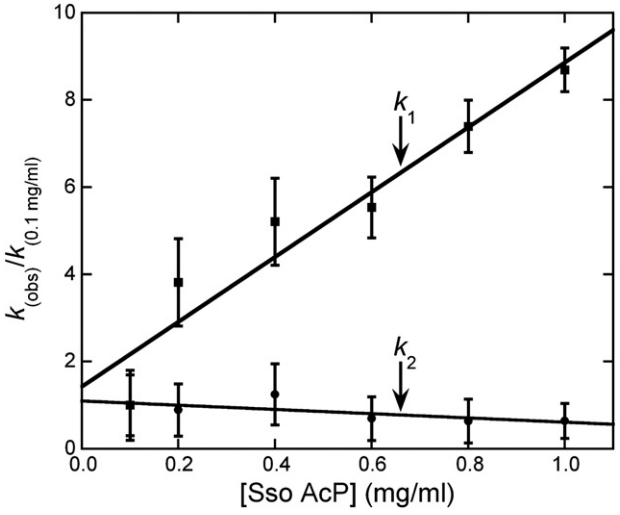

Fig. 5. The figure shows the ratio between the rate constants for the first phase k_1 (■) and second phase k_2 (●) of aggregation observed at a given protein concentration and the corresponding values measured at 0.1 mg ml^{-1}. Continuous lines represent best fits of experimental data to a linear function.

peptide having the sequence of the Sso AcP N-terminal segment, MKKWSDTEVFE. We will refer to this peptide as N11; (2) a 14-residue peptide having the sequence of the Sso AcP N-terminal segment and the initial three residues of the first β-strand, MKKWSDTEVFEMLK. We will refer to this molecule as N14; (3) an 11-residue peptide sharing the same amino-acid content as N11 but a different sequence, TMFKDWESEKV. We will refer to this molecule as scrambled-N11; (4) an 11-residue peptide designed to be soluble and charged at pH 5.5. The sequence of the peptide is KSRAHNGKSAQ. We will refer to this molecule as control peptide. N14 has been used to check the possibility that the role played by the N-terminal segment also involves a few residues downstream this segment. Scrambled-N11 has been used to check if the possible effects induced by N11 are due to its primary sequence or to its overall physico-chemical properties. Finally, the control peptide has been used to control possible non-specific effects of the added peptide on the aggregation process.

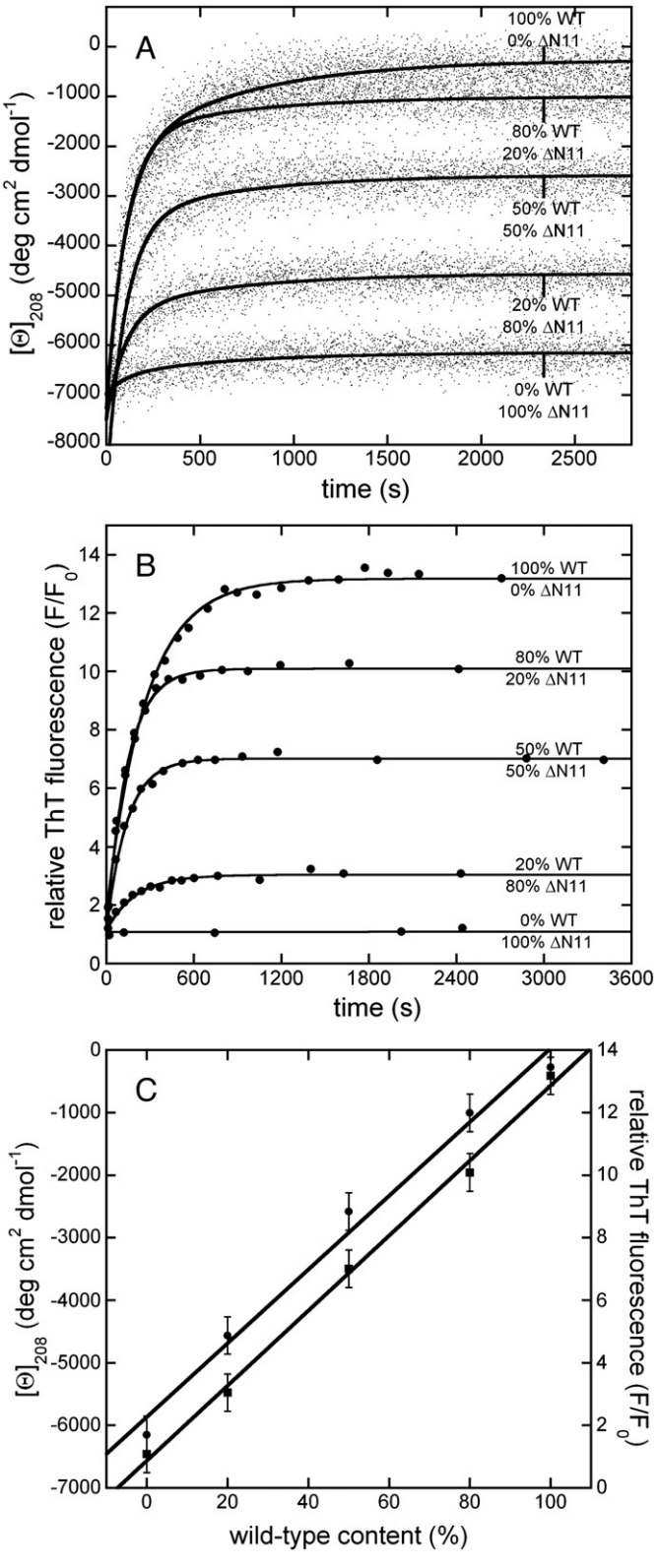

Fig. 6. (A) Aggregation of 34 μM Sso AcP in 50 mM acetate buffer at pH 5.5, 20% (v/v) TFE and 25 °C monitored by means of far-UV CD at 208 nm. Although the total protein concentration is constant (34 μM), the traces refer to different relative amounts of wild-type and ΔN11 Sso AcP variants. Continuous lines represent best fits of experimental data to Eq. (1). (B) Aggregation of 34 μM Sso AcP in 50 mM acetate buffer at pH 5.5, 20% (v/v) TFE and 25 °C monitored by means of ThT fluorescence. The signal is shown as a ratio of ThT fluorescence in the presence (F) and absence (F_0) of protein. Although the total protein concentration is constant (34 μM), the traces refer to different relative amounts of protein wild-type and ΔN11 Sso AcP variants. Continuous lines represent best fits of experimental data to Eq. (2). (C) Plateau mean residue ellipticity at 208 nm (●) and ThT fluorescence (■) versus relative content of wild-type in the experiments reported in panels (A) and (B). Continuous lines represent best fits of experimental data to a linear equation.

We have first investigated possible effects induced by the four peptides on the behavior of ΔN11 Sso AcP. Incubation of ΔN11 Sso AcP with an equimolar amount of N11 or scrambled-N11 does not induce a significant increase, as detected with DLS, in protein dimension compatible with Sso AcP dimers or oligomers (data not shown). Moreover, samples containing 34 μM ΔN11 Sso AcP in aggregating conditions and in the presence of N11 and N14 at molar excesses ranging from 1-fold to 25-fold do not undergo any detectable increase in ThT fluorescence (Fig. 7A). These observations show that the N-terminal segment is able to induce aggregation of Sso AcP only when covalently bound to the globular part of a monomer, while the same effect is not observed when this segment is free in solution, even in large excess. This finding suggests that each N-terminal segment interacts only with the globular unit of another monomer to form the early aggregates and thus these experiments rule out aggregation mechanisms based on a bridging effect of the N-terminal segment between two globular units of two Sso AcP molecules (models 3, 4, and 10 in Supplementary Data). Models based on intra-molecular interactions between the unstructured segment and the globular part of Sso AcP that give rise to an aggregation-prone state (models 6, 7, 12 and 13 in Supplementary Data) are also excluded.

In another set of experiments we have studied the effect of the various peptides on the aggregation of wild-type Sso AcP. We have followed both the first phase of aggregation, using static light scattering, and the second phase, using ThT fluorescence (see Materials and Methods). The first phase has been followed at 208 nm, rather than at the higher wavelengths in the visible region that are normally used to monitor light scattering. Indeed, this low wavelength allows to monitor the small aggregates that form during the first phase of aggregation. In the presence of a 4-fold molar excess of N11 and N14 formation of early aggregates is significantly slower (Fig. 7B). The rate constants for the first phase (k_1), determined by best fits of experimental data to Eq. (3), are equal to $(3.4\pm0.3)\cdot10^{-2}$ s^{-1}, $(1.8\pm0.2)\cdot10^{-2}$ s^{-1} and $(1.7\pm0.2)\cdot10^{-2}$ s^{-1} for Sso AcP without peptide, Sso AcP in the presence of a 4-fold molar excess of N11 and Sso AcP in the presence of a 4-fold molar excess of N14, respectively. Neither the scrambled-N11 nor the control peptide is able to induce the same effect on the process (Fig. 7B). In fact, the rate constants obtained for Sso AcP in the presence of a 4-fold molar excess of these two peptides are $(3.0\pm0.3)\cdot10^{-2}$ and $(3.4\pm0.3)\cdot10^{-2}$ s^{-1}, respectively. Peptides show the same effects when the first phase of aggregation is monitored with static light scattering at different wavelengths (data not shown).

Similar results were achieved for the second phase of aggregation (Fig. 7C). Addition of a 10-molar excess of N11 or N14 peptides

significantly slows down formation of protofibrils (Fig. 7C). The resulting rate constants (k_2), determined by best fits of experimental data to Eq. (2), are equal to $(3.7\pm0.3)\cdot10^{-3}$ s^{-1} and $(8.5\pm0.8)\cdot10^{-4}$ s^{-1} for wild-type Sso AcP in the absence and presence of either peptide, respectively. By contrast, the rate constants obtained in the presence of 10-fold molar excesses of scrambled-N11 and control peptide are $(4.7\pm0.4)\cdot10^{-3}$ and $(5.8\pm0.5)\cdot10^{-3}$ s^{-1}, respectively. The fact that these two peptides induce even a slight acceleration of the process shows that the deceleration observed in the presence of N11 and N14 is due to the primary sequence of these peptides rather than other parameters (e.g. physicochemical properties or other non-specific effects). Taken together, these results show that the N11 and N14 peptides compete with the N-terminal unstructured segment of Sso

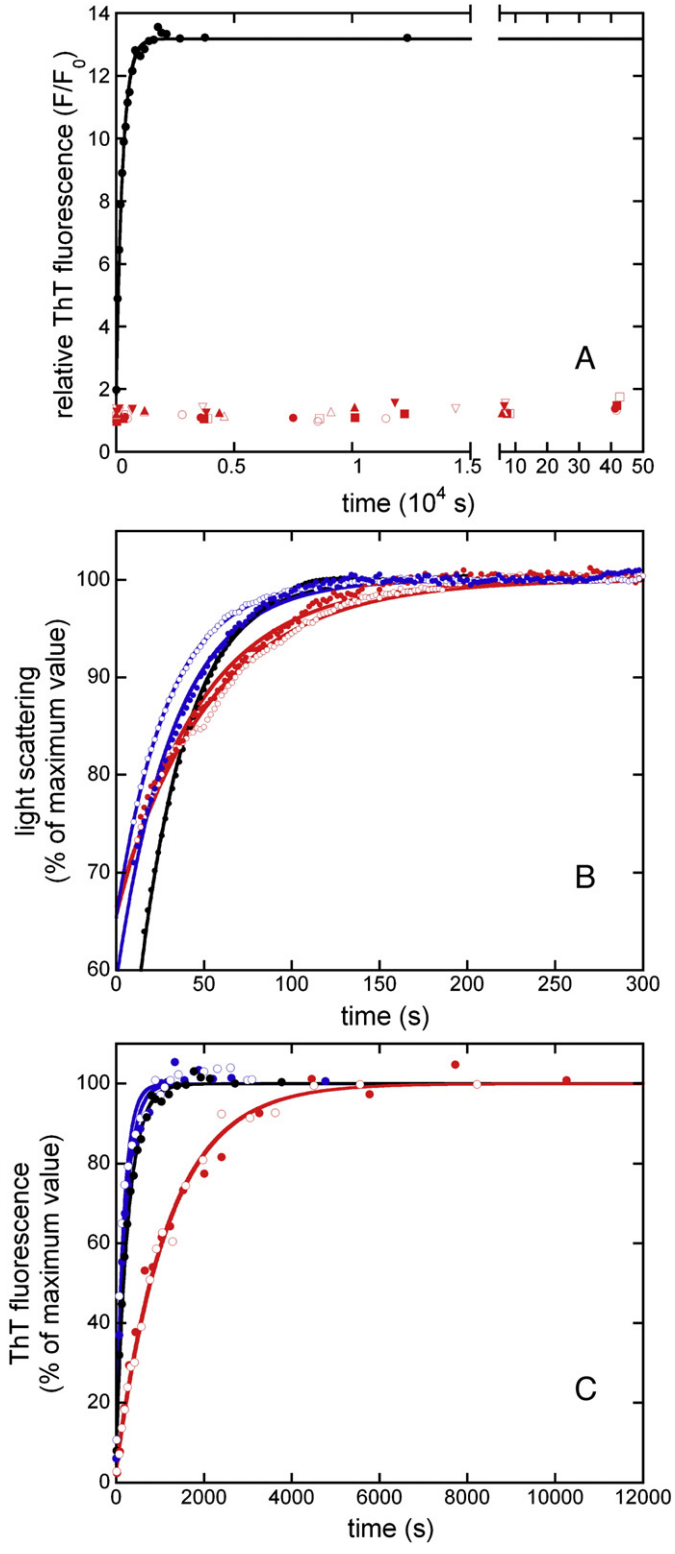

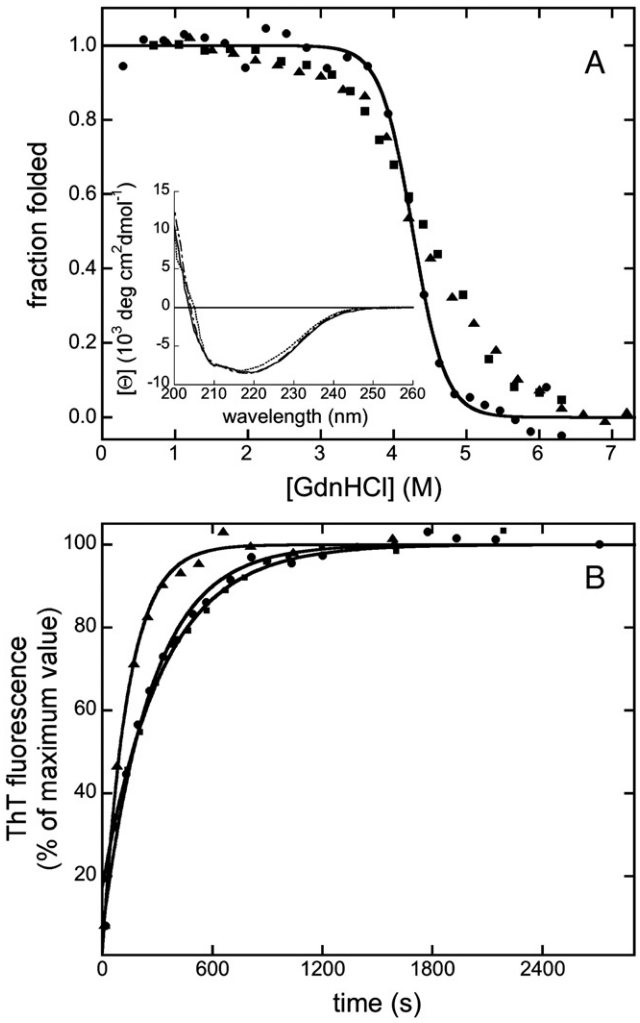

Fig. 8. (A) Equilibrium unfolding curves of wild-type (●), 85Dim (■) and 6Dim (▲) Sso AcP in 50 mM acetate buffer at pH 5.5, 37 °C. The continuous line represents best fit of experimental data to the Santoro and Bolen model [23]. The inset shows far-UV CD spectra of wild-type (continuous line), 85Dim (dotted line) and 6Dim (dashed line) Sso AcP. (B) ThT fluorescence during aggregation of wild-type (●), 85Dim (■) and 6Dim (▲) Sso AcP in 50 mM acetate buffer at pH 5.5 containing 20% (v/v) TFE, 25 °C. Continuous lines represent best fits of experimental data to Eq. (2).

Fig. 7. (A) Time course of ThT fluorescence during incubation of ΔN11 Sso AcP in 50 mM acetate buffer at pH 5.5, 20% (v/v) TFE and 25 °C in the presence of different molar excesses of N11 (red filled symbols) and N14 (red empty symbols). Data are shown for 2-fold (red ■ and □), 5-fold (red ● and ○), 10-fold (red ▲ and △) and 25-fold (red ▼ and ▽) molar excesses. The signal is shown as a ratio between ThT fluorescence in the presence (F) and in the absence (F_0) of protein. The kinetic trace for wild-type Sso AcP in the same conditions with no peptides (black ●) is shown for comparison. The continuous line represents the best fit of experimental data to Eq. (2). (B) First phase of aggregation, monitored using static light scattering recorded at 208 nm, for 34 μM wild-type Sso AcP in 50 mM acetate buffer at pH 5.5, 20% (v/v) TFE and 25 °C in the presence of a 4-fold molar excesses of various peptides. Signal normalized to the maximum value is shown versus time in this panel. Traces are shown for Sso AcP without peptides (black ●), Sso AcP and N11 peptide (red ○), Sso AcP and N14 peptide (red ●), Sso AcP and scrambled-N11 (blue ●), Sso AcP and control peptide (blue ○). Continuous lines represent best fits of experimental data to Eq. (3). (C) Second phase of aggregation, monitored using ThT fluorescence for 34 μM wild-type Sso AcP in 50 mM acetate buffer at pH 5.5, 20% (v/v) TFE and 25 °C in the presence of 10-fold molar excesses of peptides. Traces are shown for Sso AcP without peptides (black ●), Sso AcP and N11 peptide (red ○), Sso AcP and N14 peptide (red ●), Sso AcP and scrambled-N11 (blue ●), Sso AcP and control peptide (blue ○). Continuous lines represent best fits of experimental data to Eq. (2).

AcP for binding to a specific portion of the wild-type molecule and that this interaction retards aggregation. The interaction seems to be inter-molecular as the peptides induce a deceleration, rather than an acceleration of the process. Several models of aggregation are excluded following these results (see models 1, 3, 6, 7, 11, 12, 14 and 15 in Supplementary Data).

3.5. Aggregation of Sso AcP dimers does not support strand-to-strand or N-to-N-terminus interactions

Taking advantage of the absence of cysteine residues in wild-type Sso AcP, we have produced, by site-directed mutagenesis, two protein variants carrying a single cysteine in two different positions. These are D6C, presenting a cysteine in the N-terminal segment and D85C, presenting a cysteine in the β-strand 4. We have then induced the oxidative formation of disulphide bridges in both D6C and D85C Sso AcP and we have obtained two homodimers in which two N-termini and two β-strands 4 are forced to interact. We will refer to these homodimeric variants as to 6Dim Sso AcP and 85Dim Sso AcP, respectively.

In a first set of experiments we have investigated the native states of the dimers. Far-UV CD spectra of native 6Dim and 85Dim Sso AcP are fully superimposable to spectra of native wild-type Sso AcP, suggesting that dimerization does not affect the secondary structure content of the native states (inset to Fig. 8A). The conformational stabilities of 6Dim and 85Dim Sso AcP have been measured in equilibrium unfolding experiments carried out in 50 mM acetate buffer at pH 5.5 and 37 °C (Fig. 8A). Both mutants recover enzymatic activity following refolding, suggesting reversible unfolding processes (data not shown). When analyzed with a two-state model both dimers show a C_m value equal to 4.4±0.1 M GdnHCl. This is similar to the value of 4.2±0.1 measured for monomeric wild-type Sso AcP under the same conditions. However, the dimers have m values of 4.5±0.5 kJ mol^{-1} M^{-1}, remarkably lower than the value measured for the wild-type monomeric protein, 11.4±0.5 kJ mol^{-1} M. The m value is related to the change in solvent accessible area upon unfolding [26]. The observed decrease in m value can be explained with an interaction between the Sso AcP molecules that form the dimer in the unfolded state. Nevertheless, the equilibrium unfolding curves of both dimers in the transition zone are reminiscent of a three-state unfolding. Indeed, the experimental data do not fit satisfactorily to a two state model and a decrease of steepness is apparent halfway through the transition in both curves (Fig. 8A). Thus, it is possible that the two Sso AcP molecules forming the dimer unfold in two separate steps, giving rise to an apparent three-state transition.

Aggregation of the two dimers has been followed by ThT fluorescence (Fig. 8B). 6Dim Sso AcP and 85Dim Sso AcP induce the same increase in ThT fluorescence as the wild-type protein. Although the process is slightly accelerated in the case of 6Dim Sso AcP, aggregation of dimers occurs on a time scale comparable to that of the wild-type protein. Rate constants k_2, determined by best fits of experimental data to Eq. (2), are equal to $(3.7\pm0.4)\cdot10^{-3}$ s^{-1}, $(3.1\pm0.4)\cdot10^{-3}$ s^{-1} and $(7.3\pm0.6)\cdot10^{-3}$ s^{-1} for wild-type, 85Dim and 6Dim Sso AcP, respectively. The Far-UV CD spectra of the early aggregates formed by the dimers is comparable to that of the early aggregates formed by wild-type protein, with a single negative peak at 224 nm (data not shown). In both cases the protofibrillar aggregates at the plateau of the kinetic experiment bind to the CR dye (data not shown).

These data show that forcing two N-termini or two β-strands 4 to interact does not strongly accelerate aggregation, suggesting that the interaction that leads to the formation of early aggregates is not established between corresponding segments of two different Sso AcP molecules (see models 2, 5, 9, 11, 15 and 16 in Supplementary Data). Two different segments interact in early aggregates. These include the N-terminus and the β-strand 4 or another region of the globular part of Sso AcP. Structural inspection of wild-type Sso AcP shows that a possible interaction between the unstructured N-terminal segment of an Sso AcP molecule and the globular unit of another Sso AcP molecule (for example β-strand 4) would not be inhibited in the 6Dim and 85Dim dimers. In fact, even the formation of the disulphide bridge in the 85Dim does not create a steric hindrance for the β-strand 4 to interact with the N-terminal segment of another dimerized molecule.

4. Discussion

4.1. A model for the aggregation of Sso AcP

The data collected in this work allow the formulation of a model for the aggregation mechanism of Sso AcP under conditions in which the protein adopts initially a native-like state (Fig. 9). This model takes into account all the experimental evidence presented in this manuscript and in our previous work [11–13,20]. Under the conditions tested here Sso AcP initially populates an ensemble of native-like conformations. In this ensemble the native topology is retained, but the presence of TFE increases the flexibility of the protein so that some regions are transiently exposed to the solvent via structural fluctuations that are distinct from the unfolding reaction.

The first phase of aggregation is an inter-molecular process in which the N-terminal unstructured segment of an Sso AcP molecule establishes interactions with the globular part of another Sso AcP

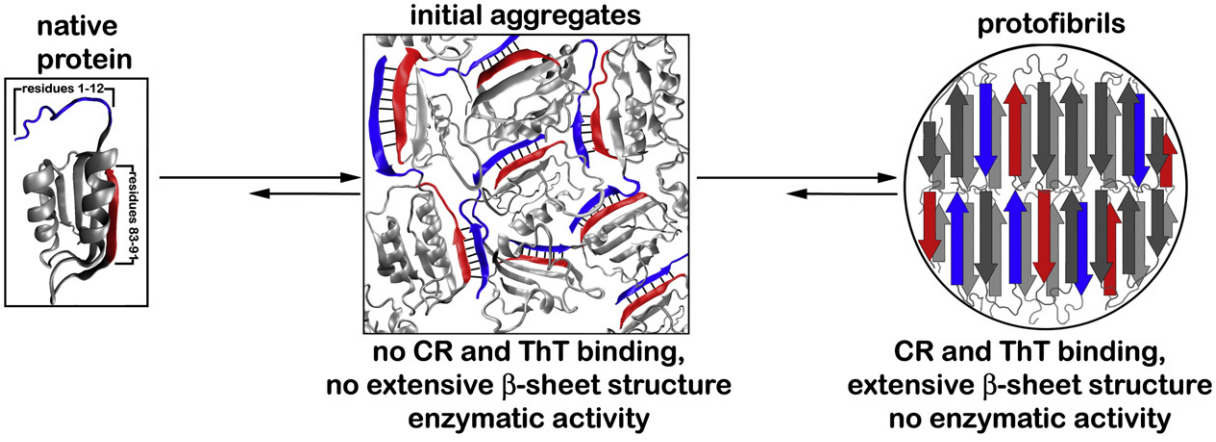

Fig. 9. Model for Sso AcP aggregation under conditions in which the protein is initially native-like. The unstructured N-terminal segment is depicted in blue; the β-strand 4 is depicted in red. The model is discussed in the text.

molecule, possibly the peripheral β-strand 4 (Fig. 9). The intermolecular nature of this interaction is indicated by the decrease in aggregation rate of the wild-type protein induced by the N11 and N14 peptides and by the observation that moving the segment to the C-terminus does not result in any difference in the process. The interaction seems to be specific rather than generic as the scrambled-N11 peptide does not induce the same effect as the N11 and N14 peptides. The interaction can induce formation of a β-strand in the N-terminal segment, as depicted in Fig. 9, but also have a different nature. Aggregation cannot proceed via N- to N-terminus or β-strand 4-to-β-strand 4 interactions. This is shown by the finding that both ΔN11 and the N11 and N14 peptides are fully soluble in conditions promoting aggregation of wild-type Sso AcP [13] and by the observation that forcing two N-termini or two β-strand 4 to interact via a covalent bond does not induce a dramatic increase in aggregation rate. In the resulting early aggregates the individual protein molecules retain a native-like topology and even exhibit enzymatic activity [12]. It is possible that other interactions, in addition to those between the N-terminus and β-strand 4, are present and stabilize these assemblies, but these do not seem to participate to the rate-determining step [13].

The second phase of aggregation is a process in which the initial aggregates convert into amyloid-like protofibrils characterized by β-sheet structure and an ability to bind ThT and CR [12]. This structural conversion occurs directly with no need to disassembly and re-assembly of the aggregated protein molecules and consists, for each protein molecule, in a cooperative conversion involving the whole structure. This is suggested by the observation that k_2, unlike k_1, does not depend on protein concentration and by the previously reported inverse correlation between k_2 and the conformational stability of the native state in a group of Sso AcP variants bearing mutations at various positions [13].

The model presented in this work is conceptually different from those proposed for proteins presenting a globular domain and an unfolded segment. In most cases it was found that the unstructured domains are able to self-assemble autonomously [27–29]. By contrast, our model is similar to another aggregation mechanism proposed for Ure2p from *Saccharomices cerevisiae*, in which the unstructured domain is proposed to interact with the globular part of another molecule [30,31]. In agreement with this model, it has been recently shown that the molecular chaperone YDJ1 is able to bind the globular part of the Ure2p molecule and inhibit fibril formation [32].

4.2. Conclusions

Globular proteins spend the majority of their life-span in a folded conformation. The recognition that evolution has devised several strategies to avoid aggregation of folded proteins [33] is by itself an indication that aggregation phenomena directly involving the folded structure are indeed realistic. Indeed, aggregation mechanisms starting from native-like states have been observed for a handful of proteins including the protein S6 from *Thermus thermophilus* [10], human ataxin-3 [9], human superoxide dismutase-type 1 [34], acylphosphatase from *Drosophila melanogaster* [35] and the system studied here [11]. In all these cases aggregation is likely to occur via structural fluctuations that occur from the native state and not involving a full unfolding across the major free energy barrier.

Sso AcP possesses a lower number of protective elements at the level of the peripheral β-strand 4 and a higher content of unstructured portions than other members of the acylphosphatase-like structural family shown to aggregate via unfolding as a first necessary step [20]. The aggregation mechanism outlined from the results presented here shows that co-existence of unprotected peripheral β-strands and highly flexible portions dramatically increases the possibility of intermolecular interactions that trigger self-assembly between protein molecules in their native-like states. Only with further investigation we will achieve the goal of completely understanding the mechanisms of amyloid formation starting from folded states and the parameters that determine such processes.

Acknowledgments

This work was supported by grants from the Italian MIUR (FIRB project n° RBIN04PWNC and PRIN project n° 2006058958), EMBO (Young Investigator Program 2005) and European community (project LSHM-CT-2006-037525). FB was supported by the Accademia dei Lincei, LV is supported by a pre-doctoral grant from the Junta de Andalucia (FQM-123), AIA is a recipient of a Return research contract from the Junta de Andalucia. The authors do not declare any conflict of interest.

Appendix A. Supplementary data

Supplementary data associated with this article can be found, in the online version, at doi:10.1016/j.bbapap.2008.08.021.

References

[1] F. Chiti, C.M. Dobson, Protein misfolding, functional amyloid, and human disease, Annu. Rev. Biochem. 75 (2006) 333–366.
[2] M. Sunde, C.C. Blake, The structure of amyloid fibrils by electron microscopy and X-ray diffraction, Adv. Protein Chem. 50 (1997) 123–159.
[3] W.S. Gosal, S.L. Myers, S.E. Radford, N.H. Thomson, Amyloid under the atomic force microscope, Protein Pept. Lett. 13 (2006) 261–270.
[4] M.R. Krebs, E.H. Bromley, A.M. Donald, The binding of thioflavin-T to amyloid fibrils: localisation and implications, J. Struct. Biol. 149 (2005) 30–37.
[5] M.R. Nilsson, Techniques to study amyloid fibril formation in vitro, Methods 34 (2004) 151–160.
[6] F. Chiti, P. Webster, N. Taddei, A. Clark, M. Stefani, G. Ramponi, C.M. Dobson, Designing conditions for in vitro formation of amyloid protofilaments and fibrils, Proc. Natl. Acad. Sci. U. S. A. 96 (1999) 3590–3594.
[7] J.I. Guijarro, M. Sunde, J.A. Jones, I.D. Campbell, C.M. Dobson, Amyloid fibril formation by an SH3 domain, Proc. Natl. Acad. Sci. U. S. A. 95 (1998) 4224–4228.
[8] V. Villegas, J. Zurdo, V.V. Filimonov, F.X. Avilés, C.M. Dobson, L. Serrano, Protein engineering as a strategy to avoid formation of amyloid fibrils, Protein Sci. 9 (2000) 1700–1708.
[9] M.K. Chow, A.M. Ellisdon, L.D. Cabrita, S.P. Bottomley, Polyglutamine expansion in ataxin-3 does not affect protein stability: implications for misfolding and disease, J. Biol. Chem. 279 (2004) 47643–47651.
[10] J.S. Pedersen, G. Christensen, D.E. Otzen, Modulation of S6 fibrillation by unfolding rates and gatekeeper residues, J. Mol. Biol. 341 (2004) 575–588.
[11] G. Plakoutsi, N. Taddei, M. Stefani, F. Chiti, Aggregation of the Acylphosphatase from *Sulfolobus solfataricus*: the folded and partially unfolded states can both be precursors for amyloid formation, J. Biol. Chem. 279 (2004) 14111–14119.
[12] G. Plakoutsi, F. Bemporad, M. Calamai, N. Taddei, C.M. Dobson, F. Chiti, Evidence for a mechanism of amyloid formation involving molecular reorganisation within native-like precursor aggregates, J. Mol. Biol. 351 (2005) 910–922.
[13] G. Plakoutsi, F. Bemporad, M. Monti, D. Pagnozzi, P. Pucci, F. Chiti, Exploring the mechanism of formation of native-like and precursor amyloid oligomers for the native acylphosphatase from *Sulfolobus solfataricus*, Structure 14 (2006) 993–1001.
[14] A. Corazza, C. Rosano, K. Pagano, V. Alverdi, G. Esposito, C. Capanni, F. Bemporad, G. Plakoutsi, M. Stefani, F. Chiti, S. Zuccotti, M. Bolognesi, P. Viglino, Structure, conformational stability, and enzymatic properties of acylphosphatase from the hyperthermophile *Sulfolobus solfataricus*, Proteins 62 (2006) 64–79.
[15] K. Miyazono, Y. Sawano, M. Tanokura, Crystal structure and structural stability of acylphosphatase from hyperthermophilic archaeon *Pyrococcus horikoshii* OT3, Proteins 61 (2005) 196–205.
[16] K. Pagano, M. Ramazzotti, P. Viglino, G. Esposito, D. Degl'Innocenti, N. Taddei, A. Corazza, NMR solution structure of the acylphosphatase from *Escherichia coli*, J. Biomol. NMR 36 (2006) 199–204.
[17] A. Pastore, V. Saudek, G. Ramponi, R.J. Williams, Three-dimensional structure of acylphosphatase. Refinement and structure analysis, J. Mol. Biol. 224 (1992) 427–440.
[18] M.M. Thunnissen, N. Taddei, G. Liguri, G. Ramponi, P. Nordlund, Crystal structure of common type acylphosphatase from bovine testis, Structure 5 (1997) 69–79.
[19] S. Zuccotti, C. Rosano, M. Ramazzotti, D. Degl'Innocenti, M. Stefani, G. Manao, M. Bolognesi, Three-dimensional structural characterization of a novel *Drosophila melanogaster* acylphosphatase, Acta Crystallogr. D Biol. Crystallogr. 60 (2004) 1177–1179.
[20] G. Soldi, F. Bemporad, F. Chiti, The degree of structural protection at the edge b-strands determines the pathway of amyloid formation in globular proteins, J. Am. Chem. Soc. 130 (2008) 4295–4302.
[21] G. Camici, G. Manao, G. Cappugi, G. Ramponi, A new synthesis of benzoyl phosphate: a substrate for acyl phosphatase assay, Experientia 32 (1976) 535–536.
[22] F. Bemporad, C. Capanni, M. Calamai, M.L. Tutino, M. Stefani, F. Chiti, Studying the folding process of the acylphosphatase from *Sulfolobus solfataricus*. A comparative analysis with other proteins from the same superfamily, Biochemistry 43 (2004) 9116–9126.

[23] M.M. Santoro, D.W. Bolen, Unfolding free energy changes determined by the linear extrapolation method. 1. Unfolding of phenylmethanesulfonyl alpha-chymotrypsin using different denaturants, Biochemistry 27 (1988) 8063–8068.
[24] G. Ramponi, C. Treves, A.A. Guerritore, Aromatic acyl phosphates as substrates of acyl phosphatase, Arch. Biochem. Biophys. 115 (1966) 129–135.
[25] M. Stefani, N. Taddei, G. Ramponi, Insights into acylphosphatase structure and catalytic mechanism, Cell. Mol. Life Sci. 53 (1997) 141–151.
[26] J.K. Myers, C.N. Pace, J.M. Scholtz, Denaturant m values and heat capacity changes: relation to changes in accessible surface areas of protein unfolding, Protein Sci. 4 (1995) 2138–2148.
[27] A. Balguerie, S. Dos Reis, C. Ritter, S. Chaignepain, B. Coulary-Salin, V. Forge, K. Bathany, I. Lascu, J.M. Schmitter, R. Riek, S.J. Saupe, Domain organization and structure–function relationship of the HET-s prion protein of *Podospora anserina*, EMBO J. 22 (2003) 2071–2081.
[28] U. Baxa, K.L. Taylor, J.S. Wall, M.N. Simon, N. Cheng, R.B. Wickner, A.C. Steven, Architecture of Ure2p prion filaments: the N-terminal domains form a central core fiber, J. Biol. Chem. 278 (2003) 43717–43727.
[29] J.R. Glover, A.S. Kowal, E.C. Schirmer, M.M. Patino, J.J. Liu, S. Lindquist, Self-seeded fibers formed by Sup35, the protein determinant of [PSI+], a heritable prion-like factor of *S. cerevisiae*, Cell 89 (1997) 811–819.
[30] L. Bousset, N.H. Thomson, S.E. Radford, R. Melki, The yeast prion Ure2p retains its native alpha-helical conformation upon assembly into protein fibrils in vitro, EMBO J. 17 (2002) 2903–2911.
[31] N. Fay, V. Redeker, J. Savistchenko, S. Dubois, L. Bousset, R. Melki, Structure of the prion Ure2p in protein fibrils assembled in vitro, J. Biol. Chem. 280 (2004) 37149–37158.
[32] H. Lian, H. Zhang, Z. Zhang, H.M. Loovers, G.W. Jones, P.J.E. Rowling, L.S. Itzhaki, J. Zhou, S. Perrett, Hsp40 interacts directly with the native state of the yeast prion protein Ure2 and inhibits formation of amyloid-like fibrils, J. Biol. Chem. 282 (2007) 11931–11940.
[33] J.S. Richardson, D.C. Richardson, Natural b-sheet proteins use negative design to avoid edge-to-edge aggregation, Proc. Natl. Acad. Sci. U. S. A. 99 (2002) 2754–2759.
[34] A. Nordlund, M. Oliveberg, Folding of Cu/Zn superoxide dismutase suggests structural hotspots for gain of neurotoxic function in ALS: parallels to precursors in amyloid disease, Proc. Natl. Acad. Sci. U. S. A. 103 (2006) 10218–10223.
[35] G. Soldi, F. Bemporad, S. Torrassa, A. Relini, M. Ramazzotti, N. Taddei, F. Chiti, Amyloid formation of a protein in the absence of initial unfolding and destabilization of the native state, Biophys. J. 89 (2005) 4234–4244.
[36] W. Humphrey, A. Dalke, K. Schulten, VMD — Visual Molecular Dynamics, J. Molec. Graphics 14 (1996) 33–38.

Supplementary Data

1. Aggregation of wild-type Sso AcP in the presence of phosphate buffer

In order to further investigate the role of the destabilization induced by the N-terminal segment on Sso AcP aggregation we took advantage of the catalytic properties of Sso AcP. This protein is an enzyme able to hydrolyze phosphoanhydridic bonds of acylphosphates [1]. All proteins belonging to the acylphosphatase structural family follow standard Michaelis-Menten Kinetic theory and phosphate ion is a well known competitive inhibitor of their activity [2]. In the presence of phosphate the equilibrium between folded and unfolded protein will the following:

$$F\text{-}P_i \overset{K_i}{\rightleftharpoons} F + P_i \overset{K_U}{\rightleftharpoons} U + P_i$$

where F-P_i is the folded state bound to phosphate, F, U and P_i are folded and unfolded protein and phosphate ion, K_i is the affinity constant of phosphate and K_U is the unfolding constant. The amount of native protein will increase following addition of phosphate and the resulting stabilization $\Delta\Delta G_{U-F}^{P_i}$ can be calculated as follows:

$$\Delta\Delta G_{U-F}^{P_i} = RT \ln\left(1 + \frac{C_P}{K_i}\right) \qquad (1)$$

where C_P is the phosphate concentration, R is the ideal gas constant and T is the temperature. Equation (1) allows the phosphate concentration to be calculated that induces the desired stabilization on Sso AcP. We have determined the affinity constant of Sso AcP for phosphate ion in the aggregation promoting conditions. In these conditions K_i is equal to 1.12±0.1 mM (supplementary Fig. 1A). Then we have followed ThT fluorescence in the presence of 34 μM wild-type protein in 44.1 mM acetate and 4.8 mM phosphate buffer at pH 5.5, 20% (v/v) TFE and 25°C (figure 4B). In these conditions wild-type protein has the same conformational stability as ΔN11 Sso AcP, as determined by equation (1), while the overall ionic strength does not vary. The fluorescence of the dye increases to reach a

plateau in a single exponential phase. Aggregation rate constant, determined by best fit of experimental data to equation (3), is equal to $(2.6\pm0.3) \cdot 10^{-6}$ s^{-1} (supplementary Fig. 1B). The species populated at the plateau of the kinetic experiment binds to Congo red dye (data not shown). Aggregation rate constants for wild-type Sso AcP and I72V-ΔN11 Sso AcP are $(3.7\pm0.4) \cdot 10^{-3}$ s^{-1} and $(8.1\pm0.8) \cdot 10^{-6}$ s^{-1}, respectively (see text). Thus, this control experiment shows that a destabilized ΔN11 protein variant aggregates slower than a stabilized wild-type protein. This lends further support to the idea that the N-terminal unstructured segment does not promote aggregation of the protein because of its destabilizing effect. The significant decrease in aggregation rate induced by the phosphate is probably due to the ability of this ion to bind to the catalytic site and to decrease the conformational fluctuations of the protein [3].

2. Methods

Enzymatic activity of 2.0 μg ml^{-1} ΔN11 Sso AcP was measured at 25°C in 50 mM acetate buffer at pH 5.5, TFE with 20% (v/v) and a benzoyl phosphate concentration ranging from 0.2 to 8 mM. The experiment was carried out both in the absence and in the presence of 1.5 mM sodium phosphate. Affinity constant for phosphate was calculated using standard Michaelis-Menten theory.

ThT fluorescence has been measured as reported in the text (see Materials and Methods).

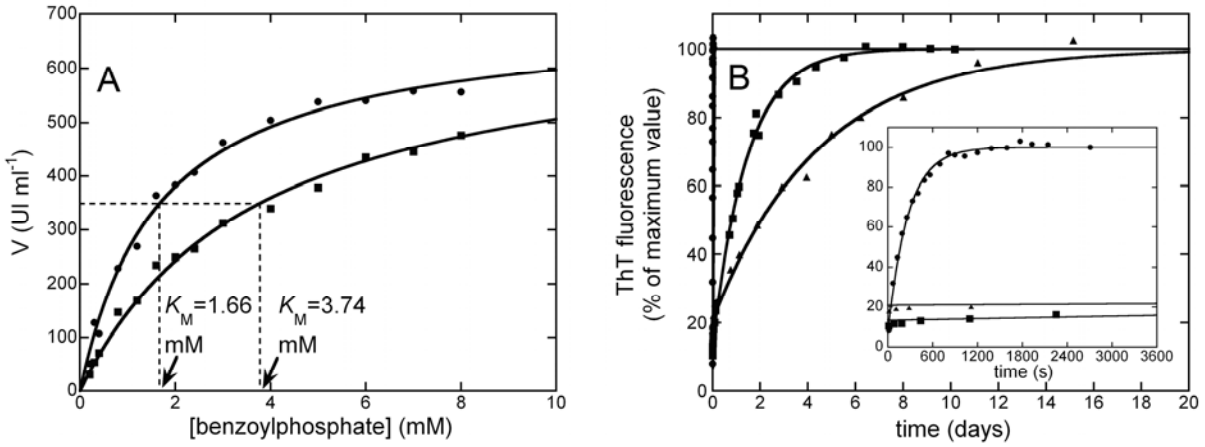

Supplementary figure 1. (A) Michaelis-Menten plot of ΔN11 Sso AcP in the absence (●) and in the presence (■) of 1.5 mM phosphate. Apparent K_M values are shown. The resulting K_i is equal to 1.12±0.1 mM. (B) ThT fluorescence during aggregation of Sso AcP in different conditions. Traces are shown for 34 μM wild-type in 50 mM acetate buffer at pH 5.5, 20% (v/v) TFE and 25°C (●), 34 μM wild-type in 44.1 mM acetate and 4.8 mM phosphate buffer at pH 5.5, 20% (v/v) TFE and 25°C (■), and 34 μM I72V-ΔN11 (▲) Sso AcP in 50 mM acetate buffer at pH 5.5, 20% (v/v) TFE and 25°C. The inset shows the first hour of recording. Continuous lines represent best fits of experimental data to equation (3).

3. Modelling the aggregation mechanism of Sso AcP

In this paragraph a set of possible models for the first phase of amyloid-like aggregation of Sso AcP are presented. The models are discussed taking into account the results presented in this manuscript and the following previously published observations:

1. At the end of the first phase of aggregation a large assembly is populated in which the Sso AcP molecules retain their native-like fold [4].
2. It was shown that two regions play a key role in the aggregation of the protein: the N-terminal unstructured segment and the β-strand 4 [5]. These two regions are depicted in red in the models.
3. A peptide that has the sequence of the N-terminal segment is not able to aggregate in conditions promoting aggregation of wild-type Sso AcP [5].
4. An Sso AcP protein variant in which the N-terminal segment has been removed (ΔN11 Sso AcP) is not able to aggregate in conditions promoting aggregation of wild-type Sso AcP [5].

In the models the N-terminal segment is depicted in blue and the β-strand 4 is depicted in red.

MODEL 1

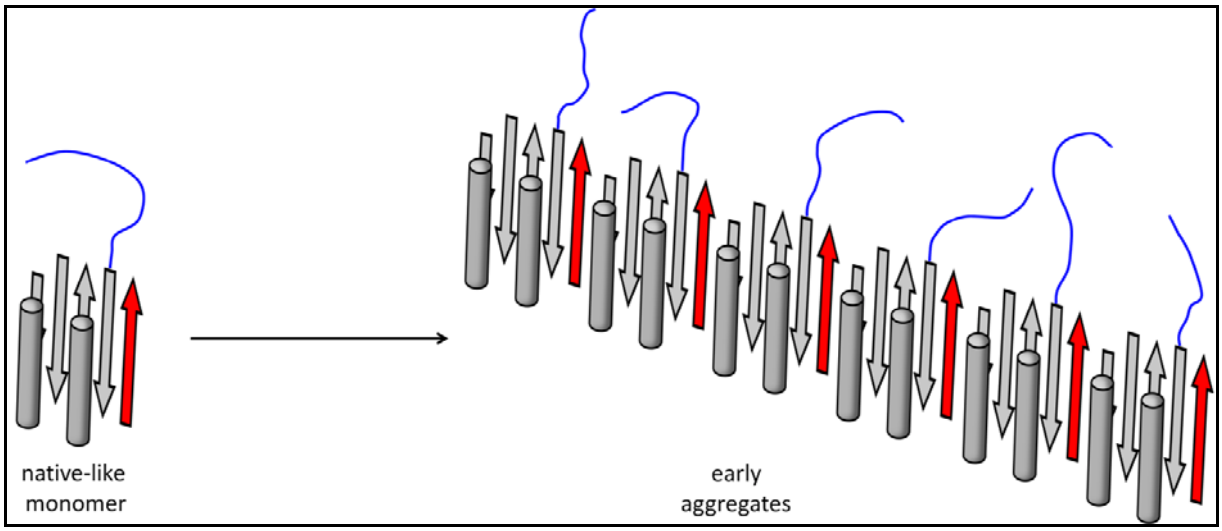

- **DESCRIPTION:** According to this model the early aggregates are stabilized by interactions between the β-strand 4 and a different region of the molecule (for instance the fifth β-strand is shown in the figure). No role is played by N-terminal segment.
- **EXPERIMENTAL OBSERVATIONS AGAINST THE MODEL:**
    1. ΔN11 Sso AcP should aggregate;
    2. One more region should be found to play a major role in promoting aggregation, i.e. the region that interacts with β-strand 4.
    3. Peptides N11 and N14 should not slow down the first phase of aggregation.
    4. Wild-type and ΔN11 Sso AcP should co-aggregate.

MODEL 2

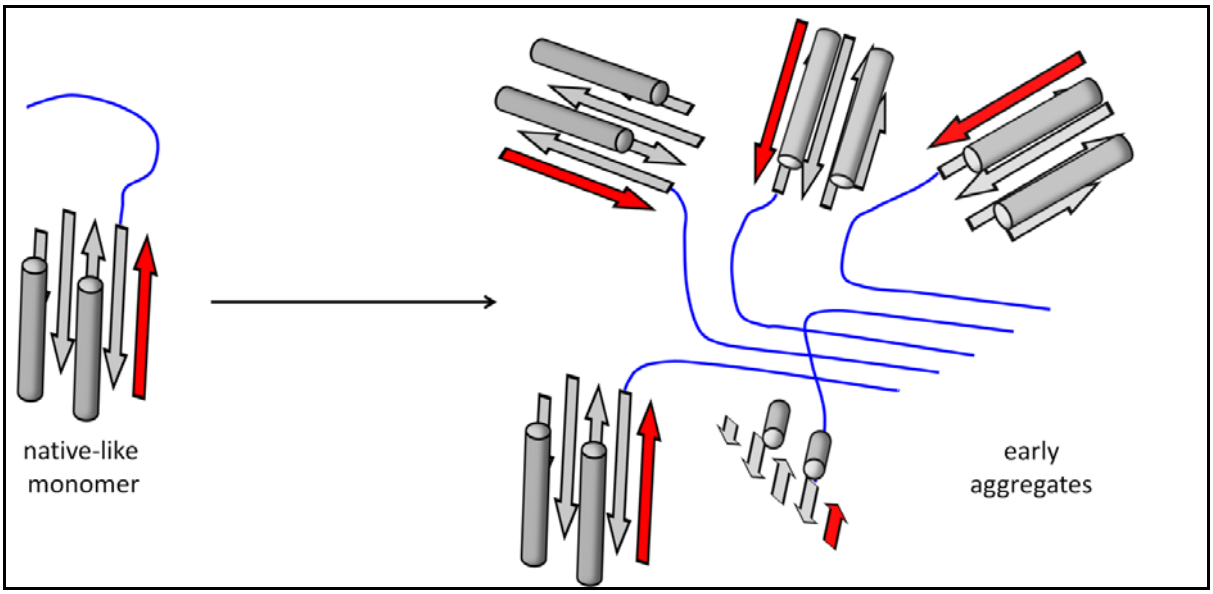

- **DESCRIPTION:** In this model the early aggregates are stabilized by intermolecular interactions between N-terminal segments of different molecules. The globular part of Sso AcP participates only to the second phase of the process.
- **EXPERIMENTAL OBSERVATIONS AGAINST THE MODEL:**
    1. The peptides N11 and N14 should aggregate in the conditions promoting aggregation.
    2. β-strand 4 should not appear important in promoting aggregation of the protein.
    3. 6Dim Sso AcP Sso AcP should show dramatic increases in aggregation rate.

MODEL 3

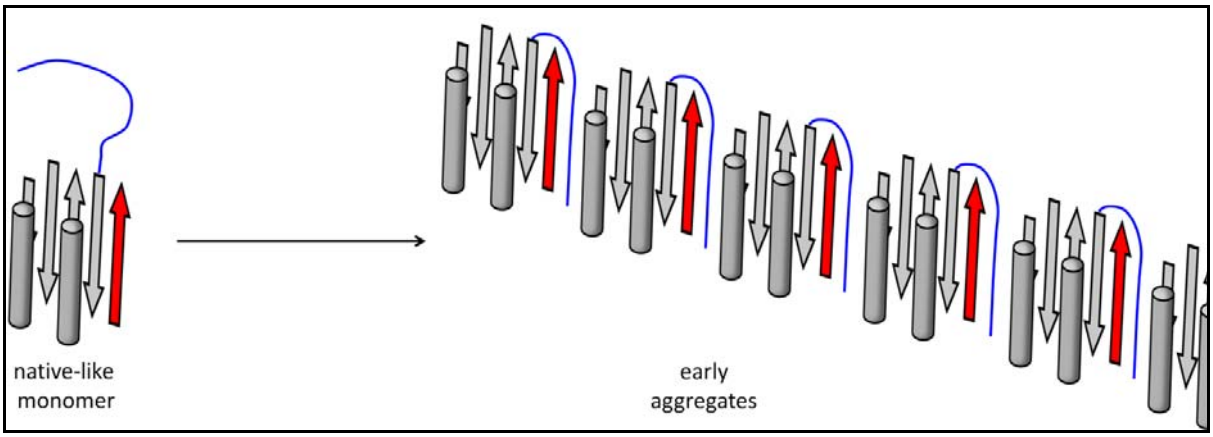

- **DESCRIPTION:** In this model the N-terminal segment of a molecule acts as a bridge between the β-strand 4 of the same molecule and another region of another molecule (for instance the other edge β-strand is shown in the figure). This induces formation of early aggregates.
- **EXPERIMENTAL OBSERVATIONS AGAINST THE MODEL:**
    1. At least one more region should play a key role in the aggregation in addition to the N-terminus and β-strand 4.
    2. Wild-type Sso AcP should aggregate more rapidly in the presence of N11 and N14 peptides.
    3. ΔN11 Sso AcP should aggregate in the presence of N11 and N14 peptides.
    4. ΔN11 and wild-type Sso AcP should co-aggregate.

MODEL 4

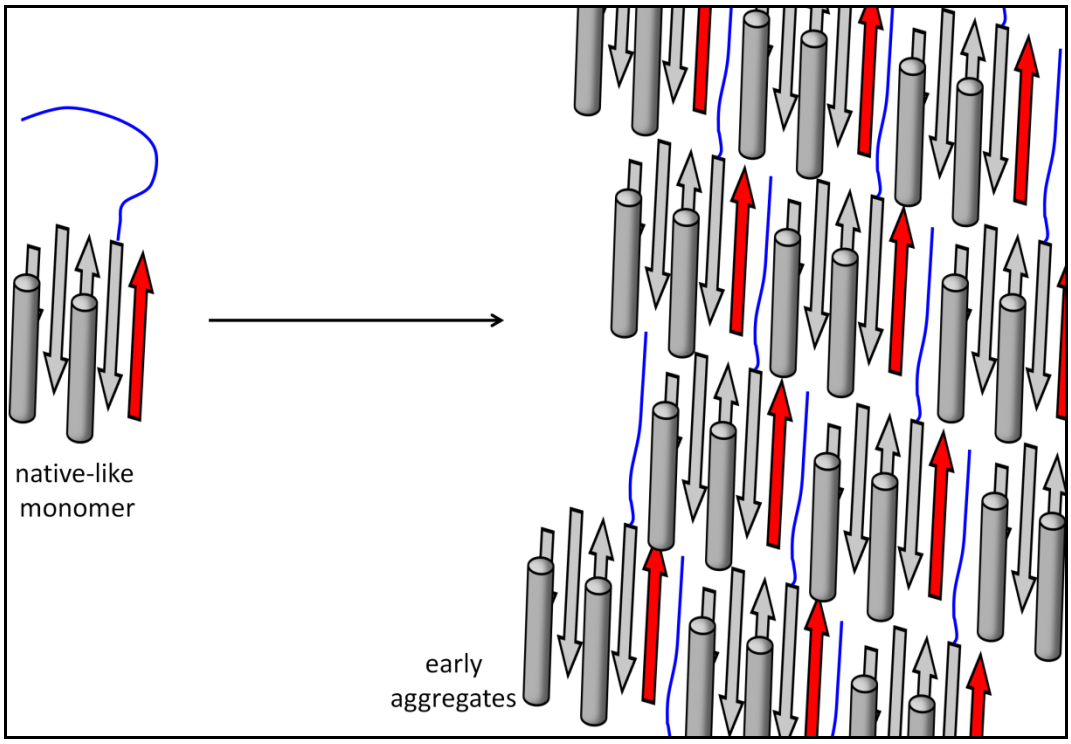

- **DESCRIPTION:** This is a variant of the previous model. In this case bridging of the N-terminal segment does not give rise to a filamentous polymer but to a larger assembly that can expand in three dimensions.
- **EXPERIMENTAL OBSERVATIONS AGAINST THE MODEL:**
    1. At least one more region should play a key role in the aggregation in addition to the N-terminus and β-strand 4.
    2. Wild-type Sso AcP should aggregate more rapidly in the presence of N11 and N14 peptides.
    3. ΔN11 Sso AcP should aggregate in the presence of N11 and N14 peptides.
    4. ΔN11 and wild-type Sso AcP should co-aggregate.

MODEL 5

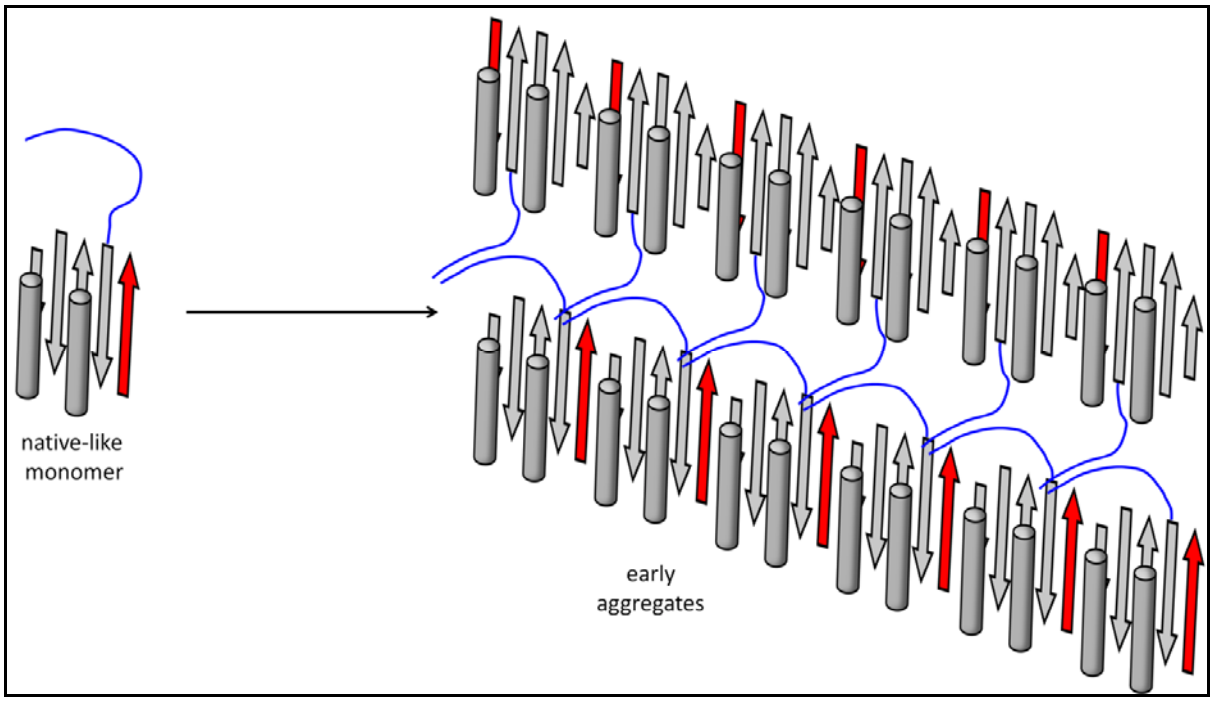

- **DESCRIPTION:** In this model both the N-terminus and the β-strand 4 play a major role in the process. Aggregation of Sso AcP is mediated by interactions between the β-strand 4 of a molecule and the globular part of another molecule and by intermolecular interactions of N-terminal segments of different molecules.
- **EXPERIMENTAL OBSERVATIONS AGAINST THE MODEL:**
    1. ΔN11 Sso AcP should give rise to oligomers in the aggregation promoting conditions.
    2. The peptides N11 and N14 should aggregate in the aggregation promoting conditions or at least form dimers.
    3. Wild-type and wild-type Sso AcP should co-aggregate.
    4. At least one more region should play a key role in the aggregation in addition to the N-terminus and β-strand 4.
    5. 6Dim Sso AcP and 85Dim Sso AcP should show dramatic increases in aggregation rate.

MODEL 6

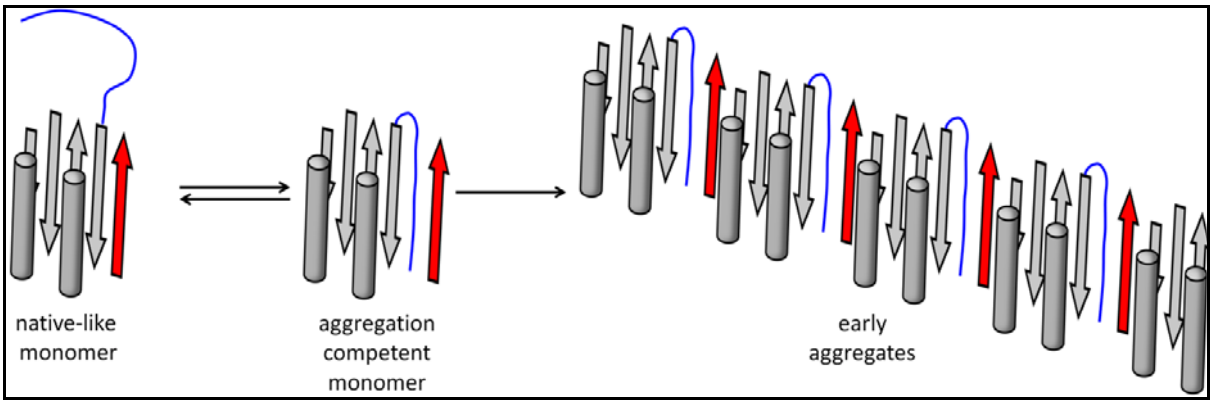

- **DESCRIPTION:** The N-terminal segment gives rise to an intra-molecular interaction with β-strand 4. Thus, an aggregation-competent conformation forms that polymerizes generating the early aggregates.
- **EXPERIMENTAL OBSERVATIONS AGAINST THE MODEL:**
    1. Aggregation of C-tail Sso AcP should show significant differences relative to the process observed for wild-type protein as any intra-molecular interaction is necessarily affected by moving the segment.
    2. Since the interaction is intra-molecular, presence of peptides N11 and N14 should speed up or have no effect on aggregation of wild-type Sso AcP and induce aggregation of ΔN11 Sso AcP.
    3. At least one more aggregation promoting region should be found.

MODEL 7

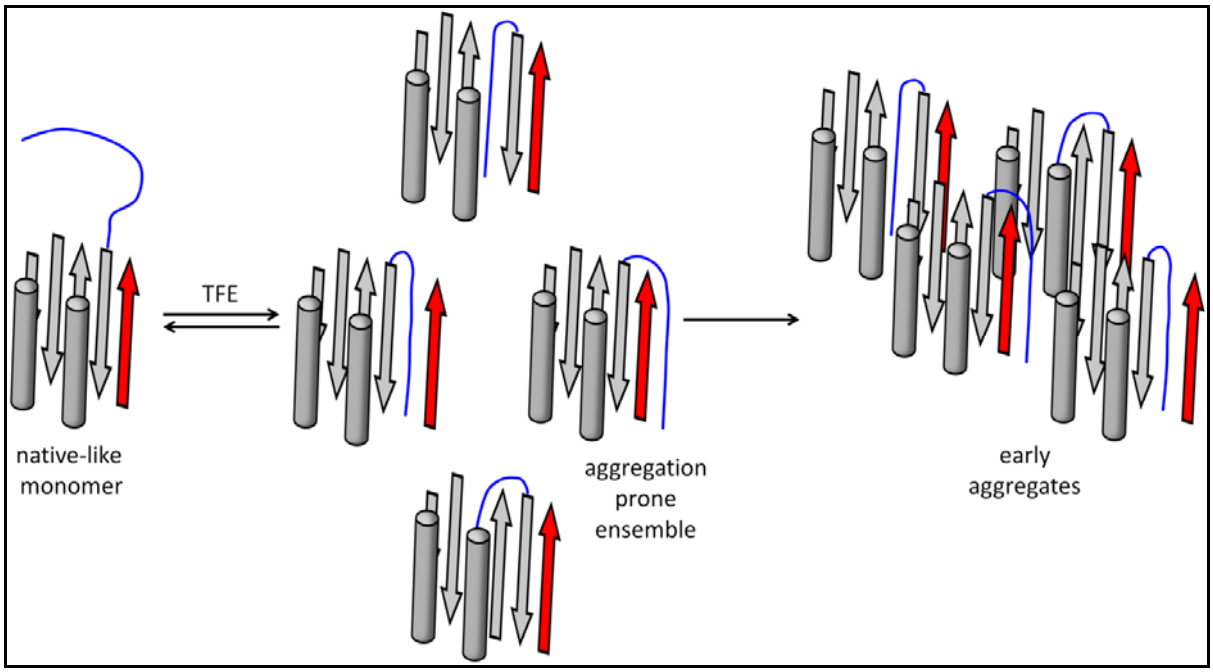

- **DESCRIPTION:** The N-terminal segment gives rise to a non-specific intra-molecular interaction with different regions of the globular part of Sso AcP. This interaction destabilizes the globule and generates an ensemble of conformations able to oligomerize.
- **EXPERIMENTAL OBSERVATIONS AGAINST THE MODEL:**
    1. Since the interaction is intra-molecular, presence of peptides N11 and N14 should speed up or have no effect on aggregation of wild-type Sso AcP and induce aggregation of ΔN11 Sso AcP.
    2. Since the interaction is non-specific, some regions in the globular part should not be more important than others.

MODEL 8

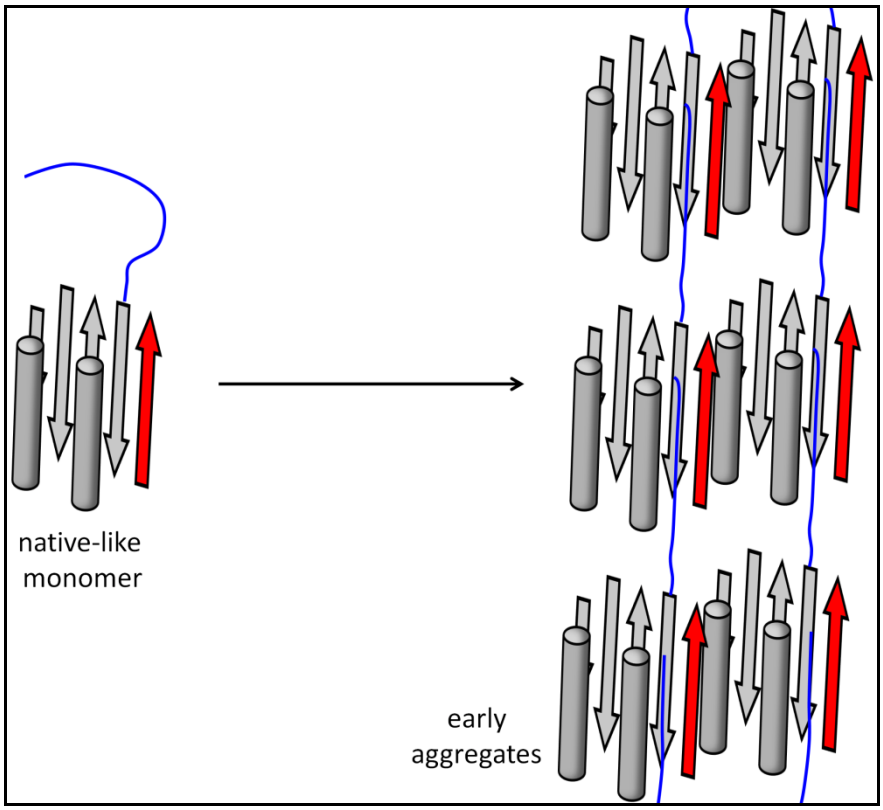

- **DESCRIPTION:** In this model both N-terminal segment and β-strand 4 play a major role in the process. However, they do not interact with each other. They both interact specifically with different regions of other molecules.
- **EXPERIMENTAL OBSERVATIONS AGAINST THE MODEL:**
    1. ΔN11 Sso AcP should give rise to dimers at least in the aggregation promoting conditions.
    2. At least two more regions should be found to play a role in aggregation.

MODEL 9

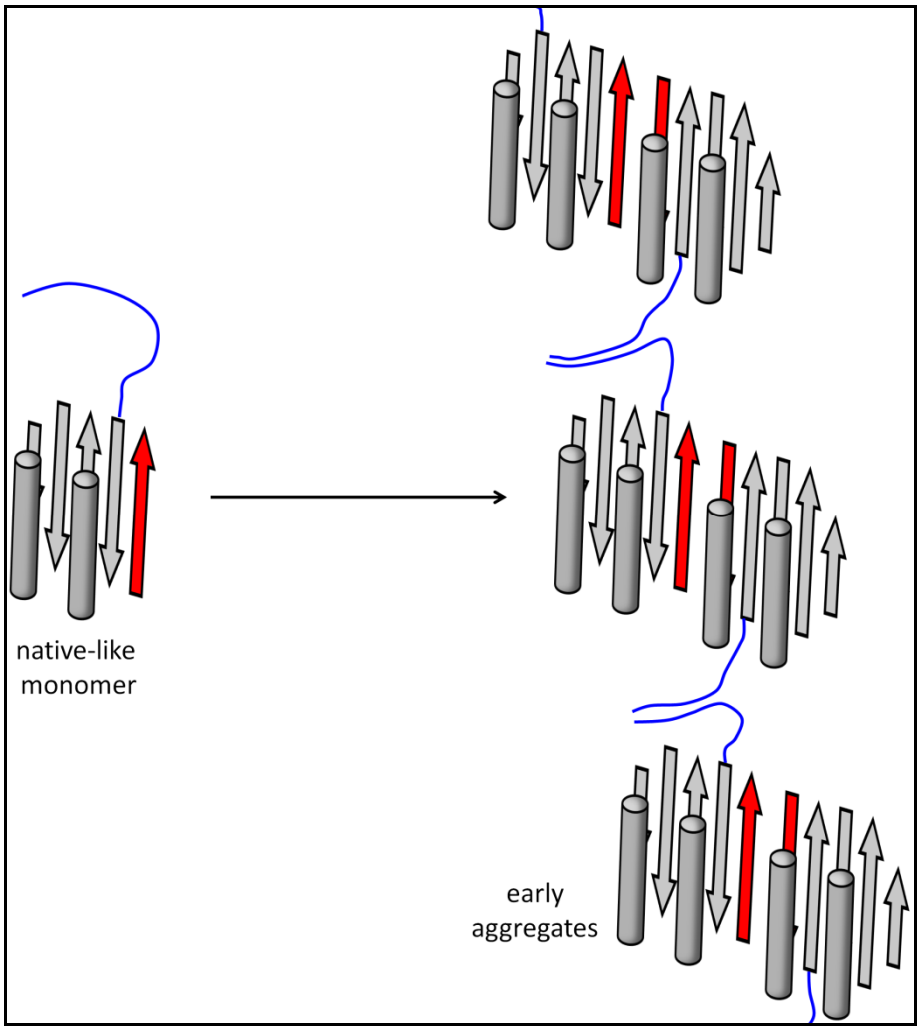

- **DESCRIPTION:** This model is built on the idea that early aggregates are stabilized by segment-to-segment interactions and strand-to-strand interactions. In the figure the strands stack onto each other giving rise to an antiparallel sheet but one can imagine a parallel sheet as well.
- **EXPERIMENTAL OBSERVATIONS AGAINST THE MODEL:**
    1. ΔN11 Sso AcP should give rise to dimers in the aggregation promoting conditions.
    2. The peptides N11 and N14 should aggregate in the aggregation promoting conditions or form at least dimers.
    3. 6Dim Sso AcP and 85Dim Sso AcP should show dramatic increases in aggregation rate.

MODEL 10

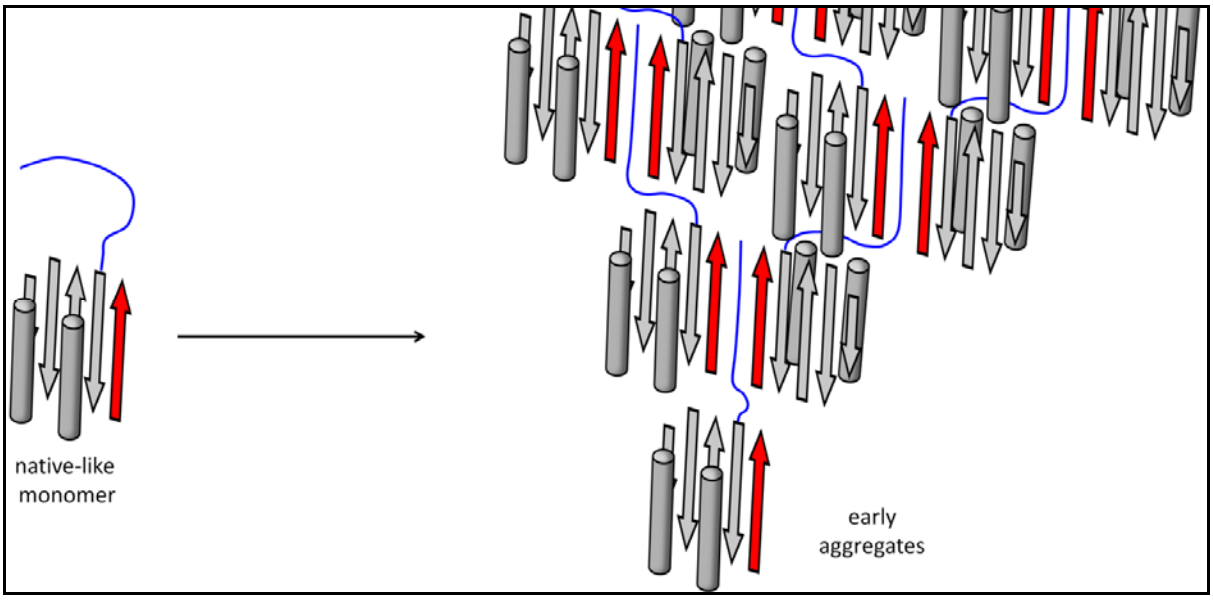

- **DESCRIPTION:** This is another possible model built using only the N-terminus and the β-strand 4. In this case an interaction between the strands of two molecules is mediated by the N-terminus of a third molecule. Following this interaction a pyramid-like aggregate forms.
- **EXPERIMENTAL OBSERVATIONS AGAINST THE MODEL:**
    1. ΔN11 Sso AcP should form dimers in aggregation promoting conditions in the presence of N11 and N14 peptides.

MODEL 11

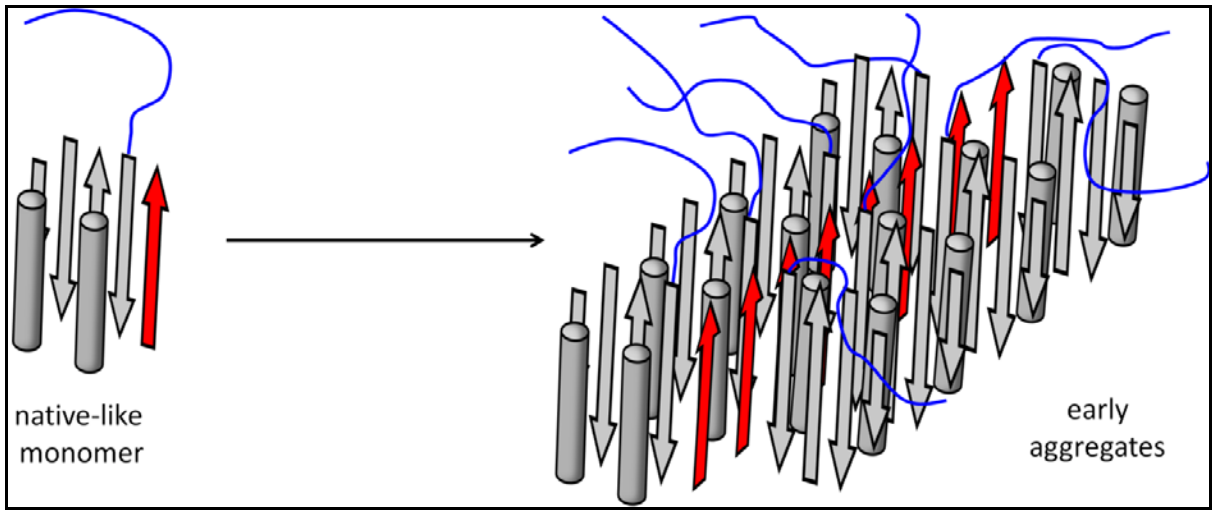

- **DESCRIPTION:** In this model the N-terminal segment and the β-strand 4 play different roles in the process. The N-terminal segment destabilizes the globular part of Sso AcP, facilitating fluctuations within the native-like state with subsequent aggregation via strand-to-strand interactions.
- **EXPERIMENTAL OBSERVATIONS AGAINST THE MODEL:**
    1. I72V-ΔN11 Sso AcP should aggregate on the same time scale as the wild-type.
    2. Peptides N11 and N14 should not affect aggregation of wild-type Sso AcP.
    3. 85Dim Sso AcP should show dramatic increases of the aggregation rate.

MODEL 12

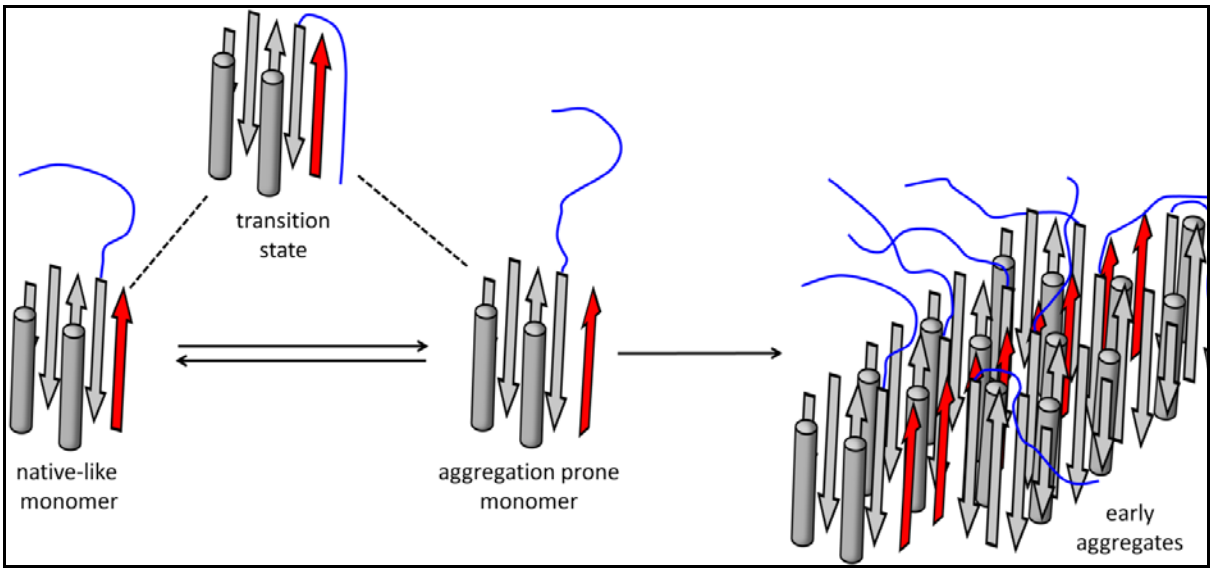

- **DESCRIPTION:** The native monomer is in equilibrium with an aggregation prone monomer in which the β-strand 4 adopts an amyloidogenic conformation. The segment plays a major role in the transition state of this equilibrium by interacting specifically with the β-strand 4. Early aggregates form via strand-to-strand interactions.
- **EXPERIMENTAL OBSERVATIONS AGAINST THE MODEL:**
    1. Peptides N11 and N14 should promote aggregation of ΔN11 Sso AcP.
    2. Peptides N11 and N14 should increase the aggregation rate of wild-type Sso AcP.
    3. C-tail Sso AcP should not aggregate.

MODEL 13

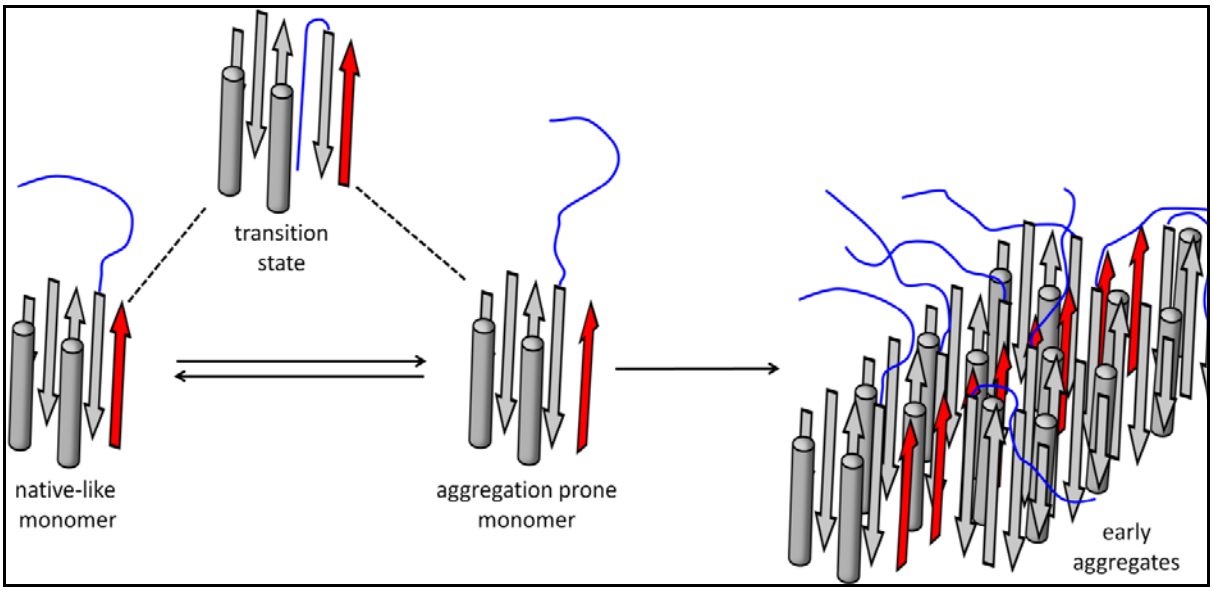

- **DESCRIPTION:** The native monomer is in equilibrium with an aggregation prone monomer in which the β-strand 4 adopts an amyloidogenic conformation. The segment plays a major role in the transition state of this equilibrium by interacting with the globular unit in a non-specific way. Early aggregates form via strand-to-strand interactions.
- **EXPERIMENTAL OBSERVATIONS AGAINST THE MODEL:**
    1. Peptides N11 and N14 should promote aggregation of ΔN11 Sso AcP.
    2. Peptides N11 and N14 should increase the aggregation rate of wild-type Sso AcP.

MODEL 14

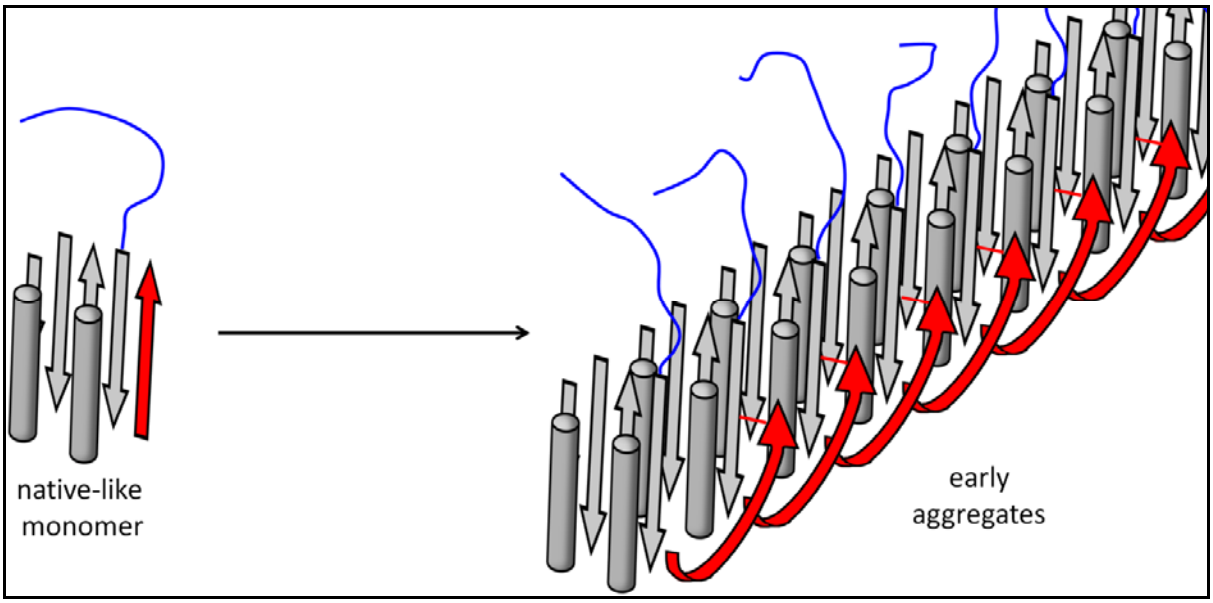

- **DESCRIPTION:** This model is based on domain swapping. β-strand 4 of a molecule replaces β-strand 4 of the following molecule, leading to the formation of early aggregates.
- **EXPERIMENTAL OBSERVATIONS AGAINST THE MODEL:**
    1. ΔN11 Sso AcP should aggregate.
    2. ΔN11 and wild-type Sso AcP should co-aggregate.
    3. I72V-ΔN11 Sso AcP should aggregate.
    4. Peptides N11 and N14 should have no effect on the aggregation of wild-type Sso AcP.

MODEL 15

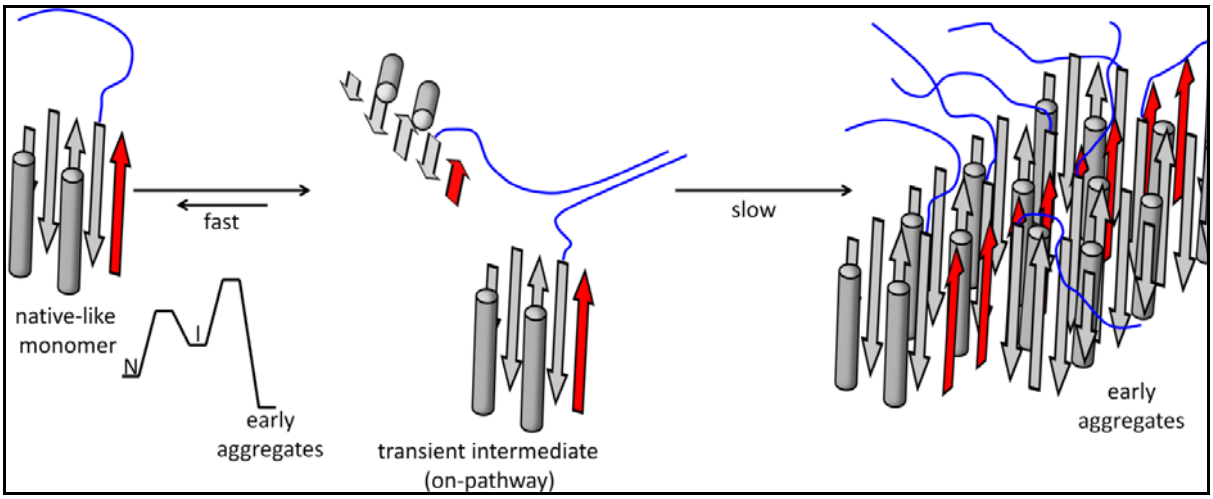

- **DESCRIPTION:** According to this model the N-terminal segment mediates the formation of a transient on-pathway intermediate (I). This eventually converts into early aggregates stabilized by interactions between β-strands 4 of different molecules.
- **EXPERIMENTAL OBSERVATIONS AGAINST THE MODEL:**
    1. Peptides N11 and N14 should have no effect on the aggregation of wild-type Sso AcP.
    2. The rate constant of the first phase of aggregation (k_1) should depend on the second power of monomer concentration.
    3. 6Dim Sso AcP should show dramatic increases in aggregation rate.

MODEL 16

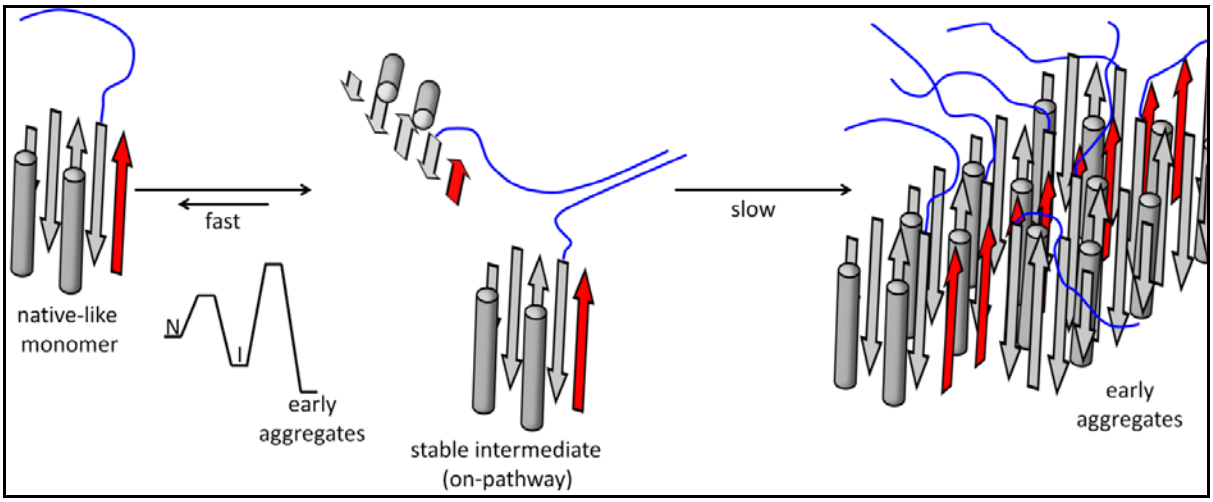

- **DESCRIPTION:** According to this model the N-terminal segment mediates the formation of a stable intermediate (I). This eventually converts into early aggregates stabilized by interactions between β-strands 4 of different molecules.
- **EXPERIMENTAL OBSERVATIONS AGAINST THE MODEL:**
    1. Peptides N11 and N14 should aggregate or at least form dimers.
    2. 6Dim Sso AcP should show dramatic increases in aggregation rate.

MODEL 17

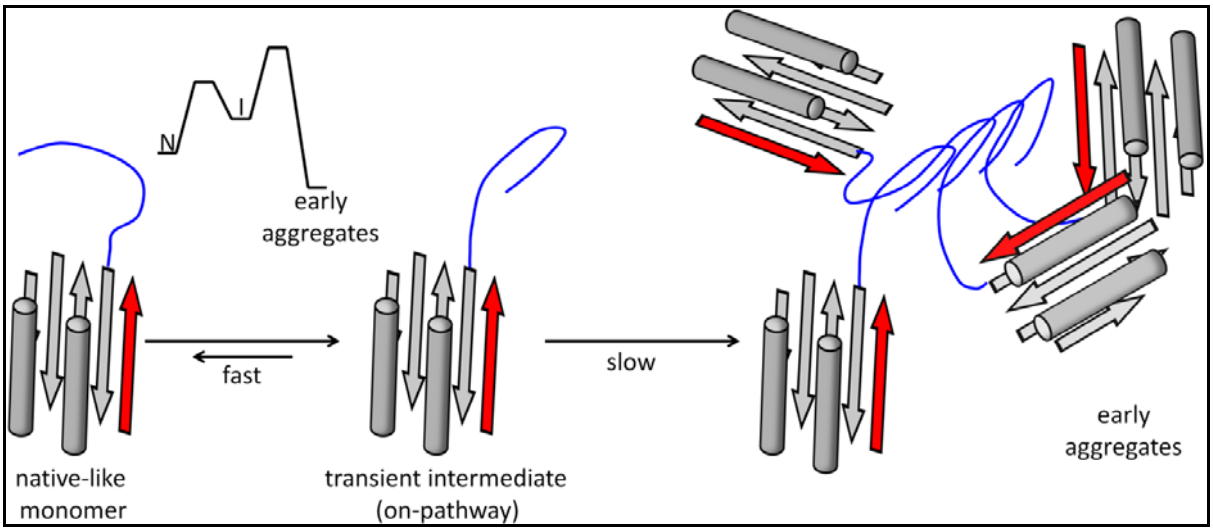

- **DESCRIPTION:** In aggregation promoting conditions, the flexibility of the native state induces the formation of a transient intermediate (I) with the N-terminal segment in a conformation prone to self-assemble. An early aggregate eventually forms via interactions between the segments adopting this conformation.
- **EXPERIMENTAL OBSERVATIONS AGAINST THE MODEL:**
    1. The N-terminal segment is initially unstructured and can sample all possible conformations in the native state. Thus, wild-type Sso AcP and peptides N11 and N14 should aggregate in the absence of TFE.
    2. Aggregation of C-tail Sso AcP should show significant differences relative to the process observed for wild-type protein.

References to supplementary material

[1] A. Corazza, C. Rosano, K. Pagano, V. Alverdi, G. Esposito, C. Capanni, F. Bemporad, G. Plakoutsi, M. Stefani, F. Chiti, S. Zuccotti, M. Bolognesi, P. Viglino, Structure, conformational stability, and enzymatic properties of acylphosphatase from the hyperthermophile Sulfolobus solfataricus, Proteins 62 (2006) 64-79.

[2] M. Stefani, N. Taddei, G. Ramponi, Insights into acylphosphatase structure and catalytic mechanism, Cell. Mol. Life. Sci. 53 (1997) 141-151.

[3] G. Soldi, G. Plakoutsi, N. Taddei, F. Chiti, Stabilization of a native protein mediated by ligand binding inhibits amyloid formation independently of the aggregation pathway, J. Med. Chem. 49 (2006) 6057-6064.

[4] G. Plakoutsi, F. Bemporad, M. Calamai, N. Taddei, C.M. Dobson, F. Chiti, Evidence for a mechanism of amyloid formation involving molecular reorganisation within native-like precursor aggregates, J. Mol. Biol. 351 (2005) 910-922.

[5] G. Plakoutsi, F. Bemporad, M. Monti, D. Pagnozzi, P. Pucci, F. Chiti, Exploring the mechanism of formation of native-like and precursor amyloid oligomers for the native acylphosphatase from Sulfolobus solfataricus, Structure 14 (2006) 993-1001.

FEBS Letters 583 (2009) 801–806

FEBS Letters

journal homepage: www.FEBSLetters.org

A single mutation in an SH3 domain increases amyloid aggregation by accelerating nucleation, but not by destabilizing thermodynamically the native state

Lorena Varela, Bertrand Morel, Ana I. Azuaga, Francisco Conejero-Lara *

Departamento de Química Física e Instituto de Biotecnología, Facultad de Ciencias, Universidad de Granada, Campus Fuentenueva, 18071 Granada, Spain

ARTICLE INFO

Article history:
Received 17 December 2008
Revised 10 January 2009
Accepted 19 January 2009
Available online 6 February 2009

Edited by Jesus Avila

Keywords:
Amyloid
Thermodynamics
Protein stability
Differential scanning calorimetry
Dynamic light scattering

ABSTRACT

We investigated the relationship between thermodynamic stability and amyloid aggregation propensity for a set of single mutants of the alpha-spectrin SH3 domain (Spc-SH3). Whilst mutations destabilizing the domain at position 56 did not enhance fibrillation, the N47A mutation increased the rate of amyloid fibril formation by 10-fold. Even under conditions of identical thermodynamic stability, the aggregation rate was much higher for the N47A mutant than for the WT domain. We conclude that the N47A mutation does not change the apparent mechanism of fibrillation or the morphology of the amyloid fibrils, and that its amyloidogenic property is due to its effect upon the rate of the conformational events leading to nucleation and not to its overall destabilizing effect.

© 2009 Federation of European Biochemical Societies. Published by Elsevier B.V. All rights reserved.

1. Introduction

Amyloid fibril aggregation is involved in the development of a group of important diseases, generically known as amyloidoses, which include Alzheimer and Parkinson diseases, several systemic amyloidoses, diabetes type II or diverse encephalopathies [1,2]. Effective therapies or methods of prevention for this type of diseases are still very scarce, mainly because little is known about the molecular mechanisms of these aggregation processes. Formation of amyloid structures by globular proteins requires the accumulation of a critical concentration of protein in partially-folded conformations exposing a significant segment of the polypeptide chain to solvent under conditions in which stable intermolecular interactions can be formed [3–5].

A number of studies have reported an inverse correlation between the propensity of proteins to aggregate into amyloid-like structures and the thermodynamic stability of the native state [6–8]. Furthermore, recent studies have proposed that stabilization of the native fold results in the modulation of the conformational ensemble favoring structural cooperativity and reducing sampling of partially-folded amyloidogenic conformations [5,9]. This has led to promising therapeutic strategies for amyloid-related diseases based on stabilization of the native state by specific drugs [10]. There are however examples in which kinetic stability, rather than thermodynamic stability, controls fibrillation [11] and in some cases the formation of amyloid fibrils is preceded by an assembly of quasi-native or native-like structures into aggregates [12,13]. Thus, a detailed understanding of the thermodynamic and kinetic factors determining accumulation of amyloidogenic species in proteins still remains far from complete.

Src-homology region 3 (SH3) domains are small modules found as part of proteins that mediate transient protein–protein interactions relative to many cellular processes [14,15]. Due to their small size, high solubility, simple structure and uncomplicated folding mechanism, the folding and stability of these modular domains have been extensively studied [16–20]. Moreover, SH3 domains can form amyloid fibrils at acid pH [4,9,21], being among the first examples of proteins unrelated to amyloidoses that form amyloid fibrils. In the case of the SH3 domain of α-spectrin (Spc-SH3), the mutation of asparagine 47 to alanine, placed within the folding nucleus of the domain, strongly accelerates the formation of amyloid fibrils [21]. Here we investigate whether the increased tendency of the N47A mutant to form amyloids relative to the WT domain is exclusively due to a thermodynamic destabilization on the native structure or it is related to other specific effects exerted by the mutation. We have compared the thermodynamic stability of

Abbreviations: Spc-SH3, Src-homology 3 domain of α-spectrin; DSC, differential scanning calorimetry; ThT, thioflavin T; DLS, dynamic light scattering; TEM, transmission electron microscopy

* Corresponding author. Fax: +34 958 272879.
E-mail address: conejero@ugr.es (F. Conejero-Lara).

0014-5793/$34.00 © 2009 Federation of European Biochemical Societies. Published by Elsevier B.V. All rights reserved.
doi:10.1016/j.febslet.2009.01.033

the native state and the amyloid aggregation propensity between the WT Spc-SH3 domain and several single mutants. In addition, we have compared the kinetics of fibril formation of the WT protein and the N47A mutant under conditions of identical thermodynamic stability. The results demonstrate that thermodynamic destabilization of the native state produced by the mutation is not the main factor favoring fibril formation by this small domain. Instead, the amyloidogenic effect appears to be due to an increase in the rate of conformational events taking place during nucleation of the fibrils.

2. Materials and methods

2.1. Protein samples

The Spc-SH3 domain variants were expressed and purified as described [19]. Protein aliquots were dialyzed extensively against pure water and lyophilized. For aggregation experiments the lyophilized protein was dissolved, unless otherwise stated, in 100 mM glycine, 100 mM NaCl, pH 3.2, at 4 °C, centrifuged for 2 min at 14000 rpm in a micro-centrifuge and filtered through a 0.2 μm filter. The protein concentration was determined by measurement of absorbance at 280 nm using extinction coefficients of 15512 M^{-1} cm^{-1} and 15220 M^{-1} cm^{-1} for the WT and N47A variants, respectively.

2.2. Differential scanning calorimetry

Temperature scans were performed at a protein concentration of 0.8 mg/mL in a VP-DSC microcalorimeter (MicroCal, Northampton, MA, USA) between 5 and 100 °C at a scan rate of 1.5 °C min^{-1}. The reversibility of the thermal unfolding was always checked in a second consecutive scan of the same sample. Instrumental baselines were subtracted to the experimental thermograms of the samples and the time response of the calorimeter was then corrected. The partial molar heat capacity curves (Cp) were calculated and analyzed using Origin 8.0 (OriginLab, Northampton, MA, USA). Cp curves were analyzed according to the two-state unfolding model [22].

2.3. Thioflavin T binding assay

Thioflavin T (ThT) binding assays were performed to monitor amyloid fibril aggregation [23] using a Perkin Elmer LS-55 spectrofluorimeter (Perkin Elmer, Shelton, CT, USA). A 250 μM stock solution of ThT was freshly prepared in 25 mM potassium phosphate buffer (pH 6.0). Protein aliquots (10 μl) were diluted into the phosphate buffer containing 12.5 μM ThT and adjusted to a final volume of 1 mL. Fluorescence emission intensity was measured out at room temperature using a 10 mm path-length cuvette.

2.4. Dynamic light scattering

Dynamic light scattering (DLS) measurements were performed with a DynaPro MS-X instrument (Wyatt Technology Corporation, Santa Barbara, CA, USA) using a 30 μL quartz thermostated sample cuvette. The protein solutions and the buffer were centrifuged and filtered through 0.02 μm Anotop filters (Whatman plc, Brentford, Middlesex, UK) immediately before measurements. Sets of DLS data at constant temperature (37 °C) were acquired every 45 s until saturation of the signal. Laser power was adapted to avoid early saturation of the instrument. Dynamics software (Wyatt Technology Corporation, Santa Barbara, CA, USA) was used in data collection and processing.

2.5. Transmission electron microscopy

Protein samples were diluted 10-fold with buffer and a 15 μL aliquot was placed on a formvar-coated copper grid and left for 4 min. The grid was then washed twice with distilled water and stained with 1% (w/v) uranyl acetate for 1 min. The dried samples were then observed in a Zeiss 902 electron microscope operating at 80 kV.

3. Results

3.1. The thermodynamic stability of single mutants does not correlate with their propensity to form amyloid aggregates

The propensity to form amyloid fibrils of the WT Spc-SH3 and several single-point mutants was analyzed by ThT fluorescence under the conditions described previously for the N47A mutant [21], i.e., at 37 °C in 100 mM glycine buffer pH 3.2, in the presence of 100 mM NaCl and a protein concentration of 8.2 mg/mL (Fig. 1a). The mutations are located at two different regions within the putative folding nucleus of the Spc-SH3 domain [17]. Most of the variants except the A56 K mutant formed amyloid fibrils when incubated at 37 °C for long periods, with morphologies similar to those of the N47A mutant, as observed by transmission electron microscopy (TEM) (not shown). The aggregation rates of the WT domain and the A56G and A56E mutants were similar but they all aggregated considerably slower than the N47A mutant and their

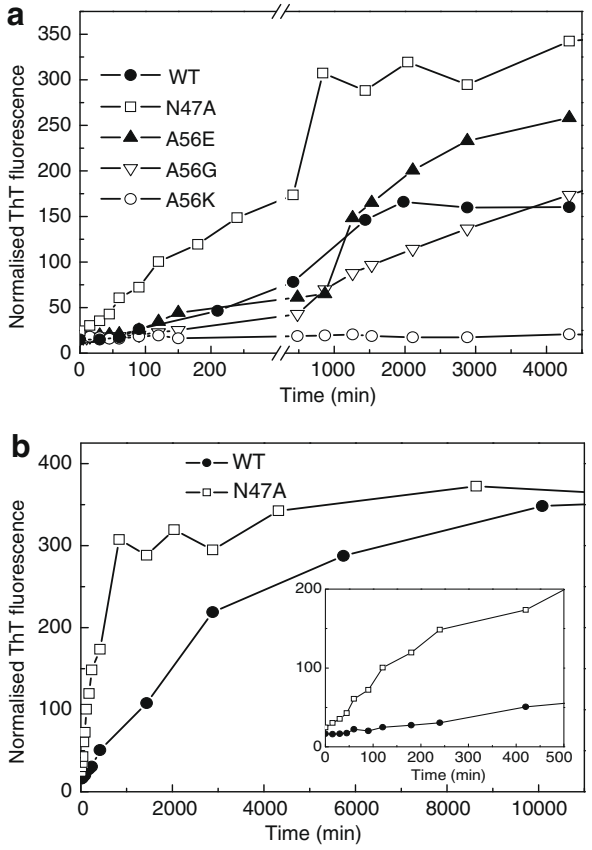

Fig. 1. Kinetics of amyloid fibril growth of variants of Spc-SH3 domain measured by ThT fluorescence. (a) Aggregation was followed at 37 °C in 100 mM glycine buffer pH 3.2, with 100 mM NaCl, at an equal protein concentration of 8.2 mg mL^{-1} for several variants as indicated. (b) Aggregation was followed as in panel (a) but at pH 2.78 for WT and pH 3.20 for N47A. The inset shows an expansion of the first 500 min of incubation.

Table 1
Thermodynamic parameters of the equilibrium thermal unfolding of Spc-SH3 variants determined by DSC.

Variant	pH	T_m (°C)	ΔH_m (kJ mol^{-1})
WT		53.9	165
N47A		50.9	149
A56G	3.2	49.3	148
A56E		50.1	146
A56K		53.3	160
WT	2.0	43.1	125
	2.5	49.5	144
	3.0	52.4	159
	3.2	54.8	168
	3.5	58.9	182
N47A	2.0	36.8	106
	2.5	40.0	114
	3.0	49.5	148
	3.2	51.2	152
	3.5	55.4	170

kinetics presented longer lag phases, suggesting a slower formation of aggregation nuclei.

The thermodynamic stability of all the variants was analyzed by differential scanning calorimetry (DSC) at pH 3.2 and protein concentrations sufficiently low (0.8 mg/mL) to avoid aggregation during the thermal unfolding. The WT and the N47A mutant were also studied by DSC at different pH values between 2.0 and 3.5. Under these conditions, the thermal unfolding of all variants was highly reversible and followed the two-state unfolding model. Identical DSC thermograms were obtained for some of the variants using different scan rates between 1 and 2 °C/min (not shown), indicating that the thermal unfolding occurs under equilibrium during the entire DSC scan. The thermodynamic parameters (Table 1) do not correlate whatsoever with the aggregation propensities of the mutants. For instance, the A56E and A56G mutants, with stabilities similar to the N47A mutant, form amyloid fibrils at slower rate than the latter but at similar rate as the more stable WT domain. In contrast, the A56 K mutant has practically identical stability as the WT domain but it does not form amyloid aggregates within the time period analyzed.

3.2. Under conditions of identical stability the WT and N47A Spc-SH3 domains have different propensity to form amyloids

A plot of the unfolding enthalpies, ΔH_m, versus the unfolding temperatures, T_m, measured for the different variants at pH 3.2 and for the WT and N47A variants at several pH values, shows a single linear dependence (not shown). This indicates that the changes in enthalpy of unfolding are only due, within the experimental error, to the its dependence with temperature due to the heat capacity change of unfolding, $\Delta C_p = d\Delta H/dT$, common to all domain variants [24]. This is consistent with insignificant changes in the native structure produced by the pH or the mutations. Using the heat capacity change of unfolding derived from the slope of the plot (3.6 ± 0.1 kJ K^{-1} mol^{-1}) and the thermodynamic data of Table 1, we calculated the Gibbs energy change of unfolding at 37 °C as described elsewhere [16] as a function of pH and determined that the WT Spc-SH3 domain at pH 2.78 and the N47A mutant at pH 3.20 have the same Gibbs energy change of unfolding, i.e., identical thermodynamic stability. Thus, to exclude the influence of the native state stability, we compared the kinetics of amyloid formation at 37 °C of the WT Spc-SH3 domain at pH 2.78 and the N47A mutant at pH 3.20 (Fig. 1b). The N47A mutant still aggregates much faster than the WT domain, which indicates that the amyloidogenic effect of this mutation is not related to a global destabilization of the native state. This difference is neither due to the pH difference affecting the net charge of the protein because the rate of fibrillation of the N47A mutant increases with the pH reduction (results not shown).

3.3. The WT and the N47A Spc-SH3 domains form amyloid fibrils of similar morphology

We compared by TEM the morphology of the particles appearing during the aggregation process of WT and N47A Spc-SH3 under conditions of equal thermodynamic stability (Fig. 2). At early times of incubation (30 min) the N47A forms protofibrillar and amorphous aggregates of protein (Fig. 2a), which quickly reorganize after only 60 min of incubation into small curly fibrils with diameter of 6–7 nm and lengths between few tenths and several hundreds of nanometers (Fig. 2b). These fibrils elongate further for longer incubation times. In the case the WT domain, at 30 min of incubation only few small globular and amorphous aggregates were sparsely visible (not shown) but a variety of irregular aggregate clusters form at 60 min of incubation (Fig. 2d), which become reorganized later to form fibrillar structures as observed at 180 min of incubation (Fig. 2e). After long incubation

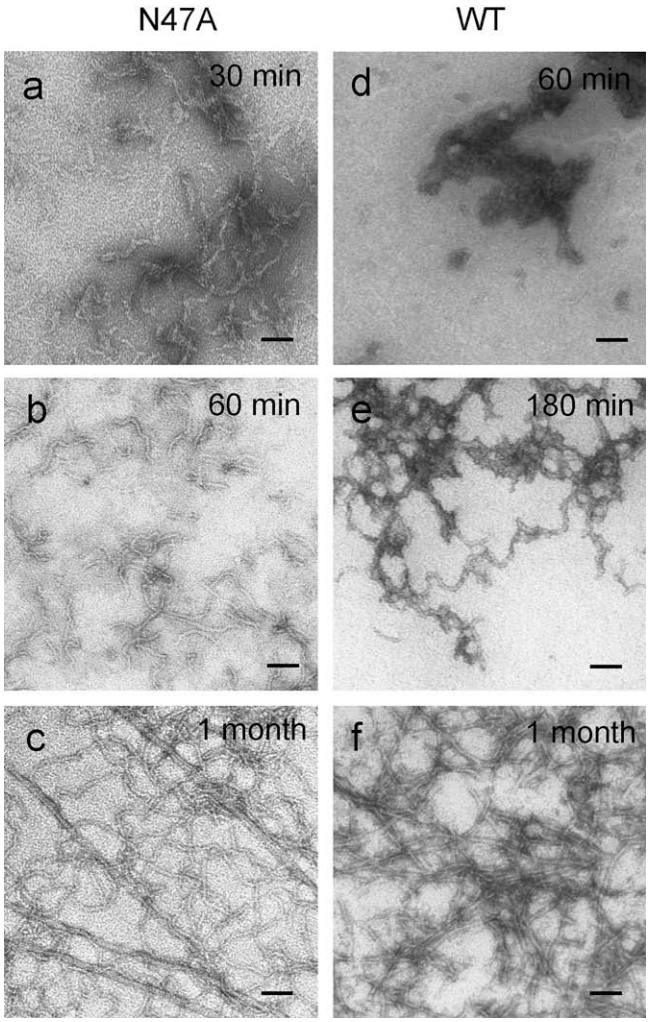

Fig. 2. Electron microscopy images of aggregated N47A (panels a, b and c) and WT (panels d, e and f) Spc-SH3 variants after different times of incubation at 37 °C: (a) 30 min; (b and d) 60 min; (e) 180 min; (c and f) 1 month. Incubation conditions are identical to those of Fig. 1b for each variant. The length of the black segments corresponds to 100 nm in all images.

times both variants presented a tangle of amyloid fibrils with similar apparent curly morphology and diameter (Fig. 2c and f) and few mature amyloid fibrils already appeared in the N47A samples.

It appears that for both protein variants amyloid fibril formation involves similar early events, i.e., an initial formation of amorphous prefibrillar aggregates and a subsequent reorganization of these aggregates into fibrils. Both events occur more rapidly in the N47A mutant than in the WT form.

3.4. The amyloidogenic mutation N47A accelerates formation of early oligomers

We followed by DLS the early stages of aggregation of the WT and N47A variants at 37 °C under conditions of identical thermodynamic stability (Fig. 3). The growth of the scattering signal (Fig. 3a) has a much shorter lag time for the N47A mutant, indicating a faster formation of aggregation nuclei. From the DLS data we calculated the size distribution of particles in the mixture as a function of the incubation time. The time evolution of the apparent hydrodynamic radius, R_h, for the two smallest peaks in the distributions are shown in Fig. 3b. At the start of the incubation, the size distribution of particles shows for both protein variants only particles with an apparent R_h of ≈ 1.7 nm, consistently with the value reported for native Spc-SH3 [20]. This R_h increases from ≈1.7 to ≈3.2 nm in N47A at around 100 min of incubation. In our previous work we interpreted this observation as indicative of oligomerisation following a conformational change in the protein [21]. In the case of the WT domain this event is delayed more than 300 min of incubation, corresponding approximately to the duration of the lag phase observed by ThT fluorescence.

Simultaneously, within few minutes from the start of the incubation additional species appeared with an apparent R_h starting at ≈7–9 nm and increasing progressively with the incubation time. These particles were identified previously as small protofilaments of 6–7 nm in diameter elongating as the aggregation progresses [21]. The fibril elongation is slightly slower for the WT, as indicated by the slower increase in their average R_h, which reaches ≈40 nm at ≈300 min (≈150 min for the N47A mutant). The apparent R_h of the fibrils stops increasing because of the lack of linear persistence of the fibrils. This apparent R_h would correspond to fibril lengths of about 250–500 nm [25]. Finally, at long incubation times larger particles with apparent R_h reaching up to several micrometers became developed for both proteins corresponding to long amyloid fibrils (not shown).

To test the effect of the presence of preformed nuclei of N47A mutant upon the fibril nucleation of the WT protein, we preincubated an 8.2 mg mL^{-1} sample of N47A mutant at 37 °C for 100 min allowing formation of oligomeric species. Then, we immediately added a 10% of this sample to an identical fresh sample of WT protein and incubated the mixture at 37 °C while measuring the DLS signal (Fig. 3a and c). The presence of N47A nuclei reduced significantly the lag phase of aggregation of WT but did not affect importantly the growth rate of fibrils as observed by the similar slope of the increase in the DLS signal. Importantly, the formation of oligomeric species of WT Spc-SH3 with apparent R_h of ≈3.2 nm was accelerated significantly, indicating that pre-existing N47A oligomers could catalyze formation of WT oligomers and facilitate nucleation.

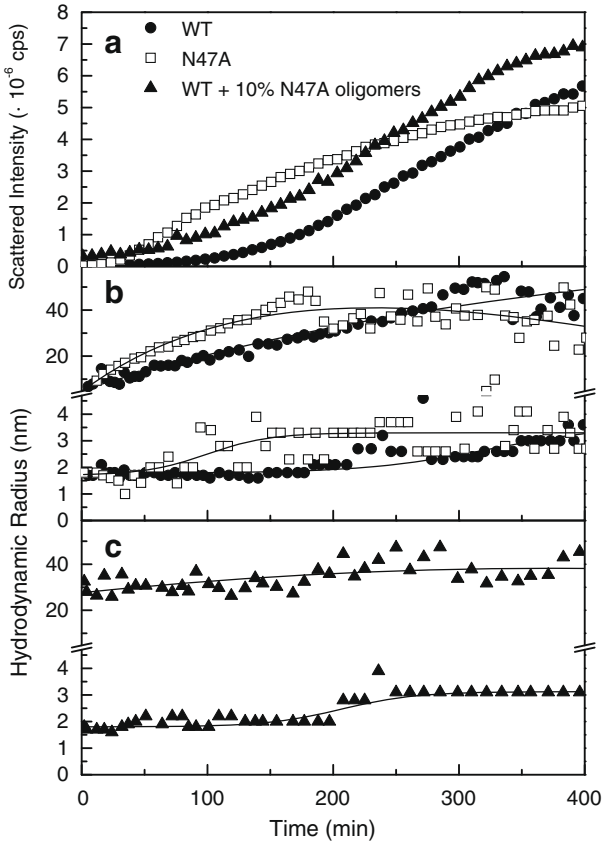

Fig. 3. Aggregation kinetics at 37 °C of WT and N47A Spc-SH3 followed by DLS. Experimental conditions are identical to those of Fig. 1b. (a) Time dependence of the scattering intensity for WT (filled circles), N47A (open squares) and WT in the presence of 10% N47A preincubated for 100 min (filled triangles). (b) Apparent hydrodynamic radius, R_h, determined by DLS for the two smallest species during the course of aggregation at 37 °C observed in the size distributions for WT (filled circles), N47A (open squares). (c) Same as in (b) for WT in the presence of 10% N47A preincubated for 100 min. Symbols (filled triangles) correspond to the maximum of each peak in the size distributions. The lines are drawn only for the sake of clarity.

4. Discussion

Here we have demonstrated that the effect of mutations in Spc-SH3 upon the thermodynamic stability of the native state does not correlate with the changes in the rates of amyloid aggregation. Whilst the destabilizing mutation N47A at the tip of the distal loop of the domain greatly enhances amyloid aggregation, other similarly destabilizing mutations at the 3_{10} helix do not change importantly the aggregation propensity. We have also shown that even under conditions where the WT and the N47A mutant have identical stability their kinetics of aggregation are markedly different. These results demonstrate that an overall thermodynamic destabilization of the native state is not the main factor driving amyloid formation in this small domain.

The fibrillation presents a much shorter lag phase for the N47A mutant than for the WT domain, suggesting a faster formation of aggregation nuclei. In addition, the rate of fibril elongation observed by DLS is roughly 2-fold higher for the N47A mutant than for the WT, in great contrast with a roughly 10-fold difference in the growth of fibril mass observed by ThT fluorescence. This indicates that the amyloidogenic effect of the N47A mutation occurs mainly at the stage of the conformational events previous to nucleation or at the nucleation step itself. In fact, the analysis by DLS shows that formation of early oligomers occurs earlier for the N47A mutant than for the WT and this event appears crucial in the development of fibrillar aggregates, thus conditioning all the subsequent fibrillation process. Indeed, for both variants the duration of the lag phase in fibril formation is very similar to that of formation of oligomers (see Figs. 1b and 3). This suggests that these oligomers may be the competent species of fibril nucleation or may even constitute themselves the aggregation nuclei. The

presence of oligomeric species in rapid equilibrium with the monomeric form has also been reported as critical for fibril nucleation as for example in Abeta [26] or yeast prion Sup35p [27] and the importance of their characterisation is emphasized by their implication in a number of neurotoxic processes [28].

The observation that preformed aggregation nuclei of the N47A mutant could accelerate significantly nucleation of the WT protein whereas the rate of fibril elongation was not affected is of particular interest because it suggests that nuclei pre-existing in the mixture can catalyze formation of additional aggregation nuclei, likely through transient intermolecular interactions.

Our results may appear in conflict with previous studies, which have found a significant inverse correlation between native stability and the propensity to form amyloids. For instance, several mutants of the B1 domain IgG-binding protein G induced amyloid aggregation in inverse correlation with their native stability [8,29]. Similarly, a significant inverse correlation has been found between native stability of a series of acylphosphatase mutants and their susceptibility to amyloid fibrillation induced by TFE [6]. These studies concluded that key requirement for fibril formation was an increase in the population of intermediate folding conformations that become favoured by destabilizing the native state. On the other hand, a mutational analysis of the fibrillation of the thermophilic protein S6 has revealed no correlation whatsoever between native stability and fibril formation [12]. Instead, the unfolding rates correlated directly with the lag phases of amyloid aggregation suggesting that the nucleation occurs from a quasi-native state. In this case, certain amino acid residues locally grouped in the structure were found to act as "gate keepers" inhibiting the access to specific states that trigger the aggregation cascade. Additional evidence supporting the importance of local effects has been provided by the study of two amyloidogenic variants of human lysozyme [5,30], in which transient unfolding of a specific region of the protein including the beta domain and the C-helix is favoured by the mutations.

Our previous studies by native state hydrogen-deuterium exchange have revealed that under native conditions at acid pH the Spc-SH3 domain undergoes a variety of conformational fluctuations ranging from local distortions of flexible regions to extensive unfoldings [19,31]. Moreover, we reported that single mutations changing the native stability produced redistributions of the conformational ensemble that differed depending of the mutational position [32,33]. Although both the 47 and 56 positions are located within the putative folding nucleus of the Spc-SH3 domain [17], they differ in conformational flexibility in the native state. A local destabilization at position A56 affects the whole domain's core lowering the energy of highly unfolded states but leaving unchanged the distribution of the most accessible states. By contrast, the N47A mutation destabilizing the flexible distal loop produces a redistribution of highly populated states, which may favor particular states prone to aggregation. This view is consistent with our finding that similarly destabilizing mutations such as N47A and A56G produce disparate amyloidogenic effects.

It appears, therefore, that although transient exposure of certain regions of the polypeptide chain is a common and obligatory step in amyloid fibril formation by globular proteins, the precise details of the mechanism by which this event conducts to nucleation and the subsequent aggregation cascade may strongly differ between proteins and determine whether or not a correlation between stability of the native state and amyloid aggregation propensity is found in a mutational analysis. In the case of the small Spc-SH3 domain, not all mutations destabilizing the native state are intrinsically amyloidogenic and it seems that the N47A mutation produces a particular redistribution of the conformational ensemble of the protein leading specifically to a significant reduction in the energy barrier of nucleation of the fibrillation process.

Acknowledgements

This research has been funded by Grants FQM-00123 and FQM-02838 from the Andalucia Regional Government and BIO2006-15517.C02.01 from the Spanish Ministry of Education and Science. L.V. and B.M. are recipients of predoctoral and postdoctoral contracts respectively funded by the Andalucia Government. A.I.A. also acknowledges a "Return Research Contract" from the Andalucia Government.

References

[1] Rochet, J.-C. and Lansbury Jr, P.T. (2000) Amyloid fibrillogenesis: themes and variations. Curr. Opin. Struc. Biol. 10, 60–68.
[2] Chiti, F. and Dobson, C.M. (2006) Protein misfolding, functional amyloid, and human disease. Annu. Rev. Biochem. 75, 333–366.
[3] Uversky, V.N. and Fink, A.L. (2004) Conformational constraints for amyloid fibrillation: the importance of being unfolded. Biochim. Biophys. Acta 1698, 131–153.
[4] Guijarro, J.I., Sunde, M., Jones, J.A., Campbell, I.D. and Dobson, C.M. (1998) Amyloid fibril formation by an SH3 domain. Proc. Natl. Acad. Sci. USA 95, 4224–4228.
[5] Dumoulin, M., Canet, D., Last, A.M., Pardon, E., Archer, D.B., Muyldermans, S., Wyns, L., Matagne, A., Robinson, C.V., Redfield, C. and Dobson, C.M. (2005) Reduced global cooperativity is a common feature underlying the amyloidogenicity of pathogenic lysozyme mutations. J. Mol. Biol. 346, 773–788.
[6] Chiti, F., Taddei, N., Bucciantini, M., White, P., Ramponi, G. and Dobson, C.M. (2000) Mutational analysis of the propensity for amyloid formation by a globular protein. EMBO J. 19, 1441–1449.
[7] Kim, Y., Wall, J.S., Meyer, J., Murphy, C., Randolph, T.W., Manning, M.C., Solomon, A. and Carpenter, J.F. (2000) Thermodynamic modulation of light chain amyloid fibril formation. J. Biol. Chem. 275, 1570–1574.
[8] Ramirez-Alvarado, M., Merkel, J.S. and Regan, L. (2000) A systematic exploration of the influence of the protein stability on amyloid fibril formation in vitro. Proc. Natl. Acad. Sci. USA 97, 8979–8984.
[9] Espargaro, A., Castillo, V., de Groot, N.S. and Ventura, S. (2008) The in vivo and in vitro aggregation properties of globular proteins correlate with their conformational stability: The SH3 case. J. Mol. Biol. 378, 1116–1131.
[10] Rochet, J.C. (2007) Novel therapeutic strategies for the treatment of protein-misfolding diseases. Expert Rev. Mol. Med. 9, 1–34.
[11] Hurshman Babbes, A.R., Powers, E.T. and Kelly, J.W. (2008) Quantification of the thermodynamically linked quaternary and tertiary structural stabilities of transthyretin and its disease-associated variants: the relationship between stability and amyloidosis. Biochemistry 47, 6969–6984.
[12] Pedersen, J.S., Christensen, G. and Otzen, D.E. (2004) Modulation of S6 fibrillation by unfolding rates and gatekeeper residues. J. Mol. Biol. 341, 575–588.
[13] Plakoutsi, G., Taddei, N., Stefani, M. and Chiti, F. (2004) Aggregation of the Acylphosphatase from *Sulfolobus solfataricus*: the folded and partially unfolded states can both be precursors for amyloid formation. J. Biol. Chem. 279, 14111–14119.
[14] Kay, B.K., Williamson, M.P. and Sudol, M. (2000) The importance of being proline: the interaction of proline-rich motifs in signaling proteins with their cognate domains. FASEB J. 14, 231–241.
[15] Mayer, B.J. (2001) SH3 domains: complexity in moderation. J. Cell Sci. 114, 1253–1263.
[16] Viguera, A.R., Martinez, J.C., Filimonov, V.V., Mateo, P.L. and Serrano, L. (1994) Thermodynamic and kinetic analysis of the SH3 domain of spectrin shows a two-state folding transition. Biochemistry 33, 2142–2150.
[17] Martinez, J.C., Pisabarro, M.T. and Serrano, L. (1998) Obligatory steps in protein folding and the conformational diversity of the transition state. Nat. Struct. Biol. 5, 721–729.
[18] Plaxco, K.W., Guijarro, J.I., Morton, C.J., Pitkeathly, M., Campbell, I.D. and Dobson, C.M. (1998) The folding kinetics and thermodynamics of the Fyn-SH3 domain. Biochemistry 37, 2529–2537.
[19] Sadqi, M., Casares, S., Abril, M.A., Lopez-Mayorga, O., Conejero-Lara, F. and Freire, E. (1999) The native state conformational ensemble of the SH3 domain from alpha-spectrin. Biochemistry 38, 8899–8906.
[20] Casares, S., Sadqi, M., Lopez-Mayorga, O., Conejero-Lara, F. and van Nuland, N.A. (2004) Detection and characterization of partially unfolded oligomers of the SH3 domain of alpha-spectrin. Biophys. J. 86, 2403–2413.
[21] Morel, B., Casares, S. and Conejero-Lara, F. (2006) A single mutation induces amyloid aggregation in the alpha-spectrin SH3 domain: analysis of the early stages of fibril formation. J. Mol. Biol. 356, 453–468.
[22] Martinez, J.C., Viguera, A.R., Berisio, R., Wilmanns, M., Mateo, P.L., Filimonov, V.V. and Serrano, L. (1999) Thermodynamic analysis of alpha-spectrin SH3 and two of its circular permutants with different loop lengths: discerning the reasons for rapid folding in proteins. Biochemistry 38, 549–559.
[23] LeVine 3rd, H. (1999) Quantification of beta-sheet amyloid fibril structures with thioflavin T. Methods Enzymol. 309, 274–284.

[24] Privalov, P.L. (1979) Stability of proteins: small globular proteins. Adv. Protein Chem. 33, 167–241.
[25] Lomakin, A., Teplow, D.B., Kirschner, D.A. and Benedek, G.B. (1997) Kinetic theory of fibrillogenesis of amyloid beta-protein. Proc. Natl. Acad. Sci. USA 94, 7942–7947.
[26] Bitan, G., Kirkitadze, M.D., Lomakin, A., Vollers, S.S., Benedek, G.B. and Teplow, D.B. (2003) Amyloid beta -protein (Abeta) assembly: Abeta 40 and Abeta 42 oligomerize through distinct pathways. Proc. Natl. Acad. Sci. USA 100, 330–335.
[27] Serio, T.R., Cashikar, A.G., Kowal, A.S., Sawicki, G.J., Moslehi, J.J., Serpell, L., Arnsdorf, M.F. and Lindquist, S.L. (2000) Nucleated conformational conversion and the replication of conformational information by a prion determinant. Science 289, 1317–1321.
[28] Haass, C. and Selkoe, D.J. (2007) Soluble protein oligomers in neurodegeneration: lessons from the Alzheimer's amyloid beta-peptide. Nat. Rev. Mol. Cell Biol. 8, 101–112.
[29] Ramirez-Alvarado, M. and Regan, L. (2002) Does the location of a mutation determine the ability to form amyloid fibrils? J. Mol. Biol. 323, 17–22.
[30] Booth, D.R., Sunde, M., Bellotti, V., Robinson, C.V., Hutchinson, W.L., Fraser, P.E., Hawkins, P.N., Dobson, C.M., Radford, S.E., Blake, C.C. and Pepys, M.B. (1997) Instability, unfolding and aggregation of human lysozyme variants underlying amyloid fibrillogenesis. Nature 385, 787–793.
[31] Sadqi, M., Casares, S., Lopez-Mayorga, O. and Conejero-Lara, F. (2002) The temperature dependence of the hydrogen exchange in the SH3 domain of [alpha]-spectrin. FEBS Lett. 527, 86–90.
[32] Casares, S., Sadqi, M., Lopez-Mayorga, O., Martinez, J.C. and Conejero-Lara, F. (2003) Structural cooperativity in the SH3 domain studied by site-directed mutagenesis and amide hydrogen exchange. FEBS Lett. 539, 125–130.
[33] Casares, S., Lopez-Mayorga, O., Vega, M.C., Camara-Artigas, A. and Conejero-Lara, F. (2007) Cooperative propagation of local stability changes from low-stability and high-stability regions in a SH3 domain. Proteins 67, 531–547.

The Thermodynamic Stability of Amyloid Fibrils Studied by Differential Scanning Calorimetry

Bertrand Morel, Lorena Varela, and Francisco Conejero-Lara*

Departamento de Química Física e Instituto de Biotecnología, Facultad de Ciencias, Universidad de Granada, 18071 Granada, Spain

Received: October 28, 2009; Revised Manuscript Received: January 12, 2010

In contrast to the thermal unfolding of native proteins, very few studies of the thermally induced melting of amyloid fibrils have been reported to date due to the complex nature of these protein aggregates and the lack of theoretical formalisms to rationalize the data. In this work, we analyzed the thermal melting of the amyloid fibrils of the N47A mutant of the α-spectrin SH3 domain by differential scanning calorimetry (DSC). The thermal melting of the isolated fibrils occurred in single endothermic transitions, yielding the fully unfolded protein. The enthalpy and heat capacity changes of fibril melting were significantly lower than those of the unfolding of the native protein, indicating a lower density of interactions and a higher solvent-exposed surface area for the protein within the fibrils relative to the native state. In addition, these magnitudes did not change significantly between fibrils showing different morphology. The independence of the transitions with the scan rate and the observation of a considerable mass-action-like effect upon the melting temperatures indicated that the fibril melting is not separated significantly from equilibrium and could be considered in good approximation as a reversible process. A simple equilibrium model of polymerization coupled to monomer unfolding allowed us for the first time to interpret quantitatively the thermal melting of amyloid fibrils. The model captured very well the general features of the thermal behavior of amyloid fibrils and allowed us to estimate the partitioning of the energy of overall melting into the unfolding of monomers and fibril elongation. We conclude that with the use of appropriate models of analysis DSC has an extraordinary potential to analyze the thermodynamic determinants of amyloid fibril stability.

Introduction

Amyloid aggregates of proteins have become recently of fundamental importance because they have been recognized as a hallmark in a number of pathological disorders of great importance such as Alzheimer and Parkinson diseases, type II diabetes, and several encephalopathies among others.[1,2] Amyloid structures form when proteins misfold and aggregate into extended fibrils with characteristic structural and morphological properties.[3] A large variety of proteins, either involved in disease or unrelated to any disease, can form amyloid fibrils under the appropriate conditions, which has led to the proposal that the formation of the highly organized amyloid aggregates is a generic property of polypeptides and not simply a feature of the proteins associated with pathological conditions.[4]

Despite the lack of sequence homology between the peptides and proteins associated with each disease, the amyloid fibrils exhibit similar external morphology and internal structure. They interact with specific dyes such as Congo red or thioflavin T (ThT) and have characteristic circular dichroism (CD) and infrared spectra typical of a high content in β-sheet secondary structure.[5] When observed by transmission electron microscopy (TEM) or atomic force microscopy (AFM) *in vitro*, the fibrils usually consist of a number of filaments (typically between two and six), each 2−6 nm thick, that twist, forming rope-like fibrils, or associate laterally to form ribbons.[6,7] X-ray fiber diffraction analysis indicates that in each filament the protein molecules are arranged in a highly ordered cross-β structure, forming β-sheets that extend throughout the entire length of the fibril.[8] Recent advances in solid-state NMR spectroscopy[9] together with the recent success in growing nano- and microcrystals of short peptides with amyloid characteristics[10] have allowed a great level of detail to be obtained on the internal molecular structure of the fibrils. For instance, in the fibrils of the Alzheimer's amyloid β-peptide (Abeta) each peptide molecule contributes to two β-strands, each one being part of a different parallel and in-register β-sheet.[11]

It is nowadays well established that amyloid fibril assembly has a mechanism of nucleation and growth, typical of crystallization. The time course of fibril formation shows a typical lag phase or nucleation phase of variable length followed by an exponential growth.[12] The formation of the nuclei of aggregation is usually the rate limiting step of the process. Once a nucleus is formed, it progresses toward the fibrillation by a series of elongation steps with addition of protein molecules to the ends of the fibril.[13] As in all nucleation-dependent processes, the lag phase can be shortened or even removed by "seeding" with preformed nuclei or fibrillar species to the protein sample prior to the start of the aggregation.[14] The nucleation phase can also be affected by changes in the experimental conditions or by mutations in the protein sequence.[15]

Notwithstanding the great advances in understanding the structure of amyloid fibrils and the kinetic mechanism of their formation, relatively few attempts have been made to characterize the thermodynamics of fibril growth and fibril stability,[13,16,17] which is essential to understand the fundamental forces governing the aggregation process.

The analysis of the thermally induced unfolding of proteins monitored by DSC has been used for decades as a key technique

* To whom correspondence should be addressed. E-mail: conejero@ugr.es. Phone: +34 958 242371. Fax: +34 958 272879.

10.1021/jp9102993 © XXXX American Chemical Society

to advance our understanding of the thermodynamics of protein folding and stability,[18−20] although the effectivity of this method has been often impaired by the presence of time-dependent irreversible denaturation processes accompanying the thermal unfolding and precluding the thermodynamic interpretation of the calorimetric data.[21,22] Among these processes, one of the most frequent is aggregation, which has been considered traditionally as an essentially irreversible process. It has been recently observed, however, that amyloid aggregation can often exhibit reversibility[23−25] even under assembly conditions.[17] We and others have previously shown that protein aggregates of several proteins, including amyloid fibrils, can be melted and dissociated by heating at high temperatures, giving rise to characteristic endothermic transitions in DSC experiments.[26−29] In remarkable contrast, other authors have reported that heating protofibrils or amyloid fibrils of lysozyme, β-microglobulin, or Abeta peptide in a DSC calorimeter produces astonishing large heat capacity decreases.[30−32] These contrasting results highlight the complex nature of amyloid aggregates and the great difficulty in studying and rationalizing their thermal behavior. To date, no quantitative analyses of the thermal stability of amyloid fibrils have been reported in the literature. This has been likely due to the complicated mechanism of the aggregation and disaggregation processes, the difficulty in obtaining homogeneous and reproducible samples of this type of aggregates, and, especially, the lack of theoretical formalisms to interpret the experimental data.

The N47A mutation in the α-spectrin SH3 domain (Spc-SH3) renders this small globular domain highly susceptible to form amyloid fibrils at 37 °C under mild acid conditions.[29,33] The rate of fibril formation depends on the conditions of aggregation in a controllable way, which makes this small protein domain a very suitable model to investigate the stability of amyloid fibrils. In this work, we analyze in detail the thermally induced melting of amyloid fibrils of the N47A mutant of Spc-SH3. Fibrils prepared by incubation at 37 °C under mild acid conditions were isolated, and their thermal melting was analyzed by circular dichroism spectroscopy (CD) and DSC. We show here that the fibril melting process occurs in a single, endothermic transition and can be considered in good approximation as a reversible process. Using a simple model of reversible aggregation to interpret quantitatively the calorimetric data, we provide for the first time meaningful thermodynamic magnitudes characterizing the thermal stability of amyloid fibrils. The results show that DSC has an extraordinary potential to study the thermodynamic determinants of amyloid fibril stability.

Experimental Methods

Preparation and Isolation of Amyloid Fibrils. The N47A mutant of the Spc-SH3 domain was overexpressed in *E. coli* cells and purified as described.[34,35] Lyophilized protein samples were freshly dissolved at 4 °C in the appropriate buffer, centrifuged for 2 min in a microcentrifuge, and filtered through a 0.2 μm filter to remove insoluble material. Protein concentration was determined by UV absorption at 280 nm, using an extinction coefficient of 15 220 M^{-1} cm^{-1}.

Amyloid fibrils were prepared by incubation of the fresh protein solutions at 37 °C at pH 3.2 in glycine buffer (100 mM glycine/HCl, pH 3.2, 100 mM NaCl).[29] The fibrils were isolated from the soluble protein by ultracentrifugation at 30 000 rpm for 180 min at 4 °C. Some fibrils remained in the supernatant after the procedure of separation. The fibrils in the pellets were resuspended in the same incubation buffer by light agitation at 4 °C and kept in ice for further analysis. The total monomer concentration in the fibril samples was determined by (1:50) dilution in 6 M GuHCl and further measurement of UV absorption at 280 nm using the theoretical value of the extinction coefficient for the unfolded protein (15 470 M^{-1} cm^{-1}).

Differential Scanning Calorimetry. Calorimetric experiments were made in a DASM4 instrument.[36] DSC scans were conducted between 3.4 and 110 °C. Instrumental baselines, obtained by filling both calorimeter cells with glycine buffer, were systematically subtracted from the sample experimental thermograms, and the time response of the calorimeter was corrected. The scan rate was varied between 0.5 and 2 °C min^{-1} to investigate specifically the dependence with time of the observed thermal effects.

Circular Dichroism Spectroscopy. CD experiments were performed on a JASCO J-715 (Tokyo, Japan) spectropolarimeter equipped with a thermostatized cell holder. Measurements of the far-UV CD spectra (260−210 nm) were made with a 0.1 mm path length quartz microcuvette. The resulting spectrum was the average of eight scans. In thermal melting experiments, the CD signal was monitored as a function of temperature at 215 nm. For the experiments carried out at a fibril concentration of 1 mg mL^{-1}, a 1 mm path length cuvette was used.

Transmission Electron Microscopy (TEM). Amyloid fibril samples were diluted 10 times in the same buffer of their preparation and 15 μL placed on a Formvar carbon coated copper grid, allowing them to stand for 4 min. The grid was then washed twice with distilled water and the samples stained with 1% uranyl acetate for 1 min. The dried samples were analyzed with a Zeiss 902 electron microscope (Oberkochen, Germany) operating at an accelerating voltage of 80 kV and observed at a magnification of 50 000×.

Results

Amyloid Fibril Morphology Studied by Transmission Electron Microscopy. We prepared amyloid fibrils of the Spc-SH3 N47A mutant by incubation of fresh native protein solutions at 8 mg mL^{-1} in glycine buffer at 37 °C for several lengths of time. Under these conditions and after 1 day of incubation, a majority of the protein formed long and relatively curly filaments with a diameter of 6−7 nm, as observed by transmission electron microscopy (TEM).[29] After 10 days of incubation, most of the fibrillar material remained similar in morphology, although a few thicker and straighter fibrils appeared sporadically in the samples (Figure 1a). These fibrils seem to be formed by several coiled filaments with a similar appearance to those described elsewhere for the PI3-SH3 domain.[37] The samples incubated for 1 month consisted of a mixture of single curly filaments and thicker fibrils with the latter predominating in the mixture (Figure 1b).

DSC Analysis of the Thermal Melting Amyloid Fibrils. The amyloid fibrils could be separated from the soluble fraction of the incubation mixture by ultracentrifugation (see Experimental Methods). The resuspended fibrils showed no apparent morphological changes produced by the isolation procedure, as observed by TEM (not shown). The suspensions of fibrils were carefully loaded into the DSC cell at 4 °C. Even though the samples consisted of a mixture of fibrils with different lengths and morphologies, the resulting DSC thermograms showed a single endothermic peak corresponding to the average heat response of the fibrils in the sample (Figure 2). The occurrence of a single transition reflects a very homogeneous thermal behavior for the fibril mixture. Similar DSC peaks were previously unequivocally assigned to the melting of the fibrils, yielding the monomeric unfolded protein.[29] As a comparison,

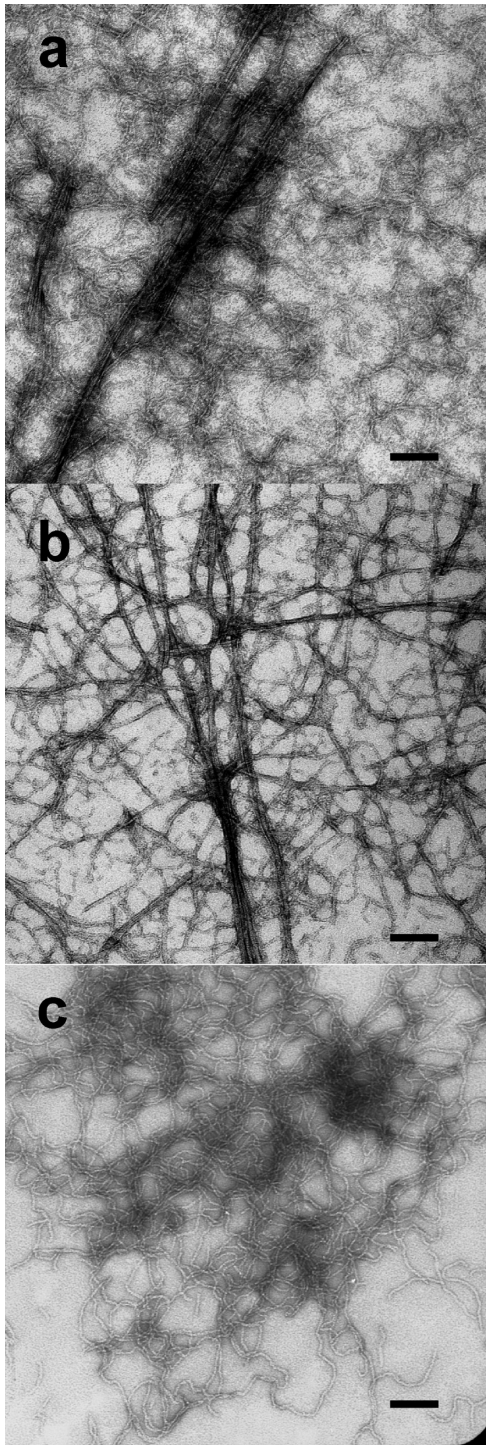

Figure 1. TEM images of amyloid fibrils of N47A Spc-SH3 assembled under different conditions. (a, b) Fibrils were produced by incubation of an 8 mg mL^{-1} fresh protein sample at 37 °C in glycine buffer. The time of incubation was 10 days (a) and 1 month (b). Fibrils were separated from the soluble protein by ultracentrifugation and resuspended in the same buffer. (c) Fibrils reassembled upon cooling to 40 °C after the thermal melting of the amyloid fibrils shown in part a. The black segment represents 100 nm in all of the panels.

the DSC trace corresponding to the thermal unfolding of the native protein under the same conditions is also shown in Figure 2. Amyloid fibrils are much more stable against thermal melting than the native protein, although the enthalpy change involved is considerably lower (see Table 1), suggesting that the density of interactions within the amyloid structure is lower than that in the native protein.[16,29] The apparent heat capacity changes

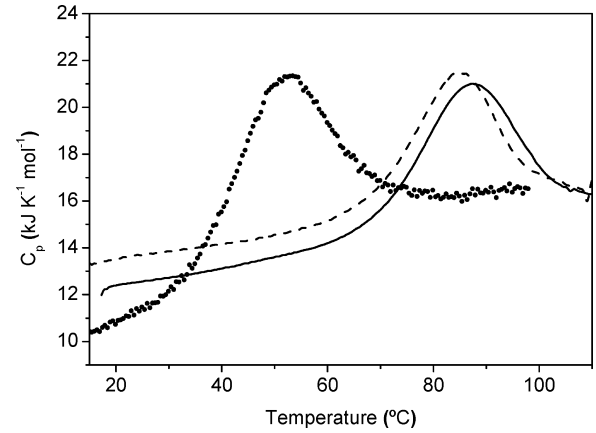

Figure 2. DSC thermograms of amyloid fibrils of N47A Spc-SH3. Fibril samples were obtained as those shown in Figure 1. Solid line: Fibrils prepared by 1 month of incubation at 37 °C and resuspended at 6 mg mL^{-1}. Dashed line: Fibrils prepared by 10 days of incubation at 37 °C and resuspended at 7.5 mg mL^{-1}. The DSC thermogram of the native protein obtained at 1.8 mg mL^{-1} under the same experimental conditions is also shown in dots.

obtained from the difference between the linear extrapolations of the DSC curves from both sides of the transitions are also considerably lower than the heat capacity changes of unfolding of the native Spc-SH3 domain either measured here or reported in the literature.[34,35]

The temperature of melting (T_m), defined as the temperature of the maximum of a DSC transition, increases with the length of incubation of the samples, indicating an increase in the thermal stability of the fibrils. The enthalpy change of the fibril melting, normalized per protein monomer, does not appear however to change importantly with the time of incubation of each fibril preparation. Interestingly, identical fibrils resuspended at different concentrations showed a considerable T_m dependence with the total concentration of protein in the DSC cell (Figure 3). This mass-action-like stabilizing effect suggested that the thermal disaggregation of the amyloid fibrils may behave as a reversible process from a thermodynamic point of view. If dissociation of the fibrils into the fully unfolded protein monomer was an irreversible process, there would not be any opposing force and the DSC transitions would be independent of the protein concentration.

Reversibility of the Thermally Induced Fibril Melting. To confirm reversibility of fibril melting, we tested the reproducibility of consecutive DSC scans after stopping the heating at different temperatures and cooling down (Figure 4a). The melting profile subsequent to each cooling depended on the stopping temperature of the previous scan, which indicated that the overall process of fibril melting is not reversible in the typical sense used for protein unfolding. The presence of a peak at about 50 °C in the DSC scans recorded after substantial fibril melting indicates that part of the protein becomes refolded to the native state during cooling. There was also formation of aggregates or fibrils with different stabilities, as evidenced by the presence of several high-temperature peaks. When the fibrils were melted completely within the DSC cell and cooled down, two transitions appeared during the second consecutive scan, one with T_m similar to that corresponding to the unfolding of the native monomer and another with high T_m, typical of fibril melting (results not shown). This indicates that during the cooling within the DSC cell only a fraction of the protein reassembles into fibrils while the remainder refolds to the native state. When the fibrils were analyzed by DSC at low concentration, the second

TABLE 1: Enthalpy Changes, ΔH_m, and Temperatures of Melting, T_m, of the Native State and the Amyloid Fibrils of N47A Spc-SH3

time of incubation[a]	protein concentration (mg mL^{-1})	T_m (°C)	ΔH_m[b] (kJ mol^{-1})	$\Delta C_{p,M}$[c] (kJ K^{-1} mol^{-1})
10 days	0.95	74.5	n.d.	1.9
	2.0	77.9	95	
	4.3	82.0	102	
	7.5	85.5	104	
1 month	1.8	82.6	n.d.	1.8
	3.0	84.7	98	
	6.1	89.3	125	
native protein	1.8	49.2	148	2.8

[a] Fibrils were prepared by incubation of fresh native protein samples at 8 mg mL^{-1} in glycine buffer. The fibrils were isolated by ultracentrifugation and resuspended in the same buffer for DSC analysis. The native protein was dialyzed in the buffer and analyzed by DSC at low concentration to avoid aggregation. [b] The enthalpy changes were calculated by direct integration of the DSC endothermic peaks after manual baseline subtraction. [c] The heat capacity changes were estimated as the difference between the C_p traces extrapolated from both sides of the melting transition.

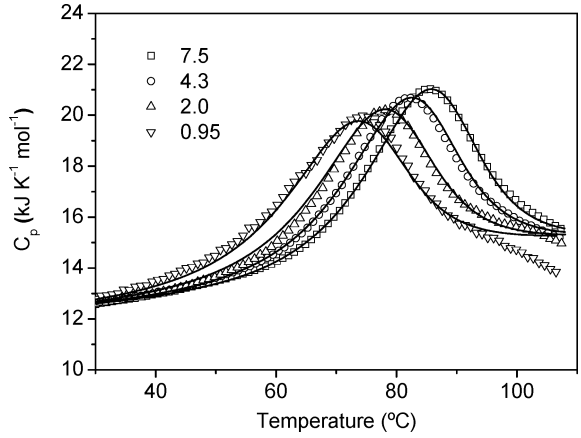

Figure 3. Effect of protein concentration on the stability of the amyloid fibrils. DSC scans of fibrils prepared by incubation for 10 days at 37 °C in glycine buffer and resuspended in the same buffer at different protein concentrations, as indicated in the plot in mg mL^{-1}. Symbols correspond to the experimental DSC curves. Continuous lines represent the best global fit using the equations of the model described in the Appendix.

scan after their melting showed only the transition corresponding to the two-state unfolding of the native Spc-SH3 domain, although diminished in area possibly due to partial protein damage produced by the heating at very high temperature. These results indicate that, once the fibrils have been melted at high temperatures, the reassociation of the unfolded protein back into fibrils during cooling is not fully efficient. This is probably due to the lack of proper nucleation conditions during cooling, which may allow all or part of the protein to refold into the native state.

We recorded the DSC thermograms with fibrils isolated as described above during both the heating and cooling scans (Figure 4b). The cooling thermogram shows an exothermic transition at about 65 °C corresponding to the reassembly of new fibrils. This transition is, however, greatly shifted toward lower temperature compared to the melting transition (87 °C), suggesting that the fibril assembly during cooling does not correspond to the reversal of the melting process.

We also monitored the melting and reassembly of the preformed amyloid fibrils during heating and cooling scans by far-UV CD at a scan rate of 2 °C min^{-1} (Figure 4c). The CD signal at 215 nm showed a steep dependence with temperature, reaching a minimum near 70 °C. The fibril melting took place with a decrease in negative ellipticity in agreement with the disruption of β-sheet structure. The transition temperature was

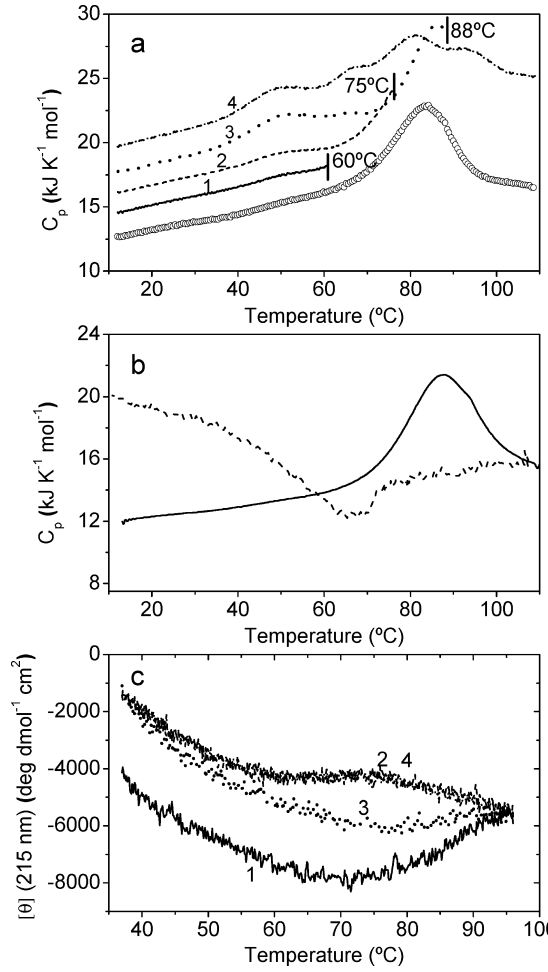

Figure 4. Reversibility analysis of the thermal melting of amyloid fibrils. (a) Consecutive DSC scans of amyloid fibrils of N47A Spc-SH3 prepared by incubation for 10 days and resuspended at a sample concentration of 2 mg mL^{-1}. Scans were stopped at the indicated temperatures and cooled down for the next consecutive scan. The consecutive scans are indicated by the numbers alongside each curve. The entire first scan with identical fibrils is represented by open symbols. The scans have been artificially shifted along the vertical axis for clarity. (b) Consecutive heating and cooling DSC curves obtained with isolated amyloid fibrils at a concentration of 2.8 mg mL^{-1}. (c) Heating and cooling of amyloid fibril samples monitored by CD at 215 nm. Fibrils were prepared by incubation for 1 week at 37 °C. Heating (1 and 3) and cooling (2 and 4) scans were made at 2 °C min^{-1}.

consistent with the T_m observed in the DSC data. The CD signal did not revert immediately upon cooling until the occurrence

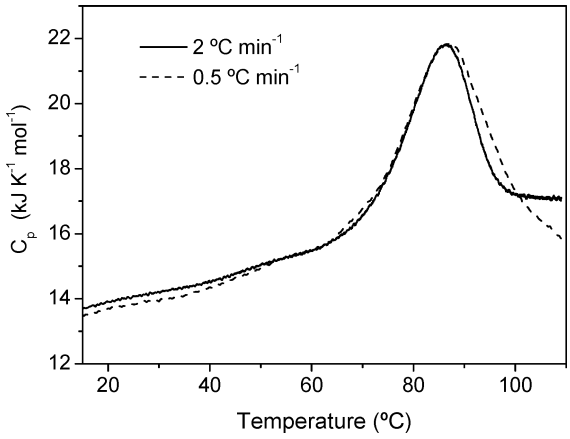

Figure 5. Effect of the scan rate on the DSC curves of amyloid fibrils. Two identical samples of isolated fibrils were prepared by incubation for 1 month at 37 °C in glycine buffer and resuspended in the same buffer at a concentration of 5.5 mg mL^{-1}. The fibrils were analyzed by DSC at different scan rates as indicated.

of a transition corresponding to the fibril reassociation around 65 °C, in good agreement with the transition observed by DSC during cooling, although the magnitude of the original negative ellipticity was not fully recovered. The shift in the temperature of the fibril reassembly transition was not reduced when the scans were performed at a lower scan rate of 0.5 °C min^{-1} (not shown). Further cooling produced a steep increase in ellipticity, with a slope similar to that observed during the heating. During the second consecutive heating, the transition of fibril melting was again reproduced, although the amplitude of the ellipticity change was smaller than that in the first scan. This indicates that only a fraction of the protein reassembled into the fibrils during the cooling after their thermal melting. The curve corresponding to the second cooling was identical to that of the first one.

We analyzed by TEM sample aliquots taken at several temperatures during the heating and cooling and frozen directly into liquid N_2. The TEM images confirmed that fibrils dissociate during the heating and reassemble with identical morphology during the cooling transition (see Figure 1c and Figure S9 in the Supporting Information). These results indicated that the melting of fibrils can be reversed but the reassociation process shows a kind of hysteresis, suggesting that after melting of the fibrils their reassembly during the cooling is delayed until proper nucleation conditions are achieved. In this respect, the process appears to have some degree of resemblance with the melting of pure ice or with the dissolution of a salt crystal in equilibrium with its saturated solution, both of which are reversible processes from a thermodynamic point of view. The reverse processes (water freezing or salt crystallization) can display significant delay, with formation of supercooled water or supersaturated salt solution, unless nucleation is favored by seeding.

Heating Rate Analysis of Fibril Melting Transitions. The key question to undertake the analysis of the data was whether fibrils could be considered to melt under equilibrium or alternatively the process was controlled kinetically. To check this, two identical amyloid fibrils samples were analyzed by DSC at equal concentrations and different scan rates, namely, 2 and 0.5 °C min^{-1}. The resulting DSC transitions showed no significant difference in T_m and were practically identical except for some deviation at the high temperature side (Figure 5). These results demonstrate that most of the fibril melting process is not controlled kinetically and, therefore, appears to occur under equilibrium.[21,22,38] The scan rate independence together with the mass-action-like effects observed for the thermal melting of the amyloid fibrils indicate that the endothermic transitions measured by DSC for the fibril melting do not exhibit during most of their extent a significant kinetic behavior. Accordingly, the reversibility of the fibril melting process needs to be interpreted as a microscopic reversibility in the sense that the process could be reversed after an infinitesimal perturbation. On the other hand, when the perturbation is large (for example, when all of the amyloid fibrils are unfolded), the fibril melting process does not revert through the same path because kinetic factors such as nucleation come into play for fibril reassociation. We conclude therefore that under our experimental conditions fibril melting could be considered in good approximation as an equilibrium process and it may be therefore acceptable using thermodynamic approaches in their interpretation.

A Simple Equilibrium Model Describing the Melting of Protein Aggregates. A plausible thermodynamic interpretation of the DSC transitions corresponding to reversible amyloid disaggregation induced by heating may come from the use of a simple polymerization model:[39]

$$A_i \leftrightarrow A_{i-1} + M \qquad (I)$$

In this model, the fibrils disaggregate through a series of consecutive steps of reversible monomer dissociation. M represents a monomeric state of the protein that dissociates from a fibril end, and the A_i species represent aggregates of i protein monomers. We assumed that all of the dissociation steps are reversible and sufficiently fast so that the whole system is not separated significantly from equilibrium during the heating. The M species are also supposed to be in rapid equilibrium with the fully unfolded state, U:

$$M \leftrightarrow U \qquad (II)$$

The idea of separating the fibril melting process into these two equilibrium processes was aimed at evaluating the partitioning of the global energy of fibril stability in two individual contributions, i.e., the energy of fibril elongation and the energy of folding the protein chain into its appropriate aggregating conformation. Accordingly, we define the equilibrium constants for each association step, K_A, and for the folding of the monomers, K_F (eqs 1 and 2 in the Appendix). Here, we assumed for simplicity that the association constant, K_A, does not depend on the size of the aggregate. This model was elaborated mathematically as described in detail in the Appendix to solve the temperature dependence of the population of each species. This has allowed us the calculation of the heat capacity of the system as a function of temperature, which is the type of information derived experimentally from the DSC experiments.

We performed exhaustive simulations of the heat capacity curves (Figures S1−S6 in the Supporting Information). Using appropriate values for the parameters, we have simulated DSC transitions similar to those obtained experimentally with the fibrils.

We explored initially the effect of a maximum allowed aggregate size, N, upon the simulated DSC transitions. Strikingly, for N higher than roughly 20, the curves become indistinguishable, indicating that the heat effect of melting of large aggregates with more than a few tenths of monomers is independent of their size, as it is mainly governed by the energy of dissociation of a monomer from a large particle. The model also reproduces very well the increase in the melting temper-

atures with the total protein concentration, P_0, as observed experimentally (Figure 3). An exhaustive exploration of the effect of changing the thermodynamic parameters of the model upon the simulated curves allowed us to derive the following conclusions:

(a) Keeping constant the set of thermodynamic parameters of monomer unfolding, the melting temperature of the aggregates, T_m, depends on the product between the association equilibrium constant and the total protein monomer concentration, $K_A \cdot P_0$. In fact, K_A and P_0 appear always together as a product in all of the equations of the model.

(b) For values of $K_A \cdot P_0$ higher than roughly 10, i.e., $P_0 \gg 1/K_A$, T_m changes linearly with the logarithm of P_0 and the slope of this plot depends inversely on the total enthalpy change of fibril melting but does not depend on the monomer unfolding temperature. This implies that the abscissa intercept of such a linear plot is proportional to $-\log K_A$ and, therefore, to the Gibbs energy of fibril elongation, ΔG_A, per mole of protein monomer.

(c) The shape of the melting transitions is highly dependent on the enthalpy change of association, with more asymmetric transitions when the association process is more endothermic. The asymmetry of the transitions does not change so much with the enthalpy of monomer unfolding. Keeping constant the total enthalpy change of melting, the transitions become sharper for more endothermic association and more endothermic unfolding.

These simulations suggest that a quantitative analysis of DSC transitions corresponding to amyloid fibril melting using this model may allow us to extract relevant thermodynamic information about the process.

Using the equations derived from the model, we attempted to reproduce quantitatively the sets of experimental DSC curves obtained under the various conditions at different protein concentrations. When fitted individually, the DSC curves could be reproduced very well (Figures S7 and S8 in the Supporting Information) but the adjustable parameters showed a high interdependency due to their relatively large number. To impose additional constraints to the analysis, we fitted simultaneously the complete sets of DSC curves obtained with identical fibrils at different protein concentrations using a single set of thermodynamic parameters. Both the shape of the DSC transitions and the effect of the protein concentration could be reproduced surprisingly well (see Figure 3).

The thermodynamic parameters obtained from the fits are compiled in Tables S1 and S2 in the Supporting Information. The fits yielded high association constants, K_A (between 2×10^5 and 4×10^5), and large negative association enthalpies, while the monomer unfolding enthalpies were relatively low. These results suggest that most of the stability of the fibrils resides in the intermolecular interactions between protein molecules, whereas the dissociating monomers have a low intrinsic structure.

In spite of the apparent success of this type of analysis, there is still relatively high interdependency between the adjustable parameters and they should be considered therefore just as approximate estimates. Nevertheless, this simple equilibrium model for amyloid thermal disaggregation constitutes a first attempt to describe quantitatively the thermal melting of amyloid aggregates and appears to capture the essential features of this intricate process. Moreover, this model could serve as a useful tool to rationalize the thermodynamic determinants of the stability of amyloid fibrils by means of a simpler analysis of the observed effects of external parameters or variables upon the melting temperatures as follows.

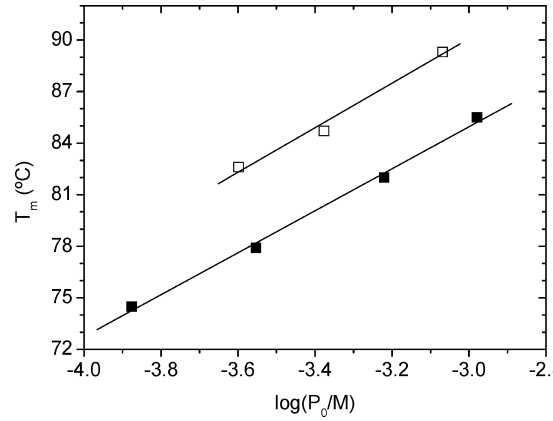

Figure 6. Concentration dependencies of the melting temperatures of amyloid fibrils. Melting temperatures, T_m, correspond to the maximum of the DSC transitions obtained with isolated amyloid fibrils. The data correspond to fibrils prepared by incubation of 8 mg mL^{-1} native protein solution at 37 °C, isolated by ultracentrifugation and resuspended at different concentrations. Filled squares correspond to fibrils obtained by 10 days of incubation. Open squares correspond to fibrils prepared by 1 month of incubation. Solid lines represent the linear regression of the data.

Figure 6 shows the experimental melting temperatures, T_m, measured by DSC versus the logarithm of the concentration of protein, P_0. The plots are approximately linear, as predicted by the model, and have very similar slopes for fibrils prepared by different incubation times. Considering that for fibrils analyzed under the same experimental conditions the stability of the monomer would only depend on temperature, the shift observed in T_m with the increase in the time of incubation would then reflect an increase in the apparent equilibrium constant of association, K_A. As discussed above, the change in the association constant ($-\Delta \log K_A$) with the time of incubation can be estimated from the shift along the abscissa axis of the linear plots of T_m vs $\log P_0$. According to this, increasing the time of the incubation of the fibrils at 37 °C from 10 days to 1 month increases the association constant 2.5-fold. This agrees well with the increase in order observed by TEM with the time of incubation for the fibrils. In contrast, the total enthalpy change of fibril melting does not change significantly with the time of incubation, as indicated by the similar slope of the linear plots of T_m vs $\log P_0$ and the similar areas of the DSC peaks, except for an expected effect of temperature related to the heat capacity change of melting (Table 1). This implies that the increase in fibril stability during fibril maturation does not involve the creation of new interactions within the fibrils but an enhancement in the entropy gain attained with the monomer association.

Discussion

In this work, we characterized carefully the thermally induced melting of amyloid fibrils of an SH3 domain and demonstrated that it occurs as single endothermic transitions that can be observed by DSC. Direct integration of the DSC transitions has provided the overall enthalpy change for the complete melting of the amyloid fibrils under a set of experimental conditions. The enthalpy changes are around 100−120 kJ mol^{-1} and do not change much with the length of the fibril incubation or with the apparent degree of order of the fibrils. In spite of the relatively high melting temperatures of the amyloid fibrils, their specific melting enthalpies ($\approx$14−17 J g^{-1}) are much lower in magnitude than the similar values of the native Spc-SH3 domain[35] or than those typical of native compact globular

proteins at similar temperatures, which usually range between 35 and 45 J g^{-1}.[18] This indicates that the melting of amyloid fibrils involves a much lower net balance of interactions than the unfolding of compact globular proteins. Similarly, the apparent heat capacity changes accompanying the melting of the fibrils are also considerably lower than that of the native Spc-SH3 domain, suggesting a higher area of hydrated surface for the protein monomer in the fibrillar state relative to the native protein. These thermodynamic magnitudes are in agreement with the view that amyloid fibrils are composed of partially structured, assembled protein monomers.[3]

The analysis by DSC of the thermally induced melting of amyloid fibrils presented here provides significant insight into the thermodynamic properties determining the fibril stability and their correlation with the structural properties of the fibrils. Few studies in the literature have reported thermodynamic parameters of amyloid fibril formation and disaggregation. For instance, Wetzel and co-workers obtained for the Aβ(1−40) peptide a standard Gibbs energy of fibril elongation of −35 kJ mol^{-1} at 37 °C in PBS buffer using the final monomer concentration at equilibrium of aggregation.[17] Similar experiments performed by Y. Goto and colleagues on β_2-microglobulin at pH 2.5 and different temperatures yielded Gibbs energies of fibril elongation in the neighborhood of −40 kJ mol^{-1}.[16] Our results give equilibrium constants for fibril elongation at 50 °C corresponding to Gibbs energy changes ranging between −33 and −35 kJ mol^{-1}, similar to the above values.

Previous detailed DSC analyses of amyloid fibrils are almost exclusively limited to the work of Y. Goto and co-workers. These authors reported striking DSC results obtained with amyloid fibrils from a variety of proteins including β_2-microglobulin, Abeta peptide, and lysozyme.[30−32,40,41] In all cases, the DSC thermograms showed extraordinary exothermic effects, which were highly dependent upon the heating rates in the DSC scans. These effects were generally interpreted by the authors as large heat capacity effects produced by heat-induced fibril association. Our results with amyloid fibrils of N47A Spc-SH3 did not show such exothermic effects but only single cooperative transitions corresponding to the fibril melting. These contrasting results may be related to different properties of the amyloid fibrils of each protein and/or to the experimental conditions used in each study.

An important conclusion of our study is that the time of fibril maturation does not influence significantly the overall enthalpy change of fibril melting, despite the considerable changes observed in morphological properties. The stability differences appear to have therefore an entropic origin. Goto and colleagues determined by isothermal titration calorimetry that the enthalpy changes of amyloid elongation of β_2-microglobulin are considerably lower than that of the native protein and even exothermic below 13 °C,[16] indicating that amyloid formation is mainly driven by entropy gain and suggesting a decreased internal packing within the amyloid structures. The same authors also analyzed the GuHCl-induced melting of β_2-microglobulin in the presence of varying concentrations of ammonium sulfate.[42] Using a linear disaggregation model to analyze their data, they reported a Gibbs energy of fibril polymerization of −41 kJ mol^{-1}, which increased strongly in magnitude with the increase in the ammonium sulfate concentration, suggesting an important role of the entropic effects in stabilizing the amyloid fibrils. Knowles et al. have recently reported that the rate of insulin amyloid aggregation is controlled by a competition between two opposing effects of similar orders of magnitude: the process is entropically favorable but enthalpically unfavorable.[43,44] All of these findings support the conclusion that the amyloid aggregates are mainly stabilized by an overall entropy increase attained with their assembly, which points toward hydration effects playing a major role in this process.

Conclusions

We have shown here that the thermally induced melting of amyloid fibrils of the N47A Spc-SH3 domain can be monitored by DSC as a single, cooperative endothermic transition and in good approximation the process may be considered as a reversible equilibrium process, at least under the conditions of this study. With the use of a simple equilibrium model of linear polymerization coupled to unfolding, we have been able to rationalize the experimentally observed thermal transitions and extract meaningful thermodynamic information about the process of aggregation−disaggregation of the amyloid fibrils. We believe that this type of approach may be of general use to get insight into the energetic determinants of amyloid fibrils of other proteins.

Acknowledgment. This research has been funded by grants FQM-00123 and FQM-02838 from the Andalusia Regional Government, grant BIO2009-07317 from the Spanish Ministry of Science and Innovation, and funds for the European regional development from the European Union. L.V. and B.M. are recipients, respectively, of a predoctoral and a postdoctoral research contract financed by the Andalusia Government.

Appendix

Here, we describe in detail the mathematical elaboration of the model for thermally induced melting of aggregates (eqs I and II). According to this model, fibrils disaggregate through a series of consecutive steps of reversible monomer dissociation. M represents a monomeric state of the protein that dissociates from a fibril end, and the A_i species represent aggregates of i protein monomers. We assumed that each dissociation step is reversible and sufficiently fast so that the system is not separated significantly from equilibrium during the heating. The M species are also supposed to be in rapid equilibrium with the fully unfolded state, U.

Starting from eqs I and II, we define the equilibrium constants for each association step and for the folding of the monomers as

$$K_A = \frac{[A_2]}{[M]\cdot[M]} = \frac{[A_3]}{[A_2]\cdot[M]} = \frac{[A_i]}{[A_{i-1}]\cdot[M]} (i: 2, \ldots, N) \quad (1)$$

$$K_F = \frac{[M]}{[U]} \quad (2)$$

Using these definitions, the total concentration of protein monomers in solution, P_0, can be written as

$$P_0 = [U] + [M] + \sum_{i=2}^{N} i\cdot[A_i] = [U] + \sum_{i=1}^{N} i\cdot K_A^{i-1}\cdot[M]^i = [U] + \sum_{i=1}^{N} i\cdot K_A^{i-1}\cdot K_F^i\cdot[U]^i \quad (3)$$

and dividing by P_0:

$$1 = x_U + \sum_{i=1}^{N} i \cdot (K_A \cdot P_0)^{i-1} (K_F \cdot x_U)^i \quad (4)$$

In eq 4, N represents the maximum size of the aggregates and each member of the sum is the fraction of protein monomers in aggregates of size i. Solving numerically, eq 4 gives the mole fraction of protein in the unfolded state for given values of N, the equilibrium constants K_F and K_A, and the total protein concentration, P_0. In principle, this would be only feasible for not very large values of N, but fortunately, there is a shortcut to sort this out. Multiplying eq 4 by $K_A \cdot P_0$, it holds that

$$K_A \cdot P_0 \cdot (1 - x_U) = \sum_{i=1}^{N} i \cdot (K_A \cdot P_0 \cdot K_F \cdot x_U)^i \quad (5)$$

If we call $x = K_A \cdot P_0 \cdot K_F \cdot x_U$ and consider that there is no limit for the size of the aggregates ($N \rightarrow \infty$), the right-hand side of eq 5 is then an infinite power series, S. Using the binomial expansion, it can be easily demonstrated that S is convergent to a finite value:

$$S = \sum_{i=1}^{\infty} i \cdot x^i = x + 2x^2 + 3x^3 + ... + ix^i + ... = \frac{x}{(1 - x)^2} \quad (6)$$

And therefore eq 5 becomes

$$(1 - x_U) = \frac{K_F \cdot x_U}{(1 - K_A \cdot P_0 \cdot K_F \cdot x_U)^2} \quad (7)$$

which can be written as

$$B^2 \cdot x_U^3 - [B^2 + 2B] \cdot x_U^2 + [2B + K_F + 1] \cdot x_U - 1 = 0 \quad (8)$$

where $B = K_A \cdot P_0 \cdot K_F$.

Taking the temperature derivative of eq 8:

$$\frac{dx_U}{dT} = - \frac{2B\frac{dB}{dT}x_U^3 - \left[2B\frac{dB}{dT} + 2\frac{dB}{dT}\right]x_U^2 + \left[2\frac{dB}{dT} + \frac{dK_F}{dT}\right]x_U}{3B^2 x_U^2 - 2(B^2 + 2B)x_U + (2B + K_F + 1)} \quad (9)$$

where

$$\frac{dB}{dT} = K_A P_0 \frac{dK_F}{dT} + K_F P_0 \frac{dK_A}{dT} \quad (10)$$

Equations 8−10 give the temperature evolution of x_U, independently of the maximum aggregate size. As shown below, the maximum size of the aggregates does not need to be very large to allow for the validity of these equations because the series convergence is fast.

TABLE 2: Enthalpy of Each Species in the Aggregate Mixture according to the Simple Polymerization Model

species	H_i (per particle)	H_i (per protein monomer)	ΔH_i (relative to M)
U	H_U	H_U	ΔH_U
M	H_M	H_M	0
A_2	$2H_M + \Delta H_A$	$H_M + (1/2)\Delta H_A$	$(1/2)\Delta H_A$
A_3	$3H_M + 2\Delta H_A$	$H_M + (2/3)\Delta H_A$	$(2/3)\Delta H_A$
...	...		
A_i	$4H_M + (i - 1)\Delta H_A$	$H_M + [(i - 1)/i]\Delta H_A$	$[(i - 1)/i]\Delta H_A$

The equilibrium constants K_F and K_A will change with temperature according to the van't Hoff equation:

$$\frac{dK_F}{dT} = K_F \frac{-\Delta H_U}{RT^2} \quad (11)$$

$$\frac{dK_A}{dT} = K_A \frac{\Delta H_A}{RT^2} \quad (12)$$

For convenience, eq 11 is expressed using the enthalpy of unfolding of the monomer, ΔH_U. ΔH_A is the enthalpy change of each aggregation step and for simplicity is assumed independent of the aggregate size. These equations need to be integrated in a certain temperature interval. Once the evolution of x_U with temperature has been evaluated, the mole fraction of the monomer and each aggregate species can be easily calculated as

$$x_M = K_F x_U \quad (13)$$

$$x_{A_i} = i \cdot (K_A \cdot P_0)^{i-1} (K_F \cdot x_U)^i \qquad (i = 2, 3, 4, ...) \quad (14)$$

Since the main objective of this model was the analysis of DSC data obtained with amyloid aggregates, we needed to derive equations for the temperature dependence of the enthalpy and the heat capacity of the system.

Each species present in the mixture would have an enthalpy according to Table 2. Accordingly, the average enthalpy of the whole system per mole of protein, relative to the monomeric state M, will be therefore

$$\langle \Delta H \rangle = \Delta H_U \cdot x_U + \Delta H_A \sum_{i=2}^{\infty} [(i - 1)/i] \cdot x_{A_i} = \Delta H_U \cdot x_U + \frac{\Delta H_A}{K_A \cdot P_0} \sum_{i=2}^{\infty} (i - 1)(K_A \cdot P_0 \cdot K_F \cdot x_U)^i \quad (15)$$

In eq 15, the sum is again a convergent power series so that it can be simplified to

$$\langle \Delta H \rangle = \Delta H_U \cdot x_U + \Delta H_A \cdot \frac{K_A \cdot P_0 \cdot (K_F \cdot x_U)^2}{(1 - K_A \cdot P_0 \cdot K_F \cdot x_U)^2} = \Delta H_U \cdot x_U + \Delta H_A \cdot \frac{B \cdot K_F \cdot x_U^2}{(1 - B \cdot x_U)^2} \quad (16)$$

The excess heat capacity of the system is obtained by taking the temperature derivative of eq 16:

$$\Delta C_p = \Delta C_{p,\mathrm{U}} \cdot x_\mathrm{U} + \Delta H_\mathrm{U} \cdot \frac{\mathrm{d}x_\mathrm{U}}{\mathrm{d}T} + \Delta C_{p,\mathrm{A}} \cdot \frac{B \cdot K_\mathrm{F} \cdot x_\mathrm{U}^2}{(1 - B \cdot x_\mathrm{U})^2} + \Delta H_\mathrm{A} \cdot \frac{\mathrm{d}}{\mathrm{d}T}\left[\frac{B \cdot K_\mathrm{F} \cdot x_\mathrm{U}^2}{(1 - B \cdot x_\mathrm{U})^2}\right] \quad (17)$$

where $\Delta C_{p,\mathrm{U}}$ and $\Delta C_{p,\mathrm{A}}$ are the heat capacity changes of the unfolding and the aggregation processes, respectively. We have omitted for simplicity the explicit derivative in the last term of eq 17. Finally, the partial heat capacity of the system is obtained by

$$C_p = C_{p,\mathrm{M}} + \Delta C_p \quad (18)$$

To evaluate C_p as a function of temperature, it is necessary to have analytical functions describing the temperature dependencies of the heat capacities of the accessible states. The heat capacity of the unfolded state can be appropriately described by a second-order polynomial that can be calculated from the protein sequence:[45,46]

$$C_{p,\mathrm{U}} = a + b \cdot T + c \cdot T^2 \quad (19)$$

For the sake of simplicity, we have assumed linear functions for the heat capacity of the monomer and the aggregates:

$$C_{p,\mathrm{M}} = d + e \cdot T \quad (20)$$

$$C_{p,\mathrm{A}} = f + g \cdot T \quad (21)$$

Using these heat capacity functions, the temperature dependences of the enthalpy changes, ΔH_U and ΔH_A, and the equilibrium constants K_F and K_A can be evaluated by integration of the Kirchhoff and van't Hoff relations:

$$\Delta H_\mathrm{U} = \Delta H_\mathrm{U}(T_\mathrm{U}) + (a - d) \cdot (T - T_\mathrm{U}) + \frac{(b - e)}{2} \cdot (T^2 - T_\mathrm{U}^2) + \frac{c}{3} \cdot (T^3 - T_\mathrm{U}^3) \quad (22)$$

$$\Delta H_\mathrm{A} = \Delta H_\mathrm{A}(T_0) + (f - d) \cdot (T - T_0) + \frac{(g - e)}{2} \cdot (T^2 - T_0^2) \quad (23)$$

$$\ln K_\mathrm{F} = \frac{\Delta H_{U_0}}{R}\left(\frac{1}{T} - \frac{1}{T_\mathrm{U}}\right) - \frac{(a - d)}{R} \ln\left(\frac{T}{T_\mathrm{U}}\right) - \frac{(b - e)}{2R}(T - T_\mathrm{U}) - \frac{c}{6R}(T^2 - T_\mathrm{U}^2) \quad (24)$$

$$\ln K_\mathrm{A} = \ln K_\mathrm{A}(T_0) - \frac{\Delta H_{A_0}}{R}\left(\frac{1}{T} - \frac{1}{T_0}\right) + \frac{(f - d)}{R} \ln\left(\frac{T}{T_0}\right) + \frac{(g - e)}{2R}(T - T_0) \quad (25)$$

In eqs 22−25, T_U is the melting temperature of the monomer (the temperature at which $K_\mathrm{F} = 1$) and T_0 is a reference temperature chosen as 50 °C for convenience. ΔH_{U_0} and ΔH_{A_0} stand for the unfolding and association enthalpies at 0 K.

To reduce the number of parameters, we have assumed that the slopes of the heat capacity functions of the monomer and the aggregates are equal; i.e., the heat capacity change of association is independent of temperature. In addition, we have assumed that the heat capacity changes of unfolding and association are proportional to their respective enthalpies.

Supporting Information Available: Simulations of DSC thermograms using the model of fibril melting by reversible monomer dissociation coupled to monomer unfolding. Analysis of the experimental DSC curves corresponding to the melting of N47A Spc-SH3 fibrils using the proposed model for thermal melting. This material is available free of charge via the Internet at http://pubs.acs.org.

References and Notes

(1) Rochet, J.-C.; Lansbury, P. T., Jr. Amyloid fibrillogenesis: themes and variations. *Curr. Opin. Struct. Biol.* **2000**, *10*, 60–68.

(2) Stefani, M.; Dobson, C. M. Protein aggregation and aggregate toxicity: new insights into protein folding, misfolding diseases and biological evolution. *J. Mol. Med.* **2003**, *81*, 678–699.

(3) Chiti, F.; Dobson, C. M. Protein Misfolding, Functional Amyloid, and Human Disease. *Annu. Rev. Biochem.* **2006**, *75*, 333–366.

(4) Dobson, C. M. The structural basis of protein folding and its links with human disease. *Philos. Trans. R. Soc. London, Ser. B* **2001**, *356*, 133–145.

(5) Nilsson, M. R. Techniques to study amyloid fibril formation in vitro. *Methods* **2004**, *34*, 151–160.

(6) Saiki, M.; Honda, S.; Kawasaki, K.; Zhou, D.; Kaito, A.; Konakahara, T.; Morii, H. Higher-order molecular packing in amyloid-like fibrils constructed with linear arrangements of hydrophobic and hydrogen-bonding side-chains. *J. Mol. Biol.* **2005**, *348*, 983–998.

(7) Serpell, L. C. Alzheimer's amyloid fibrils: structure and assembly. *Biochim. Biophys. Acta* **2000**, *1502*, 16–30.

(8) Makin, O. S.; Atkins, E.; Sikorski, P.; Johansson, J.; Serpell, L. C. Molecular basis for amyloid fibril formation and stability. *Proc. Natl. Acad. Sci. U.S.A.* **2005**, *102*, 315–320.

(9) Heise, H. Solid-state NMR spectroscopy of amyloid proteins. *ChemBioChem* **2008**, *9*, 179–189.

(10) Nelson, R.; Sawaya, M. R.; Balbirnie, M.; Madsen, A. O.; Riekel, C.; Grothe, R.; Eisenberg, D. Structure of the cross-beta spine of amyloid-like fibrils. *Nature* **2005**, *435*, 773–778.

(11) Tycko, R. Solid-state NMR as a probe of amyloid structure. *Protein Pept. Lett.* **2006**, *13*, 229–234.

(12) Ferrone, F. Analysis of protein aggregation kinetics. *Methods Enzymol.* **1999**, *309*, 256–274.

(13) Wetzel, R. Kinetics and Thermodynamics of Amyloid Fibril Assembly. *Acc. Chem. Res.* **2006**, *39*, 671–679.

(14) Harper, J. D.; Lansbury, P. T., Jr. Models of amyloid seeding in Alzheimer's disease and scrapie: mechanistic truths and physiological consequences of the time-dependent solubility of amyloid proteins. *Annu. Rev. Biochem.* **1997**, *66*, 385–407.

(15) Pedersen, J. S.; Christensen, G.; Otzen, D. E. Modulation of S6 fibrillation by unfolding rates and gatekeeper residues. *J. Mol. Biol.* **2004**, *341*, 575–588.

(16) Kardos, J.; Yamamoto, K.; Hasegawa, K.; Naiki, H.; Goto, Y. Direct measurement of the thermodynamic parameters of amyloid formation by isothermal titration calorimetry. *J. Biol. Chem.* **2004**, *279*, 55308–55314.

(17) O'Nuallain, B.; Shivaprasad, S.; Kheterpal, I.; Wetzel, R. Thermodynamics of Aβ(1−40) Amyloid Fibril Elongation. *Biochemistry* **2005**, *44*, 12709–12718.

(18) Privalov, P. L. Stability of proteins: small globular proteins. *Adv. Protein Chem.* **1979**, *33*, 167–241.

(19) Makhatadze, G. I.; Privalov, P. L. Energetics of protein structure. *Adv. Protein Chem.* **1995**, *47*, 307–425.

(20) Freire, E. Differential scanning calorimetry. *Methods Mol. Biol.* **1995**, *40*, 191–218.

(21) Sanchez-Ruiz, J. M.; Lopez-Lacomba, J. L.; Cortijo, M.; Mateo, P. L. Differential scanning calorimetry of the irreversible thermal denaturation of thermolysin. *Biochemistry* **1988**, *27*, 1648–1652.

(22) Conejero-Lara, F.; Sanchez-Ruiz, J. M.; Mateo, P. L.; Burgos, F. J.; Vendrell, J.; Aviles, F. X. Differential scanning calorimetric study of carboxypeptidase B, procarboxypeptidase B and its globular activation domain. *Eur. J. Biochem.* **1991**, *200*, 663–670.

(23) Calamai, M.; Canale, C.; Relini, A.; Stefani, M.; Chiti, F.; Dobson, C. M. Reversal of Protein Aggregation Provides Evidence for Multiple Aggregated States. *J. Mol. Biol.* **2005**, *346*, 603–616.

(24) Cellmer, T.; Douma, R.; Huebner, A.; Prausnitz, J.; Blanch, H. Kinetic studies of protein L aggregation and disaggregation. *Biophys. Chem.* **2007**, *125*, 350–359.

(25) Morgan, D.; Keller, R. K. What evidence would prove the amyloid hypothesis? Towards rational drug treatments for Alzheimer's disease. *J. Alzheimer's Dis.* **2002**, *4*, 257–260.

(26) Azuaga, A. I.; Dobson, C. M.; Mateo, P. L.; Conejero-Lara, F. Unfolding and aggregation during the thermal denaturation of streptokinase. *Eur. J. Biochem.* **2002**, *269*, 4121–4133.

(27) Litvinovich, S. V.; Brew, S. A.; Aota, S.; Akiyama, S. K.; Haudenschild, C.; Ingham, K. C. Formation of amyloid-like fibrils by self-association of a partially unfolded fibronectin type III module. *J. Mol. Biol.* **1998**, *280*, 245–258.

(28) Rezaei, H.; Choiset, Y.; Eghiaian, F.; Treguer, E.; Mentre, P.; Debey, P.; Grosclaude, J.; Haertle, T. Amyloidogenic Unfolding Intermediates Differentiate Sheep Prion Protein Variants. *J. Mol. Biol.* **2002**, *322*, 799–814.

(29) Morel, B.; Casares, S.; Conejero-Lara, F. A single mutation induces amyloid aggregation in the alpha-spectrin SH3 domain: analysis of the early stages of fibril formation. *J. Mol. Biol.* **2006**, *356*, 453–468.

(30) Sasahara, K.; Naiki, H.; Goto, Y. Kinetically Controlled Thermal Response of β2-Microglobulin Amyloid Fibrils. *J. Mol. Biol.* **2005**, *352*, 700–711.

(31) Sasahara, K.; Yagi, H.; Naiki, H.; Goto, Y. Heat-Triggered Conversion of Protofibrils into Mature Amyloid Fibrils of β2-Microglobulin. *Biochemistry* **2007**, *46*, 3286–3293.

(32) Sasahara, K.; Yagi, H.; Naiki, H.; Goto, Y. Thermal response with exothermic effects of beta2-microglobulin amyloid fibrils and fibrillation. *J. Mol. Biol.* **2009**, *389*, 584–594.

(33) Varela, L.; Morel, B.; Azuaga, A. I.; Conejero-Lara, F. A single mutation in an SH3 domain increases amyloid aggregation by accelerating nucleation, but not by destabilizing thermodynamically the native state. *FEBS Lett.* **2009**, *583*, 801–806.

(34) Sadqi, M.; Casares, S.; Abril, M. A.; Lopez-Mayorga, O.; Conejero-Lara, F.; Freire, E. The native state conformational ensemble of the SH3 domain from alpha-spectrin. *Biochemistry* **1999**, *38*, 8899–8906.

(35) Viguera, A. R.; Martinez, J. C.; Filimonov, V. V.; Mateo, P. L.; Serrano, L. Thermodynamic and kinetic analysis of the SH3 domain of spectrin shows a two-state folding transition. *Biochemistry* **1994**, *33*, 2142–2150.

(36) Privalov, P. L.; Plotnikov, V. V. Three generations of scanning microcalorimeters for liquids. *Thermochim. Acta* **1989**, *139*, 257–277.

(37) Jimenez, J. L.; Nettleton, E. J.; Bouchard, M.; Robinson, C. V.; Dobson, C. M.; Saibil, H. R. The protofilament structure of insulin amyloid fibrils. *Proc. Natl. Acad. Sci. U.S.A.* **2002**, *99*, 9196–9201.

(38) Freire, E.; van Osdol, W. W.; Mayorga, O. L.; Sanchez-Ruiz, J. M. Calorimetrically determined dynamics of complex unfolding transitions in proteins. *Annu. Rev. Biophys. Biophys. Chem.* **1990**, *19*, 159–188.

(39) Oosawa, F.; Kasai, M. A theory of linear and helical aggregations of macromolecules. *J. Mol. Biol.* **1962**, *4*, 10–21.

(40) Sasahara, K.; Naiki, H.; Goto, Y. Exothermic Effects Observed upon Heating of β2-Microglobulin Monomers in the Presence of Amyloid Seeds. *Biochemistry* **2006**, *45*, 8760–8769.

(41) Sasahara, K.; Yagi, H.; Naiki, H.; Goto, Y. Heat-induced Conversion of β2-Microglobulin and Hen Egg-white Lysozyme into Amyloid Fibrils. *J. Mol. Biol.* **2007**, *372*, 981–991.

(42) Narimoto, T.; Sakurai, K.; Okamoto, A.; Chatani, E.; Hoshino, M.; Hasegawa, K.; Naiki, H.; Goto, Y. Conformational stability of amyloid fibrils of β2-microglobulin probed by guanidine-hydrochloride-induced unfolding. *FEBS Lett.* **2004**, *576*, 313–319.

(43) Knowles, T. P. J.; Shu, W.; Devlin, G. L.; Meehan, S.; Auer, S.; Dobson, C. M.; Welland, M. E. Kinetics and thermodynamics of amyloid formation from direct measurements of fluctuations in fibril mass. *Proc. Natl. Acad. Sci. U.S.A.* **2007**, *104*, 10016–10021.

(44) Knowles, T. P.; Fitzpatrick, A. W.; Meehan, S.; Mott, H. R.; Vendruscolo, M.; Dobson, C. M.; Welland, M. E. Role of Intermolecular Forces in Defining Material Properties of Protein Nanofibrils. *Science* **2007**, *318*, 1900–1903.

(45) Makhatadze, G. I.; Privalov, P. L. Heat capacity of proteins. I. Partial molar heat capacity of individual amino acid residues in aqueous solution: hydration effect. *J. Mol. Biol.* **1990**, *213*, 375–384.

(46) Privalov, P. L.; Makhatadze, G. I. Heat capacity of proteins. II. Partial molar heat capacity of the unfolded polypeptide chain of proteins: protein unfolding effects. *J. Mol. Biol.* **1990**, *213*, 385–391.

JP9102993

SUPPORTING INFORMATION

1. Simulations of DSC thermograms using the model of fibril melting by reversible monomer dissociation coupled to monomer unfolding.

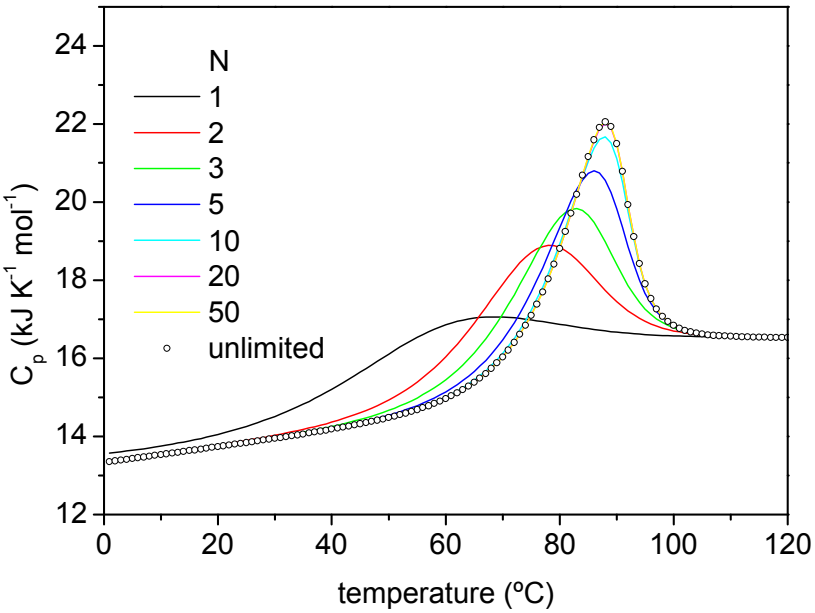

Figure S1: Effect of the maximum aggregate size, N, on the DSC thermograms calculated with the equations of the model. In all curves the monomer unfolding temperature, T_U, is 50 ºC, the total heat capacity change of fibril melting at 50ºC is 1.5 kJ K^{-1} mol^{-1} and the slope of the C_p function for both the aggregates and the monomer is 0.02 kJ K^{-2} mol^{-1}. The enthalpy changes of monomer unfolding and association are respectively: ΔH_U (50ºC) = 60 kJ mol^{-1} ; $\Delta H_A = 0$.

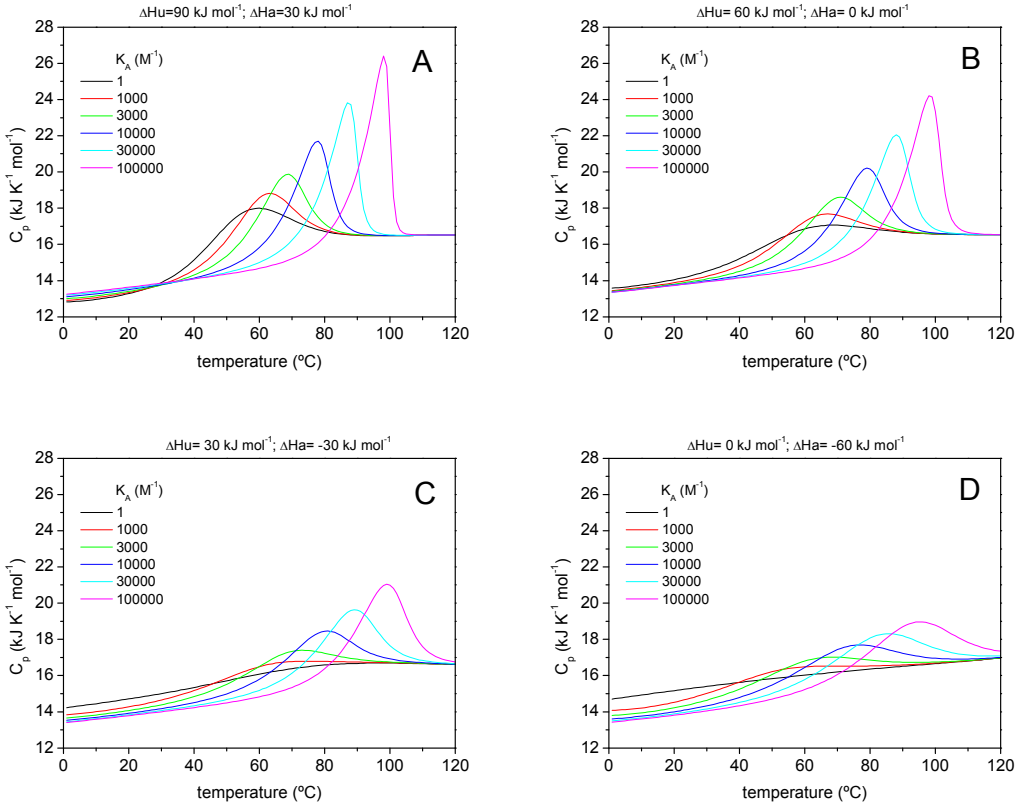

Figure S2: **Effect of the association constant K_A**. DSC thermograms calculated for different values of the association equilibrium constant, K_A, at 50 ºC, for a fixed total protein concentration, P_0, equal to 1 mM. In all curves the monomer unfolding temperature, T_U, is 50 ºC, the total enthalpy and heat capacity changes of fibril melting at 50ºC are 60 kJ mol^{-1} and 1.5 kJ K^{-1} mol^{-1} respectively and the slope of the C_p function for both the aggregates and the monomer is 0.02 kJ K^{-2} mol^{-1}. **Panel A:** ΔH_U (50ºC) = 90 kJ mol^{-1} and ΔH_A (50ºC) = 30 kJ mol^{-1}. **Panel B**: ΔH_U (50ºC) = 60 kJ mol^{-1} and ΔH_A (50ºC) = 0 kJ mol^{-1}. **Panel C:** ΔH_U (50ºC) = 30 kJ mol^{-1} and ΔH_A (50ºC) = –30 kJ mol^{-1}. **Panel D:** ΔH_U (50ºC) = 0 kJ mol^{-1} and ΔH_A (50ºC) = –60 kJ mol^{-1}.

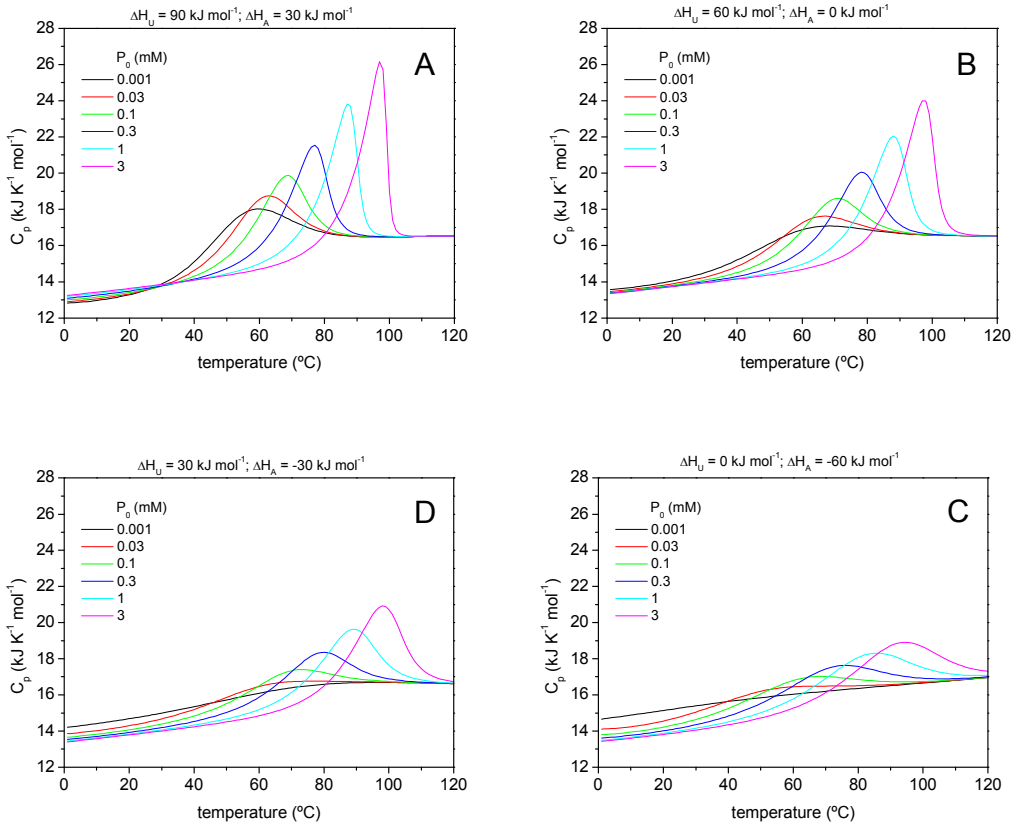

Figure S3: Effect of the total protein concentration. DSC thermograms calculated for different values of the protein concentration P_0 from 1 μM to 3 mM. K_A was fixed to 3×10^4 M^{-1} at 50ºC. All the rest of parameters in each panel are as in Figure S2.

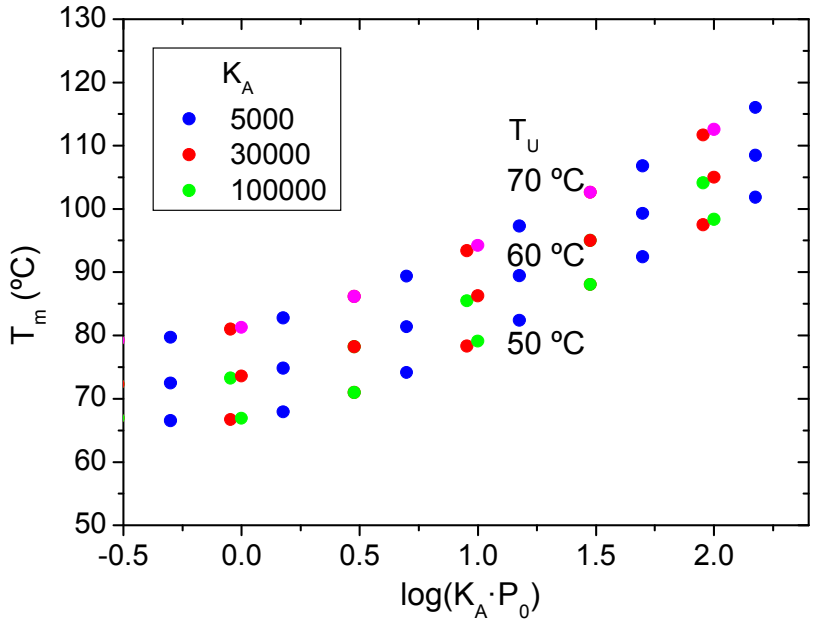

Figure S4: Combined effect of K_A and P_0. Temperature of maximum C_p, T_m, versus $\log(K_A \cdot P_0)$ for different values of the unfolding temperature of the monomer, T_U. The values of K_A are indicated in the plot and P_0 varies from 1μM to 10 mM. The rest of the parameters are as in Figure S2.

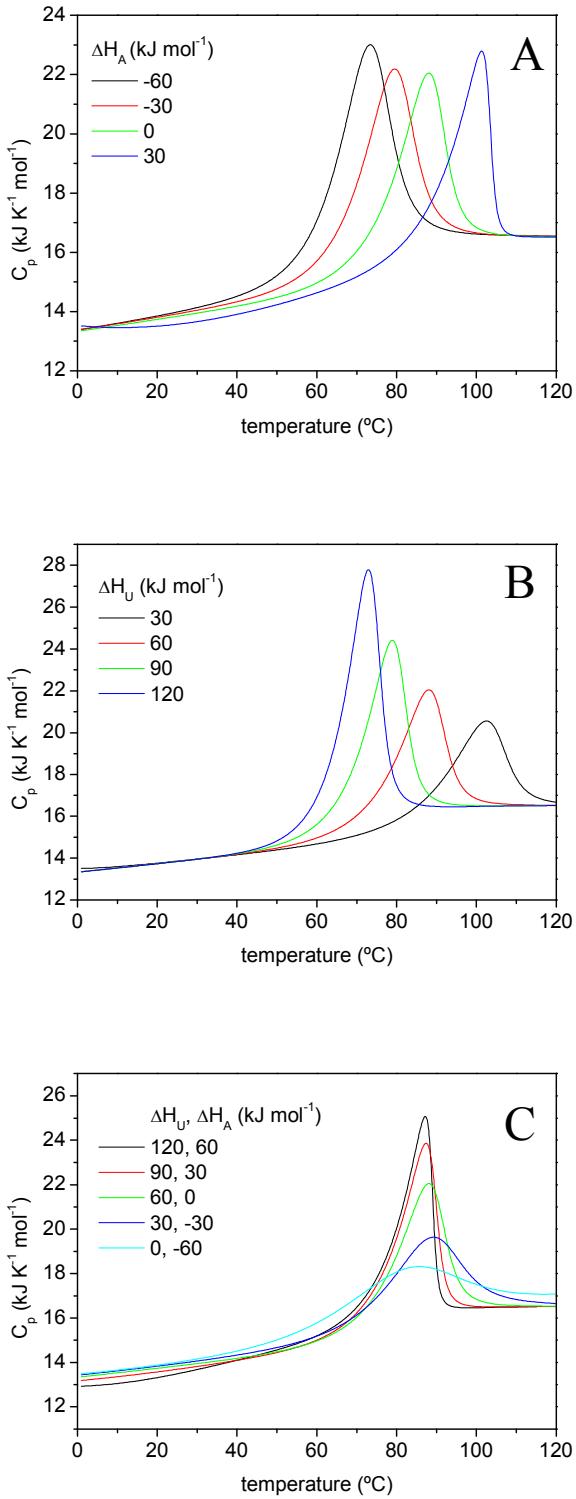

Figure S5: Effect of the enthalpies of aggregation and monomer unfolding. (A) Enthalpy of monomer unfolding fixed to 60 kJ mol^{-1}. (B) Enthalpy of association fixed to 0 kJ mol^{-1}. (C) Total enthalpy of fibril melting is fixed to 60 kJ mol^{-1}. K_A and P_0 are fixed in all simulations to 3×10^4 and 1 mM, respectively. The rest of the parameters are as in Figure S2.

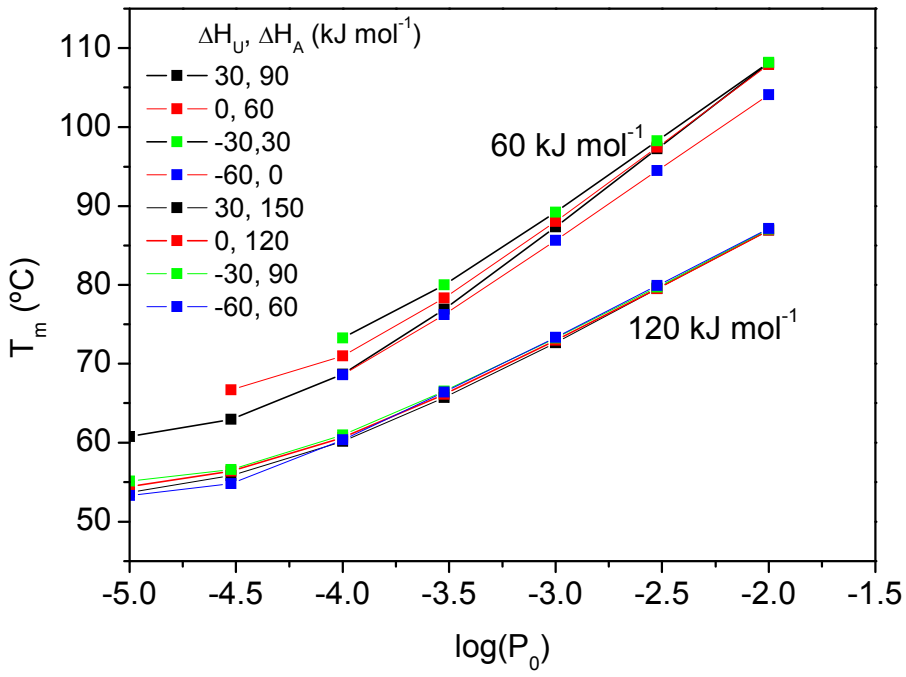

Figure S6: Dependence of the melting temperature with the total protein concentration and the enthalpy changes of association and monomer unfolding. Both the enthalpy of association and monomer unfolding are varied to keep constant the total enthalpy of fibril melting as indicated along the plots. In all simulations K_A was kept constant and equal to 3×10^4 M^{-1}. All remaining parameters are as in Figure S2.

2**. Analysis of the experimental DSC curves corresponding to the melting of N47A Spc-SH3 fibrils using the proposed model for thermal melting.**

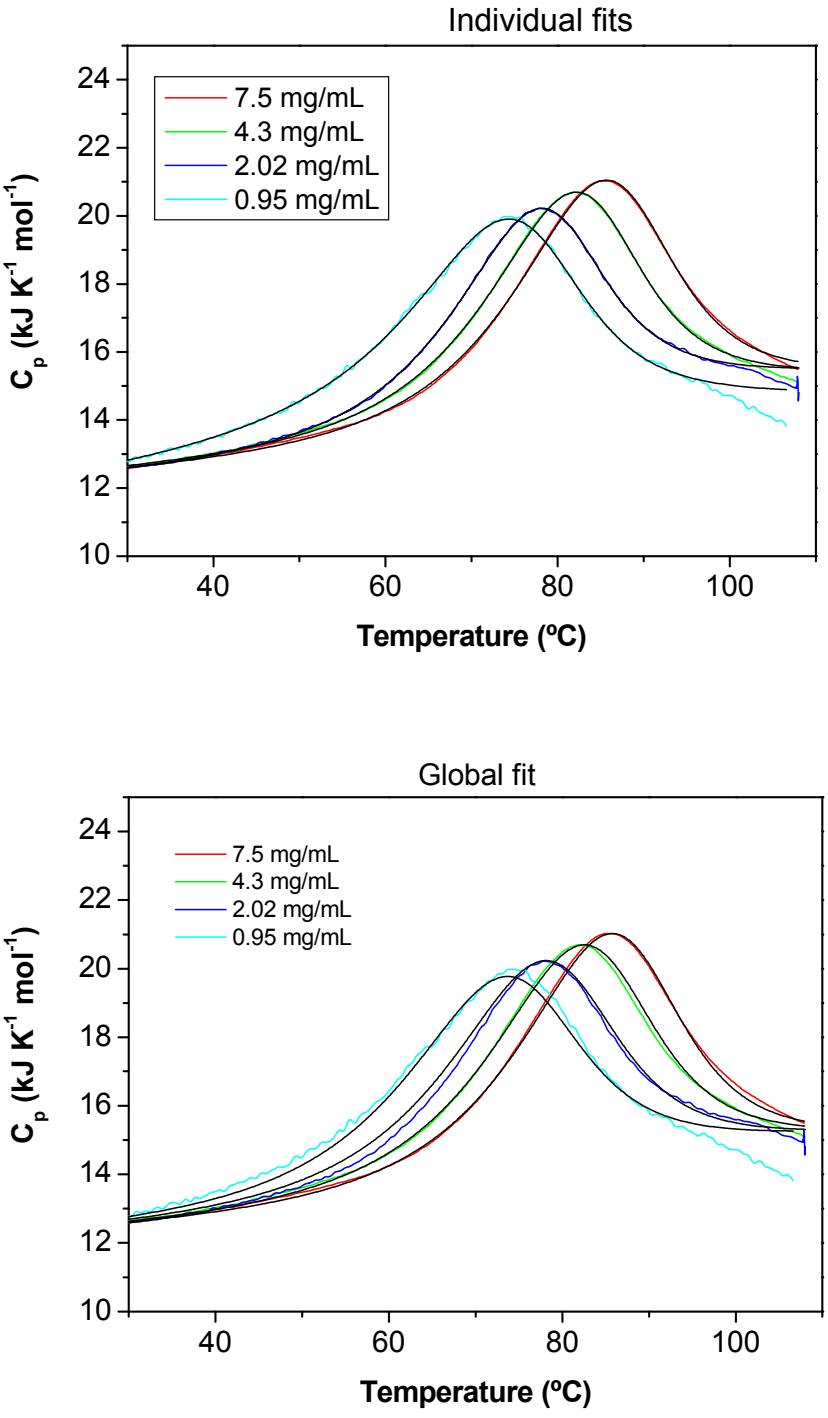

Figure S7: DSC data of fibrils prepared by incubation at 37ºC for 10 days in the presence of 100 mM NaCl and analysed at different protein concentrations as indicated. The black lines correspond to the best fits according to the model. The individual fits of each DSC curve are shown in the upper panel and the global fit to the whole set of curves in the bottom panel.

Table S1: Thermodynamic parameters of the fits shown in figure S7.					
P_0 (mg/ml)	7.5	4.3	2.02	0.95	Global fit
ΔH_A (kJ mol^{-1})	-116.9 ± 7.0	-109.6 ± 6.1	-98.7 ± 7.2	-128.7 ± 0.55	-120.5 ± 0.9
K_A	433093 ± 165499	370452 ± 161401	385668 ± 213348	351721 ± 1405	398182 ± 13686
T_U (ºC)	48 ± 52	39 ± 63	-3.5 ± 79	79.6 ± 0.5	77.17 ± 2.46
ΔH_U (kJ mol^{-1})	7.4 ± 6.9	10 ± 9	7.3 ± 12.3	46.5 ± 0.2	13.2 ± 1.3
ΔC_p (kJ K^{-1} mol^{-1})	1.59 ± 0.14	1.63 ± 0.11	1.89 ± 0.12	0.61 ± 0.01	1.51 ± 0.02
Slope Cp(M) (kJ K^{-2} mol^{-1})	0.021 ± 0.001	0.021 ± 0.0015	0.019 ± 0.0018	0.032 ± 0.0006	0.019 ± 0.0005

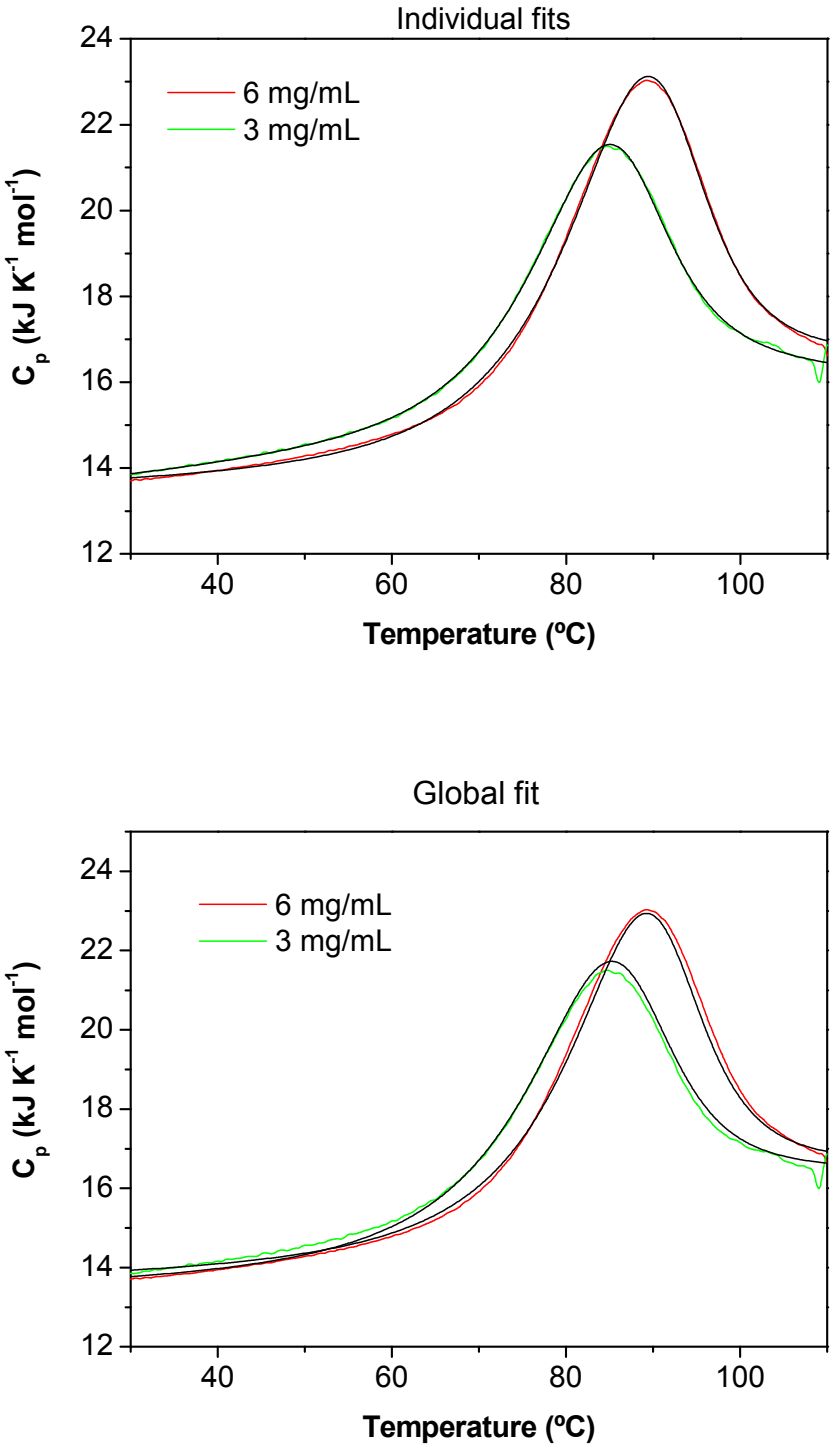

Figure S8: DSC data of fibrils prepared by incubation at 37ºC for 1 month in the presence of 100 mM NaCl and analysed at different protein concentrations as indicated. The black lines correspond to the best fits according to the model. The individual fits of each DSC curve are shown in the upper panel and the global fit to the whole set of curves in the bottom panel.

Table S2: Thermodynamic parameters of the fits shown in figure S8.			
P_0 (mg/ml)	6.1	3.0	Global fit
ΔH_A (kJ mol^{-1})	-91.6 ± 2.0	-60.1 ± 5.1	-85.6 ± 2.6
K_A	524836 ± 139343	64362 ± 12391	231532 ± 20920
T_U (ºC)	48.9 ± 44	73.74 ± 0.56	72.88 ± 1.7
ΔH_U (kJ mol^{-1})	11.5 ± 7.3	60.5 ± 3.8	31.2 ± 2.3
ΔC_p (kJ K^{-1} mol^{-1})	2.07 ± 0.06	1.37 ± 0.02	1.74 ± 0.03
Slope Cp(M) (kJ K^{-2} mol^{-1})	0.0089 ± 0.0017	0.016 ± 0.002	0.0068 ± 0.0013

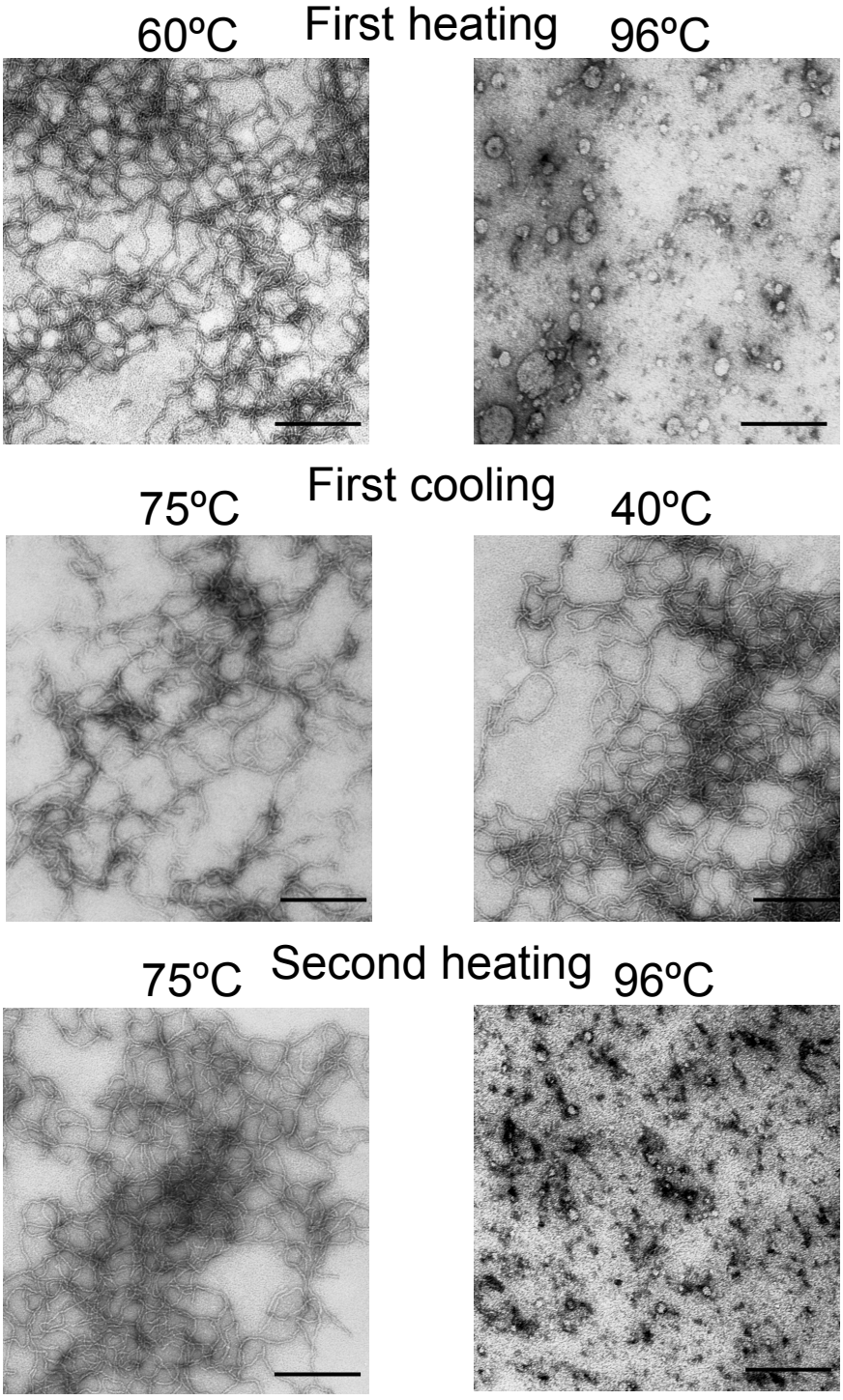

Figure S9. TEM images of amyloid fibrils of N47A Spc-SH3 at several temperatures during consecutive heating and cooling scans. Fibrils were produced by 5-day incubation at 37ºC of an 8 mg mL^{-1} fresh protein sample in 100 mM glycine buffer pH 3.2, in the presence of 100 mM NaCl, and separated from the supernatant by ultracentrifugation. Resuspended fibrils were heated and cooled in a water bath at 2ºC min^{-1}. Sample aliquots were taken at the indicated temperatures and frozen in liquid N_2 for TEM analysis. The black segment represents 233 nm in all the panels.